

THE LOWEST TRIPLET STATE OF
TETRAMETHYL-1, 3-CYCLOBUTANEDITHIONE

By

JOSEPH PETER BAIARDO

A DISSERTATION PRESENTED TO THE GRADUATE COUNCIL
OF THE UNIVERSITY OF FLORIDA IN
PARTIAL FULFILLMENT OF THE REQUIREMENTS
FOR THE DEGREE OF DOCTOR OF PHILOSOPHY

UNIVERSITY OF FLORIDA
1982

JM 10 82 2044

In memoria di mio padre

Ottavio Nino

e per la mia cara madre

Gisella

and to my wife Nancy, whose love,
encouragement and endless sacrifices kept
my spirit alive and whose terrific menu did
wonders for me;

to Joseph, your daily welcome home dash
and embrace made everything bearable;

to Jonathan, your eagerness to help me
was always my inspiration;

and Justin, your echoes and answering service
has been the song in my mind.

To all of you who somehow managed to transform
the daily valleys into peaks.

ACKNOWLEDGEMENTS

I would like to express my deepest appreciation to Professor Martin T. Vala whose encouragement and optimism coupled with his sage advice and infinite patience over the years have been a source of inspiration without which this work would not have been possible.

I gratefully acknowledge Dr. Ib Trabjerg who spent countless hours recording the Zeeman spectra.

To my fellow students, past and present, thank you for sharing good times and bad and for giving an ear when it was needed the most.

To Drs. Jean Claude Rivoal, Ranajit Mukherjee and Marek Kreglewski, I owe a great deal of thanks for the many stimulating discussions and timely advice which they shared with me.

Special thanks are due to the Northeast Regional Data Center for making available the many hours of computer time over the years.

And of course to Ms. Joan Raudenbush, whose long hours of patient typing made possible the speedy completion of this work without sacrificing quality, I owe a great many thanks.

I wish to thank Professor William Weltner for helpful discussions on some parts of Chapter 5, and Professor M. Vala and our draftsman, Jeff Pate, for drafting most of the figures.

I am grateful to Professor Willis Person for his encouragement over the years.

TABLE OF CONTENTS

	Page
ACKNOWLEDGEMENTS -----	iii
LIST OF TABLES -----	vii
LIST OF FIGURES -----	ix
ABSTRACT -----	xii
CHAPTER	
1. INTRODUCTION -----	1
General Background -----	1
Motivation and Direction -----	11
2. RESULTS OF <i>ab initio</i> SCF CALCULATIONS ON CARBONYL ANALOGUES -----	15
Computational Details -----	24
Results and Discussion -----	25
Ionization Potentials -----	25
Excited $n \pi^*$ States -----	27
3. THE $T_1 \leftarrow S_0$ ELECTRONIC TRANSITION IN CRYSTALLINE TETRAMETHYL-1,3-CYCLOBUTANEDITHIONE -----	40
Introduction -----	40
Spectroscopic Technique -----	40
Crystal Symmetry -----	41
Crystal States -----	43
Effect of External Fields -----	44
Features of Crystal Spectra -----	45
Crystal Vibrations -----	45
Electronic Absorption -----	47

Crystal Structure -----	49
Crystal Growth -----	53
Crystal Orientation -----	54
Experimental Details -----	55
Results -----	59
Low Temperature -----	59
Temperatures Above 10K -----	59
Vibrational Analysis of the $T_1 + S_0$ Transition -----	61
The 0-0 Band -----	61
The 300 cm^{-1} Band -----	62
The 600 cm^{-1} Band -----	65
The 970 cm^{-1} Band -----	65
Polarization c -----	65
Summary -----	65
Crystal Vibrations in TMCBDT -----	67
The Double Minimum Potentials -----	70
Fitting Procedure and Results -----	70
The Calculated Spectra at 1.6K -----	75
Temperature Dependence of Spectra -----	80
Physical Nature of DMP -----	80
Summary -----	88
4. SPIN-ORBIT COUPLING IN TETRAMETHYL-1,3-CYCLOBUTANEDI- THIONE -----	90
Introduction -----	90
$T_1 + S_0$ Crystal Transition Moment for TMCBDT -----	90
Evaluation of Matrix Elements: $\langle H_{so} \rangle$ and $\langle m \rangle$ -----	98
Spin-Orbit Hamiltonian -----	98
Choice of Wavefunction -----	98
Evaluation of $\langle H_{so} \rangle$ With Respect to EHT Wave- functions -----	102
Transition Moments With Respect to EHT Wave- functions -----	107
Choice of Parameters Used in the Calculation -----	111
Results -----	111
Summary -----	121
5. ZEEMAN SPECTROSCOPY OF TETRAMETHYL-1,3-CYCLOBUTANE- DITHIONE -----	122
Introduction -----	122
Theory -----	125

Zeeman Intensity Ratio for an Arbitrary Field	126
Direction -----	129
Polarized Zeeman Absorption -----	136
Unpolarized Zeeman Absorption -----	137
Zero-field Absorption (ZFA) -----	
Effect of Zero-Field Splitting Parameters -----	138
Calculation of Zero-Field Splitting Parameters -----	145
Influence of Triplet-State Perturbers -----	147
Localized and Delocalized Excitation -----	152
Comment on Xanthione -----	153
Experimental Details -----	156
Apparatus -----	156
Crystal Mounting -----	157
Experimental Results -----	163
Low Temperature Results: 1.6 K -----	163
Temperatures Above 4 K -----	164
Measurement Errors -----	176
Discussion -----	180
Temperatures above 4 K -----	180
Zeeman Ratio as Function of R_x , R_z , ψ and ϕ -----	187
Summary -----	201
Low Temperature and Field Dependent Results -----	202
Discrepancies -----	213
ρ and g Tensor Consideration -----	213
Summary of Zeeman Absorption Experiments -----	222
6. CONCLUSIONS AND SUGGESTIONS -----	224
APPENDIX I -----	230
APPENDIX II -----	248
REFERENCES -----	265
BIOGRAPHICAL SKETCH -----	273

LIST OF TABLES

TABLE	Page
2-1. ATOMIC COORDINATES FOR TMCBD AND CBD -----	36
2-2. ORBITAL ENERGIES FOR CBD, TMCBD (<i>ab initio</i> , D_{2h}) -----	37
2-3. VERTICAL TRANSITION ENERGIES (ΔSCF) FOR THE $1,3n\pi^*$ STATES CALCULATED USING D_{2h} WAVEFUNCTIONS -----	38
2-4. COMPARISON OF VERTICAL TRANSITION ENERGIES (ΔSCF) of $1n\pi^*$ OF TMCBD STATES WITH OBSERVED AND SEMIEMPIRICAL METHODS -----	39
3-1. VIBRATIONAL ANALYSIS OF $T_1 \leftarrow S_0$ ABSORPTION OF CRYSTAL-LINE TMCBDT POLARIZED PERPENDICULAR TO c -----	63
3-2. (STATIC) CORRELATION BETWEEN MOLECULAR (SITE) GROUP AND FACTOR GROUP -----	66
3-3. DMP DESCRIPTION OF THE LOW FREQUENCY VIBRATIONS OBSERVED AT 1.6 K IN CRYSTALLINE TMCBDT SPECTRA -----	72
3-4. CORRELATION TABLE FOR THE DISTORTED MOLECULAR EXCITED STATE -----	78
4-1. PARAMETERS USED IN EHT CALCULATIONS -----	112
4-2. CONTRIBUTIONS TO $T_1 \leftarrow S_0$ TRANSITION MOMENT FROM SINGLET STATE PERTURBATIONS OF $T_1(3n\pi^*)$ -----	115
4-3. CONTRIBUTIONS TO $T_1 \leftarrow S_0$ TRANSITION MOMENT FROM TRIPLET STATE PERTURBERS OF S_0 -----	116
4-4. TRANSITION MOMENTS, OSCILLATOR STRENGTHS AND LIFETIMES OF THE TRIPLET SUBLEVELS -----	119
5-1. MOLECULAR AXES IN UNIT CELL FRAME AND THEIR DIRECTION COSINES WITH RESPECT TO \vec{H} -----	133
5-2. OBSERVED RATIOS FOR THE ZEEMAN ABSORPTION (CRYSTAL B) OF THE 5943 Å BAND AT 16 K AS A FUNCTION OF POLARIZER ANGLE -----	168

5-3.	OBSERVED RATIOS FOR THE ZEEMAN ABSORPTION (CRYSTAL C) OF THE 5943 Å BAND AT 5 K AS A FUNCTION OF POLARIZER ANGLE -----	171
5-4.	ZERO-FIELD ABSORPTION VS. POLARIZATION -----	184
5-5.	OBSERVED Δ VALUES FROM FIELD DEPENDENT ABSORPTION OF 5943 Å BAND AND EMISSION OF 6003 Å TRAP -----	186
5-6.	COMPARISON OF CALCULATED TO EXPERIMENTAL ZEEMAN MEASUREMENTS AT 1.6 K -----	206
5-7.	POLARIZED ZEEMAN ABSORPTION INTENSITIES FOR CRYSTALS B AND C -----	210
5-8.	INTENSITIES FOR CRYSTAL C CALCULATED USING $X=+2$, $Y=Z=-1$ -----	218

LIST OF FIGURES

Figure	Page
2-1. Through-space and through-bond interactions in TMCBD -----	18
2-2. Density and contour maps for the $n_+(b_{1u})$ and $n_-(b_{3g})$ molecular orbitals of CBD -----	20
2-3. Net orbital populations for CBD in C_s -----	31
2-4. Molecular orbitals and their one-electron energies for TMCBDT as calculated by Extended Hückel method -----	34
3-1. Orientation of TMCBDT molecules within the tetragonal unit cell -----	50
3-2. Low temperature absorption spectrum of single crystal TMCBDT polarized perpendicular to c -----	58
3-3. Absorption spectrum of single crystal TMCBDT at 20 K and 47 K -----	60
3-4. Double minimum potential for ground state -----	73
3-5. Double minimum potential for triplet excited state-----	74
3-6. Simulated absorption and emission spectra calculated using the DMP model as a function of temperature--	82
3-7. Molecular displacements involved in the B_{2g} lattice vibration -----	86
5-1. Coordinate system used in the derivation of Zeeman intensities for an arbitrary magnetic field orientation in the Faraday configuration -----	131
5-2. Effect of zero-field-splitting parameters on the Zeeman spectra -----	141
5-3. Light-pipe and coils assembly used in the Zeeman experiments -----	158

5-4.	Zeeman absorption spectrum at 1.6 K of the 594 nm band of single crystal TMCBDT po- larized perpendicular to c -----	160
5-5.	Unpolarized Zeeman absorption spectrum at 1.6 K of the 594 nm band of single crystal TMCBDT-----	162
5-6.	Polarized Zeeman absorption spectra of the 594 nm band at 16 K as a function of polarizer orientation -----	166
5-7.	Polarized Zeeman absorption spectra of the 594 nm band at 5 K as a function of polarizer orientation -----	170
5-8.	Polarized zero-field absorption spectra of the 594 nm band at 5 K as a function of polarizer orientation -----	173
5-9.	Unpolarized Zeeman absorption spectra of the 594 nm band at 5 K as a function of magnetic field strength -----	175
5-10.	Unpolarized Zeeman emission spectra of the 600 nm trap at 5 K as a function of magnetic field strength -----	178
5-11.	Effect of ϕ on the calculated Zeeman intensity ratio for $\psi=5^\circ$ and one spin-orbit route in the absence of zero-field splitting -----	189
5-12.	Effect of ϕ on the calculated Zeeman intensity ratio for $\psi=20^\circ$ and one spin-orbit route in the absence of zero-field splitting -----	191
5-13.	Effect of z spin-orbit route on the Zeeman inten- sity ratio in the absence of zero-field split- ting -----	193
5-14.	Effect of x spin-orbit route on the Zeeman inten- sity ratio in the absence of zero-field split- ting -----	195
5-15.	Comparison of the calculated Zeeman ratio for the y spin-orbit route with average experimental ratios as a function of polarizer orientation---	198
5-16.	Comparison of the theoretical Zeeman ratio using the transition moments determined from the EHT- spin-orbit-coupling calculation -----	200

5-17. Simulated Zeeman spectra of crystal A for the two molecules in the unit cell and their sum---	207
5-18. Simulated Zeeman spectra of crystal F for the two molecules in the unit cell and their sum---	209
5-19. Plot of calculated and experimental band posi- tions as a function of magnetic field strength for $D > 0$ and spin axes coincident with molecular symmetry axes -----	214
5-20. Plot of calculated and experimental band posi- tions as a function of magnetic field strength for $D < 0$ and spin axes coincident with molec- ular symmetry axes -----	215
5-21. Plot of calculated and experimental band positions as a function of magnetic field strength for the case of non-coincident molecular symmetry and spin axes -----	217

Abstract of Dissertation Presented to the Graduate Council
of the University of Florida in Partial Fulfillment of the
Requirements for the Degree of Doctor of Philosophy

THE LOWEST TRIPLET STATE OF
TETRAMETHYL-1,3-CYCLOBUTANEDITHIONE

By

Joseph Peter Baiardo

May, 1982

Chairman: Martin T. Vala
Major Department: Chemistry

The lowest energy band in the absorption spectrum of tetramethyl-1,3-cyclobutanedithione (TMCBDT) is determined to be due to ${}^3A_u(n\pi^*) \leftarrow {}^1A_g$ by Zeeman spectroscopy. The polarized single crystal absorption spectrum in zero field at 1.6 K consists of bands polarized exclusively perpendicular to c, with the 0-0 band at 594.3 nm. A model in which a double minimum potential (DMP) in both the ground and excited states, involving either a ring torsion mode or a lattice mode, is shown to account for the observed temperature dependence of the spectra. Vibrations observed in the triplet region are assigned to the C=S stretch at 970 cm^{-1} , skeletal vibrations at 309 and 600 cm^{-1} , and a C-C stretch or methyl bend at 913 cm^{-1} .

A detailed analysis of spin-orbit-coupling (SOC) in TMCBDT predicts that this transition should be polarized exclusively along the C=S bonds, in agreement with experiment, and that two ${}^3B_{2g}, n\pi^*$

states significantly perturb the ground state and contribute 60% of the free molecule transition moment via $T_n + T_1$ allowed transitions. The most influential singlet state perturbing T_1 is the ${}^1B_{2u}, {}^1\pi_+, \pi_-^*$ state which adds 18% to the transition moment.

An expression for the Zeeman intensity for an arbitrary magnetic field orientation in the Faraday configuration, is derived. It is shown that the observed polarization dependence is due to field misalignment rather than multiple spin-orbit routes and that the observed Zeeman data is consistent with the SOC calculation results.

Field-strength-dependent Zeeman spectra demonstrate that the zero-field splitting (D) in single crystal TMCBDT is smaller than that found for xanthione by Burland. The SOC contributions to D are discussed in terms of localized vs. delocalized excited states and it is shown that both the extent of excitation-localization and the singlet-triplet splitting of perturbing states are important.

An orbital symmetry unrestricted calculation (double- ζ) is performed at the *ab initio* SCSCF level on the parent molecule cyclobutanedione. It is found that the localized description of the $1,3_n\pi^*$ (and 2_n) states gives a transition energy (and ionization potential) which is more in accord with experiment than that given by the delocalized solutions to the SCF equations. These results are used to qualitatively discuss the effect of localization on the SOC contributions to D.

CHAPTER 1 INTRODUCTION

General Background

Within the framework of molecular orbital (MO) theory the lowest energy electronic transition of a single carbonyl group is described as arising from the promotion of an electron in the highest occupied MO, the nonbonding lone pair of oxygen (n), to the lowest unoccupied MO, the antibonding carbonyl π orbital (π^*). This has come to be known as a $\pi^* \leftarrow n$ (or $n \rightarrow \pi^*$) transition and usually occurs in the near-ultraviolet region of the spectrum. This explanation was made by McMurry in 1941 in a spectroscopic study of aldehydes and ketones (1).

In a subsequent study of dicarbonyl compounds, McMurry (2) described the interaction of the carbonyl groups in terms of the simple LCAO-MO theory by taking symmetric and antisymmetric (+ and -) linear combinations of both the n orbitals and π^* orbitals. He considered the n orbitals as strictly localized on the oxygen atoms and not interacting while he allowed for an interaction between the π^* orbitals thereby introducing a splitting between the π^*_+ and π^*_- MO's (the latter being of higher energy due to an additional node). This was rationalized on the basis of the conjugative properties of π orbitals and explained the observed splitting of the lowest $n \rightarrow \pi^*$ carbonyl band in the dichromophoric compounds. In 1955 Sidman and

McClure (3) applied McMurry's approach in their study of the electronic spectra of the α -dicarbonyl biacetyl; they explained the split $n \pi^*$ band in this compound in terms of transitions from the degenerate n_+ and n_- MO's to the split π_+^* and π_-^* MO's.

Tetramethyl-1,3-cyclobutanedione (TMCBD), a β -dicarbonyl which has been studied recently by Vala and his coworkers (4-9), was first studied spectroscopically by LaLancette and Benson (10) in 1961 and in 1963 by Kosower (11). Kosower interpreted the solution spectrum of TMCBD in terms of two $n \pi^*$ transitions (in the region 225 nm to 375 nm) resulting from transannular interaction between the carbonyl π^* MO's, giving the split π_+^* and π_-^* linear combination. In 1970 Ballard and Park (12) compared the solution spectra of TMCBD and TMCBDT and verified the observation of Kosower regarding the split $n \pi^*$ band of TMCBD and concurred on the transannular interaction of the π^* orbitals. In addition, however, they noted that if the n orbitals were also split, four symmetry forbidden $n \pi^*$ transitions would then arise in TMCBD, two of them A_u ($n_+ \pi_-^*$ and $n_- \pi_+^*$) and two B_{1g} ($n_+ \pi_+^*$ and $n_- \pi_-^*$) as expressed in the D_{2h} point group of the molecule. No indication of four $n \pi^*$ transitions was reported by Ballard and Park, however.

For the corresponding dithione, on the other hand, Ballard and Park (12) found that the solution spectrum contained a weak broad band in the region 400 to 625 nm having six poorly resolved maxima. These were assigned as vibrations because of the regularity of the 1460 cm^{-1} spacing between the peaks and their approximate Gaussian distribution. Although Ballard and Park noted that the excited state frequency of the C=S stretch is expected to decrease from the $\sim 1100 \text{ cm}^{-1}$ value in

the ground electronic state in response to the bond weakening due to the $n\pi^*$ transition, these authors nevertheless assigned the 1460 cm^{-1} spacing to the C=S stretch. In addition they assigned a band at 294 nm as an $n\sigma^*$ transition and another, very intense band, in which no splitting was observed, at 200 nm was assigned as $\pi\pi^*$. From these considerations Ballard and Park concluded that the $n\pi^*$ band in TMCBDT is not split by a transannular π interaction as in the corresponding dione, and therefore suggested (12) that the transannular distance between the thiocarbonyl carbons must be greater in TMCBDT than in TMCBD.

At about this time the theoretical interpretation of interacting chromophoric groups was revolutionized by Hoffman and coworkers (13-15) who, in a series of Extended Hückel Theory (EHT) (16) and CNDO/2 (17) calculations, demonstrated that the non-bonding orbitals in a molecule containing two or more symmetry related heteroatoms can interact by two different mechanisms and thereby split. These mechanisms were termed through-space and through-bond interactions. Through-space interaction between two orbitals n_a and n_b , for example, occurs when their spatial overlap S_{ab} is significant. The transannular interaction mechanism invoked by Kosower and Ballard and Park, for example, is of this type. If S_{ab} is small, however, the two orbitals n_a and n_b may still interact indirectly via the σ framework orbitals as follows. The linear combinations n_+ and n_- formed from n_a and n_b are still degenerate; however, these now transform as two different irreducible representations of the molecular point group. If there is significant overlap between one or both of these linear combinations with a framework MO of the

same symmetry, usually lower in energy, than the n_+ and n_- combinations will interact differently with the framework orbitals thereby splitting. Normally through-space interaction above is considered to produce the n_- combination at higher energy than the n_+ while the through-bond mechanism may destabilize the n_+ orbital more than the n_- and could result in n_+ lying above n_- .

In 1971 Cowan et al. (13) using molecular photoelectron spectroscopy (PES) (19) determined experimentally the order and splitting of the n orbitals in TMCBD and several other dicarbonyl molecules. They found that in TMCBD the through-bond interaction causes n_+ to lie 0.7 eV higher in energy than n_- . This was a significant result because it directly confirmed the prediction of Swenson and Hoffman (14) and suggested that Ballard and Park's (12) observation of the possibility of four $n\pi^*$ transitions in TMCBD may be observable.

Using the powerful technique of low temperature single crystal polarized absorption spectroscopy, Spafford et al. (7) later demonstrated that each of the two $n\pi^*$ transitions previously observed (11,12) are further split into two $n\pi^*$ bands. Based on the polarization of bands, vibrational assignments, and crystal and site symmetries (discussed in Chapter 3) they were able to assign four singlet-singlet $n\pi^*$ bands in the order $A_u < B_{2g} < B_{2g} < A_u$ (in D_{2h}) by invoking a distorted geometry in each of the four excited states: C_{2v} in the first and third and C_{2h} in the second and fourth. The other important interpretations advanced in this work are the additional verification of the through-bond mechanism (*vide supra*) and the introduction of a circumannular interaction whereby the π^* orbitals are split because of a preferential destabilization of the π_+ orbital by the bonding σ C(ring)-C(methyl)

orbitals; this is another manifestation of the through-bond interaction mechanism.

A theoretical analysis advanced by Baiardo et al. (8) compared three semiempirical MO methods in their ability to correctly predict the four $n\pi^*$ transitions in cyclobutane-1,3-dione (CBD) and TMCBD. It was found that the EHT method was more accurate and reasons were advanced for this; the mechanisms of through-bond interactions active in both the n -orbital and π^* -orbital splittings were said to outweigh the through-space mechanisms, in accord with the previously observed PES (19) results regarding the n orbital ordering and splitting.

Working independently Gordon et al. (20) simultaneously reported a very similar result for the $n\pi^*$ transitions of TMCBD. The band positions agreed with those of Spafford et al. (7) but a different vibrational and electronic state assignment was given resulting in different excited state distortions and only three $n\pi^*$ bands. The fourth was assigned as a CH stretch vibronic origin based on comparison with d_{12} isotope spectra.

These are the first published reports of direct experimental evidence for more than two $n\pi^*$ transitions in a dicarbonyl molecule, thus providing additional experimental evidence for the n orbital and π^* orbital splitting in these molecules.

Investigation of n orbital splittings has been intensely pursued in the azabenzenes and azanaphthalenes using PES by Heilbronner and his coworkers (21-23) and in the dicarbonyl compounds also using PES by Cowan et al. (19), Dougherty and McGlynn (24) and Dougherty et al. (25).

Unlike their dicarbonyl analogues dithiocarbonyls have received very little attention spectroscopically over the years. The same comparison is true for the monochromophoric compounds, but to a lesser extent.

Thiophosgene has been studied by Brand et al. (26), Oka et al. (27) and Okabe (28); thiobenzophenone by Gupta et al. (29) and a number of monothiones by Blackwell et al. (30). An important result of the work of Blackwell et al. (30) is the appearance of singlet-triplet transitions in five out of the six compounds studied, which are not observed as readily in the corresponding carbonyl compounds. The aromatic thione, xanthione (XS), has been studied more extensively (31-36).

Bruhman and Huber (33) studied the quenching of the XS triplet state in solution and determined the deactivation to be physical in nature and diffusion controlled. Similarly, in a study involving quenching of the XS triplet state by other thioketones and dithioketones (including TMCBDT) Rajee and Ramamurthy (34) concluded that the quenching process must take place by an "out of phase" contact, whereby the thio-carbonyl moieties approach and contact each other in an anti-parallel fashion, and that the sulfur non-bonding orbital of the ground state molecule must be responsible for the quenching of the triplet $n \pi^*$ state. The interesting point in this work is that no photoproducts could be found even after more than 10 days of irradiation. Furthermore all the quenchers chosen had the lowest T state lying above that of XS precluding T-T energy transfer. This suggests that the sulfur atom of the quencher may have acted as an external-heavy atom inducing more efficient intersystem crossing to the ground state, possibly via a S-S exciplex.

More recently, Maki et al. (35) have reported a large zero-field splitting (D) in the XS lowest triplet state (in an n-hexane matrix at 1.1°K) and attributed it to spin-orbit perturbation of T_1 . Burland (36) determined the splitting to be -11 cm^{-1} and -20 cm^{-1} for the two sites of XS doped into xanthone host crystals.

While most of these authors emphasize the role of spin-orbit effects in the spectra and zero-field splitting (35,36) of the triplet state, only Maki et al. (35) have advanced a reasonable, though limited, account of the spin-orbit activity in xanthione. A recent review of the interesting thiocarbonyl photochemical properties has recently been given by de Mayo (37).

Very little work has been done on the dithiocarbonyl compounds. Of particular interest here is the crystal structure determination of TMCBDT by Shirrell and Williams (38) in 1973; they found that the transannular distance in TMCBDT is equal (within experimental error, less than 0.01 \AA) to that of TMCBD, which unambiguously refuted the arguments of Ballard and Park, discussed previously.

Soon after this, work began in this laboratory (39) on the single crystal polarized absorption spectrum of TMCBDT at 12°K with the aim of searching for multiple $n\pi^*$ transitions as found for TMCBD (7). However, due to difficulties with the handling of the crystals and the varying crystal habit progress was slow. Concurrently, in an investigation of the bisimines of TMCBD, Worman et al. (40) reassigned the TMCBDT solution spectrum in the light of Shirrell and Williams' work, as being due to two $n\pi^*$ transitions split because of the n orbital interaction, which was as yet unconfirmed by direct PES measurements. These were carried out in 1977 by Behan et al. (41) and it was

found that the n orbital splitting in TMCBDT is 0.42 eV, the orbital order (n_+ above n_- or vice versa) was not given, however. This PES result was later confirmed by Basu et al. (42) who also reported the n orbital splitting as 0.42 eV; in addition, these workers suggested the appearance of four $n\pi^*$ transitions in TMCBDT based on a room temperature (presumably) unpolarized single crystal spectrum, the PES results and analogy to TMCBD (7,8). This is unfortunately no more informative than Ballard and Park's solution spectrum; the lack of polarization and vibrational resolution renders these experimental findings speculative.

In 1979 a definitive experiment was reported (43) which unambiguously showed that the lowest energy band in the TMCBDT single crystal spectrum was a singlet-triplet transition: the low temperature high field Zeeman absorption spectrum recorded by Trabjerg and Vala (44). Also reported at that time was a detailed account of the spin-orbit activity and the nature of the perturbing states in the free molecule as well as the emission spectrum of TMCBDT single crystals in the temperature range 1.6 K-16 K. The result of the latter experiments is that the emission is found to occur solely from traps and not from the exciton band (43).

Gordon et al. (45) recently reported the polarized single crystal spectrum of TMCBDT at 4 K. Their results are in agreement with Trabjerg et al. (43) on the 3A_u assignment of the lowest energy transition, however their published spectrum shows that the 0-0 band of the triplet is more than twice as intense as the singlet (1A_u or $^1B_{1g}$) vibronic origin of the same $n\pi^*$ transition. Their assignment to

3A_u of the lowest energy band (16829 cm^{-1} for TMCBDT- h_{12}) is based solely on the basis of the appearance of a single origin in a single polarization which is consistent with the spin-orbit activity in TMCBD (6,20). No attempt is made to explain the discrepancy of intensities in the 3A_u vs. 1A_u transitions. Trabjerg et al. (43) on the other hand reported that the singlet transition is much more intense than the triplet.

Gordon et al. (45) also report two $^1n\pi^*$ transitions with nearly degenerate vibronic origins near 18000 cm^{-1} (1A_u , $^1B_{lg}$) and "probably" the other set at about 19500 cm^{-1} . Their spectra as reported (45) show remarkably little vibrational structure for a 4°K single crystal sample examined with polarized light. In the region 18000 cm^{-1} to 23000 cm^{-1} , (both $\perp c$ and $\parallel c$ polarizations) for example, only 22 bands and 17 shoulders can be discerned. Work on this same system has shown that in fact over 100 bands can easily be resolved.

A strict interpretation of the analogies to TMCBD used by Gordon et al. (45) in their TMCBDT assignments should include the circumannular type of through-bond interaction (7,8) to describe the π^* splitting. The assignments of the $^1n\pi^*$ transitions proposed by Gordon et al. (45) however preclude any π^* orbital splitting.

Work on the interesting molecule tetramethyl-3-thio-1,3-cyclobutanedione (TMTCBD) has also been reported (42,46), and although most bands are disappointingly broad (FWHM as large as 1000 cm^{-1} and as small as 150 cm^{-1}) (46) the assignments (46) demonstrate that the thiocarbonyl and carbonyl chromophores act fairly independently. Assignments to 3A_2 and 1A_2 ($n\pi^*$ of C=S) states and a 3A_2 ($n\pi^*$ of C=O)

state were made for bands appearing at ca. 17050 cm^{-1} , 18350 cm^{-1} and 27430 cm^{-1} .

While Hoffman's explanation of the n orbital splittings (Δn) using MO theory has been successful in most cases (21-23) Wadt and coworkers (47,48) have demonstrated that, in the case of pyrazine, an equally accurate description of Δn can be given using a Valence-Bond (VB) approach. They showed that the observed (21) order of the n and π orbitals can be predicted from a configuration interaction approach using a double zeta basis. Furthermore, the $n\pi^*$ excitation energies are also well reproduced. The outstanding feature of the method is that the n orbitals are split while remaining 90% localized on the nitrogen atoms. Thus an electron excited out of an n orbital can be treated as coming from one nitrogen only, leaving a "localized hole". This is referred to as the localized excitation picture.

In contrast Hoffman's interaction scheme mixes σ orbital character into the n orbitals and vice versa resulting in nonbonding orbitals which are delocalized, sometimes extensively, in the σ molecular framework (8). An excitation out of the nonbonding orbital now has to be regarded as delocalized; i.e., the hole is now distributed over a large portion of the molecule.

The effect of localization is to lower the ionization and excitation energies. This effect has been investigated by various authors and confirmed (47-53); the amount of energy lowering depends on the symmetry constraints on the wave functions and can vary from one to two or more electron volts. It may happen, however, that the energy lowering can be overcompensated and the calculated result then lies below

the experimental one. Thus the results should be used with caution when comparing absolute energies. Inclusion of a modest amount of configuration interaction, however, seems reliable (48). The PES spectrum of pyrazine has been calculated by Von Niessen et al. (54) using a many-body Green's function approach and the orbital ordering and energies compare very well both with experiment (21) and VB calculations (48).

Motivation and Direction

As discussed above, the conclusion of Ballard and Park (12) regarding the absence of a $n\pi^*$ splitting in the lowest absorption band in the TMCBDT solution spectrum is subject to question in light of the finding by Shirrell and Williams (38) that the transannular distance in TMCBD and TMCBDT is the same. Furthermore the number of bands in the solution spectrum (12) is greater than that expected for the $n\pi^*$ transition region, even if all four transitions in fact occur as in TMCBD (7). Thus in view of the greater spin-orbit activity due to the sulfur atoms it seemed likely that one or more of the weakest bands in the solution spectrum of TMCBDT could be due to direct singlet-triplet absorption.

In view of the excellent results obtained in this laboratory (7) and by others (20) using the low temperature single crystal polarized absorption technique, it was decided that its application to TMCBDT was necessary to elucidate the $n\pi^*$ region in this interesting molecule. In addition, the availability of a high field pulsed Zeeman apparatus (55) made the investigation of the Zeeman absorption and emission spectra of TMCBDT possible and desirable.

The spin-orbit activity of carbonyl compounds as applied to absorption and emission involving singlet-triplet transitions is well understood; however, as pointed out above very little has been done in this regard for thiocarbonyls. Thus a fairly detailed semi-quantitative study has been carried out for TMCBDT using conventional methods (56). Due to the expected proximity of the ${}^3B_{2g} \text{ } n\pi^*$ states to the lowest 3A_u state in TMCBDT and the generally lower energies in these states compared to corresponding carbonyl compounds (31), special attention is directed toward the perturbation of the ground electronic state by these triplet states and the ensuing intensity borrowing from electronically allowed triplet-triplet transitions (56).

As a result of the crystal structure of TMCBDT, electronic transitions polarized along the C=S bonds and out of the molecular plane cannot be distinguished by polarization measurements as in the case of TMCBD. Polarized Zeeman absorption measurements are therefore indicated to ascertain the extent of these two intensity contributions (57). The third direction, in-plane but \perp to the C=S bond axis, can be distinguished from the other two directions by the zero-field polarization measurements.

The excellent work by Maki et al. (35) and Burland (36) demonstrating the existence of a large zero-field splitting (zfs) in the aromatic monoketone xanthione, has stimulated interest in the effects of the zfs on the TMCBDT Zeeman spectrum. Since this effect in xanthione has been attributed to spin-orbit coupling, examination of spin-orbit contributions to the zfs in TMCBDT is carried out. Now two interesting questions arise.

(1) What are the effects of the two sulfurs on the zfs of TMCBDT? (2) How does the localization or delocalization of the observed $^3n\pi^*$ transition and/or the perturbing triplet states affect the magnitude of the zfs? Theoretical work on the localized excitation effects (47-53) has thus far been restricted to the determination of excitation energies, ionization potentials, and orbital splittings. Although application of the Generalized Valence Bond technique (58) to the calculation of force constants has produced good results (59), determinations of other properties has not been done to our knowledge.

With these considerations in mind a qualitative investigation of these effects is carried out for TMCBDT in connection with the Zeeman study. The discussion makes use of some recent *ab initio* calculations on TMCBD and CBD which have been carried out in this laboratory; the results of this work have been reported elsewhere (60). Because these calculations are performed on the carbonyl analogues of TMCBDT and due to the lack of configuration interaction at present, only those results necessary for the qualitative discussion of the localization effects as they apply to the TMCBDT zfs discussion are included in this work. For comparison the results of the EHT calculation of the TMCBDT $n\pi^*$ energies are also included.

The results of the *ab initio* calculations are given in Chapter 2. The $^3A_u \leftarrow ^1A_g$ absorption spectrum of single crystal TMCBDT is given in Chapter 3. Effects of lattice vibrations and the possible excited state distortion are discussed in terms of double minimum potentials in the ground and excited electronic states. The temperature dependence

of the absorption and emission (discussed elsewhere, (43)) are predicted using this model.

In Chapter 4 the spin-orbit coupling calculations are presented and the relative contributions to the crystal transition moment are discussed.

Because of apparent inconsistencies in the early polarized Zeeman absorption measurements, the effect of field alignment on the observed Zeeman splitting pattern is investigated theoretically using equations derived for a general field orientation with respect to the unit cell axes. This is included in Chapter 5 along with the interpretation of the Zeeman spectroscopy of the $(n\pi^*)^3A_u \leftarrow ^1A_g$ transition in TMCBDT. Discussion of the spin-orbit effects on the zfs parameters is also given in Chapter 5; the results of the calculations presented in Chapter 2 are used to discuss qualitatively the effects of spin-orbit coupling on the zfs parameters.

Finally, in Chapter 6 the work is summarized and suggestions for future research are given.

CHAPTER 2
RESULTS OF *ab initio* SCF CALCULATIONS ON CARBONYL ANALOGUES

In a previously reported study on the spectroscopy of the multiple $n \pi^*$ singlet-singlet transitions (7) Baiardo et al. (8) compared the ability of the EHT and CNDO (/2 and /S) methods to predict the observed $^1_n \pi^*$ transitions in TMCBD (4). For this molecule the highest occupied MO's have been assigned as n_+ (b_{1u})¹ lying above n_- (b_{3g}) in the PES work of Cowan et al. (19) and Dougherty et al. (25), in agreement with the semiempirical MO calculations. Since the observed order of the $^1_n \pi^*$ excited states was found to be (4) $A_u < B_{2g} < B_{2g} < A_u$ the π^*_+ (b_{3u}) π^*_- (b_{2g}) orbitals must be ordered with the + lying above the -, in agreement with EHT but not with either CNDO parameterization. The resulting excitation energies as calculated in the three methods showed that EHT gave the best correlation with the observed spacings between the $^1_n \pi^*$ states, while CNDO/S-SECI gave the best correlation with the lowest A_u state, differing from the experimental result by only 0.02 ev. For this reason and because of its simplicity the EHT method was chosen for the spin-orbit-coupling calculations in this study (Chapter 4).

1. The choice of axis system here does not follow the conventional one as given by R. S. Mulliken, J. Chem. Phys. 23, 1997 (1955). Instead, z was arbitrarily chosen parallel to the crystal c axis in the later chapters and x out of plane. This differs also from that used in ref. 8.

Making use of Hoffman's ideas (14-16) the observed ordering of excited $n\pi^*$ states was explained by a through-bond mechanism applied to the n and π^* orbitals. Here it was necessary to invoke the so-called "circumannular" interaction of the π^* orbitals (+ and - linear combinations) through the relay¹ orbitals localized in the C (ring)-C(methyl) bonds; it was argued that this effect must dominate the through-space, or "transannular", interaction for the observed state order to be consistent with the PES assignment of the n orbital order (19,25). These mechanisms are diagrammed in Fig. 2-1.

As a result of the through-bond interaction the n orbitals are delocalized in the ring. The extent of this delocalization is demonstrated by means of orbital contour and orbital density plots in Fig. 2-2a for the $n_+(b_{1u})$ and Fig. 2-2b for the $n_-(b_{3g})$ molecular orbitals. These plots were made with molecular orbitals from an *ab initio* SCF calculation for CBD(61).

Further work was initiated to obtain excited state energies for the $^1n\pi^*$ and $^3n\pi^*$ states of TMCBD and CBD. The spacings between the $n\pi^*$ states could then be compared with experiment (7). The results of these calculations relevant to later discussions (Chapter 5) are presented in this chapter. It would also be interesting to apply the method of Wadt and coworkers (47) to CBD to see if the n orbital splitting and $n\pi^*$ state splittings could be reproduced.

Additional motivation for this came from the work of Hehenberger (51) on the (localized) calculation of furan ionization potentials and Jonkman's (53) study of the lowest $n\pi^*$ excited states of

1. The term "relay orbitals" in through-bond interaction was coined by Heilbronner and Schmeltzer (Helv. Chim. Acta 58, 936 (1975)) to describe the common orbital which causes the n orbitals to split.

Figure 2-1. Through-space and through-bond interactions in TMCBD. The energy levels shown are not to scale.

- (a) No interaction of any type, n and π orbitals degenerate.
- (b) Through-space interaction affects only the π orbitals (only π^* shown) and not the n orbitals. Antisymmetric combination, π^*_- , is above the symmetric one. n_+ and n_- combinations still degenerate.
- (c) Through-bond interaction in the n orbitals occurs through the ring σ (C-C) bonds. The n_+ interaction with $\sigma(b_{1u})$ is greater than the interaction of n_- with $\sigma(b_{3g})$; n_+ lies above n_- .
- (d) Through-bond interaction in the π^* orbitals occurs through the methyl bonds, σ_{CC} , to a greater extent than the interaction in (b) and as a result π^*_+ lies above π^*_- .

Figure 2-2. Density and contour maps for the n_+ and n_- orbitals in CBD. These are obtained using the HIDEPLOT program (61) for *ab initio* SCSCF (see text) wavefunctions. For all plots the wavefunction is evaluated in the molecular plane containing the C=O groups. In the "contour" plots each curve represents a value of constant orbital density. The "density" plots give the value of the square of the wavefunction (ϕ^2) on the vertical axis as a function of position in the molecular plane thus there are peaks in only one direction. The "orbital" plots give the value of the wavefunction (ϕ) on the vertical axis as a function of position in the molecular plane, thus there are positive (up) and negative (down) regions.

(a) i. Contour plot of the n_+ MO.

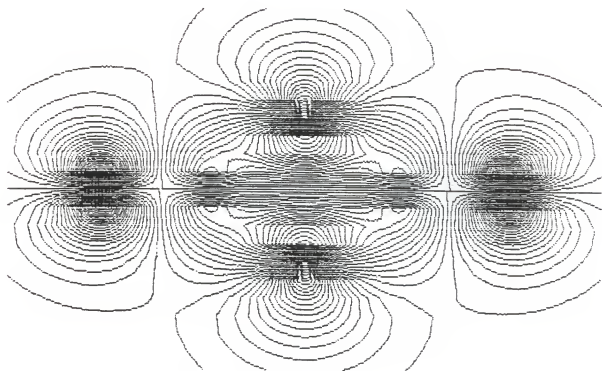
(a) ii. Orbital plot of the n_+ MO.

(a) iii. Density plot of the n_+ MO viewed from above and below the molecular plane.

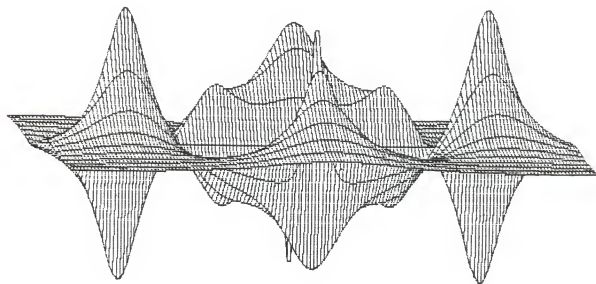
(b) i. Contour plot of the n_- MO.

(b) ii. Orbital plot of the n_- MO.

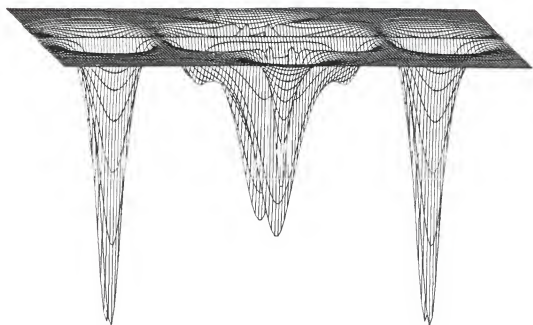
(b) iii. Density plot of the n_- MO.



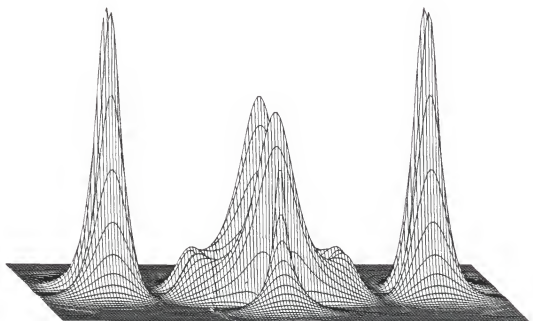
(a) i.

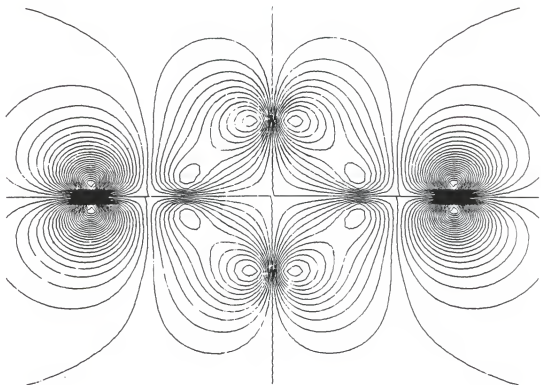


(a) ii.

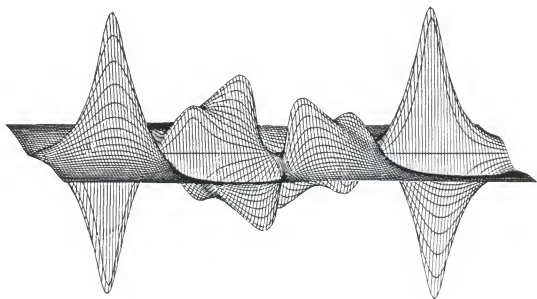


(a) iii.



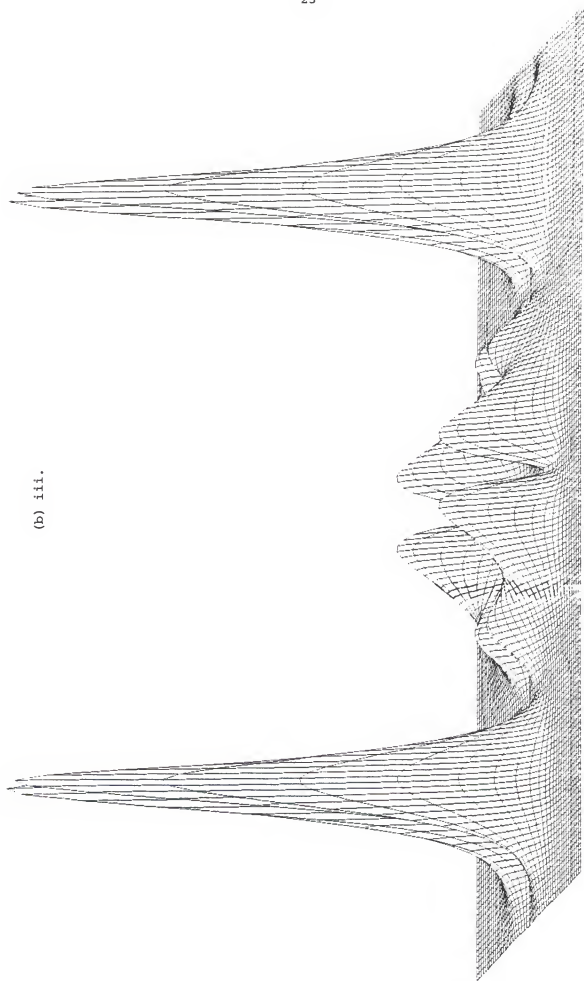


(b) i.



(b) ii.

(b) iii.



benzoquinone, we decided to repeat the calculation on CBD using a reduced symmetry constraint on the wavefunction so that the oxygen atoms were no longer treated as symmetry equivalent centers. A thorough discussion of the symmetry breaking and its effects within the Restricted Hartree Fock formalism has been given by Jonkman (53) and more recently by Canuto et al. (62).

Computational Details¹

The *ab initio* calculations were performed with the MOLECULE-ALCHEMY program package which employs the MOLECULE integral program written by Dr. J. Almlöf (63) of the University of Uppsala, Sweden. The ALCHEMY SCF program was written by Bagus et al. (64) and was interfaced to MOLECULE by Dr. U. Wahlgren and P. S. Bagus at the IBM San Jose Research Laboratory.

The double-zeta basis set of Dunning-contracted Gaussian functions (65) was used in all the calculations. For the carbon and oxygen atoms a 9s5p primitive basis contracted to 4s2p while for the hydrogen atoms a 4s/2s contraction using Dunning's (65) coefficients was employed. The hydrogen exponents were all scaled to fit a Slater orbital exponent of 1.20 by multiplying all the hydrogen primitive Gaussian exponents by $(1.2)^2$ (ref.65). This basis set was used by Dykstra and Schaefer (66) in their study of the ground and lowest excited states of glyoxal. A calculation of the ground state and lowest excited singlet and triplet states ($^1,^3A_u$) was first carried out to become familiar with the

1. The many helpful discussions with Drs. Michael Hehenberger, Joseph Worth, Gregory Born, Jack Smith and Henry Kurtz during the (now and then) course of these *ab initio* calculations is deeply appreciated. Many thanks are due also to Drs. George Purvis and Richard Lozes for making their versions of the programs available.

various options of the MOLECULE-ALCHEMY package and it was found that the total energies in our calculations were higher than those of ref. 66 by 0.003 au. The orbital order was the same, however. Communication with C. Dykstra revealed that scaled hydrogen exponents were used in their calculation. All subsequent calculations were performed using the scaled exponents for hydrogen.

The vector coupling coefficients necessary for the calculation of the excited states were obtained from M. Hehenberger (67).

All integral calculations were performed neglecting those smaller than 10^{-10} and approximating (63) those less than 10^{-8} . In the case of the low (C_s) symmetry these tolerances were set to 10^{-8} and 10^{-6} , respectively. The convergence tolerance in the SCF procedure was usually 10^{-5} with respect to eigenvectors.

The atomic coordinates used in these calculations are given in Table 2-1, calculated from the X-ray work of Riche and Janot (68) for TMCBD, but taking the ring to be square. For CBD the same coordinates as ref. 8 are used with a C-H bond length of 1.09 \AA . The coordinates for TMCBDT are taken from Shirrell and Williams (38) and are listed in full in Table 4-1.

Results and Discussion

Ionization Potentials

The MO order predicted by the *ab initio* calculation for the n orbitals is reversed from that observed by PES for both CBD and TMCBD. Basu et al. (42) obtained the same result for CBD using Gaussian 70 (QCPE N-236); however, the lowest unoccupied orbital (LUMO) (π_+^*) from their calculation lies approximately 15 eV above the highest occupied

orbital (HOMO) (n_-). In our calculation the (π_+^*) LUMO is about 12 ev above the n_- orbital. Comparison with the results on the azabenzenes obtained by Von Niessen et al. (54) shows that in these molecules the occupied-virtual separation is about 13 ev. It is pointed out that in such cases, where the HOMO-LUMO separation is small, the many-body corrections to the ionization energies can be expected to be large; hence, Koopmans' theorem breaks down and the orbital ordering from an SCF calculation may not correspond to that observed in the PES (54). Thus it appears that CBD and TMCBD fall into this category, and investigation using many-body methods would be of great value.

Using a double-zeta quality basis and a limited configuration space Wadt et al. (48) demonstrated that the correct order of the highest occupied orbitals of pyrazine is obtained when configuration interaction is included in the calculation of the ionization potentials. Thus it seems that the relaxation of the symmetry constraint on the wavefunction somehow introduces correlation corrections (64).

The energies of the highest four occupied orbitals in CBD and TMCBD are given in Table 2-2. It can be seen that attempting to account for electron reorganization in the cationic state (TMCBD) by calculating the total energy for both ground state and ionized state ($^2n_+$) and taking the difference (Δ SCF) does not correct the order on the splitting of the n orbitals. What is lacking is the correlation correction. It should be noted that EHT gives the correct order of n orbital energies and a reasonably good splitting, although the absolute value is not good. The lone pair ionization potential

in the reduced symmetry calculation is included in Table 2-2 for comparison with the Koopmans value. If we take the difference between the Δ SCF and Koopmans values for TMCBDT and use it to estimate a Δ SCF for CBD, we see that the reduced symmetry value is still lower by about 1 ev.

Excited $n\pi^*$ States

Using the ground state geometry for CBD and TMCBD a separate single-configuration-SCF calculation was carried out on each of the four singlet and triplet $n\pi^*$ states of both molecules. The results of the Δ SCF vertical transition energies are given in Table 2-3. Although the n orbital ordering is reversed with respect to the experimental (PES), the calculated transition energies give the correct ordering of states in terms of symmetry species; the $n_{+}\pi_{-}^*$ configuration is expected to be lowest, however. The absolute energies are not expected to agree with experiment at this level of approximation (62,66).

Comparison of the energy spacings of the lowest singlet $n\pi^*$ states with the experimental values and the EHT/CNDO(S) results (8) are given in Table 2-4. These results indicate that EHT gives $n\pi^*$ state splittings which are closer to experiment than any of the other methods at the present level of approximation.

Comparison of the singlet-triplet splitting with experiment is possible for the lowest A_u state. Spafford et al. (6) assigned the 3A_u origin in TMCBD (single crystal) as 25718 cm^{-1} and the corresponding 1A_u has been found to be (7) 27122 cm^{-1} ; this gives a ΔE_{ST} of $\sim 1400\text{ cm}^{-1}$ compared with that calculated by the vertical Δ SCF of $\sim 1700\text{ cm}^{-1}$ and $\sim 1790\text{ cm}^{-1}$ for the two A_u states. The agreement here

is rather good. Recalculating the CBD singlet and triplet $n\pi^*$ excited state vertical transition energies with reduced symmetry (C_s , as described in the previous section) gives the following results:

$$\Delta SCF (^1n\pi^*) = 3.434 \text{ eV}$$

$$(^3n\pi^*) = 3.095 \text{ eV}$$

$$\Delta E_{ST} = 0.338 \text{ eV (2730 cm}^{-1}\text{)}$$

The energy lowering for the singlet excited state amounts to 2.65 eV while 2.78 eV is found for the triplet state. By comparison the energy decrease for pyrazine due to localization is (62) 1.2 eV for the singlet $n\pi^*$ state and 1 eV for the triplet, while for benzoquinone (53) the values are 2.51 eV and 2.36 eV for the singlet and triplet states, respectively.

The ΔE_{ST} for CBD is seen to increase (cf. Table 2-3) as a result of symmetry breaking whereas for both pyrazine and benzoquinone ΔE_{ST} decreases.¹ This is due to a localization of both the n and π^* (on adjacent atoms) in CBD because the carbonyl groups are not conjugated, whereas the π^* orbital remains essentially delocalized in the other two cases and can avoid the localized n orbital more efficiently.

It is often desirable to determine the amplitude of a particular orbital on a given center, as on the oxygen atoms in CBD or the sulfur atoms in CBDT. The one center spin-orbit-coupling matrix elements, for example, are proportional to the product of two orbital amplitudes on the atom (cf. the term immediately preceding Eq. 4-25). Wadt and

1. For pyrazine ΔE_{ST} in D_{2h} is 0.73 eV and in C_{2v} it is 0.56 (62). For benzoquinone ΔE_{ST} is 0.33 eV in D_{2h} and 0.23 eV in C_{2v} (53).

Goddard (47,48) have demonstrated that in the $1,3B_{3u}$ and $1,3B_{2g}$ $n\pi^*$ states in pyrazine, the n orbital is localized on one of the nitrogens and the π^* orbital adjusts itself so as to make the exchange integral

$$K = \langle n(1)\pi^*(2) | r_{12}^{-1} | \pi^*(1)n(2) \rangle$$

a minimum for the singlet state and a maximum for the triplet state.

This comes about because the energy of the two states is given by (48)

$${}^1E = E_o + K_s$$

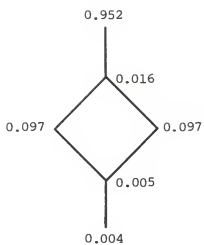
$$\text{and } {}^3E = E_o - K_t$$

Because K is positive the triplet state energy will be minimized if K is maximum and the singlet energy will be minimized when K is minimum. Thus if the orbital part of the wavefunction is allowed to be different for the singlet and triplet states of a given spatial symmetry the singlet will have less π^* electron density near the nitrogen atom which has the n orbital localized on it whereas the triplet will have more.

To demonstrate this effect in CBD we again consider the C_s symmetry calculation and look at the net populations in the n and π^* orbitals of the self consistent excited state. The diagrams in Fig. 2-3 give these quantities in the appropriate points on the molecular framework. The net population is chosen because it most closely resembles the orbital amplitude on the atom. It is readily seen that for both the triplet and singlet states the n orbital population on the excited oxygen is the same, whereas for the π^* orbital the triplet state clearly has a greater π^* density on the excited oxygen than does the singlet.

Figure 2-3. Net orbital populations for CBD in C_s

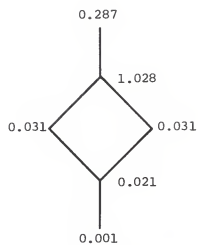
- (a) Net orbital populations for n and π^* orbitals of singlet state.
- (b) Net orbital populations for n and π^* orbitals of triplet state.



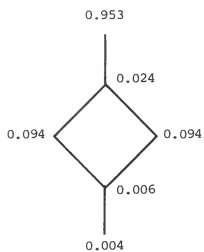
n

S

(a)



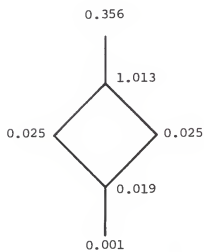
π^*



n

T

(b)



π^*

This also demonstrates quite clearly that the excitation is exclusively localized on one of the carbonyl chromophores. This is to be contrasted with the greater mobility of the π^* orbital in pyrazine and benzoquinone which is due to the inherent delocalized nature of the planar benzenoid structures. We conclude that the charge-transfer-like nature of the localized carbonyl excitation is responsible for the greater magnitude of the ΔE_{ST} change in going from the delocalized (D_{2h}) picture to the localized (C_s) picture in CBD.

As was mentioned earlier, the *ab initio* results which have been included here will be used in a later discussion of the spin-orbit contributions to the zero-field splitting parameters in TMCBDT taken up in Chapter 5.

Having briefly mentioned the success of the EHT method in predicting the $n\pi^*$ interstate energy separations for TMCBD, it is appropriate to include the analogous calculation for TMCBDT at this time. The bands in the TMCBDT solution spectrum and the calculated values of the transitions are given below:

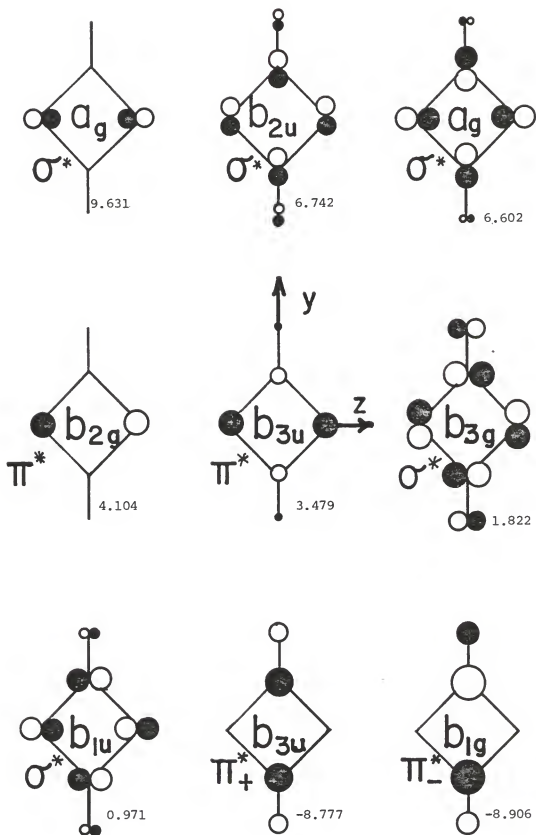
<u>State</u>	<u>EHT</u>	<u>Ref.12</u>
2^1A_u	+ 6050	+ 5600
2^1B_{2g}	+ 5000	+ 2800
1^1B_{2g}	+ 1050	+ 1600
1^1A_u	18710 cm^{-1}	18400 cm^{-1}

It will be informative to have orbital diagrams for the later discussions on electronic distributions, thus the orbital energies and MO diagrams (EHT) are given in Fig. 2-4.

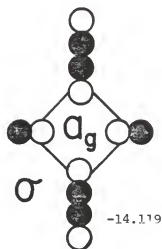
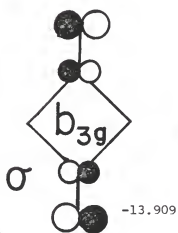
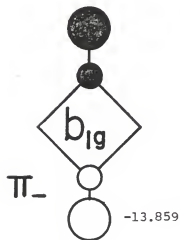
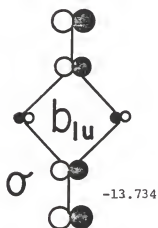
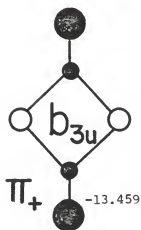
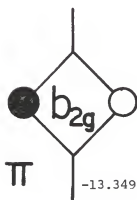
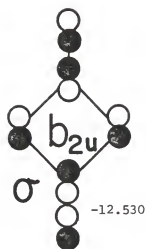
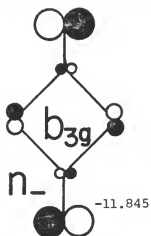
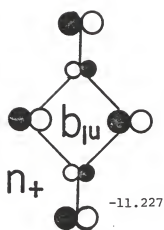
Figure 2-4. Molecular orbitals and their one electron energies for TMCBDT as calculated by Extended Hückel method. The coordinate system is given on the center Figure in (a). All orbital energies are given in ev.

(a) The lowest 9 virtual orbitals of TMCBDT.

(b) The highest 9 occupied orbitals of TMCBDT.



(a)



(b)

TABLE 2-1
ATOMIC COORDINATES FOR TMCBD AND CBD^a

<u>TMCBD</u>			
<u>Atom</u>	<u>x</u>	<u>y</u>	<u>z</u>
C1	0.0	0.0	2.084575
C2	0.0	2.084575	0.0
CM	2.320533	3.679436	0.0
O	0.0	0.0	4.352295
H1	3.823699	2.794608	0.0
H2	2.480797	4.748543	-1.368850

<u>CBD</u>			
C1	0.0	0.0	2.084410
C2	0.0	2.084410	0.0
O	0.0	0.0	4.352120
H	1.763150	3.186140	0.0

a. TMCBD coordinates calculated from bond lengths and angles of ref. 67. For CBD bond lengths and angles are from ref. 8. All are given in atomic units.

TABLE 2-2
 ORBITAL ENERGIES (ev) FOR CBD, TMCBD (*ab initio*, D_{2h})^a

	<u>Koopmans</u>		<u>ΔSCF</u>	<u>PES</u>	<u>EHT</u>
	CBD	TMCBD	TMCBD	TMCBD	TMCBD
$n_- (b_{3g})$	-11.31	-10.37	-9.44	-9.53	-12.00
$n_+ (b_{1u})$	-11.65	-10.73	-9.79	-8.80	-11.36
$\pi_+ (b_{3u})$	-14.02	-13.46	-	-	-
$\pi_- (b_{2g})$	-15.20	-14.57	-	-	-
Δn	0.34	0.37	0.35	0.73	0.64
$\Delta \pi$	1.17	1.11	-	-	-
2_n	-9.29 ^b				

a. Wavefunction utilizing full D_{2h} point group symmetry.

b. Wavefunction utilizing only C_s^{2h} symmetry, with σ_h as the molecular plane. Value given is Δ SCF.

TABLE 2-3
VERTICAL TRANSITION ENERGIES (ΔE in eV) FOR THE $1, 3, n \pi^*$ STATES
CALCULATED USING D_{2h} WAVEFUNCTIONS

State	CBD			TMCBD		
	Singlet	Triplet	ΔE_{ST}^a	Singlet	Triplet	ΔE_{ST}^a
$A_u (n \pi^*)$	5.900	5.679	1784	6.085	5.873	1708
$B_{2g} (n \pi^*)$	6.501	6.095	3272	6.769	6.345	3419
$B_{2g} (n \pi^*)$	6.741	6.437	2451	6.829	6.525	2453
$A_u (n \pi^*)$	7.250	7.034	1745	7.469	7.247	1792

Ground State Total Energies;

CBD = -303.3838872 au.

TMCBD = -459.1751617 au.

a. The singlet-triplet energy splittings are given in cm^{-1} .

TABLE 2-4
COMPARISON OF VERTICAL TRANSITION ENERGIES (Δ SCF) OF $1_n \pi^*$ STATES
FOR TMCBD WITH OBSERVED AND SEMIEMPIRICAL METHODS^{a,b}

<u>State</u>	<u>Expt.</u>	<u>EHT</u>	<u>CNDO/S</u>	<u>ΔSCF</u>
2 A _u	0.99	0.89	0.64	1.38
2 B _{2g}	0.61	0.64	0.41	0.74
1 B _{2g}	0.37	0.26	0.22	0.68
1 A _u	0	0	0	0
	(3.363) ^c	(2.328)	(4.962)	(6.085)

a. All energies are in ev.

b. Experimental values and semiempirical results are from ref. 8.

c. All values in parantheses refer to the absolute value of the lowest state.

CHAPTER 3
THE $T_1 \leftarrow S_0$ ELECTRONIC TRANSITION IN CRYSTALLINE
¹TETRAMETHYL-1,3-CYCLOBUTANEDITHIONE

Introduction

The spectroscopic technique to be used in this study is that of low temperature, single-crystal, polarized absorption spectroscopy. Each aspect of this technique possesses distinct characteristics, the combination of which allows one to extract a much greater amount of useful spectroscopic information than the more conventional room temperature solution spectroscopy.

Spectroscopic Technique

An isolated molecule possesses many sharp rotational and vibrational energy levels within a given electronic state. In condensed phases, however, rotational energy levels cannot be resolved due to the lack of free rotation. In solution the vibrational structure is severely broadened due to the random interaction of molecules with the solvent; this causes merging of the vibrational features into an unresolvable spectrum. The extent of this effect also depends on the solvent. In the crystalline state, on the other hand, the molecules are fixed in space as part of the crystal lattice and therefore are subject to uniform interactions with their surroundings. The result is that crystalline absorption spectra allow resolution of a much greater amount of vibrational structure.

In the context of this technique, "low temperature" refers to temperatures below 77 K (the boiling point of liquid nitrogen). In this study, the temperatures used lie in the range from 1.6 K to about 50 K. In this temperature range molecular vibration is usually restricted to its lowest eigenstate, thus eliminating the vibrational hot bands which are the result of transitions originating in higher vibrational eigenstates. For polyatomic molecules containing low frequency vibrations, as is the case of TMCBDT, the quenching of hot bands is not achieved until liquid helium temperature, 4.2 K or lower. With reference to the crystalline state, lowering the temperature causes the molecules to be more rigidly fixed in the crystal lattice thereby reducing the crystal lattice vibrations to their lowest eigenstates. This reinforces the crystal-induced resolution of the vibrational structure.

In addition to vibrational resolution, crystal spectra can lead to a great deal of information about the direction of the electronic transition moments. By proper orientation of the crystal it is possible to achieve a fixed and known orientation of the molecules with respect to the electric field vector of the incident plane polarized light and thereby obtain information about the polarization direction of a given absorption band. The results of polarized single crystal spectra cannot usually be interpreted in terms of transitions in the free molecule, however, but must be considered in the framework of the crystal symmetry.

Crystal Symmetry

The molecular crystal can be identified with a particular crystal class. Within the crystal class further classification is achieved by

determining the space group to which the crystal lattice belongs. The overall symmetry is described by both point and translational symmetry; the lattice is invariant under operations of both kinds, the complete set of these constitutes the elements of the space group. It is possible to imagine another group, in which the translational subgroup of the space group behaves like an identity element and the remaining elements of this group consist of the cosets $R_i T$, where R_i is a point operation and T is the translational subgroup. This new group is called the factor group of the space group and is isomorphic with one of the 32 crystallographic point groups (69); this property will provide a means of correlating states in the free molecule with those of the crystal.

This correlation is dependent on the particular site occupied by the molecule within the translationally invariant unit cell. Each site is characterized by a particular local symmetry which can be described by its own rotation axes and reflection planes, but which necessarily has relationships to those of the full factor group and thus to the symmetry axes and planes of the unit cell. The number of possible sites of a given point group, called site groups, which are admitted by a particular factor group is limited only to those which are a subgroup of the particular factor group. However the distribution of sites differs with the space group for each of the factor groups. The site group can never contain symmetry elements not belonging to the free molecule and is generally of lower symmetry.

With this background, it is appropriate to further amplify that aspect of the technique just described which pertains to the interpretation of crystal spectra.

Crystal States

Since the molecules in a unit cell occupy sites, it is clear that the site state corresponding to a given molecular electronic or vibrational state is found by correlation in the two symmetry point groups. These site states are not symmetry-adapted in the factor group, however. This adaptation is carried out in a manner completely analogous to the symmetry adaptation of atomic orbitals to form (symmetry adapted) molecular orbitals in a polyatomic molecule. Whereas one operates on the localized atomic orbitals with the symmetry operations of the molecular point group in that case, the symmetry operations of the crystal factor group are used to operate on the site states (or functions) (70) in the crystal to obtain a reducible representation from which the crystal states can be projected out as linear combinations of site states. Thus for the case of n molecules per unit cell n factor group states are obtained, each characterized by an irreducible representation of the factor group.

In general, if interaction between the molecules is allowed, the n factor group states are not expected to lie at equal energies. Therefore a single molecular state can split into n factor group states in a crystal with n molecules per unit cell. This type of splitting is called "factor group splitting" or "Davydov splitting". The appearance of this effect in molecular crystal spectra can lead to a greater amount of information concerning intermolecular interactions, at the expense of a more complex spectrum, however.

Thus far no specification has been made of the particular molecular or site state and in this respect the application is to a molecular state having the equilibrium geometry of the ground electronic state. In molecular excited electronic states, however, there is often a change in the equilibrium geometry from that in the ground electronic state. For the free molecule this case is discussed in terms of the subgroup common to both the excited state and ground state point groups. When considering a distorted molecular state in a crystal environment, the distortion may be taken as a local perturbation in which the effective site symmetry is then defined by the symmetry elements common to both the distorted molecular point group and the invariant factor group. We will make use of this excited state site symmetry correlation later.

Effect of External Fields

When an external field is applied to a crystal the symmetry of the site is reduced; the extent of this symmetry breaking is dependent on the field orientation with respect to the crystal axes of symmetry (71). The resulting symmetry is determined by taking the symmetry elements in common between the site group (where the effect of the field is expected to cause the greatest perturbation) and the group $C_{\text{oo}h}^1$. Obviously, if the field is not along a crystal symmetry axis or in a symmetry plane, the resulting overall symmetry will be C_1 . In ref. 71, the symmetry of the point group resulting from application of an external electric or magnetic field applied along a symmetry axis of the point group is tabulated.

1. The magnetic field is $C_{\text{oo}h}$ and electric field $C_{\text{oo}v}$.

Features of Crystal Spectra

The proper interpretation of any type of spectrum depends on the amount of information available about the system being studied. With respect to electronic absorption spectra it is important to know the vibrational frequencies of the molecule being considered; although these may be different in the excited electronic state from the ground state, it is often possible to correlate one with the other. Then by comparing the frequency shifts and the intensity distribution of the vibrational bands in the spectrum, it is possible to infer the changes in the potential function which governs that vibrational mode.

Since we shall be concerned with spectra of molecular crystals, it will be useful to briefly outline the two most pertinent features found therein; these are crystal vibrations and their effect on optical absorption in the crystal.

Crystal Vibrations

Within a molecular crystal the intermolecular forces are much weaker than the forces acting between the atoms of a single molecule so that, in a first approximation, the molecules retain their individuality. On this basis all possible vibrations of the atoms in a molecular crystal may be divided into two main categories (72)

1. Internal vibrations: these are the intramolecular vibrations of the atoms in a molecule relative to one another. In these vibrations, the center of mass (c.o.m) of the molecule is not displaced and there is no rotation of the molecule as a whole. These vibrations are encountered in the isolated molecule. We will also refer to these as molecular vibrations.
2. External vibrations: are the vibrations which describe the relative motion of the molecules with respect to one another. They arise because of the rotational and translational degrees

of freedom of the molecules even as they are held rigidly in the crystal lattice. These vibrational frequencies bear no correspondence to those of the molecule in the vapor or solution phase, hence they are called lattice vibrations. The frequencies of these vibrations depend on the wave vector \vec{q} , unlike the internal vibrations which, in the absence of coupling with external vibrations, do not. The range covered by these vibrations is from $0 \sim 100 \text{ cm}^{-1}$ (72).

In a real lattice of course, there is coupling between the two types of vibrations and the distinction between them vanishes. This is especially true when the molecular vibrations have frequencies comparable to those of the lattice vibrations. Indeed, the molecular vibrations are influenced by the lattice which results in frequency shifts and factor group splitting, as was discussed for electronic states (vide supra). The discussion of symmetry as applied to crystal states applies equally well to crystal vibrations. It is possible to deduce the number and symmetry types of crystal vibrations from knowledge of the number and symmetry types of molecular vibrations and the factor group and site symmetry (69). A breakdown of the various classes¹ of lattice vibrations may be summarized as follows(72).

In a molecular crystal which contains n molecules per unit cell and p atoms per molecule there are a total of $3np$ crystal vibrations for each wave vector \vec{q} . Henceforth our discussion will focus on the point $\vec{q}=0$. Three of these classes constitute acoustical modes which are characterized by a change of the c.o.m. of the unit cell and, at $\vec{k}=0$ have zero frequency. The rest of the vibrations ($3np-3$) constitute the optical class of vibrations, characterized by nonzero frequencies at $\vec{q}=0$.

1. The terms class, branch and mode are all applicable and frequently interchanged. The term used here will be "mode".

Out of all $3np$ modes of vibrations of the crystal, $6n$ modes belong to the lattice vibrations (external), three of these are the acoustical modes and the rest, $6n-3$, are optical. The optical modes are further divided into $3(n-1)$ translational-vibrational modes and $3n$ rotational modes.

All of the remaining $n(3p-6)$ vibrational modes will be determined by the internal (molecular) vibrations of the n molecules in the unit cell and are all optical. Having discussed the vibrational characteristics of the crystal lattice, we now summarize the qualitative aspects of the interaction of the electronic excitation with the crystal lattice.

Electronic Absorption

Optical absorption in a molecular crystal results in the formation of an exciton. This is an excitation which corresponds to the formation of an electronically excited molecular state on one of the molecules in the crystal. This excitation may then propagate throughout the crystal by hopping from one molecule to another or by fast delocalization in the exciton band. At the instant of its formation the exciton may simultaneously create and/or annihilate a lattice phonon and in so doing cause an additional band to appear in the optical spectrum.

The extent of interaction of the electronic excitation (exciton) and the lattice vibration (phonon) will determine the spectral outcome and can be characterized by a parameter called the Stokes loss. Di Bartolo and Powell (73) give simulated spectra for various values of this parameter. One description of this parameter is that it is analogous to the nuclear recoil which occurs with gamma ray emission in Mössbauer spectroscopy. In the crystal case it corresponds to a shift in the equilibrium position of the molecules within the unit cell.

The exciton-phonon interaction manifests itself in phonon sidebands. These often have structure which may or may not bear correspondence to Raman frequencies observed for the crystal. Furthermore, the intramolecular vibrations which fall in the optical phonon branch may have frequencies comparable to those of the lattice optical modes, indeed may even intersect the acoustical modes at $\vec{q} \neq 0$. Because lattice vibrations are described in terms of all possible motions within the crystal, there is no longer a sharp distinction between intermolecular vibrations and pure intramolecular ones.

Three cases may be distinguished by the Stokes loss (ℓ) parameter (74):

1. $\ell \ll 1$: the excitation which propagates through the lattice consists mainly of delocalized excitons (electronic excitation). The appearance of the Franck-Condon envelope for this case (cf. Ref. 73, p. 410) is similar to that observed for the $+970 \text{ cm}^{-1}$ and 600 cm^{-1} bands in the TMCBDT crystal spectrum (Fig. 3-2). Using Eq. 10.11.15 of Ref. (73) it can be estimated that ℓ for these modes is about 0.1 and 0.3 respectively.
2. $\ell \approx 1$: the excitons are strongly coupled with phonons: the excitation propagates in the form of a polaron which is described as the electronic excitation together with lattice phonons. Since the electronic excitation is polarized, this process has the lattice phonons moving along the preferred direction determined by the exciton. The spectral manifestation of this is not seen in the TMCBDT spectra (75).
3. $\ell \gg 1$: the excitation is completely localized at the site of the exciton formation. In this case the intensity of the phonon sideband is comparable to that of the zero-phonon line and peaks at a frequency equal to ℓ quanta of the phonon mode.

Thus (qualitative) information on the nature of exciton migration may be obtained by noting the appearance of the absorption profile (Franck-Condon envelope). Comparison of the phonon sidebands in the corresponding emission spectrum can supplement the information obtained

from the absorption spectrum. In the case of low temperature ($\sim 2^\circ\text{K}$) the absorption in the $l \ll 1$ case takes place to the $\vec{k}=0$ zero-phonon level (74) and to various $\vec{k}+\vec{q}=0$ transitions involving phonons of wave vector \vec{q} which give rise to the phonon sideband. At this low temperature (2K) the excitation will relax into the $\vec{q}=0$ level (in the case of an exciton band having a concave-up dispersion curve) and transitions will only be possible to the $\vec{q}=0$ phonon levels of the ground electronic state. Thus, for $l \ll 1$ only $\vec{q}=0$ optical phonons will appear in the emission spectrum; this amounts to discrete emissions with little (or no) phonon sidebands and is indicative of delocalized excitons.

In the other coupling cases mentioned, the emission spectrum will contain broad phonon sidebands ($l \sim 1$) because the $\vec{q}=0$ selection rule does not hold since the phonon and exciton remain coupled. In the localized exciton case ($l \gg 1$) the phonon sideband in emission will bear a close resemblance to that observed in the corresponding absorption spectrum.

Crystal Structure

TMCBDT crystallizes in the tetragonal crystal class, in the space group $P4_2/mnm$ with two molecules per unit cell (38). Figure 3-1 shows the unit cell and the relative orientations of the two translationally inequivalent molecules which are located at the points (0,0,0) and (1/2,1/2,1/2). The site symmetry at these points is D_{2h} , which requires at least D_{2h} symmetry for the molecules which occupy these sites. The molecular structure is found (38) to be D_{2h} with the methyl groups eclipsed with respect to one another. The C=S bonds are collinear and both lie in the molecular plane defined by the

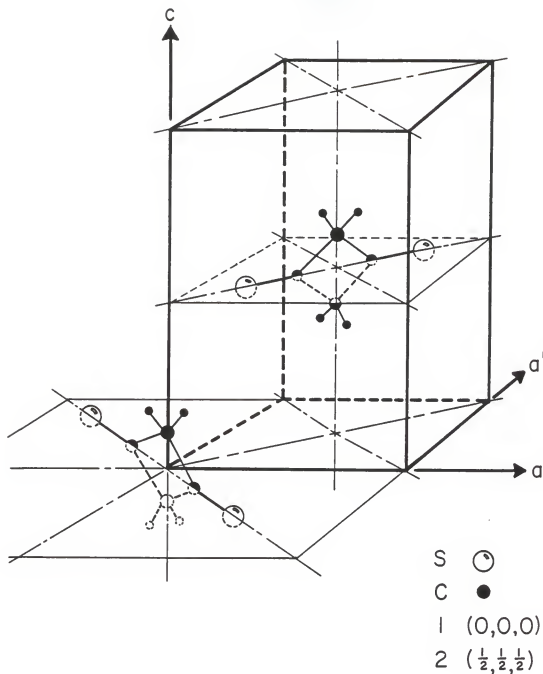


Figure 3-1. Orientation of TMCBDT molecules within the tetragonal unit cell. The unit cell dimensions are: $c=12.549 \text{ \AA}$, $a=6.330 \text{ \AA}$ (ref. 38). The molecular and cell dimensions are not drawn to scale here, (cf. Figure 3-7). The methyl carbon atoms are shown slightly smaller than those of the ring. The methyl hydrogens have been omitted.

cyclobutane (planar) ring (cf. Fig. 3-1); the molecular planes of the translationally inequivalent molecules are mutually perpendicular and lie at 45° with respect to the ac planes. The long in-plane axis of the molecule is along the C=S bonds (these are mutually perpendicular), we will label this the y molecular axis. The short in-plane axis will be taken as the z molecular axis and is parallel to the c crystal axis; the z molecular axes are parallel. The molecular x axis is out-of-plane and makes an angle of 45° (as the y) with the a crystal axis and is perpendicular to the c crystal axis.

This choice of coordinate system is not unique, but with a right handed axis system on each molecule and the molecular z axes parallel the correlation between molecular (or site) states and factor group states allows construction of factor group symmetry adapted functions by inspection. This is because with this system the symmetric (+) combination of B_{1u} molecular states correlates with the A_{2u} representation, while the antisymmetric (-) combination correlates with B_{2u} in the factor group.

If the molecular z axes were chosen antiparallel, the correlation would be $B_{1u}(+)/(-) \rightarrow B_{2u}/A_{2u}$. Unless otherwise specified the axis system used throughout this study will be that described above; it seems that having the z molecular axis parallel to the crystal symmetry axis justifies circumventing the more conventional choice of the z axis parallel to the C=S bonds.

The molecular coordinates calculated from the thermally corrected bond lengths and angles (38) are given in Table 4-1.

As mentioned previously the site and factor group symmetry is usually lower than the molecular symmetry; this leads to a breakdown of the symmetry selection rules operative in the free molecule, thus permitting the appearance of symmetry forbidden transitions in the free molecule. In the case of TMCBDT, on the other hand, the factor group symmetry is higher than the site and molecular symmetry. This arises because the two translationally inequivalent molecules are at right angles to one another thereby requiring a rotation of $\pi/2$ (followed by a non-primitive translation of $[0,0,1/2]$ to interchange them¹.)

The consequence of this relationship is that the molecular x and y direction (and therefore the B_{3u} and B_{2u} molecular electronic or vibrational states) which belong to one-dimensional irreducible representations in the molecular point group correlate with the two-dimensional irreducible representation of the D_{4h} factor group (E_u). This means that while molecular transitions polarized along the x and y molecular directions in the free molecule could in principle be distinguished, in the TMCBDT crystal these transitions are now both polarized $\parallel c$ and indistinguishable. Table 3-2 gives the correlations between the free molecule (and undistorted site group) and the crystal factor group for TMCBDT.

The uniaxial nature of the crystal is another consequence of the molecular arrangement within the unit cell². This property is manifested in the optical equivalence of the a and a' directions, that is, any orientation of the electric field vector of plane polarized light

1. The operation consisting of rotation about an axis by $2\pi/n$ followed by a non-primitive translation is called an n-fold screw axis (70).
2. This discussion applies only in the absence of external fields, see Chapter 5.

in the aa' plane is equivalent to any other orientation in this plane. On the other hand if the plane polarized light is incident on an ac face, the $\parallel c$ and $\perp c$ directions will be mutually exclusive. Thus a single crystal placed with the ac face parallel to a set of crossed polarizers will cause total extinction when the crystal is rotated so that the c crystal axis is parallel to one of the polarizers. If total extinction does not occur, it means that the c axis is not exactly parallel to the polarizer, which in turn could mean that the c axis is not parallel to the developed plane of the crystal.

The most important consequence of the molecular orientations in the unit cell is that for any electric dipole allowed transition in the free molecule there can be no factor group splitting in the crystal states. This is a consequence of the symmetry correlation discussed above. The x and y polarized states in the molecule each become degenerate (E_u), while the z polarized molecular states become A_{2u} (+ combination of site states) and B_{2u} (- combination of site states). The E_u are electric dipole allowed $\perp c$. The A_{2u} is allowed $\parallel c$ but the B_{2u} will not be seen unless the transition is assisted (vibronic) by a b_{2g} crystal vibration--this gives both factor group components $\parallel c$ polarization, or by an e_g crystal vibration which gives the (-) combination $\perp c$ polarization.

This effect is interesting but not observed in the TMCBDT triplet spectrum and will therefore not be considered further.

Crystal Growth

Earlier work (39) has shown that the preferred method for TMCBDT crystal growth is that of sublimation. TMCBDT readily sublimates at room temperature and will form minute crystals on the container walls even

while stored at $\sim 10^{\circ}\text{C}$. A few of these crystals were placed in a pyrex glass tube which was evacuated to $\sim 10^{-2}$ torr at 77 K for 15 to 30 minutes and then sealed. The tubes were then mounted (at $\sim 45^{\circ}$ angle from the vertical, and in a dark room) about one meter above a hot plate whose temperature was $\sim 50^{\circ}\text{C}$ - 60°C . The distance from the hot plate was varied to get sublimation rates which were slow enough to produce as few growing nuclei as possible; these usually formed at the end of the tube farthest from the hot plate. When well-developed single crystals failed to form, the tubes were simply inverted with the newly formed crystals now toward the hot plate.

Several other methods were tried but none gave good results. For example, attempting to cool a minute spot on the opposite end of the tube immediately resulted in many pin-point centers which disappeared when cooling ceased. The most successful method, described above, produced good crystals in about two weeks.

Crystal Orientation

The crystals used in this work were all similar in habit; their general appearance is shown in Fig. 5-3 in connection with the Zeeman apparatus; they may be described as being nearly hexagonal plates with the c axis lying in the face of the developed plane. Identification of the c axis direction was done by x-ray crystallography (76) and the alignment of the crystal for mounting was achieved through conoscopic examination with a polarizing microscope. By far the best results were obtained with those crystals which could be used directly without polishing (crystal D).

Experimental Details

The polarized absorption spectrum was recorded on Tri-X film (77). The sample was mounted in an immersion type liquid helium dewar and cooled to approximately 1.6K by evacuating the helium vapor. Some spectra were photographed above 4.2 K after the liquid helium level had dropped just below the sample. These were given minimum exposure times (1 minute) and no attempt was made to control the temperature. The optical arrangement consisted of a quartz-iodine lamp focussed onto the sample and the transmitted light refocussed onto the slit of a Jena 2 meter spectrograph by a reflecting microscope objective placed after the sample. The slit width of 50μ and the grating dispersion of 7.28 \AA/mm provided a resolution of about 0.3 \AA , about 0.9 cm^{-1} at 5900 \AA . A Wollaston prism adjacent to the slit produced both parallel and perpendicular polarizations simultaneously. To compensate for the polarizing effect of the grating a circularly-polarizing $\lambda/4$ plate was placed between the Wollaston prism and the slit, effectively scrambling the radiation incident on the slit.

Spectra taken at temperatures above 10K were recorded on a Cary 14 spectrophotometer using slit widths from about 60μ to about 100μ , giving a resolution of about 2.1 \AA and 3.5 \AA (corresponding to ~ 5 and 9 cm^{-1}) respectively. The crystals were mounted between an indium mask and a copper plate attached to the cold finger of a closed cycle helium cryostat (Air Products, Displex CSW-202). A gold-chromel thermocouple was mounted as close to the crystal as possible with cryogenic grease, and connected to a digital voltmeter. The reference junction was immersed in an ice bath at 0°C . It is estimated that temperatures measured in this manner are accurate to ± 1 .

Densitometer tracings of the films from the low temperature spectra were recorded with a Leeds and Northrup Model 6700-A2 micro-densitometer equipped with an RCA 1P28 photomultiplier tube. The signal from the photomultiplier was amplified by a Keithley Model 416 picoammeter and recorded on a Heath Model 700C strip-chart recorder.

The band positions were determined by comparison with a potassium discharge tube spectrum recorded on one of the films. The Wollaston spectra consisted of sets of two adjacent exposures containing the TMCBDT spectra. The potassium spectrum was superimposed on the perpendicular to c polarization of one of the sets. A recording of this exposure gave the distance of the TMCBDT absorption 0-0 band with respect to the longest wavelength potassium line (5895.923 \AA). The 25 potassium lines between 5895 \AA and 4641 \AA were used to obtain a least squares fit to the quadratic equation

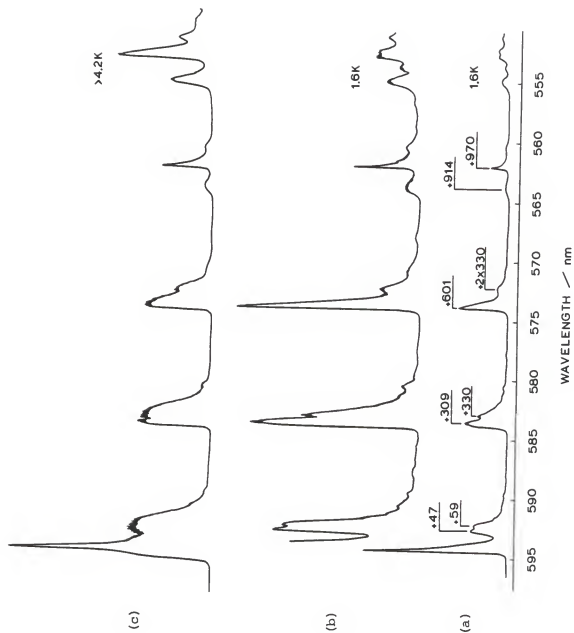
$$\lambda = b_0 + b_1 d + b_2 d^2$$

where d is the distance from the 5895.9 \AA potassium line. The root mean square deviation of the fit was $\pm 0.134 \text{ \AA}$. The constants, b_1 , have to be determined for each chart recorder speed and densitometer scan speed combination. For the tracings presented here the values $b_0 = 5896.1396$, $b_1 = -1.8068877$ and $b_2 = -2.2417152 \times 10^{-5}$ were used; this gives a wavelength of 5943.104 \AA for the 0-0 band of TMCBDT. The other band positions are calculated using the above formula with d equal to their distance from the TMCBDT 0-0 band plus the distance of the 0-0 band from the 5895.9 \AA potassium line. This method insures that the band positions are correct relative to the 0-0 band.

The potassium emission lines were very sharp and determining ' d ' for these involves little error (± 0.2 division). It is estimated

Figure 3-2. Low temperature absorption spectrum of single crystal TWCBDT polarized perpendicular to c. All three are densitometer traces.

- (a) Singlet-triplet transition region at 1.6K. Band positions are in cm^{-1} .
- (b) Expanded scale of (a).
- (c) Same as (a) and (b) but at a temperature between 4K and 10K (exact value unknown).



that for the TMCBDT bands which are not as sharp, the band position is in error by about $\pm 3 \text{ cm}^{-1}$.

Results

Low Temperature

Polarized absorption spectra (single beam mode) of several crystals were taken at temperatures below 10K in the spectral range of 600 nm to 400 nm. Bands to the blue of 550 nm were much more intense and required greater exposure times. The latter region has been reported as the vibronic $^1A_u \leftarrow ^1A_g$ transition (43, 45) and will not be discussed here. Densitometer traces of several exposures were made and the best ones chosen; these will be referred to as crystals D (taken at 1.6K) and F (taken somewhat above 4.2K but below 10K). These are shown in Fig. 3-2. The frequency (in cm^{-1}) and vibrational assignments are given in Table 3-1.

Temperatures Above 10K

Crystal E was run on the Cary 14 (double beam mode) at 11K, 20K and 47K. There was no difference between the first two of these in either band position, band contour or intensity; the 20K and 47K spectra are shown in Fig. 3-3. As for the low temperature spectra, bands to the blue of 550 nm were very intense. Although some changes with temperature appeared to take place in this region, the resolution was inadequate for proper observation of these effects. The blue shift and broadening of the bands in the triplet region (600 nm to 555 nm) will be discussed later.

In addition, because the developed planes of this crystal were not parallel, the subsequent polishing resulted in a mounting with uncertain c axis direction. Since the cryostat could only be rotated

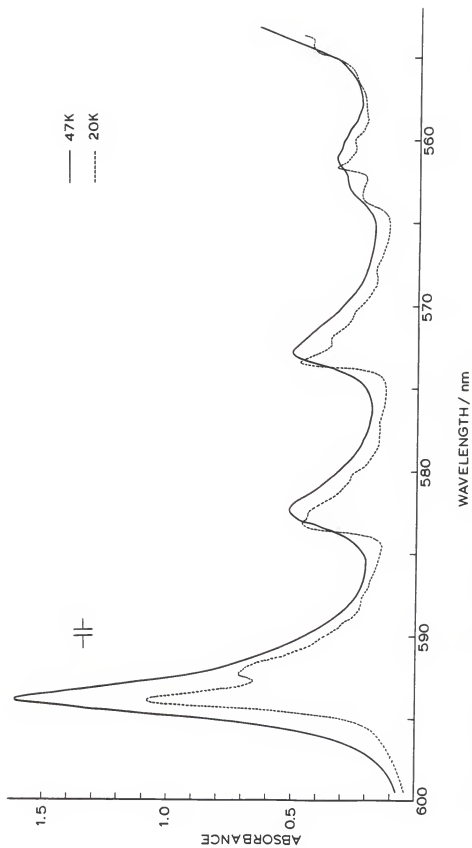


Figure 3-3. Absorption spectrum of single crystal TMCBDT at 20 K and 47 K. Cary 14 spectra (unpolarized.)

about its vertical axis, it was not possible to remove the contaminating $||c$ polarization. Although the intensity variation serves to reinforce the conclusion that Eq. 5-20 fits the observed polarization behavior, the polarization contamination in the region below 555 nm (where the 1A_u transition occurs) renders the temperature dependence in that region useless.

In the next section an account of the temperature dependence and band intensity distribution is presented.

Vibrational Analysis of the $T_1 \leftarrow S_0$ Transition

Table 3-1 lists the observed frequencies, displacements from the origin, assignments and calculated positions (*vide infra*). The major bands are located at 0 cm^{-1} , $\sim 300\text{ cm}^{-1}$, 600 cm^{-1} and $\sim 950\text{ cm}^{-1}$ from the electronic origin (0-0). These bands are discussed in turn below.

The 0-0 Band

The pure electronic origin located at 16822 cm^{-1} (5943.1 \AA) is assigned as the $^3E_u \leftarrow ^1A_{1g}$ crystal transition (43); this is an electric dipole allowed transition which arises via spin-orbit coupling of the $^3A_{1u}$ crystal state to 1E_u crystal states. This corresponds to the lowest $^3n\pi^*(^3A_u)$ state in the free molecule, in which the spin-orbit coupling is mainly to $^1\pi\pi^*(^1B_{2u}\text{ or }^1B_{3u})$ states. The dominant pathways for spin-orbit interaction in TMCBDT are treated in detail in Chapter 4. Table 3-2 gives a correlation diagram between the molecular point group (D_{2h} = site group) and the crystal factor group (D_{4h}).

The 0-0 band is $\sim 3\text{ cm}^{-1}$ wide (FWHM), has a very sharp red edge and somewhat broadened blue edge. This is a good example of the band shape that arises in the case of weak exciton-phonon interaction, $l \ll 1$, as discussed earlier. (See also Ref. 78.)

A series of very weak, irregularly spaced bands is found on a broad absorption whose maximum occurs at $\sim 50 \text{ cm}^{-1}$. Two of them (+47 and +87) are built on the other strong vibronic bands: this sequence could be due to lattice modes or a low frequency molecular vibration (*vide infra*). Regardless of their origin, their energy distribution can be described by a double minimum potential (DMP). A brief description of the fitting procedure and resulting potential function parameters will be given later.

Table 3-1 gives the calculated values of these energy levels. A similar series of bands is observed in the emission spectrum of crystalline TMCBDT¹ at 1.6 K, except that in the latter spectrum the bands are very intense, some are very sharp, and overlapping with trap emission bands occurs. A DMP was fit to this sequence of bands giving the potential function for the ground electronic state.

The 300 cm^{-1} Band

This band, located at $+309 \text{ cm}^{-1}$, has a somewhat different appearance than the 0-0 band and the other sharp bands at $+600 \text{ cm}^{-1}$ and $+970 \text{ cm}^{-1}$. There is also a shoulder at $+329 \text{ cm}^{-1}$ which undoubtedly causes the broadening. The red edge is not sharp and appears to be lacking the zero-phonon line. A look at Fig. 3-2 and Fig. 3-3 shows that upon increasing the temperature above 4K (but below 20K) the band at $+329 \text{ cm}^{-1}$ increases relative to the one at $+309 \text{ cm}^{-1}$. This might indicate that the 329 cm^{-1} band represents a transition from a level located about 20 cm^{-1} above the zeroth level in the ground state, which becomes more populated on warming. However, since this band is seen at 1.6 K we assign it as a separate molecular mode.

1. The emission experiments (43) will not be included in this work, but will be referenced as needed to complement the discussion of the absorption experiments.

TABLE 3-1
 VIBRATIONAL ANALYSIS OF $T_1 + S_8$ ABSORPTION OF
 CRYSTALLINE TMCBDT POLARIZED PERPENDICULAR TO c

Observed Frequency (cm^{-1})	$\Delta\nu_{-1}$ (cm^{-1})	Assignment ^a (cm^{-1})	Calculated ^b (cm^{-1})	$\Delta\nu_{-1}$ (cm^{-1})
O1 16822	0	$0^+ - 0^+$	-	-
16869	47	1+	47	0
16880	58	1-	54	+4
16897	75	lattice	75	0
(16907)	(85)	2+	87	-2
16925	103	2-	106	-3
16956	134	3+	133	+1
17007	185	4+	186	-1
O2 17131	309	309	-	-
O3 17151	329	329	-	-
17197	375	329 + 47	376	-1
17223	401	309 + 87	396	+5
17248	426	329 + 87	416	+10
17311	489	309 + 2 x 87	483	+6
O4 17422	600	600	-	-
17471	649	600 + 47	647	+2
		2 x 329	658	-9
		309 + 329	638	+11
17513	691	600 + 87	687	+4

 continued

TABLE 3-1 continued

		2 x 329 + 47	705	-14
		309 + 329 + 47	685	+6
17600	778	600 + 2 x 87	774	+4
		309 + 329		
		+ 87 + 47	772	+6
05 17735	913	913	-	-
		600 + 309	909	+4
		600 + 329	929	-14
06 17791	969	969	-	-
		913 + 47	960	+9
		600 + 329 + 47	976	-7
17843	1021	969 + 47	1016	+5
17867	1045	969 + 87	1056	-11
17898	1076	3 x 329 + 87	1074	+2
17963	1141	969 + 2 x 87	1143	-2

-
- a. Multiple assignments are given where it was not possible to make a unique assignment or where more than one band is likely to be present even if not resolved. 02 through 06 define the vibronic bands.
- b. Calculated band position based on assignment. The difference between the observed band positions relative to the 16822 cm^{-1} origin (0-0) and this calculated value appears in the last column.

The 600 cm^{-1} Band

The shape of this band resembles the 0-0 and the 970 cm^{-1} bands. It is clearly a separate vibration and has the weaker series of bands to the blue. Several possibilities are given (cf. Table 3-1) for these since any one cannot be ruled out in an obvious manner. The temperature behavior of this band is similar to the one discussed above.

The 970 cm^{-1} Bands

The broad, weak band at +913 cm^{-1} is assigned to a separate vibration for the same reasons as the 300 cm^{-1} band. A sharp band resembling the 0-0 and 600 cm^{-1} which appears at +970 cm^{-1} is assigned as a separate vibration as well. The weaker bands to the blue can be assigned as various combinations.

Polarization ||c

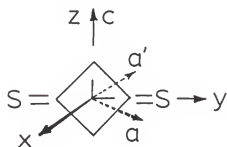
For crystal E at 1.6K a very sharp symmetrical (Gaussian like) but very weak band was noted at the same position as the 0-0 band polarized $\perp c$. All attempts to remove this by rotating the polarizer failed. The intensity ratio is about 1:620 for $||c:\perp c$. While this could be a real manifestation of a spin-orbit route inducing $||c$ intensity, a definite conclusion could not be reached.

Summary

The $T_1 \leftarrow S_0$ transition in crystalline TMCBDT is polarized exclusively $\perp c$ and therefore corresponds to spin-orbit coupling of the 3A_u molecular state with ${}^1B_{2u}$ and / or ${}^1B_{3u}$ molecular states. Of the possible choices for a ${}^3\pi\pi^*$ state (3A_u or ${}^3B_{2g}$), inspection of Table 3-2 immediately shows that the ${}^3B_{2g}$ state (${}^3n_+\pi_+^*$) could not be seen in first order. This shows that the lowest triplet state in TMCBDT is 3A_u which implies

TABLE 3-2
(STATIC) CORRELATION BETWEEN MOLECULAR (SITE) GROUP AND FACTOR GROUP

D_{2h}		D_{4h}
A_g		A_{1g}
$B_{1g}(R_z)$		$A_{2g}(R_c)$
$B_{2g}(R_y)$		B_{1g}
$B_{3g}(R_x)$		B_{2g}
		$E_g(R_a, R_{a'})$
A_u		A_{1u}
$B_{1u}(z)$		$A_{2u}(c)$
$B_{2u}(y)$		B_{1u}
$B_{3u}(x)$		B_{2u}
		$E_u(a, a')$



that 1A_u is lowest in the singlet manifold. The active vibrations in the transition are found to be 309 cm^{-1} , 330 cm^{-1} , 600 cm^{-1} , 913 cm^{-1} and 970 cm^{-1} . By analogy with TMCBD we assign the 309 cm^{-1} and 600 cm^{-1} to skeletal vibrations and the 970 cm^{-1} mode to the C=S stretch (symmetric), and the 913 cm^{-1} mode to C-C stretch or CH_3 bend.

Crystal Vibrations in TMCBDT

In the previous section the 0-0 band has been assigned to an electric dipole allowed transition induced by spin-orbit coupling. This means that any vibrations observed must have g symmetry, since the electronic state is E_u , any of the g vibrations in D_{4h} will allow the transition to be observed $\perp c$; this was experimentally observed. It is clear from the earlier general discussion of crystal vibrations, that the vibrations observed at 300 cm^{-1} , 600 cm^{-1} and 970 cm^{-1} must be due to internal modes. This leaves the low frequency vibrations built on the 0-0 band which must be explained. Because only the far infrared spectrum is available (gas phase, room temperature, see Ref. 83) for TMCBDT, it will be necessary to draw on analogies with TMCBD infrared and Raman spectra (4).

From the Raman spectra of TMCBD we find only one vibration below 200 cm^{-1} in solution, polycrystal and single crystal; this is about 160 cm^{-1} . We expect two bands corresponding to this molecular band to appear in the crystal spectrum of TMCBDT, at approximately the same value of energy and not split (see arguments on factor group splitting).

If the 216 cm^{-1} band of TMCBD is included, and if it can be assumed to shift to lower frequency, we can only account for two

of the eight observed bands in the range 0 to $\sim 200 \text{ cm}^{-1}$ relative to the 0-0 band. We can assign the 134 cm^{-1} band and 213 cm^{-1} band (cf. Table 3-3) observed in TMCBDT to correspond to the 160 cm^{-1} and 216 cm^{-1} Raman bands (see Table 3-1) of TMCBD. The 75 (or 85) cm^{-1} and the 185 cm^{-1} bands correlate with the 42 cm^{-1} and the 186 cm^{-1} bands, respectively, observed in the far IR spectrum of TMCBDT in the gas phase. This correspondence is based on analogy with the TMCBD bands at 58 cm^{-1} and 180 cm^{-1} in the gas phase which shift to 82 cm^{-1} and 186 cm^{-1} in the polycrystal. This assignment accounts for 4 of the 8 observed bands (cf. Table 3-3). If all four bands are due to internal modes, the remaining four bands must be due to lattice modes. These are examined briefly below.

To determine the lattice modes in the factor group, a correlation method will be used (69). The lattice or intermolecular vibrations are derived from the translational (transform as the molecular axis vectors) and the rotational (transform as the rotations about the molecular axes) degrees of freedom of the molecules within the lattice. Thus, we may correlate the symmetry species of these motions in the free molecule to obtain the factor group symmetry adapted coordinates for the lattice modes---these correspond to symmetry coordinates in the free molecule vibrations. Taking the appropriate linear combinations we obtain

$$(1/\sqrt{2})(R_{z1} + R_{z2}) \quad a_{2g}(+); \quad b_{2g}(-)$$

$$(1/\sqrt{2})(R_{y1} + R_{y2}) \quad e_g \quad (2, \text{ degenerate})$$

$$(1/\sqrt{2})(R_{x1} + R_{x2}) \quad e_g \quad (2, \text{ degenerate})$$

Here only the g type modes have been constructed as demanded by the E_u electronic transition. These modes correspond to in-phase and

out-of-phase rotational oscillations about the molecular axes, keeping the c.o.m. of the unit cell fixed, and are thus optical modes. Furthermore, they are all Raman active except the a_{2g} mode.

The b_{2g} and a_{2g} vibrations are acceptable because they give E_u when the direct product with the E_u electronic representation is taken. The e_g modes, however, give

$$E_u \times e_g = A_{1u} + B_{1u} + B_{2u} + A_{2u}$$

none of which are allowed. So from the 6 gerade lattice modes only two are candidates for the observed bands, the a_{2g} and b_{2g} vibrations.

Thus, there can only be two lattice mode fundamentals. If these two are assigned to the 47 cm^{-1} and 58 cm^{-1} bands the 103 cm^{-1} band can be assigned to the combination of these two. These assignments leave one band unexplained: the 85 (or 75 cm^{-1}) band.

An alternate assignment for the low frequency vibrations rests on the assumption of a large zero-field splitting in TMCBDT.

A large zero-field splitting ($D = -11\text{ cm}^{-1}$) has been found for xanthione (see Chap. 5 and references therein). If the same were true for TMCBDT, the isolated molecule 3A_u state would have two nearly degenerate spin sublevels located about 11 cm^{-1} below the third spin sublevel. The two frequencies 47 cm^{-1} and 75 cm^{-1} could now be assigned as two g lattice vibrations and transitions from the ground electronic state to one of the lower spin sublevels of the 3A_u state would appear at $0-0 + 47\text{ cm}^{-1}$ and $0-0 + 75\text{ cm}^{-1}$. Transitions to the upper spin sublevel of 3A_u would occur at 58 cm^{-1} and 86 cm^{-1} . For this to occur, however, the transition moments to the two triplet sublevels involved must be nearly equal. The spin-orbit-coupling results (Table 4-4) and analogy with carbonyl transition moments, preclude this.

Furthermore, such a large zero-field splitting would have been easily observed in the Zeeman experiments (see Chapter 5) but was not. On the basis of these inconsistencies therefore, this model is ruled out.

In the next section another model, involving a double minimum potential, is proposed that explains all the observed bands as well as the temperature behavior in absorption and the emission band positions (43).

The Double Minimum Potentials

Fitting Procedure and Results

The method of Coon, Naugle and McKenzie (79) was chosen to fit the weak irregularly spaced bands in the region $+0$ to $+220 \text{ cm}^{-1}$. This method described the DMP function as a harmonic oscillator of frequency ν_0 which is perturbed by a Gaussian barrier centered at the equilibrium position (Q_0 , the mass weighted coordinate) of a simple harmonic oscillator (SHO). To implement this method, a system of computer programs was written (Fortran IV). A more detailed documentation of these and the graphical method of Coon et al. (79) may be found in a separate report (80). A brief outline of the method and a description of the parameters is given here to facilitate discussion of the results.

The DMP function of Coon et al. can be characterized by the three parameters ρ , B and ν_0 . The parameter ρ describes the relative slopes of the barrier walls and the outer walls of the potential (79); B is related to the height of the barrier (b) through the relation $b = B\nu_0$. The wavefunction of the perturbed oscillator is taken as a

linear combination of SHO functions and the eigenvalues and eigenvectors of the various levels are determined by direct diagonalization of the perturbed SHO Hamiltonian. Due to the symmetry properties of the SHO functions (79) the resulting eigenstates will be divided into even (+) and odd (-) states. These eigenstates are described by linear combinations of even and odd SHO eigenfunctions (81) respectively. In the case of TMCBDT the symmetry of the potential is still D_{2h} and the (+) levels will be a_g while the (-) levels will have the symmetry of the mode in question.

The fitting procedure is based on the fact that the eigenvalues relative to the potential minima $[V(Q_m)]$ may be written as G/v_o and the quantity

$$v_o = \frac{G(i) - G(0^+)}{G/v_o(i) - G/v_o(0^+)} \quad (3-1)$$

is then plotted as a function of the parameter B for a given value of ρ . The $G(i)$ are the observed frequencies. The intersection of the v_o versus B curves for several levels (i), will occur only when the two parameters ρ and B give eigenvalue differences which fit those observed.

The number of basis functions to include in the SHO expansion will depend on the values of ρ and B (79,80) and is chosen to give correct eigenvalues for the lowest 14 levels.

The results of the fit to the observed absorption and emission frequencies at 1.6 K is given in Table 3-3. The DMP potentials are shown in Figs. 3-4 and 3-5. The important conclusions from the fit are

TABLE 3-3
DMP DESCRIPTION OF THE LOW FREQUENCY VIBRATIONS
OBSERVED AT 1.6K IN CRYSTALLINE TMCBDT SPECTRA

<u>$^1A_{1g}$</u>			<u>$^3A_{1u}$</u>		
<u>Emission Bands^d</u>			<u>Absorption bands^d</u>		
<u>Observed</u>	<u>Calculated</u>	<u>Assignment^e</u>	<u>Observed</u>	<u>Calculated</u>	<u>Assignment^e</u>
0	0	0 ⁺	0	0	0 ⁺
-22	14.9	0 ⁻	-	0.84	0 ⁻
-47 ^b	47.0	1 ⁺	47 ^b	46.9	1 ⁺
-68	72.6	1 ⁻	58	54.0	1 ⁻
-103 ^b	102.0	2 ⁺	85 ^b	86.6	2 ⁺
-129	130.2	2 ⁻	103	105.7	2 ⁻
-159 ^b	159.2	3 ⁺	134 ^b	133.2	3 ⁺
-183	188.1	3 ⁻	-	158.4	3 ⁻
-216 ^b	217.1	4 ⁺	185 ^b	185.5	4 ⁺
-237	246.1	4 ⁻	213 ^c	212.3	4 ⁻
-280	275.3	5 ⁺	-	239.8	5 ⁺
-	304.4	5 ⁻	-	267.2	5 ⁻
<u>DMP</u> <u>Parameters</u>					
1.80	ρ	2.10			
0.80	B	3.30			
29.3	ν_o (cm ⁻¹)	28.7			
23.4	b (cm ⁻¹)	94.7			
1.30×10^{-20}	$ Q_m $ (g ^{1/2} cm)	2.31×10^{-20}			

a. See Ref. 43.

b. Observed frequency used in fit.

c. Taken from run with more pronounced sideband.

d. All quantities are in cm⁻¹.

e. Labels refer to DMP levels, see Figures 3-4 and 3-5.

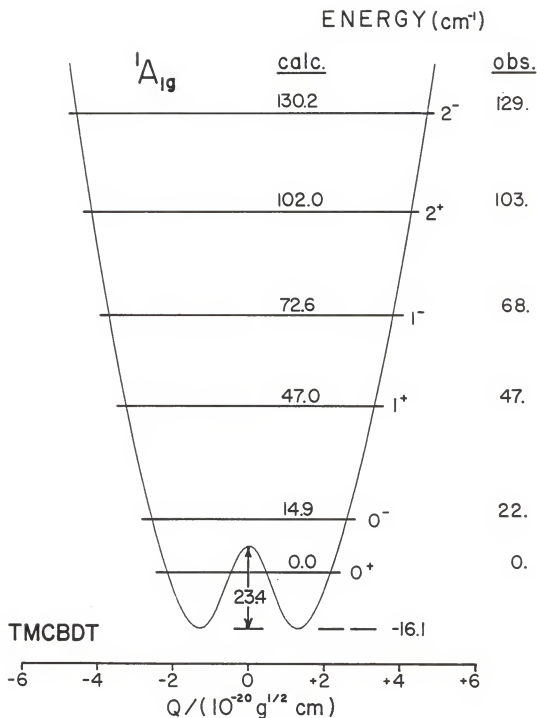


Figure 3-4. Double minimum potential for ground state. The energy levels are obtained from a fit using the emission bands (43) in Table 3-3. The parameters are $\rho=1.80$, $B=0.80$, $\nu_0=29.3 \text{ cm}^{-1}$, barrier height, b , is 23.4 cm^{-1} and minima occur at $Q=1.30 \times 10^{-20} \text{ g}^{1/2} \text{ cm}$.

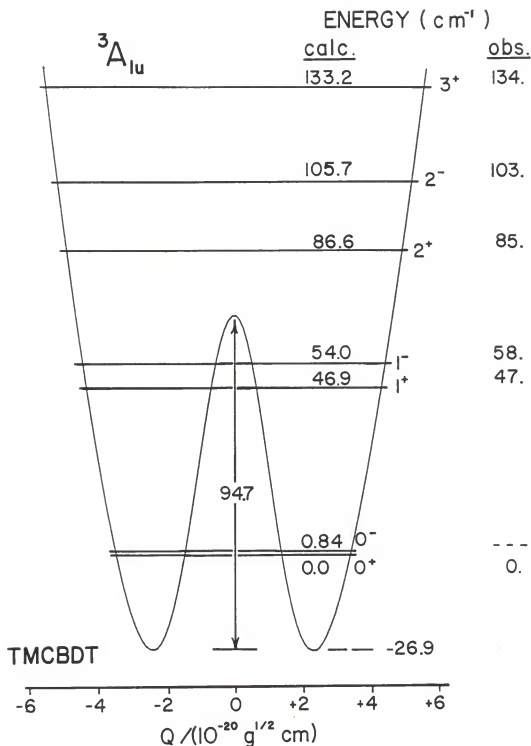


Figure 3-5. Double minimum potential for triplet excited state. The energy levels are obtained from a fit using the absorption bands in Table 3-3. The parameters are $\rho=2.10$, $B=3.30$, $\nu_0=28.7 \text{ cm}^{-1}$, barrier height, b , is 94.7 cm^{-1} and minima occur at $Q'=2.31 \times 10^{-20} \text{ g}^{1/2} \text{ cm}$.

1. The barrier height in both states is low enough to preclude observation of a bent molecular structure in the room temperature X-ray determination and infrared or Raman spectra. In fact it may be shown that for the ground electronic state based on the level populations at ambient temperature and the value of the transition amplitudes (82) only a single band will be seen at the frequency ν . (A broad band at 42 cm^{-1} is observed in the gas phase IR at room temperature (83)).
2. There is a difference in the potential minima, Q_m , between the ground and excited electronic states: although it is not possible to translate this into an angle since we do not know the reduced mass of the motion, it is seen that the Q'_m/Q''_m is about 1.8 (cf. Table 3-3). This amounts to a 77% change.
3. At 1.6 K the system is constrained to the lowest level so that the effective symmetry of the potential changes from D_{2h} (in the molecular group) to C_{2v} due to loss of the mirror plane of symmetry.

The Calculated Spectra at 1.6 K

Using the above DMP models absorption and emission spectra may be calculated as a function of temperature (80). The Franck-Condon factors may be found using

$$\underline{F} = \underline{A}' \underline{R} \underline{B} \quad (3-2)$$

where \underline{A} (\underline{B}) is the eigenvector matrix for the ground (excited) electronic state and the prime denotes the transpose. \underline{R} is the overlap matrix over the SHO eigenfunctions of the ground electronic state, ν''_0 , and those of the excited electronic state, ν'_0 . In this case since the SHO frequencies are nearly the same \underline{R} is very close to $\underline{1}$. Here it is assumed that the electronic transition moment M_e , is independent of ν (\pm), and that the electronic transition is allowed. In the case of a vibronic transition \underline{R} becomes $\langle \nu'(i) | \underline{Q} | \nu''(j) \rangle$ and the electronic transition moment now involves matrix elements of $(\partial M_e / \partial Q)_{Q_0}$ between the ground and excited electronic states (70). These will not be considered here.

To calculate the spectrum the band positions are first determined relative to the $0^+ - 0^+$ band (0 cm^{-1}). The intensity for a particular band, ($v'' = 0^+$ to $v' = 1^+$ at $+47 \text{ cm}^{-1}$, for example) is then proportional to the square of $F(|F_{0+1+}|^2 \text{ for this example})$. All the intensities are then multiplied by the appropriate fractional (Boltzmann) population factor (N_{0+} in this case) and the resulting values normalized to the largest intensity.

Normally the displacement (or normal) coordinates Q'' and Q' have the same origin in the case of two DMP functions (84); then due to the even/odd symmetry of the SHO eigenfunctions Eq. 3-2 will factor into even and odd components. The resulting spectrum is then strictly governed by the $(+)\rightarrow(+)$ and $(-)\rightarrow(-)$ selection rule and at 1.6 K the transitions to $(-)$ bands should be absent in absorption. In the present model (cf. Table 3-3) transitions to $(-)$ levels in the ground state are predicted in the emission spectrum at 1.6 K because the 0^+ and 0^- levels of the excited state have a 53% and 47% population distribution.

However, at this low temperature, we can consider the ground state system with the entire population in the 0^+ level which is just below the barrier maximum. Then the symmetry is reduced (if the model is applied to a low frequency intramolecular torsion in a planar molecule, for example, the symmetry would be reduced from D_{2h} to C_{2v}) and the point group which now determines the selection rules is the subgroup common to both. If we apply this to the TMCBDT (crystal), we find that, if the DMP describes a torsional mode, its symmetry in D_{2h} is (cf. Table 3-2) B_{3u} for the $(-)$ and A_g for the $(+)$ levels. In the crystal factor group these become $E_u(-)$ and $A_{1g}(+)$. Since the pure electronic

transition is observed $\perp c$, it is E_u which correlates with either a B_{2u} or B_{3u} molecular state. Thus the vibronic species will be

$$E_u \times \begin{cases} A_{1g} \rightarrow E_u & \text{allowed } \perp c \\ E_u \rightarrow A_{1g} + B_{1g} + B_{2g} & \text{not allowed} \end{cases}$$

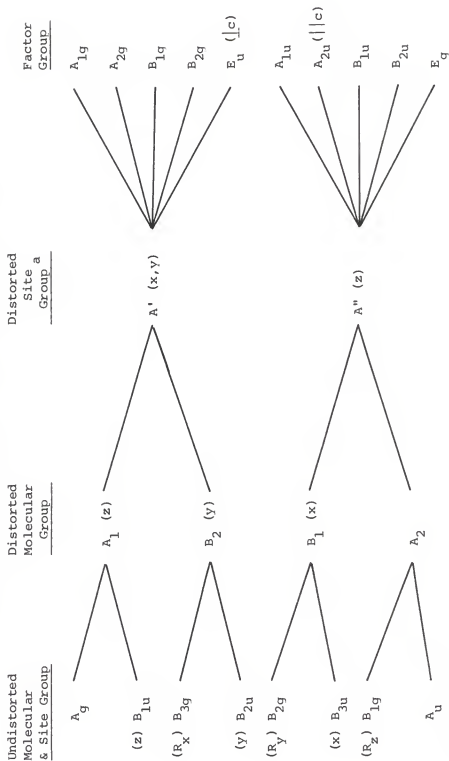
For the C_{2v} distorted molecule, the site group is determined by the symmetry elements in common with the unchanged crystal factor group; this is C_s . Table 3-4 gives the appropriate correlation among the groups. Here we label the axes differently so that the torsional mode now becomes B_{1u} . This becomes totally symmetric in the site; hence, all vibrational levels are symmetric. The electronic state now will be B_{1u} or B_{2u} which become totally symmetric in the site; thus all the vibronic levels become allowed (and $\perp c$ polarized) in the crystal factor group. (The correlation tables may be found in Ref. 81, Appendix X.)

The above argument justifies calculating R using two displaced SHO potentials, in which case it is no longer factored (80, 84) into even/even and odd/odd blocks. The displacement is taken as the difference in $|Q_m|$ between the two electronic states. Now the Franck-Condon overlaps will be nonzero for mixed even/odd integrals, even when the even/odd wavefunctions retain the higher symmetry. For example, for the transition $1^+ \rightarrow 0^-$, which occurs at $+47-15=32 \text{ cm}^{-1}$, we would have

$$\begin{aligned} \langle 0(-) | 1(+) \rangle &= \langle [0.99 \langle 1 | + 0.11 \langle 3 |] \quad | \quad [0.66 | 0 \rangle - 0.29 | 2 \rangle - 0.69 | 4 \rangle \\ &\quad - 0.1 | 6 \rangle] \rangle \\ &= (0.99 [(0.66) \langle 1 | 0 \rangle - (0.29) \langle 1 | 2 \rangle] + \dots \\ &= 0.46 + \dots \end{aligned}$$

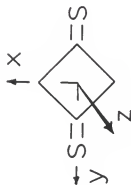
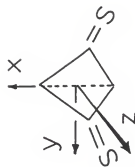
The values for the R elements ($\langle 1 | 0 \rangle$ etc.) are calculated (80, 84)

TABLE 3-4
CORRELATION TABLE FOR THE DISTORTED MOLECULAR EXCITED STATE



continued

TABLE 3-4 continued

 D_{2h}  C_{2v} C_s D_{4h}

- a. The distorted site group is that subgroup of the crystal factor group defined by the symmetry elements common to both the distorted molecular point group and the crystal factor group. The yz molecular plane (and the identity) is that symmetry element in this case, giving a distorted site group symmetry of C_s .

on the basis of $(\nu''/\nu')^{1/2} = 1$ and a displacement equal to $|Q_m'| - |Q_m''|$ from Table 3-3.

Temperature Dependence of Spectra

Using the model just described we can calculate (approximate) spectra for various temperatures; Fig. 3-6 shows the effect of raising the temperature from 2°K to 60 K. With this model, the effect of trap emission (43) can also be simulated by superimposing the $0^+ - 0^+$ band from the calculated spectrum on the wavenumber at which the trap emission onset with decreasing temperature is observed (43); only one band (-159 cm^{-1}) used in the fit corresponds to an observed trap band.

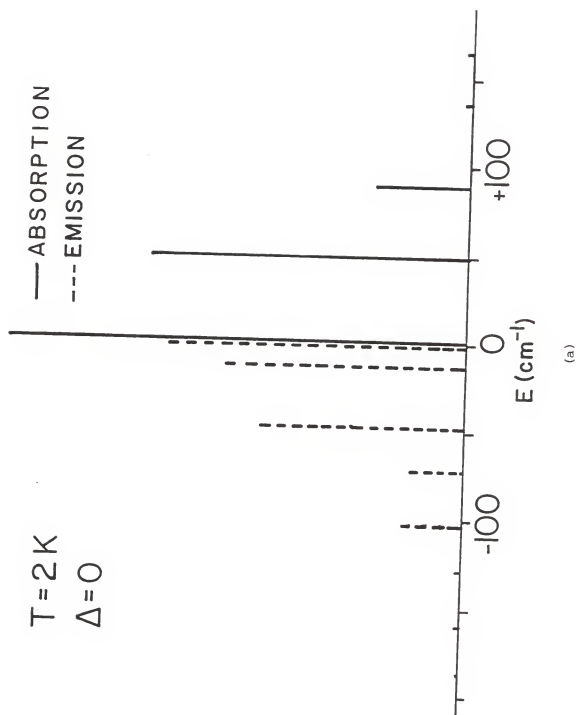
The essential features in the observed spectra which have been discussed earlier are clearly reproduced by the present model. Considering absorption only in Fig. 3-6, it can be seen that as temperature increases the $0^- \rightarrow \nu_1^+$ bands increase at the expense of the $0^+ \rightarrow \nu_1^+$ bands. As temperature increases still further, more bands to the red of the $0^+ - 0^+$ grow in. There is a limit to the increase of the $0^- - 1^+$ band at $+32 \text{ cm}^{-1}$ for example, because the population (fraction) in the 0^- level of the ground electronic state increases (from zero at 1.6K) to a maximum of about 0.31 at 40 K and then decreases as temperature increases. This trend accounts for the observed behavior in the 329 cm^{-1} band, for example, since it does not continue to increase above 47 K. In the observed spectrum, the bands continue to broaden and no large shifts in maxima occur above ~50 K.

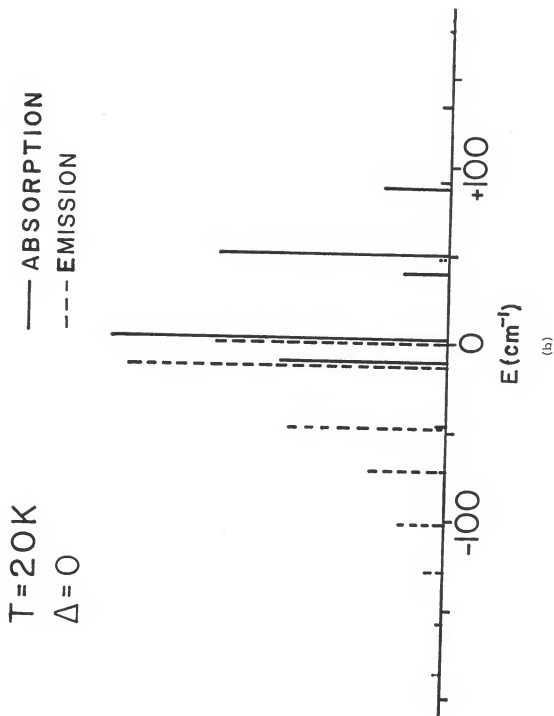
Physical Nature of DMP

Thus far the nature of the low frequency vibration that accounts for the observed series of bands built on the 0-0 band has been

Figure 3-6. Simulated absorption and emission spectra calculated using the DMP model as a function of temperature. For all three cases it is assumed that $\Delta = |Q'm| - |Q''m| = 0$. The energies are relative to the $(0 - 0)$ transition.

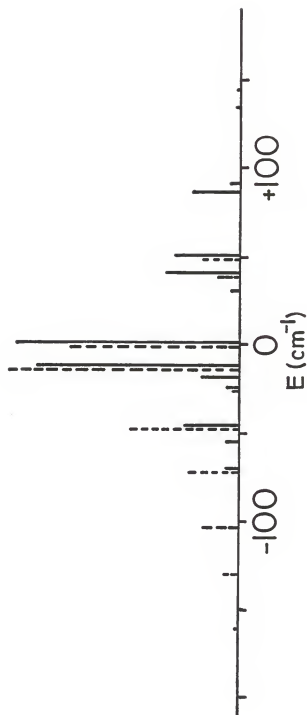
- (a) Simulated emission and absorption spectra at 2 K.
- (b) Simulated emission and absorption spectra at 20 K.
- (c) Simulated emission and absorption spectra at 60 K.





$T = 60\text{K}$
 $\Delta = 0$

— ABSORPTION
 ---- EMISSION



(c)

considered to be the TMCBDT torsional mode. This choice is rationalized on the basis of the 42 cm^{-1} vibration observed in the far-infrared spectrum of TMCBDT vapor (83). This is assigned to the b_{3u} torsion due to its low frequency and infrared activity, assuming the molecule is D_{2h} .

In this section another motion is considered which, qualitatively, is consistent with the DMP calculations. This is the lattice vibration (B_{2g}) which involves out of phase rotation about the z molecular axis. Using the molecular distances and lattice parameters from the x-ray structure (38) the spatial relationships of the molecules in the crystal is shown (to scale) in Fig. 3-7. The view is along the line $a=a'$. In this view the sulfur non-bonding p orbitals are vertical ($||c$). It can be seen that the motion described by the B_{2g} lattice vibration involves the translationally equivalent molecules all moving in phase with respect to each other and out of phase with respect to their translationally inequivalent counterparts; all the molecules labeled 1 move in phase with each other, as do the ones labeled 2, but all the 1, 2 pairs move out of phase with respect to each other.

The direction of motion is shown in Fig. 3-7 with an arrow for motion in the plane of the paper and with + and - for motion out of this plane. It can be seen that positions A and B represent points of closest approach where electrostatic repulsion might give a maximum in the potential function. If the coordinate of the motion is described by the angle of rotation about the z axis, a value of zero for this corresponds to this maximum. Motion along the coordinate simultaneously increases the sulfur-sulfur distance at A and the sulfur methyl group

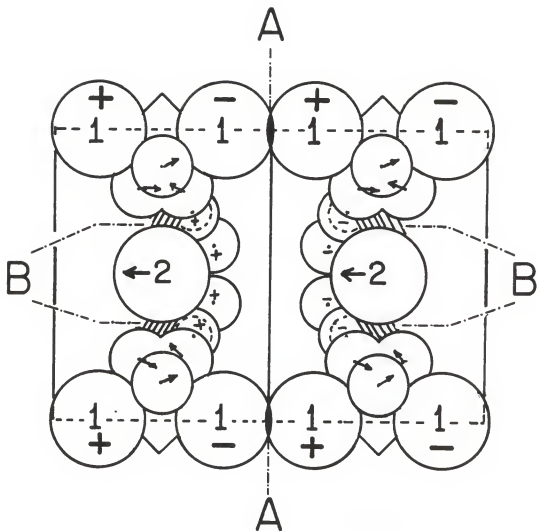


Figure 3-7. Molecular displacements involved in the B_{2g} lattice vibration. The view shown is along an aa^{2g} diagonal (cf. Fig. 3-1) in the unit cell. Two adjacent unit cells are shown. The methyl groups on one side of the molecular plane are omitted for clarity. The direction of motion is indicated by arrows for motion in the plane of the paper and by + or - for motion out of the figure plane. The circles represent van der Waals radii; those labeled 1 and 2 are the sulfur atoms, all others are methyl hydrogens. The figure is drawn to scale, taking the van der Waals radii as 1.85 Å for sulfur and 1.20 Å for hydrogen, the unit cell dimensions from Fig. 3-1 and the atomic coordinates from Table 4-1.

distance at B. This type of behavior could describe a DMP in the ground electronic state.

When the electronic transition to the ${}^3A_u(n\pi^*)$ state occurs, the C=S bond distance is expected to increase. Inspection of Fig. 3-7 shows that in this case the angle of rotation (coordinate of the B_{2g} motion) would have to increase to accommodate the elongated C=S bond, while at the zero position (where all translationally equivalent molecules are collinear) the barrier would increase. This is consistent with the DMP descriptions for the ground and excited electronic states described previously.

While both the intramolecular torsion and intermolecular lattice modes can account for the observed low frequency series of bands near the 0-0 band, there is no direct experimental evidence presently available that can confirm one model or the other. Semiempirical calculations (INDO for example) of the energy as a function of the rotation (and torsion) coordinate could be performed on a cluster of several TMCBDT molecules to determine the potential energy of the ground and lowest triplet state as a possible means to reinforce one model or the other.

In connection with Fig. 3-7 it is seen that if the van der Waals radii for the atoms are taken into account, the TMCBDT molecules are rather close together. In this respect it is not surprising that only one vibrational quantum of the C=S stretch is observed in the absorption spectrum. This fact means that the change in equilibrium position for that coordinate is slight. Whereas in the free molecule the change in this same coordinate could be expected to be greater, in the crystal the lattice restricts this expansion somewhat. A lattice distortion

then follows to achieve a new equilibrium. The lack of progressions in the other intramolecular vibrations observed (*vide supra*) can be viewed in the same way. This is consistent with the small Stokes loss parameter in terms of the exciton picture.

We can now apply the above considerations of steric hindrance to the torsional mode using Fig. 3-7. In this case both sulfur atoms would move out of plane and the methyl groups would undergo a symmetric rock in the opposite direction. It can be seen from Fig. 3-7 that the same steric effects considered above apply to the torsional motion. Thus, the harmonic torsional motion experiences a steric perturbation at the point of planarity. This implies that a DMP would not be seen in the isolated molecule case. Since there is no experimental evidence to support or reject either of these models, it must be concluded that either one or both is operative in TMCBDT.

Summary

The $T_1 \leftarrow S_0$ absorption spectrum of crystalline TMCBDT at 1.6 K has been assigned on the basis of polarization to the 3A_u molecular state. Evidence for a double minimum potential in the ground and excited state is presented and it is shown that this model accounts for all the observed low frequency bands (except the 75 cm^{-1} band) and all the non-trap band origins in emission. The physical nature of this potential is discussed and it is concluded that it may arise from either a distorted molecular configuration along the torsion coordinate or from a B_{2g} lattice vibration or a combination of both; the present data are not able to distinguish between them. The remaining low frequency vibration at 75 cm^{-1} may then be tentatively assigned to the

A_{2g} lattice mode. The other vibrations observed are assigned by analogy to the corresponding dione except the C=S stretch at 970 cm^{-1} .

CHAPTER 4
SPIN-ORBIT COUPLING IN TETRAMETHYL-1,3-CYCLOBUTANEDITHIONE

Introduction

In this chapter the expression for the zero-field transition moment of the $T_1 \leftarrow S_0$ transition in single crystal TMCBDT is derived for comparison with that obtained in Chapter 5. The various matrix elements are evaluated using Extended Hückel wavefunctions and the results of the calculations discussed.

$T_1 \leftarrow S_0$ Crystal Transition Moment for TMCBDT

For a 3A_u site (molecular) state there are two possible crystal states corresponding to the symmetric (A_{1u}) and antisymmetric (B_{1u}) combinations of site 1 and site 2 wavefunctions. These can be written

(85) as

$${}^3\psi_r \begin{Bmatrix} A_{1u} \\ B_{1u} \end{Bmatrix} = \frac{1}{\sqrt{2}} \left\{ {}^3\phi_{(A_u)}^{r(1)} \phi_o^{(2)} + {}^1\phi_o^{(1)} {}^3\phi_{(A_u)}^{r(2)} \right\} \quad (4-1)$$

where $\phi_o^{(i)}$ is the wavefunction for the ground electronic state of the i th molecule. The wave function for the crystal ground state is

$${}^1\psi_o(A_{1g}) = {}^1\phi_o^{(1)} \phi_o^{(2)}.$$

In order to mix singlet character into the triplet wavefunctions we apply the spinorbit coupling interaction via first order perturbation theory.

The spin-orbit operator used is that appropriate to a central field approach for a polyatomic molecule and may be written as (86)

$$H_{so} = \sum_i \left[\sum_{\alpha} (2m^2 c^2)^{-1} r_{i\alpha}^{-1} (\partial V(r_{i\alpha}) / \partial r_{i\alpha}) \right] \cdot \vec{\ell}_i \cdot \vec{S}_i \quad (4-2)$$

where α and i refer to nuclear and electron indexes, respectively and the quantity in [] will be referred to as A_i . $\vec{\ell}_i$ and \vec{S}_i are orbital and spin angular momentum operators respectively for the i th electron.

Since we will ultimately reduce all terms to the molecular level it will be useful to briefly comment on the spin functions. For the case of an isolated molecule in the absence of external magnetic fields the molecular spins will be aligned with the molecular symmetry axes (87). In this case the spin orbit operator is totally symmetric since both the orbital angular momentum and spin angular momentum operators transform as the rotations in the point group.

This spin alignment effect has been observed experimentally by direct paramagnetic absorption measurements on the T_1 state of naphthalene in a dilute mixed crystal of the durene host by Hutchison and Mangum (88).

In a single crystal, however, the behavior of the spin-spin interaction insofar as the spin axes orientations are concerned, is governed for the most part by the nature of the excitation interaction. In the case of triplet excitons for which the Davydov splitting is greater than the zero-field splitting of the triplet sublevels (D), the principal directions of the spin-spin interaction tensor correspond to the crystal axes (89,90). In this case, for two molecules per unit cell, both molecules have a common spin coordinate system which is space fixed and unaffected by rotations of the molecular framework (85,91).

Thus the spin operators are totally symmetric, and the spin-orbit operator now takes its symmetry properties solely from the orbital angular momentum operator. This same situation arises when an external magnetic field is present in the crystal, but in that case the spins become quantized along the field axis system (85).

For the case of the TMCBDT crystal there is no Davydov splitting in the observed $T_1 + S_0$ spectrum, indeed the FWHM line width of the 0-0 band is $\sim 3 \text{ cm}^{-1}$ which is greater than the expected zero field splitting. Hence the molecule fixed spins are the correct choice for the zero field description of the TMCBDT crystal states.

Because of the absence of intermolecular interactions the spin-orbit Hamiltonian can be written as a sum of one molecule operators having the form of Eq. 4-2. Thus we have

$$H_{so} = H_{so}(a) + H_{so}(a') + H_{so}(c) \quad (4-3)$$

$$H_{so}(a) = \ell_x^2 [(h_{so}(x))_1 + (h_{so}(x))_2] + \ell_y^2 [(h_{so}(y))_1 + (h_{so}(y))_2]$$

$$H_{so}(c) = n_z^2 [(h_{so}(z))_1 + (h_{so}(z))_2]$$

where ℓ_u and n_u are the direction cosines of the u th molecular axis with respect to the a and c crystal axes, respectively. For $H_{so}(a')$ a similar expression to that of $H_{so}(a)$ arises but with m_x and m_y . For the TMCBDT crystal structure $\ell_x^2 = m_x^2 = \ell_y^2 = m_y^2 = \frac{1}{2}$, while $n_z^2 = 1$, for both molecules.

We now apply the first order correction to the triplet wave function in Eq.4-1. Using well known methods (70,85,87,92) we obtain

$${}^3\psi_r \begin{Bmatrix} A_{1u} \\ B_{1u} \end{Bmatrix} = {}^3\psi_r \begin{Bmatrix} A_{1u} \\ B_{1u} \end{Bmatrix} + \sum_k \Delta E_k^{-1} \langle {}^1\psi_k | H_{so} | {}^3\psi_r \begin{Bmatrix} A_{1u} \\ B_{1u} \end{Bmatrix} \rangle {}^1\psi_k \quad (4-4)$$

where r is the x , y or z triplet sublevel in zero field and the summation is over all perturbing singlets, k . ΔE_i is the energy difference between the perturbing singlet and T_1 .

The above takes into account perturbation of the triplet state by singlet states of the appropriate symmetry. Perturbation of the ground state by triplet states is also possible. Indeed it was shown by Goodman and Krishna (93) that for an isolated molecule single configuration semiempirical wavefunction the contribution to the $T_1 + S_0$ transition moment from allowed $T_n + T_1$ transitions is not negligible. In fact, for pyrazine and pyrimidine this contribution is larger than that from allowed $S_n + S_0$ transitions.

To include this effect in the present case, the first order perturbation correction of the ground state has to be considered. This is

$$^1\psi_0 = ^1\psi_0 + \sum_{\ell} \Delta E_{\ell}^{-1} \langle ^3\psi_{r\ell} | H_{so} | ^1\psi_0 \rangle ^3\psi_{r\ell} \quad (4-5)$$

In the D_{4h} factor group $H_{so}(|c)$ is of A_{2g} symmetry and $H_{so}(|c)$ is of E_g symmetry. Thus, only triplet states of A_{2g} and E_g symmetry will perturb the ground state. Since B_{1g} site states correlate with A_{2g} crystal states, while B_{2g} and B_{3g} site states both correlate with E_g crystal states, we have

$$^3\psi_{r\ell} + (A_{2g}) = \frac{1}{\sqrt{2}} \left\{ \begin{matrix} 3\phi_{(B_{1g})}^{r(1)} & \phi_o^{(2)} \\ + & \phi_o^{(1)} 3\phi_{(B_{1g})}^{r(2)} \end{matrix} \right\}$$

and

$${}^3\psi_{r\ell}(E_g) = \frac{1}{\sqrt{2}} \left\{ {}^3\psi_{r(B_{2g})}^{(1)} \phi_o^{(2)} + \phi_o^{(1)} {}^3\psi_{r(B_{2g})}^{(2)} \right\} \quad (4-6)$$

$${}^3\psi_{r\ell}(E'_g) = \frac{1}{\sqrt{2}} \left\{ {}^3\psi_{r(B_{3g})}^{(1)} \phi_o^{(2)} + \phi_o^{(1)} {}^3\psi_{r(B_{3g})}^{(2)} \right\}$$

The E_g functions are doubly degenerate, thus all four must be used in the perturbation. Exactly the same applies to E_u functions which appear implicitly in Eq. 4-4. The corrected ground state wavefunction will then be

$${}^1\phi_o = {}^1\psi_o + \sum_{\ell} \Delta E_{\ell}^{-1} < {}^3\psi_{c\ell} | H_{so}(c) | {}^1\psi_o > {}^3\psi_{c\ell} \quad (4-7)$$

$$+ \sum_{\ell'} \Delta E_{\ell'}^{-1} < {}^3\psi_{a\ell'} | H_{so}(a) | {}^1\psi_o > {}^3\psi_{a\ell'} + \sum_{\ell''} \Delta E_{\ell''}^{-1} < {}^3\psi_{a,\ell''} | H_{so}(a') | {}^1\psi_o > {}^3\psi_{a,\ell''}$$

while for the ${}^3\Psi \begin{Bmatrix} A_{lu} \\ B_{lu} \end{Bmatrix}^{+,-}$ we have

$${}^3\Psi_{r+} = {}^3\psi_{+} + \sum_k \Delta E_k^{-1} < {}^1\psi_k | H_{so}(c) | {}^3\psi_{1r+} > {}^1\psi_k \quad (4-8)$$

$$+ \sum_{k'} \Delta E_{k'}^{-1} < {}^1\psi_{k'} | H_{so}(a) | {}^3\psi_{r+} > {}^1\psi_{k'} + \sum_{k''} \Delta E_{k''}^{-1} < {}^1\psi_{k''} | H_{so}(a') | {}^3\psi_{r+} > {}^1\psi_{k''}$$

In these equations the indices ℓ, ℓ' and ℓ'' refer to all site states of symmetry $B_{1g}, (B_{2g}, B_{3g})$ and (B_{2g}, B_{3g}) respectively, while k, k' and k'' refer to the analogous ungerade states, (\pm combinations).

The crystal transition moment is found by evaluating the integral $< {}^3\psi_{1+}^r | e\mathbf{r} | {}^1\psi_o >$, and it is seen that two components arise, each with the 3 spatial components a, a' and c . Because of the symmetry restrictions in the site group, the polarization directions (a, a') and c are associated with $(H_{so}(a), H_{so}(a'))$ and $H_{so}(c)$, respectively. Thus we have

$$\begin{aligned}
\langle {}^3\psi_{1u}(+) | e\vec{r} | {}^1\psi_0 \rangle &= \sum_{\vec{u}} \sum_{\vec{k} \in u} \Delta E_k^{-1} \langle {}^1\psi_k | H_{so}(u) | {}^3\psi_{1u}(+) \rangle^* \langle {}^1\psi_k | e\vec{u} | {}^1\psi_0 \rangle \\
&+ \sum_{\vec{u}} \sum_{\vec{k} \in u} \Delta E_k^{-1} \langle {}^3\psi_k | H_{so}(u) | {}^1\psi_0 \rangle \langle {}^3\psi_k | e\vec{u} | {}^3\psi_1 \rangle
\end{aligned} \quad (4-9)$$

Here u is the spatial component of r and $\vec{k} \in u$ means that the sum is over those states k whose symmetry is appropriate to u .

Now, expanding H_{so} (cf. Eq. 4-3), expressing the dipole operators in terms of molecular vectors (cf. Table 5-1), and abbreviating the wavefunctions as (for example, Eq. 6)

$${}^3\psi_r(A_{2g}) = {}^3B_{1g}^r(+) \quad \text{and} \quad {}^3\psi_r(E_g) = {}^3B_{3g}^r(+),$$

$$\text{also } |0\rangle = |{}^1\phi_0^1 \quad {}^1\phi_0^2\rangle,$$

we obtain for the transition moments to the crystal ${}^3\psi_1(+)$ states

$$\begin{aligned}
\langle {}^3\psi_{(+)} | e\vec{r} | {}^1\psi_0 \rangle &= \sum_{\vec{k}} \Delta E_k^{-1} \langle {}^1B_{1u}(+) | n_z^2 h_{so}(z) (1+2) | {}^3A_u^z(+) \rangle^* \langle {}^1B_{1u}(+) | n_z(\vec{z}_1 + \vec{z}_2) | 0 \rangle \\
&+ \sum_{\vec{k}} \Delta E_k^{-1} \langle {}^1B_{2u}(+) | \ell_y^2 h_{so}(1+2) | {}^3A_u^y(+) \rangle^* \langle {}^1B_{2u}(+) | \ell_{y2}\vec{y}_2 + m_{y1}\vec{y}_1 + m_{y2}\vec{y}_2 + \ell_{y1}\vec{y}_1 | 0 \rangle \\
&+ \text{same term for } x, {}^1B_{3u}(+) \\
&+ \sum_{\vec{k}} \Delta E_k^{-1} \langle {}^3B_{1g}(+) | n_z^2 h_{so}(1+2) | 0 \rangle \langle {}^3B_{1g}(+) | n_z(\vec{z}_1 + \vec{z}_2) | {}^3A_u^z(+) \rangle \\
&+ \sum_{\vec{k}} \Delta E_k^{-1} \langle {}^3B_{2g}(+) | \ell_y^2 h_{so}(1+2) | 0 \rangle \langle {}^3B_{2g}(+) | \ell_{y1}\vec{y}_1 + \ell_{y2}\vec{y}_2 + m_{y1}\vec{y}_1 + m_{y2}\vec{y}_2 | {}^3A_u^y(+) \rangle \\
&+ \text{same term for } x, {}^1B_{3g}(+)
\end{aligned} \quad (4-10)$$

and

$$\begin{aligned}
\langle {}^3\psi_{(-)} | e\vec{r} | {}^1\psi_0 \rangle &= \sum_{\vec{k}} \Delta E_k^{-1} \langle {}^1B_{1u}(-) | n_z^2 h_{so}(1+2) | {}^3A_u(-) \rangle^* \langle {}^1B_{1u}(-) | \vec{z}_1 + \vec{z}_2 | 0 \rangle \\
&+ \sum_{\vec{k}} \Delta E_k^{-1} \langle {}^1B_{2u}(-) | \ell_y^2 h_{so}(1+2) | {}^3A_u^y(-) \rangle^* \langle {}^1B_{2u}(-) | \ell_{y1}\vec{y}_1 + \ell_{y2}\vec{y}_2 + m_{y1}\vec{y}_1 + m_{y2}\vec{y}_2 | 0 \rangle \\
&+ \text{same term for } x, {}^1B_{3u}(-)
\end{aligned}$$

$$\begin{aligned}
& + \frac{\Delta E_{\ell}^{-1}}{\ell} \langle {}^3B_{1g}(+) | h_{soz}(1+2) \cdot n_z^2 | 0 \rangle \langle {}^3B_{1g}^z(-) | \\
& + \frac{\Delta E_{\ell}^{-1}}{\ell} \langle {}^3B_{2g}(+) | h_{soy}(1+2) \cdot \ell_y^2 | 0 \rangle \langle {}^3B_{2g}^y(-) | \ell_{y1} \vec{y}_1 + \ell_{y2} \vec{y}_2 + m_{y1} \vec{y}_1 + m_{y2} \vec{y}_2 | {}^3A_u^y(+) \rangle \\
& + \text{same term for } x, {}^3B_{3g}(+) \quad (4-11)
\end{aligned}$$

The vector $\vec{r} = (\vec{a}, \vec{a}', \vec{c})$. It can be seen from Table 5-1 that the second term above, for example, reduces to $\frac{1}{2\sqrt{2}} M_y^{s*}(\vec{a} + \vec{a}')$ with

$$\begin{aligned}
M_y^{s*} &= \frac{1}{2\sqrt{2}} \sum_k \langle h_{k,1}(y) \rangle^* m_{ok}, \\
&= \frac{1}{2\sqrt{2}} \sum_k \Delta E_k^{-1} \langle {}^1B_{2u} | h_{so}(y) | {}^3A_u^y \rangle^* \langle {}^1A_g | y | {}^1B_{2u} \rangle \quad (4-12)
\end{aligned}$$

having reduced the integrals to ones over isolated molecule states.

The superscript s refers to the contribution from S-S allowed transitions; similarly t is used for T-T allowed contributions.

Reducing all terms in the same way and setting

$$M_u = M_u^{s*} + M_u^t \quad (4-12a)$$

we have

$$\begin{aligned}
\langle {}^3\Psi(+) | e\vec{r} | {}^1\Psi_0 \rangle &= \vec{M}_a(+) + \vec{M}_{a'}(+) + \vec{M}_c(+) \\
&= \frac{1}{2\sqrt{2}} (M_x + M_y)(\vec{a} + \vec{a}') + \frac{1}{2\sqrt{2}} M_z \vec{c} \quad (4-13a)
\end{aligned}$$

and

$$\begin{aligned}
\langle {}^3\Psi(-) | e\vec{r} | {}^1\Psi_0 \rangle &= \vec{M}_a(-) + \vec{M}_{a'}(-) \\
&= \frac{1}{2\sqrt{2}} (M_x - M_y)(\vec{a} + \vec{a}') \quad (4-13b)
\end{aligned}$$

As expected for zero field, we find that the two components $\perp c$ are equal for both $+$ and $-$ crystal states. Thus if these two states exhibited a Davydov splitting one would find a band polarized along c

and two bands polarized $\perp c$. Each band $\perp c$ would be further split into the x and y triplet spin components. The z component of the + crystal state is not necessarily zero and $\parallel c$ while that for the - state is zero by symmetry.

Because there is no experimental evidence to suggest that these transitions could be separately observed the intensity of the $T_1 + S_0$ transition in the TMCBDT single crystal in zero field can be obtained by adding the intensity of the + and - components. This is given by the square of the dot product of the transition moment with the electric field vector (70); and expressed as

$$\begin{aligned}
 I(T_1 + S_0) \propto & |(M_a(+)+M_a(+)) \cdot E_{\perp c}|^2 + |M_c(+)\cdot E_{\parallel c}|^2 \\
 & + |(M_a(-)+M_a(-)) \cdot E_{\perp c}|^2 \\
 I(T_1 + S_0) \propto & \frac{1}{4} (M_x^2 + M_y^2) E_{\perp c}^2 + \frac{1}{2} M_z^2 E_{\parallel c}^2
 \end{aligned} \tag{4-14}$$

In zero field the electronic spins are sharply defined along the molecular axes and the electric field can then induce transitions only along these directions. Light propagation in the crystal is such that for unpolarized incident light, the electric vector will oscillate in two planes only, one \perp to c and one $\parallel c$. For this reason cross terms between a and c do not appear. The cross terms between x and y then cancel as a result of adding the intensity of the transition to the + and - crystal states. As will be seen later the situation is very different in the presence of a magnetic field.

In the next section the matrix elements of H_{so} and \vec{r} are evaluated.

Evaluation of Matrix Elements: $\langle H_{so} \rangle$ and $\langle \vec{m} \rangle$.

Spin-Orbit Hamiltonian

In the previous section the H_{so} operator was written in the form given by McClure (86,92,93). This is an approximation to the more rigorous magnetic Hamiltonian for a many electron system (87,94) applied to polyatomic molecules by Ginsburg and Goodman (95).

This latter Hamiltonian contains three terms which contribute to the spin orbit coupling. 1) The nuclear field term: a one electron term which describes the interaction of the spin of an electron with its own orbital motion in the electric field of the nucleus, 2) the spin-same orbit term: a two electron term which describes the same spin-orbit interaction as in 1) but in the electric field of the other electrons and 3) the spin-other-orbit term: another two electron term describing the interaction of the spin of one electron with the orbit of another electron. Neglecting all multicenter terms which arise (i.e. in 1. the interaction of an electron on nucleus A with the field of nucleus B) and using formaldehyde as a representative molecule they found, with the CNDO wavefunctions of Pople and Segal (96), that terms 2 and 3 contributed only 4 percent to the total H_{so} matrix element. Similarly (ref.21 in 95) they found the same relative magnitudes in the one and two electron terms in the spin-orbit interactions of the mono- and di-azines. The work of Ginsburg and Goodman (95) serves as a basis for justifying McClure's central field approach to the spin-orbit Hamiltonian for a polyatomic molecule, which has been widely used since. This form of the Hamiltonian seems suitable for the present work on TMCBDT.

Because of the transformation properties of the spin functions that will be used however, it is convenient to write the spin-orbit Hamiltonian as a sum of an antisymmetric (with respect to electron index interchange) part and a symmetric part. For the present case involving two optical electrons this may be written as

$$h_{so} = \sum_{i=1}^2 \sum_u R_{ui} S_{ui} = \frac{1}{2} \sum_u (R_{u1} - R_{u2}) (S_{u1} - S_{u2}) + \frac{1}{2} \sum_u (R_{u1} + R_{u2}) (S_{u1} + S_{u2}) \quad (4-15)$$

where $R_{ui} = A_i \overset{\rightarrow}{\ell}_{ui}$ and $u = x, y$ and z .

The second term (symmetric) contributes zero to the matrix elements between states of different multiplicity since it does not change the total spin. The first term however has the effect of changing triplet spin functions into the singlet spin function and vice versa. Thus we may write the spin orbit Hamiltonian as

$$h_{so} = \frac{1}{2} \sum_u \mathbf{R}_u^- \cdot \mathbf{S}_u^- \quad (4-16)$$

The notation h_{so} denotes the one electron spin orbit operator for an isolated molecule as used in Eq. 4-3.

Choice of Wavefunction

Evaluation of the H_{so} matrix elements requires that the wavefunction and energy of the perturbing states be known. To obtain these we choose the Extended Hückel method. This choice is dictated largely because of its qualitative accuracy and simplicity. Previous calculations on tetramethykcyclobutanedione (8) have shown this method to give comparable $\pi\pi^*$ transition energies to CNDO/S and in reasonably good agreement with experiment.

The higher excited states of TMCBDT have not yet been experimentally determined, although work on some Rydberg states has been done (97), so that excited state energies needed in the perturbation treatment have to be obtained from theory or estimated from experimental values of similar molecules. Unfortunately no information on similar molecules exists except for the lowest two singlet states and the lowest triplet state, for example in aromatic thiocarbonyls (29 - 35). In addition no other dithiocarbonyls have been investigated and the nature of the low lying excited states differs from the monocarbonyls; for example, S_2 is $\pi\pi^*$ in monocarbonyls while it is expected to be $n\pi^*$ in TMCBDT, by analogy with TMCBD (8). For these reasons we assume that using EHT orbital energy differences for the excited state energies in the perturbation approach gives a reasonable qualitative estimate of the true energies.

Following the approach of Masmanidis, Jaffe and Ellis (98) (without including the CI) we use the notation V_{ij} to denote a singlet state single configuration wavefunction formed by promotion of an electron from the occupied (unprimed) molecular orbital i to the virtual orbital (primed) j' . Similarly T_{np}^u will refer to a triplet state (spin sublevel u) having orbitals n and p' singly occupied. Because the H_{so} used is a one electron operator the only part of the determinantal wavefunctions which will contribute nonzero terms is that which contains the singly occupied orbitals (99). Thus we may use the following well known representations of singlet and triplet states (92)

$$V_{ij} = {}^1\phi_{ij}, {}^1\omega; \quad T_{np}^u = {}^3\phi_{np}, {}^3\omega_u.$$

The choice of spin functions ω is that appropriate to the zero field description of the triplet sublevels

$$\begin{aligned} {}^1\omega &= \frac{1}{\sqrt{2}}(\alpha_1\beta_2 - \alpha_2\beta_1) && \text{totally symmetric} \\ {}^3\omega_x &= \frac{1}{\sqrt{2}}(\beta_1\beta_2 - \alpha_1\alpha_2) && R_x \\ {}^3\omega_y &= \frac{1}{\sqrt{2}}(\beta_1\beta_2 + \alpha_1\alpha_2) && R_y \\ {}^3\omega_z &= \frac{1}{\sqrt{2}}(\alpha_1\beta_2 + \alpha_2\beta_1) && R_z \end{aligned} \quad (4-17)$$

with $i = \sqrt{-1}$, and the symmetry transformation properties of the rotations as given above. The orbital parts of the wavefunction are

$${}^1\phi_{ij} = \frac{1}{\sqrt{2}} (\phi_i(1)\phi_j(2) + \phi_i(2)\phi_j(1))$$

and (4-18)

$${}^3\phi_{np} = \frac{1}{\sqrt{2}} (\phi_n(1)\phi_p(2) - \phi_n(2)\phi_p(1))$$

Their symmetry species is the direct product of the representations of the singly occupied molecular orbitals, ϕ_n and ϕ_p , for example. The molecular orbitals ϕ are expressed as linear combinations of Slater type atomic orbitals χ

$$\phi_i = \sum_v C_{iv} \chi_v \quad (4-19)$$

The coefficients C_{iv} are those obtained from a standard EHT calculation. The parameters appropriate to the EHT calculation are given in Table 4-1 for the H, C and S atoms.

Evaluation of $\langle H_{SO} \rangle$ With Respect to EHT Wavefunctions

Now we apply the operator and wavefunction of the previous section to evaluate the m_k^s and m_k^t terms in Eq. 4-12. As mentioned earlier the spin part of the operator h_{SO} converts singlet spin functions into triplet functions and vice versa. The results of this operation are summarized as follows (δ is the Kronecker delta):

$$S_u^{-3} \omega_v = \chi^1 \omega_{uv} \delta_{uv} \quad \text{and} \quad S_u^{-1} \omega = \chi^3 \omega_u.$$

Rewriting the relevant part of Eq. 4-12 here we get (using the y component as an example)

$$\langle h_{k,1}(y) \rangle = \frac{\langle v_{ij}^{k'} | \frac{1}{2} R_y^- S_y^- | T_{np'} \rangle}{E_t - E_s} \quad (4-20)$$

Here k' refers to the k^{th} singlet state perturber with symmetry appropriate for coupling via $h_{SO}(y)$, and the T state is the triplet state in question. The second factor in this equation is the electric dipole allowed transition moment for the singlet ground state to singlet excited state perturber, $v_{ij}^{k'}$, and will be evaluated later.

Integrating out the spin from the first factor we have

$$\frac{\langle v_{ij}^{k'} | \frac{1}{2} R_y^- S_y^- | T_{np'} \rangle}{E_t - E_s} = \frac{1}{2} \cdot \chi \frac{\langle i_1 j'_2 + j'_1 i_2 | R_y^- | n_1 p'_2 - p'_1 n_2 \rangle}{E_t - E_s} \quad (4-21)$$

Where we have abbreviated using the molecular orbital indices, and the subscripts 1 and 2 refer to electrons. Expanding the operator and carrying out the integrations we find that two types of integrals arise. Since this is a one electron operator the only nonzero terms in this integral will be those involving at most three different orbitals, that is (following the notation of Ref. 98).

if either $i=n$ or $p'=j'$. These results are conveniently expressed in Table II of Ref. 98. One factor of 2 cancels after collecting identical terms from electrons 1 and 2 and we get for the right hand side

$$+ \frac{\hbar}{2} \cdot \frac{\langle i | R_y | n \rangle}{E_t - E_s} \quad \text{or} \quad - \frac{\hbar}{2} \cdot \frac{\langle j' | R_y | p' \rangle}{E_t - E_s} \quad (4-22)$$

As will be seen later this determines what type of states ($\sigma\pi^*$, $\pi\pi^*$ etc.) will be likely perturbing states for a given type of triplet state.

We now turn to the operator $R_{ui} = A_i \overset{\rightarrow}{\ell}_{ui}$, (i now references electronic coordinates) with A as defined in Eq. 4-2. Since $\overset{\rightarrow}{\ell}_u$ is the angular momentum operator (x, y or z component) it will affect only the angular part of the wavefunction. Thus after operating on the ket and integrating over the angular coordinates we are left with integrals involving the operator A and the radial part of the wavefunction with the integration over radial coordinates only. When these integrals are calculated using STO wavefunctions the results are not always good when compared to the spectroscopic values, (cf., for example, Ref. 100). More common is the practice of substituting an empirically determined spin orbit coupling constant, ζ_α , for the matrix element of A. The values given by McClure (86) were used in this work. Returning to the angular momentum operator, we recall (98) the following properties:

$$\overset{\rightarrow}{\ell}_u \phi(s) = 0; \quad \overset{\rightarrow}{\ell}_u \phi(p_v) = \pm i \hbar \delta(p_\tau) (1 - \delta_{uv}) \quad u, v, \tau = x, y, z$$

Thus s atomic orbitals will contribute nothing and p orbitals are rotated into another p orbital according to a cyclic permutation, the sign being positive in forward direction ($x \rightarrow y \rightarrow z$) and negative

in reverse ($z \rightarrow x$) direction. Similar results are found for d orbitals but are omitted here because they are not included in the wavefunction. This is justified on the grounds that even though the orbital coefficient may be found to be significant in the LCAO expansion in calculating other properties, with respect to spin-orbit coupling d electrons are expected to contribute much less than p electrons in the case of TMCBDT. This is apparent when ζ is considered. For an electron in the $n\ell$ sublevel $\zeta_{n\ell}$ is given by

$$\zeta_{n\ell} = \frac{e^2 \hbar^2}{2m c^2 a_0^3} \frac{z^4}{n^3 (\ell+1) (\ell+1/2) \ell} \quad (4-23)$$

where m is the mass of electron, c is the speed of light, a_0 is the Bohr radius, e is the electron charge, \hbar is Planck's constant $/2\pi$ and $n, \ell =$ principal and orbital angular momentum quantum numbers. It is seen that for a given z the ratio of the ζ value for a 3d electron to that of a 3p electron is $\frac{1}{5}$. Neglecting this is within acceptable limits considering the other approximations involved in the calculation. This also facilitates the EHT calculation since d electrons are not included in the version available to us (101).

Introducing the LCAO approximation Eq. 4-19 into 4-22 and integrating over the radial coordinates we have, for $j='p'$ example,

$$\langle \phi_i | \sum_{\alpha} \zeta_{\alpha} \vec{\ell}_{\alpha} | \phi_n \rangle = \frac{1}{\hbar} \sum_{\alpha} \zeta_{\alpha} \sum_{\nu} \sum_{\rho} C_{\nu i} C_{\rho n} \langle \chi_{\nu} | \vec{\ell}_y | \chi_{\rho} \rangle \quad (4-24)$$

The \hbar^{-1} factor is there because ζ is proportional to \hbar^2 (Eq. 4-23), one \hbar each from spin and orbital operators. The sums are such that both ν and ρ must be orbitals centered on the same atomic center, α , for the integral to be nonzero. This comprises the Zero Differential

Overlap approximation. Further, as mentioned above, the integral on the right hand side of 4-23 will be zero if $v=\rho$, or if ζ represents an s orbital.

Deferring until later the details of the types of states responsible for the spin-orbit coupling mechanism in the specific case of TMCBDT, it is easy to see from (8) that if the state in question is of $^3\pi\pi^*$ type, for example, the y component of the spin-orbit operator will mix in $^1\pi\pi^*$ states. This is so because the common orbital π^* will drop out to give integrals of the type

$$\langle \pi | \ell_y | \sigma \rangle \quad (j'=k')$$

Now the σ orbital may be made up of an in-plane p_z orbital centered on, say, a carbonyl oxygen and involved in a σ bond with the carbonyl carbon (z axis along the C=O bond, local C_{2v} symmetry). Then $\vec{\ell}_y(p_z) = +i \hbar p_x$, with p_x being an out of plane π type orbital, and if the p_x of oxygen from the left side, in the π molecular orbital, has a nonzero coefficient, we have

$$\frac{\frac{1}{2} \frac{1}{\hbar} \zeta_o \cdot C_{(p_x, \pi; o)} C_{(p_z, \sigma; o)} \cdot i \hbar \langle p_x | p_x \rangle}{E_t - E_s} .$$

This represents one term in the expansion of Eq. 4-21. The spin orbit coupling constant is usually given in cm^{-1} so that the term is unitless when the ΔE is in cm^{-1} . For a thorough discussion of the ideas sketched out here see Azumi, McGlynn and Kinoshita (102).

In summary, we may express these results as follows:

$$\langle h_{k'1}(y) \rangle = \frac{1}{2} \sum_{\alpha} \sum_{\nu} \sum_{\rho} C_{vi}^{k'} C_{\rho\alpha}^{\nu} \zeta_{\alpha} \zeta_{\nu} \rho (1 - \delta_{in}) / (E_1 - E_k) \quad (4-25)$$

Equation 4-25 represents one of the singlet-perturbing- T_1 terms in the sum of Eq. 4-12. The $h(y)$ will pick out the appropriate v and ρ , these being either a p_x or a p_z orbital on the α center (not hydrogen). The i and n will depend on the two states being coupled by $h(y)$.

Thus far we have detailed the evaluation of only one type of spin-orbit matrix element that arises in the transition moment between the ground state and first excited triplet state, namely, that due to intensity borrowing from electric dipole allowed singlet-singlet transitions. As pointed out earlier there are also significant contributions to the $T_1 \leftarrow S_0$ transition probability which are due to intensity borrowing from triplet-triplet transitions originating in the T_1 state (93). Evaluation of these matrix elements proceeds in a manner similar to the above, but in this case only $\langle n | R | p' \rangle$ terms (103) arise ($n=n$) because the ground state orbital wavefunction is just

$$V_0 = \phi_n \phi_n, \quad (4-26)$$

the n orbital being in common with the occupied orbital in the triplet state T_{np}^0 , which perturbs the ground state. These have a factor of $\sqrt{2}$ in front, as a consequence of the closed shell nature of the wavefunction above. It is not necessary to expand further on these latter matrix elements here.

An important part of the matrix elements discussed thus far is the energy denominator. In this regard we need only mention that the state energies are calculated from the molecular orbital energies obtained from the EHT calculation. For example, for a state described

by an excitation from an occupied orbital i to the virtual orbital j' we would have

$$E_{ij'} = 2 \sum_{k \neq i, j'}^{\text{occ}} \epsilon_k + \epsilon_i + \epsilon_{j'} \quad (4-27)$$

In the EHT approximation, however the singlet and triplet states arising from a given excitation are degenerate. This introduces an error equal to the S-T splitting (98) for that state. The magnitude of this splitting varies with the type of molecule in question, for example in aromatic hydrocarbons it can be as large as 20000 cm^{-1} (104) whereas in carbonyl systems it is usually on the order of $2000\text{-}6000 \text{ cm}^{-1}$ (104) at most. In the particular case of TMCBDT we saw in Chapter 3 that we have experimental evidence that, for the lowest excited state, the ST splitting is about 1400 cm^{-1} . As will be seen later this will amount to about 15% of the smallest energy denominator in the $\langle h \rangle$ matrix elements. This is acceptable even in view of the fact that the observed S_1 in the crystal spectrum of TMCBDT is $\sim 18200 \text{ cm}^{-1}$ and it is calculated from EHT as 18700 cm^{-1} , an error of only $\sim 3\%$, because we can be reasonably sure that the "accuracy" will decrease with increasing state energy. Thus we approximate the error in the energy denominators as being at least 15-20%.

Transition Moment With Respect to EHT Wavefunctions

Two perturbation processes render the spin forbidden $T_1 \leftarrow S_0$ transition allowed: 1) the mixing of singlet character into the triplet state (T_1) wavefunction and, 2) the mixing of triplet character into the singlet ground state (S_0) wavefunction via the spin-orbit perturbation. The intensity of the transition is determined by the sum of

the various spin and orbital symmetry allowed $S_k \leftarrow S_0$ and $T_\ell \leftarrow T_1$ transition moments whose coefficients depend on the magnitude of the $\langle h_{so} \rangle$ matrix elements. Having defined our approximate wavefunction by the EHT method we can evaluate the various transition moments needed in Eqs. 4-10 to 4-12. Once again, it would be desirable to have experimental oscillator strengths for the allowed transitions to the various perturbing states, but this data is even more scarce than the energy of the states. Since the EHT method is carried out with respect to a STO basis, a procedure similar to that of Jaffe and coworkers (92,105) is appropriate.

The transition moments to be calculated are of the type appearing in Eq. 4-12, namely:

$$\vec{m}_{ok} = \langle \phi_o^1 | \vec{er} | \phi_k^1 \rangle \quad (4-28a)$$

for the singlet-singlet transitions, while for the triplet-triplet transitions we have

$$\vec{m}_{1\ell} = \langle \phi_1^3 | \vec{er} | \phi_\ell^3 \rangle \quad (4-28b)$$

In the latter case $r=u$ ($u=x, y$ or z) because of the D_{2h} symmetry, and $u_1 = u_\ell$ since only transitions between the same sublevels are electric dipole allowed due to orthogonality of the spin functions (105). Once the spin functions are integrated out, and Eqs. 4-18 and 4-19 substituted in we find once again three types of integrals:

$\frac{1}{\sqrt{2}} \langle \phi_j | \vec{r} | \phi_i \rangle$ for the singlet-singlet transitions, while $\frac{1}{2} \langle \phi_{n_\ell} | \vec{r} | \phi_{n_1} \rangle$ and $\frac{1}{2} \langle \phi_{p_\ell} | \vec{r} | \phi_{p_1} \rangle$ apply to the triplet-triplet transitions. The subscripts on the n and p are to differentiate the initial (T_1) and final (T_ℓ) states. These are integrals over two molecular orbitals which are nonzero only if the direct product of their irreducible

representations is the same as that of the cartesian component of \vec{r} that we wish to calculate. Furthermore they are identical in form so we need only elaborate the details for $\vec{m}_{ok} = \frac{1}{\sqrt{2}} \langle \phi_j, | \vec{r} | \phi_i \rangle$.

In doing so, it will be convenient to express Eq. 4-19 in terms of atomic orbitals indexed on atomic centers as follows:

$$\phi_i = \sum_{(\alpha)} \sum_{\nu} C_{i\nu} \chi_{\nu} \quad (4-29)$$

substituting into \vec{m}_{ok} , we get

$$\vec{m}_{ok} = \sum_{(\alpha)} \sum_{\nu} C_{j\nu} \chi_{\nu} \left| e^{\vec{r}} \right| \sum_{(\alpha)} \sum_{\rho} C_{i\rho} \chi_{\rho} \quad (4-30)$$

From this it can easily be seen that four types of terms arise, and are given by Ellis and coworkers (92, 105) as

$$\begin{aligned} \vec{m}_{ok} = & \sum_{(\alpha)} \sum_{\nu} C_{j\nu} \{ C_{\nu i} \langle \nu | \vec{r} | \nu \rangle + \sum_{\rho} C_{\rho i} \langle \nu | \vec{r} | \rho \rangle \\ & + \sum_{\beta \neq \alpha} \sum_{\rho} C_{\rho i} \langle \nu | \vec{r} | \rho \rangle \} \quad (A) \quad (B) \end{aligned} \quad (4-31)$$

First, there are integrals over the same atomic orbital type centered on the same atom, these are labeled A. Second, are those involving different atomic functions on the same atom, labeled B. The last term in the above equation represents integrals over atomic functions on two centers (ν on α and ρ on β) and is broken down into cases where $\nu = \rho$ and $\nu \neq \rho$. The latter two terms will be neglected in keeping with the ZDO approximation (92). The term labeled B would also be neglected in this approximation; however, for certain types of transitions ($n\pi^*$) it is dominant and following Ellis and coworkers (92, 105) it will be retained.

The integrals in A and B then reduce to

$$A = \langle v | \vec{R}_\alpha + \vec{r}_{i\alpha} | v \rangle = \vec{R}_\alpha$$

$$B = \langle v | \vec{R}_\alpha + \vec{r}_{i\alpha} | \rho \rangle = \langle v | \vec{r} | \rho \rangle$$

where \vec{R} is the position vector for the nucleus α with respect to the molecule fixed coordinate system and \vec{r} is now the position of the electron i on atom α in the coordinate system centered on atom α . The B value will depend on the symmetry of the atomic orbitals v and ρ , and can be seen (105) to be

$$\langle s | u | p_u \rangle = \langle p_u | u | s \rangle$$

and

$$\langle p_u | u | p_v \rangle = \langle s | u | s \rangle = 0 \quad u, v = x, y, \text{ or } z.$$

We employ the STO functions (106)

$$\chi_v(r, \theta, \phi) = N_v r^{n-1} \exp(-\xi r) Y_\ell^m(\theta, \phi) \quad (4-32)$$

where n , ℓ and m are the principal, angular momentum and magnetic quantum numbers, respectively, for the orbital v ; ξ is its Slater exponent and N the normalization constant (given by $(2\xi)^{n+1/2} / [(2n)!]^{1/2}$), with r , θ and ϕ in the atomic coordinate system centered on the atom on which v is found. $Y_\ell^m(\theta, \phi)$ are the spherical harmonics which describe the angular dependence of the functions (106). We describe the p orbitals as follows:

$$p_z = Y_1^0; \quad p_x = \frac{1}{\sqrt{2}}(Y_1^1 + Y_1^{-1}); \quad p_y = \frac{i}{\sqrt{2}}(Y_1^{-1} - Y_1^1) .$$

We express the $u(x, y \text{ or } z)$ by their appropriate spherical polar representation, substitute the STO's into the integral and integrate over all space to get

$$\langle ns|eu|np_u \rangle = \frac{(2n+1)2^{2n+1}}{\sqrt{3}} \frac{(\xi_s \xi_p)^{n+(1/2)}}{(\xi_s + \xi_p)^{2n+2}} .e \quad (4-33)$$

This is multiplied by a_o to get units of Debye. The result above is true in general for the case where the orbital exponent ξ is not the same for the ns and np electrons. If $\xi_s = \xi_p$ is assumed, as is done in EHT method in this work, the above integral reduces to the more simple form

$$\langle ns|eu|np_u \rangle = \frac{(2n+1)}{2\sqrt{3}} \left(-\frac{e a_o}{\xi_n} \right), \text{ in Debye units.}$$

The transition moment terms A and B are calculated in Debye units in the subroutine MOMENT. Output from this routine consists of a detailed breakdown of the type of terms and individual atom contributions to the transition moment between two states.

Choice of Parameters used in the Calculation

Ideally the exponents of a STO for an s orbital will differ from that of a p orbital (107), however the EHT method frequently makes use of exponents as calculated by Slater's rules in which s and p orbitals with the same principal quantum number have equal exponents (108). The values of the spin-orbit coupling constants ζ for the various atoms are taken from McClure (86). These quantities are collected in Table 4-1 along with other EHT parameters used in the calculation.

Results

The results of the spin-orbit calculations for TMCBDT are summarized in Tables 4-2 to 4-5. Tables 4-2 and 4-3 list all the contributions to $\vec{M} (T_1 + S_O)$. Table 4-4 gives the total transition moment as calculated for the isolated molecule case, and represents the quantity M_u in Eq. 4-13. From these, the oscillator strengths and natural radiative lifetimes are calculated using the standard formulas

TABLE 4-1
PARAMETERS USED IN EHT CALCULATIONS

a. EHT Parameters^a

ATOM	ξ	ζ (cm ⁻¹)	α_s (e.v.)	α_p (e.v.)
C	1.625	28	-21.4	-11.4
S	1.817	382	-20.72	-11.61

b. Atomic Coordinates (Å)

ATOM	x	y	z
H1	2.075068	1.147565	0.0
H2	-2.075068	1.147565	0.0
H3	2.075068	-1.147565	0.0
H4	-2.075068	-1.147565	0.0
H5	1.315648	2.460271	0.875579
H6	1.315648	2.460271	-0.875579
H7	-1.315648	2.460271	0.875579
H8	-1.315648	2.460271	-0.875579
H9	1.315648	-2.460271	0.875579
H10	1.315648	-2.460271	-0.875579
H11	1.315648	-2.460271	0.875579
H12	1.315648	-2.460271	-0.875579
C1	0.0	0.0	1.049015
C2	0.0	0.0	-1.049015

continued

TABLE 4-1-continued

C3	0.0	1.115135	0.0
C4	0.0	-1.115135	0.0
C5	1.323484	1.880792	0.0
C6	-1.323484	1.880792	0.0
C7	1.323484	-1.880792	0.0
C8	-1.323484	-1.880792	0.0
S1	0.0	0.0	2.657015
S2	0.0	0.0	-2.657015

-
- a. The STO exponents, ξ , are calculated using Slater's rules (108) and the spin-orbit-coupling constants ζ are from McClure (86). The coulomb integrals $\alpha(H_{ii})$ for sulfur are from S. D. Thompson, D. G. Carroll, F. Watson, M. O'Donnell and S. P. McGlynn, J. Chem. Phys. 45, 1367 (1966). The α for carbon and hydrogen (-13.6 eV) are from ref. 16.

$$f_u = \frac{8\pi^2 m c v}{3 h e^2} M_u^* M_u \quad \text{and} \quad \frac{1}{\tau_p} = \frac{64 \pi^4 v^3}{3 h c} M_u^* M_u \quad .$$

The constant coefficients in these expressions are 4.703×10^{-7} and 3.136×10^{-7} , respectively, for v in cm^{-1} and M in Debye units.

With respect to the singlet states (Table 4-2) it is seen that the largest contributions to the $T_1 \leftarrow S_0$ transition moment came from electric dipole allowed $S_k \leftarrow S_0$ transitions to the low lying ${}^1\pi_{+,-}^*$ states. These have oscillator strengths of 0.81 and 0.19, respectively, and are polarized along the C=S bonds (y). The ${}^1n_{+}\sigma^*$ state at 13 ev contributes about the same as the $\pi_{+,-}^*$ state at 5.3 ev.

Inspection of Table 4-2 shows that for the x (\perp to molecular plane) direction, the perturbing states are mostly $\sigma\pi_{-}^*$ with spin-orbit matrix elements of roughly the same magnitude as that of the ${}^1B_{2u}$ states, but either the weak $S_k \leftarrow S_0$ transition moment or the large energy denominator term causes the x contributions to be small. The ${}^1n_{+}\pi^*$ state contributes nothing due to the small spin-orbit matrix element and large energy denominator. In addition to the above, the x contributions have different signs and therefore partially cancel one another, their total being a factor of 40 times smaller than for the y polarization.

The contributions to the z polarized intensity (in the molecular plane but perpendicular to the C=S bonds) are very small due to all three factors being unfavorable, and even though all have the same sign, their total is less than that of the x contributions, by about a factor of 9.

The triplet states contribute a great deal more than the singlets along the y direction (cf. Table 4-3). The largest contributions come from the two ${}^3B_{2g}(n\pi^*)$ states immediately above the 1A_u state, and

TABLE 4-2
CONTRIBUTIONS TO T_1+S_0 TRANSITION MOMENT FROM
SINGLET STATE PERTURBATIONS OF $T_1, ({}^3n_+\pi_-^*)$

State	$\langle V_{ij}^k, R_\mu T_{np'}^{1,\mu} \rangle^a$	E_k^b	\vec{m}_{ok}^c	$\langle h_\mu \rangle \cdot \vec{m}_{ok}^d$
${}^1B_{2u, +} \pi_-^*$	69.48	4.55	-6.87 \hat{y}	26.5 \hat{y}
${}^1B_{2u, +} \pi \pi_-^*$	-53.87	5.32	3.03 \hat{y}	6.7 \hat{y}
${}^1B_{2u, +} n \sigma^*$	44.65	13.05	-6.38 \hat{y}	3.3 \hat{y}
${}^1B_{1u, \sigma\pi_-}^*$	-1.64	5.80	1.28 \hat{z}	0.075 \hat{z}
${}^1B_{1u, +} n \sigma^*$	4.34	17.83	-1.35 \hat{z}	0.047 \hat{z}
${}^1B_{1u, +} n \sigma^*$	3.36	20.86	-0.16 \hat{z}	0.004 \hat{z}
${}^1B_{3u, \sigma\pi_-}^*$	61.94	3.62	-0.82 \hat{x}	4.83 \hat{x}
${}^1B_{3u, \sigma\pi_-}^*$	35.88	6.34	1.35 \hat{x}	-1.49 \hat{x}
${}^1B_{3u, \sigma\pi_-}^*$	-46.67	8.10	-2.42 \hat{x}	-2.42 \hat{x}
${}^1B_{3u, +} n \pi^*$	-0.37	15.33	3.79 \hat{x}	0.013 \hat{x}
${}^1B_{3u, \sigma\pi_-}^*$	-11.08	15.71	-0.41 \hat{x}	-0.04 \hat{x}
TOTAL x pol.= +0.88 mD z pol.= +0.13 mD y pol.= 36.5 mD				

a. SOC matrix elements in $\text{cm}^{-1}/\sqrt{-1}$. b. State energies in ev., calc. by EHT. c. Electric dipole allowed transition moments in Debyes. d. Contribution to T_1+S_0 in units of milliDebyes $/\sqrt{-1}$.

TABLE 4-3
CONTRIBUTIONS TO $T_1 \leftarrow S_0$ TRANSITION MOMENT FROM
TRIPLET STATE PERTURBERS OF S_0

State	$\langle S_0 R_\mu T_{np}^{\ell, \mu} \rangle^a$	E_ℓ^b	$\vec{m}_{1, \ell \mu}^c$	$\langle h_\mu \rangle \cdot \vec{m}_{1 \ell}^d$
${}^3B_{2g, +} \pi^+$	89.04	2.45	11.95 \hat{y}	-53.9 \hat{y}
${}^3B_{2g, -} \pi^-$	-123.26	2.94	-8.61 \hat{y}	-44.8 \hat{y}
${}^3B_{2g, 0} \pi^-$	-94.99	5.00	-5.36 \hat{y}	-12.6 \hat{y}
${}^3B_{2g, \sigma} \pi^-$	36.01	7.23	1.26 \hat{y}	-0.78 \hat{y}
${}^3B_{2g, +} \pi^+$	-25.18	14.71	-3.13 \hat{y}	-0.67 \hat{y}
${}^3B_{2g, +} \sigma^+$	-18.41	22.51	-0.97 \hat{y}	-0.10 \hat{y}
${}^3B_{1g, \sigma} \pi^-$	56.99	5.21	5.07 \hat{z}	-6.87 \hat{z}
${}^3B_{1g, \sigma} \pi^-$	109.77	6.26	-3.53 \hat{z}	7.67 \hat{z}
${}^3B_{1g, \sigma} \pi^-$	-29.46	7.34	1.66 \hat{z}	0.83 \hat{z}
${}^3B_{1g, \sigma} \pi^-$	-13.56	15.17	-0.41 \hat{z}	-0.05 \hat{z}

continued

TABLE 4-3

$^3B_{3g, \pi\pi}^*$	-0.56	5.66	-3.02 \hat{x}	-0.04 \hat{x}
$^3B_{3g, n\sigma}^*$	-42.89	17.97	0.90 \hat{x}	0.27 \hat{x}
$^3B_{3g, n\sigma}^*$	23.34	23.09	-1.07 \hat{x}	0.13 \hat{x}

TOTAL x pol.= +0.36 mD z pol.= +1.58 mD y pol.= -113. mD

a., b., c., d. same as Table 4-2.

represent the ${}^3n_{+}\pi_{+}^{*} \leftarrow {}^3n_{+}\pi_{-}^{*}$ and ${}^3n_{-}\pi_{-}^{*} \leftarrow {}^3n_{+}\pi_{-}^{*}$ transitions. These have oscillator strengths of 0.20 and 0.24, respectively. As in the case of the singlets all the contributions to the y polarized intensity have the same sign; although this is opposite to the sign of the singlet contributions, the latter appear as the complex conjugate in Eq. 4-9 and will therefore add.

As in the case of the singlet state perturbers, the x and z directions have very small contributions due to $T_{\ell} \leftarrow T_1$ transitions. In the z direction, the perturbing states are all ${}^3\sigma\pi_{-}^{*}$ and although their spin-orbit matrix elements are large, and the $T_{\ell} \leftarrow T_1$ transition moments are of about the same magnitude as those of the major y-polarized-singlet-singlet contributors, the two major contributors have opposite signs and roughly cancel one another. The total z here is a factor of about 300 smaller than the y.

In the x polarization the largest contributions come from two ${}^3n_{+}\sigma^{*}$ states, however, because these have large energy denominators and small $T_{\ell} \leftarrow T_1$ transition moments, the resulting terms are very small (about 1/70 th) relative to the y polarization.

If we now add all the terms for Tables 4-2 and 4-3 according to Eq. 4-12a we find the quantities M_u given in Table 4-4. Using these values of M_u the phosphorescence lifetimes and oscillator strengths for the transitions $T_1^u \leftarrow S_0$ are calculated. Calculating the oscillator strength in this way implies that the $T_1^u \leftarrow S_0$ transition occurs between two stationary states that are adequately described by wavefunctions which are themselves well defined. Thus we are assuming that the EHT eigenvectors, coupled with the perturbation corrections,

TABLE 4-4
TRANSITION MOMENTS, OSCILLATOR STRENGTHS AND LIFETIMES
OF THE TRIPLET SUBLEVELS

Sublevel(u)	$M_u(T_{lu} \leftarrow S_o)^a$	$f^b(T_{lu} \leftarrow S_o)$	τ_u^b
y	-149.5	1.8×10^{-4}	$3.0 \times 10^{-5} s$
z	+1.45	1.7×10^{-8}	0.32 s
x	-0.52	2.1×10^{-9}	2.5 s

a. In units of milliDebye/ $\sqrt{-1}$.

b. Calculated using the experimental $(E_{T_1} - E_{S_o}) = 16826 \text{ cm}^{-1}$.

Using the EHT calculated transition energy (18711 cm^{-1}) increases f by ~10% and decreases τ by ~27%.

give wavefunctions that adequately describe the ground state and lowest excited triplet state in TMCBDT. While this is far from true theoretically it provides a reasonable starting point for determining the qualitative nature of the spin-orbit coupling process which gives rise to the observed intense $T_1 \leftarrow S_0$ transition.

If the zero-field splitting among the triplet sublevels were observable the M_u and f values in Table 4-4 would apply. However, for the transition moments of the $T_1 \leftarrow S_0$ transition in single crystal TMCBDT Eqs. 4-13 and 4-14 (and Table 4-4) are to be used. For the $^3\Psi(+)$ state we have

$$M(+) = -53.0 \text{ i } \hat{\epsilon}_{\perp} + 1.0 \text{ i } \hat{\epsilon}_{||} \text{ (mD)}$$

while for the $^3\Psi(-)$ state

$$M(-) = +52.7 \text{ i } \hat{\epsilon}_{\perp} \text{ (mD)}$$

(where $\text{mD} = 10^{-3}$ Debye).

We may now estimate the ratio for c-polarized to a-polarized intensity as

$$\frac{I_{||}}{I_{\perp}} = \frac{1}{5588}.$$

The $\hat{\epsilon}_{||}$ and $\hat{\epsilon}_{\perp}$ are vectors parallel to the c crystal axis and the plane $\perp c$, respectively.

When considering the lifetimes calculated in Table 4-4 it should be pointed out that for the case where spin-lattice relaxation is large, that is if the temperature is such that $kT \gg D$ (zero-field splitting), thermal equilibrium may be assumed among the triplet sublevels. In that case it has been shown (109) that the emission from the triplet state obeys an exponential decay whose lifetime is given by

$$\tau^{-1} = \frac{1}{3} \sum_u \tau_u^{-1}.$$

For the present case of TMCBDT, the values in Table 4-4 give $\tau_u \sim 90\mu s$, and it can be seen that the emission would all be channeled through the γ sublevel (γ parallel to C=S bonds).

At very low temperatures where spin-lattice relaxation does not occur (perhaps at 1.6K or lower) the emission from each sublevel is in addition affected by the population in that level which is determined by the intersystem crossing matrix elements. These will not be considered here.

Summary

The two largest contributions (60%) to the isolated molecule $T_1 \leftarrow S_0$ transition moment are the ${}^3n_+\pi_+^* + {}^3n_+\pi_-^*$ and ${}^3n_-\pi_-^* + {}^3n_+\pi_+^*$ transitions, polarized along the C=S bonds. The next largest contribution is the ${}^1B_{2u} \leftarrow {}^1A_g$, $(\pi_-^* \leftarrow \pi_+)$ transition which adds 18% to this same polarization. The total contribution to the transition moment parallel to C=S from $T_0 \leftarrow T_1$ transitions is 76% and from $S_k \leftarrow S_0$ transitions 24%. The oscillator strength of about 2×10^{-4} for the largest $T_1 \leftarrow S_0$ component (γ) falls within the range of typical $\pi^* \leftarrow n$ transitions of a spin allowed nature (S-S). For the crystal, the prediction is that the $T_1 \leftarrow S_0$ absorption should be almost exclusively $\parallel c$ polarized. This is in fact observed. These results are consistent with the assignment that T_1 in TMCBDT is 3A_u , as was found for the oxygen analogue TMCBD (6).

CHAPTER 5
ZEEMAN SPECTROSCOPY OF TETRAMETHYL-1,3-CYCLOBUTANEDITHIONE

Introduction

As discussed in Chapter 4, transitions between the ground electronic state, S_0 , and the lowest triplet state, T_1 , of an organic molecule can only be seen if the spin-orbit-coupling mechanism is active in the molecule (70,102). In order to obtain useful information about the nature of the perturbing states, however, polarized spectra of oriented molecules may be taken, hence the use of single crystals. Many of the most common organic molecules having D_{2h} or C_{2v} symmetry crystallize in the $P2_1/a$ (C_{2h}^5) space group (70), usually having two molecules per unit cell. For these cases a single crystal polarized study in zero field does not yield unambiguously the symmetry of the triplet state observed because each molecular or site state correlates with two crystal states, one symmetric and one anti-symmetric with respect to a twofold rotation about the b(unique)axis. Thus, any or all of the spin-orbit routes $H_{so}(x)$, $H_{so}(y)$ or $H_{so}(z)$ may be mixing in singlet states which contribute intensity $\parallel b$ (symmetric) and/or $\perp b$ (antisymmetric). For example, if we have a 3A_u molecular state (D_{2h} point group) in the free molecule, contributions to the $^3A_u \leftarrow ^1A_g$ transition moment will come from electric dipole allowed transitions from 1A_g to $^1B_{1u}$, $^1B_{2u}$ and $^1B_{3u}$ molecular states via perturbations induced by $H_{so}(z)$, $H_{so}(y)$ and $H_{so}(x)$, respectively.

These molecular states all correlate with the A_u site state (because the only site symmetry is C_i for the particular case of the C_{2h}^5 factor group) which in turn splits into A_u and B_u factor group states, electric dipole allowed $||b$ and $\perp b$, respectively.

For the specific case where only one type of singlet state perturbs the triplet state, say $^1B_{3u}$, the ratio of b-polarized to a-polarized intensity is given by the equation(70,110)

$$\frac{I_b}{I_a} = \frac{\cos^2 \theta_{xb}}{\cos^2 \theta_{xa}} \quad (5-1)$$

where θ_{xa} is the angle between the molecular x axis and the a crystal axis. If one knows the orientation of the molecules in the crystal the ratio for that molecular direction which best fits the observed intensity ratio will tell the symmetry of the molecular singlet state which is perturbing the triplet. This is equal to the direct product of the active H_{so} component representation and that of the triplet state in question. Knowing the symmetry of the triplet state then gives the active H_{so} component symmetry.

However, if the triplet state symmetry is not known several possibilities arise. If it is found that the perturbing singlet is $^1B_{3u}$ as in the present example, then from symmetry considerations in the D_{2h} group we may have 3A_u (via $H_{so}(x)$), $^3B_{1u}$ (via $H_{so}(y)$) or $^3B_{2u}$ (via $H_{so}(z)$) for the absorbing triplet state.

All of the above considerations assume 1) one type of perturbing singlet, 2) no factor group splitting of crystal states and 3) no interactions among higher electronic states in the molecule. When any of these assumptions becomes invalid, the oriented gas ratio relationship (Eq. 5-1) does not hold.

If a Zeeman experiment is carried out on the crystal, however, Hochstrasser and coworkers (111) have shown that it is possible to obtain an unambiguous assignment of the triplet state symmetry by measuring the absorption intensity ratios among the triplet sublevels. It is shown that by considering the transition moments to the triplet sublevels using first order perturbation theory the intensity ratios among the three sublevels depend on which spin-orbit route(s) is (are) active. Specifically for the case of only one route the intensity ratio is independent of the electric field direction of the incident radiation with respect to the crystal axes. For two or more routes the ratio is very sensitive to the \vec{E} orientations. In fact, it is possible to use \vec{E} directional dependence to show the presence of as little as 0.5% of a second spin orbit route (111a).

This method depends critically on proper alignment of the crystal in the magnetic field, that is \vec{H} must be parallel or perpendicular to a crystal symmetry axis. The derivation by Castro and Hochstrasser (111a) assumes this is true and the resulting equation relating the triplet sublevel intensity ratio to the direction cosines of the molecular axes with respect to a) the crystal axis that is parallel to \vec{H} and b) the electric field \vec{E} , does not apply for a general field orientation.

In this chapter the approach of Castro and Hochstrasser (111a) is applied to the TMCBDT single crystal for the case in which the magnetic field is aligned in an arbitrary direction with respect to the crystal axes.

In addition, the case of nonvanishing zero-field splitting parameters is examined and the quantities X , Y and Z are estimated from the results of the spin-orbit coupling calculation. The motivation for these considerations comes from the large spin-orbit coupling interaction due to the sulfur atoms in TMCBDT and the influence of such interaction on the zero-field splitting parameters. An unusually large effect of this type was recently reported by Burland (36) and Maki, Svejda and Huber (35) for the molecule xanthione. Hochstrasser and Lin (112) have applied the theory of the Zeeman and Stark effects to determine the zero-field splitting parameters and electrostatic interaction matrix elements of benzophenone single crystals using optical absorption spectroscopy.

A brief outline of the experimental details is then given, followed by the results and discussion.

Theory

Although there are two molecules in the TMCBDT unit cell, x-ray crystallography (38) shows that they are oriented in such a way that Davydov splitting is not expected if only totally symmetric vibrations are active. For this case, or if there is splitting which is unobservably small, the two molecules can be treated as independent absorbers (111c) This section deals with the Zeeman absorption intensities for the case where the magnetic field is in a general direction relative to the crystal (unit cell) axes. The notation and procedure outlined in Castro and Hochstrasser (111) will be followed. Expressions for polarized and unpolarized absorption spectra are derived. The zero-field splitting parameters are calculated and their influence on the absorption spectra is discussed.

Zeeman Intensity Ratio for an Arbitrary Field Direction

For the i th molecule the transition moment can be written as

$$\vec{m}_i = m_{xi} \hat{x} + m_{yi} \hat{y} + m_{zi} \hat{z} \quad (5-1)$$

where the \hat{x} , \hat{y} and \hat{z} are unit vectors along the molecule fixed axes.

As shown in Chapter 4 the $m_{\alpha i}$ are obtained from a free molecule spin-orbit coupling calculation using a first order perturbation treatment and are of the following form

$$\begin{aligned} \vec{m}_{\alpha} = & \sum_k \Delta E_k^{-1} \langle {}^1\psi_k | H_{so}(\alpha) | {}^3\psi_1 \rangle \cdot | \vec{m}_{\alpha S_0 S_k} | \hat{\alpha} \\ & + \sum_{\ell} \Delta E_{\ell}^{-1} \langle {}^3\psi_{\ell} | H_{so}(\alpha) | {}^1\psi_0 \rangle \cdot | \vec{m}_{\alpha T_1 T_{\ell}} | \hat{\alpha} \end{aligned} \quad (5-2)$$

which includes the contributions from S-S ($\vec{m}_{\alpha S_0 S_k}$) and T-T ($\vec{m}_{\alpha T_1 T_{\ell}}$) allowed electronic transitions; \vec{m}_{α} is the allowed transition moment in the α direction in the molecular frame. The spin part of the wavefunctions are taken to be those which diagonalize the zero-field spin-spin Hamiltonian (113) for the triplet

$$\begin{aligned} |\omega_x\rangle &= \frac{1}{\sqrt{2}} (\beta_1\beta_2 - \alpha_1\alpha_2) \\ |\omega_y\rangle &= \frac{i}{\sqrt{2}} (\beta_1\beta_2 + \alpha_1\alpha_2) \\ |\omega_z\rangle &= \frac{1}{\sqrt{2}} (\alpha_1\beta_2 + \beta_1\alpha_2) \\ |{}^1\sigma_0\rangle &= \frac{1}{\sqrt{2}} (\alpha_1\beta_2 - \beta_1\alpha_2) \end{aligned} \quad (5-3)$$

The Hamiltonian for the case where the magnetic field is oriented in the general direction given by ℓ , m , and n , (the direction cosines of \vec{H} with respect to the molecular x , y , and z axes, respectively) and including the zero field-splitting-parameters is

$$H = g\beta H_0 (\ell S_x + m S_y + n S_z) - (X S_x^2 + Y S_y^2 + Z S_z^2) \quad (5-4)$$

The g tensor has been assumed isotropic and X , Y and Z are the zero-field-splitting parameters (113) and will be discussed later. The Hamiltonian matrix then becomes

$$H = \begin{bmatrix} X & -ibn & ibm \\ ibn & Y & -ibl \\ -ibm & ibl & Z \end{bmatrix} \quad (5-5)$$

The eigenvectors of this matrix are then used to transform the spin functions in the transition moment expression Eq. 5-2 from a molecule fixed basis $|\omega\rangle$, to a field fixed basis $|\sigma\rangle$.

Thus $|\sigma_s\rangle = \sum_r C_{sr} |\omega_r\rangle$ is applied to Eq. 5-2 to give

$$\begin{aligned} \vec{m}_{i+} = & \sum_k \Delta E_k^{-1} \left(\sum_r C_{+r}^{i(1)} \langle \phi_k | \sigma_o^1 | H_{so}(r) | \phi_1 \cdot \omega_r \rangle | \vec{m}_{rok} \rangle \right) \\ & + \sum_\ell \Delta E_\ell^{-1} \left(\sum_r C_{+r}^{i(1)} \langle \phi_\ell | \sigma_o^1 | H_{so}(r) | \phi_o^1 \rangle | \vec{m}_{r1\ell} \rangle \right) \end{aligned} \quad (5-6)$$

The part of the spin-orbit Hamiltonian which is effective in coupling singlet and triplet states can be written as (cf. Chapter 4)

$$H_{so}(r) = \frac{1}{2} (R_{r1}^- R_{r2}) (S_{r1} - S_{r2}) = \frac{1}{2} R_r^- S_r^- \quad (5-7)$$

The effect of S_r^- on the spin functions is $S_r^- |^1\sigma_o\rangle = \hbar |\omega_r\rangle$ and $S_r^- |\omega_s\rangle = \hbar^1\sigma_o \delta_{rs}$ so that integrating out the spin from Eq. 5-6 gives

$$\begin{aligned} \vec{m}_{i+} = & \sum_r C_{+r}^i \left[\sum_k \Delta E_k^{-1} \langle \phi_k | R_r^- | \phi_1 \rangle | \vec{m}_{rok} \rangle \right] \\ & + \sum_\ell \Delta E_\ell^{-1} \langle \phi_\ell | R_r^- | \phi_o \rangle | \vec{m}_{r1\ell} \rangle | \hat{f} \end{aligned} \quad (5-8)$$

The quantity in [] is obtained in a straightforward manner from a spin-orbit coupling calculation and can be written simply as m_r . Thus, the transition moment from the ground electronic state to the triplet sublevels may be written as

$$\vec{m}_{is} = \sum_r C_{sr}^i m_r \hat{f}_i \quad s = +, 0, - \text{ and } r = x, y, z \quad (5-9)$$

The \hat{r}_i vectors are the unit vectors on the molecule fixed frame obtained from the x-ray work (38), and are different for each molecule, i . The coefficient matrix \underline{C}^i representing the eigenvectors of 5-5 for molecule i are functions of the zero field parameters, X , Y and Z and the strength (H_0) and direction (ℓ_i, m_i, n_i) of the magnetic field. It is a simple task to obtain a general expression for the \underline{C} matrix if $X=Y=Z=0$, but not for nonzero values of these parameters. In the latter case a suitable (114) diagonalization procedure for a Hermitian matrix may be used.

In order to illustrate the application of the intensity expression in fitting the available Zeeman data we assume $X=Y=Z=0$ for which case \underline{C} is easily found to be

$$\underline{C} = \begin{array}{ccc} \begin{array}{c} |T_x\rangle \\ |T_y\rangle \\ |T_z\rangle \end{array} & \begin{array}{c} |T_x\rangle \\ |T_y\rangle \\ |T_z\rangle \end{array} & \begin{array}{c} |T_x\rangle \\ |T_y\rangle \\ |T_z\rangle \end{array} \\ \left[\begin{array}{ccc} -\frac{1}{\sqrt{2}} \frac{(\ell n - i m)}{(1-n^2)^{1/2}} & -\frac{1}{\sqrt{2}} \frac{(m n + i \ell)}{(1-n^2)^{1/2}} & \frac{1}{\sqrt{2}} (1-n^2)^{1/2} \\ \ell & m & n \\ -\frac{1}{\sqrt{2}} \frac{(\ell n + i m)}{(1-n^2)^{1/2}} & -\frac{1}{\sqrt{2}} \frac{(m n - i \ell)}{(1-n^2)^{1/2}} & \frac{1}{\sqrt{2}} (1-n^2)^{1/2} \end{array} \right] & \begin{array}{c} | +1 \rangle \\ | 0 \rangle \\ | -1 \rangle \end{array} \end{array} \quad (5-10)$$

Where the molecule subscript i has been omitted from the ℓ , m and n for simplicity, however because of the different orientations of the two translationally inequivalent molecules in the unit cell $\underline{C}_1 \neq \underline{C}_2$. This is especially true if a general direction is chosen for H . Thus, even though the quantities m_x in Eq. 5-9 are the same for the two molecules, (since they are taken from the free molecule calculation), the transition moment to the s^{th} sublevel will differ, and therefore the intensity ($I_s^i \propto m_s^i m_s^{i*}$) will also.

It should be pointed out here that for this case $C_{+r}^i = (C_{-r}^i)^*$ which leads to $I_+ = I_-$. In other words, the intensity of the $|M_s| = 1$ lines are the same. If the X, Y and Z are not zero and the field is not extremely large, i.e., $g\beta H_0 \gg D$ is not true, then there will be an imbalance in the intensity of the $|+\rangle$ and $|-\rangle$ lines. In addition the eigenvalues in this case are such that $\epsilon_+ - \epsilon_0 \neq \epsilon_- - \epsilon_0$; so there is an imbalance in the intensity and position of the $|+\rangle$ and $|-\rangle$ lines. This will be considered later with reference to some of the experimental data.

Polarized Zeeman Absorption

The intensity for the s^{th} triplet sublevel will then be given by

$$I_s = \sum_{i=1}^2 \left(\sum_r C_{sr}^i m_r \cdot \vec{E} \right) \left(\sum_r C_{sr}^i m_r \cdot \vec{E} \right)^* \quad (5-11)$$

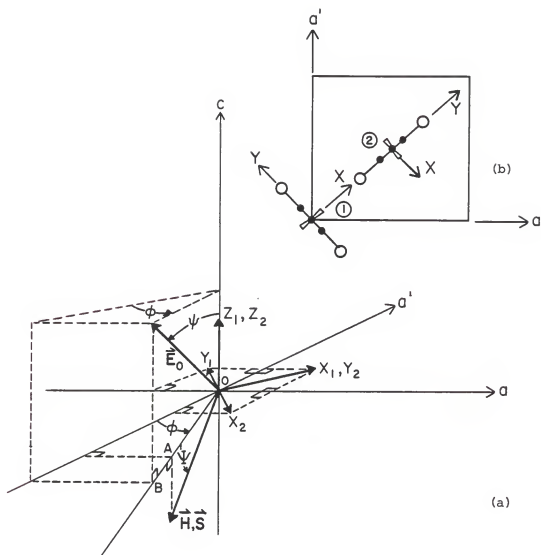
where \vec{E} is the electric field vector of the (polarized) analyzing light. To evaluate Eq. 5-11 the geometrical factors relating the molecular axes to the direction of the magnetic field and electric field, \vec{E} , have to be considered. These factors are diagrammed in Fig. 5-1. With reference to the experimental constraints on the relationship of \vec{E} and \vec{H} as explained later, we note that \vec{E} is always perpendicular to \vec{H} , (thus to consider the polarization direction θ we rotate \vec{E}_0 about \vec{H} by θ degrees). The analyzing light beam always travels in a direction collinear with \vec{H} . Since the molecular orientation with respect to the crystal axes are known, two angles (ψ and ϕ) will suffice to describe all the necessary quantities. ψ is the angle which the electric field vector of the plane polarized light makes with the c axis, while ϕ is the angle which the $\perp c$ component of this vector makes with the -a' axis. The latter component

Figure 5-1. Coordinate system used in the derivation of Zeeman intensities for an arbitrary field orientation in the Faraday configuration. Reference to Fig. 5-3 and Fig. 3-1 is helpful.

\vec{H} - Magnetic field vector.
 \vec{S} - Poynting vector.
 \vec{E} - Electric field vector, minimum absorption.
 X_i^O, Y_i, Z_i - Molecular symmetry axes.
 a_i, a'_i, c_i - Crystal symmetry axes.
 ψ - Angle which magnetic field makes with aa' plane.
 ϕ - Angle which the aa' projection of the magnetic field makes with the $-a'$ axis.

(a) General view.

(b) View along c crystal axis.



can be written in terms of its projections along a and a' . Likewise we can write the molecular axis vectors in terms of a and a' components and thus carry out the dot product in Eq. 5-11. From the definition of the polarizer angle (θ), for $\theta=0$ one has minimum zero-field absorbance. This is denoted E_0 . The (unit) vectors are written as column vectors with components a , a' and c . Thus we have from Fig. 5-1

$$\hat{a} = \begin{bmatrix} \cos\psi\sin\phi \\ -\cos\psi\cos\phi \\ -\sin\psi \end{bmatrix} \quad \text{and} \quad \hat{E}_0 = \begin{bmatrix} \sin\psi\sin\phi \\ -\sin\psi\cos\phi \\ \cos\psi \end{bmatrix} \quad (5-12)$$

For the general polarization direction θ , the projections of \vec{E} on the cell axes are found by successive application of the following rotations on the unit vector $(0,0,1)$ representing $E(\psi=\phi=\theta=0)$: rotation about a' by θ , rotation about a by ψ and rotation about c by ϕ . The result is

$$\hat{E}_\theta = \begin{bmatrix} \cos\theta\sin\psi\sin\phi + \sin\theta\cos\phi \\ -\cos\theta\sin\psi\cos\phi + \sin\theta\sin\phi \\ \cos\theta\cos\psi \end{bmatrix} \quad (5-13)$$

The l_i , m_i and n_i will be given by $l_i = \hat{z}_i \cdot \hat{a}$, $m_i = \hat{y}_i \cdot \hat{a}$ and $n_i = \hat{z}_i \cdot \hat{a}$ and are listed in Table 5-1, along with the molecular unit vectors in the unit cell frame.

The intensity expression, Eq. 5-11, can now be expanded, Letting E_a , $E_{a'}$ and E_c be the components of the electric field vector along the unit cell axes we get

TABLE 5-1
MOLECULAR AXES IN UNIT CELL FRAME AND THEIR DIRECTION COSINES WITH
RESPECT TO H. (The angles ψ and ϕ are defined in Figure 5-1.)

	Site 1	Site 2
\hat{x}^a	$\frac{1}{\sqrt{2}} (\hat{a} + \hat{a}')$	$\frac{1}{\sqrt{2}} (\hat{a} - \hat{a}')$
\hat{y}	$-\frac{1}{\sqrt{2}} (\hat{a} - \hat{a}')$	$\frac{1}{\sqrt{2}} (\hat{a} + \hat{a}')$
\hat{z}	\hat{c}	\hat{c}
ℓ^b	$\frac{1}{\sqrt{2}} \cos\psi (\sin\phi - \cos\phi)$	$\frac{1}{\sqrt{2}} \cos\psi (\sin\phi + \cos\phi)$
m	$-\frac{1}{\sqrt{2}} \cos\psi (\sin\phi + \cos\phi)$	$\frac{1}{\sqrt{2}} \cos\psi (\sin\phi - \cos\phi)$
n	$-\sin\psi$	$-\sin\psi$

-
- a. The hat $\hat{}$ denotes a unit vector; \hat{x} , \hat{y} and \hat{z} are the molecular axes vectors while \hat{a} , \hat{a}' and \hat{c} are the unit vectors in the unit cell frame.
- b. The ℓ , m and n are direction cosines for the molecular x, y and z axes, respectively, with respect to the magnetic field direction \hat{H} . Expressing the vectors \hat{H} and \hat{x} in the unit cell frame (see Eq. 5-12 for \hat{H}) we find ℓ is given by the scalar product of \hat{H} and \hat{x} . The same is done for m and n using \hat{y} and \hat{z} .

$$\begin{aligned}
I_s = & \frac{1}{2} m_x^2 [C_{sx_1} C_{sx_1}^* (E_a + E_a')^2 + C_{sx_2} C_{sx_2}^* (E_a - E_a')^2] \\
& + \frac{1}{2} m_y^2 [C_{sy_1} C_{sy_1}^* (E_a - E_a')^2 + C_{sy_2} C_{sy_2}^* (E_a + E_a')^2] \\
& + m_z^2 E_c^2 [C_{sz_1} C_{sz_1}^* + C_{sz_2} C_{sz_2}^*] \quad (5-14) \\
& + \frac{1}{2} m_x m_y (E_a'^2 - E_a^2) [(C_{sx_1} C_{sy_1}^* + C_{sy_1} C_{sx_1}^*) - (C_{sx_2} C_{sy_2}^* + C_{sy_2} C_{sx_2}^*)] \\
& + \frac{1}{\sqrt{2}} m_z E_c [m_x \{ (C_{sx_1} C_{sz_1}^* + C_{sz_1} C_{sx_1}^*) (E_a + E_a') + (C_{sx_2} C_{sz_2}^* + C_{sz_2} C_{sx_2}^*) (E_a - E_a') \} \\
& + m_y \{ (C_{sy_1} C_{sz_1}^* + C_{sz_1} C_{sy_1}^*) (E_a - E_a') + (C_{sy_2} C_{sz_2}^* + C_{sz_2} C_{sy_2}^*) (E_a + E_a') \}]
\end{aligned}$$

Now as Castro and Hochstrasser (111) have shown for the high field spin basis $|\alpha\alpha\rangle$, $|\beta\beta\rangle$ etc. terms of the type $C_{sx} C_{sx}^*$ reduce to ℓ^2 for $s=0$ and $\frac{1}{2}(1-\ell^2)$ for $s=\pm 1$, while $(C_{sx} C_{sy}^* + C_{sy} C_{sx}^*)$ reduces to $2\ell m$ for $s=0$ and $-\ell m$ for $s=\pm 1$. Similar expressions are found for y , z , xz etc. As can easily be seen from the $|0\rangle$ vector in Eq. 5-19 the same results are obtained using the zero-field eigenfunctions $|\psi\rangle$. Substituting these expressions and Eq. 5-13 into 5-14 gives the following results

$$I_o = \cos^2 \psi \cos^2 \theta \left\{ \frac{1}{2} (m_x^2 + m_y^2) (\sin^2 \psi + \tan^2 \theta) + 2m_z^2 \sin^2 \psi \right\} \quad (5-15a)$$

$$\begin{aligned}
& - 2m_z (m_x + m_y) \sin^2 \psi + \left[\frac{1}{2} (m_x^2 + m_y^2) \sin^2 2\theta + m_x m_y \cos^2 2\theta \right] x (\sin^2 \psi - \tan^2 \theta) \\
& + \left[\frac{1}{2} (m_x^2 + m_y^2) - m_x m_y \right] \sin \psi \sin 4\theta \tan \theta \}
\end{aligned}$$

$$I_{\pm} = \frac{1}{2} \{ (m_x^2 + m_y^2) (\cos^2 \theta \sin^2 \psi + \sin^2 \theta) + 2m_z^2 \cos^2 \psi \cos^2 \theta - I_o \} \quad (5-15b)$$

We now take the $\cos^2 \psi \cos^2 \theta$ factor out of the first two terms of I_+ and divide both equations by m_y^2 . After taking the ratio we find that Eq. 5-15 can be written as

$$\frac{I_0}{I_+} = \frac{2 \{A_0 + B_0 \tan \theta + C_0 \tan^2 \theta\}}{A_1 - B_0 \tan \theta + C_1 \tan^2 \theta} \quad (5-16)$$

Where the coefficients of the quadratics in $\tan \theta$ in this equation are functions of ψ, ϕ and ratios of transition moments: $R_x = (m_x/m_y)$ and $R_z = (m_z/m_y)$. These coefficients are given below

$$A_0 = \sin^2 \psi \left\{ \frac{1}{2}(R_x + 1)^2 + \frac{1}{2}(R_x - 1)^2 \sin^2 2\phi + 2R_z(R_z - R_x - 1) \right\}$$

$$A_1 = (R_x^2 + 1) \tan^2 \psi + 2R_z^2 - A_0$$

$$B_0 = \frac{1}{2}(R_x - 1)^2 \sin \psi \sin 4\phi \quad (5-16a)$$

$$C_0 = \frac{1}{2}(R_x - 1)^2 \cos^2 2\phi$$

$$C_1 = (R_x^2 + 1) / \cos^2 \psi - C_0$$

It follows immediately that for $\theta=0$ the ratio is given by $2A_0/A_1$, while for $\theta=90$ we get $2C_0/C_1$.

These results show that an important consequence of not having the magnetic field aligned with a crystal axis (that is $\phi \neq 0^\circ$ and/or $\psi \neq 0, 90^\circ$) is that if either y or x is the only active spin-orbit route a polarization dependence in the Zeeman intensity ratio arises, whereas for the z route the expected polarization independence is found for any field orientation. This occurs because the molecular z axes of the two molecules in the unit cell are translationally equivalent and therefore magnetically equivalent, whereas the x and y directions are translationally inequivalent and for the general orientation of the field these

become magnetically inequivalent. For certain field orientations, however, the x and y directions remain magnetically equivalent, as for $\phi=0, 90$ (\vec{H} in an ac plane). These considerations in connection with Eq. 5-15 lead to results identical to those of Castro and Hochstrasser (111) for one spin-orbit route. For the case where $H_{so}(z)$ is the only active spin-orbit route

$$\frac{I_o}{I_+} = \frac{2\sin^2\psi}{1-\sin^2\psi} = \frac{n^2}{\frac{1}{2}(1-n^2)} \quad (5-17)$$

and for $H_{so}(x)$ or $H_{so}(y)$ in the case where $\phi=0$

$$\frac{I_o}{I_+} = \frac{2\cos^2\psi}{2-\cos^2\psi} = \frac{l^2}{\frac{1}{2}(1-l^2)} = \frac{m^2}{\frac{1}{2}(1-m^2)} \quad (5-18)$$

Unpolarized Zeeman Absorption

The results of the previous section can be used to calculate the Zeeman ratio for the case of an unpolarized probe beam. To do this we note that the ratio I_o/I_+ involves intensities to two separately observable substates. Thus we can integrate each intensity over all polarizer angles and then take the ratio. We write this as

$$I_r(np) = \int_0^{2\pi} I_r(\theta) d\theta \quad \text{with } r = 0 \text{ and } +.$$

Then for the ratio:

$$R(np) = \frac{I_o(np)}{I_+(np)}$$

The $I(\theta)$ are obtained from Eqs. 5-15 by grouping terms in $\cos^2\theta$, $\sin^2\theta$ and $\sin\theta\cos\theta$. The $I_o(\theta)$ and $I_+(\theta)$ can be written as

$$I_o(\theta) = \cos^2\psi(\alpha \cos^2\theta + \beta \sin^2\theta + \gamma \sin\theta\cos\theta)$$

and $I_+(\theta) = \frac{1}{2}[\alpha'\cos^2\theta + \beta'\sin^2\theta - I_o(\theta)]$

Here the α , α' , β , β' and γ are not functions of θ , but depend only on ψ , ϕ and the transition moments m_x , m_y and m_z . Integrating each of the above expressions over all possible θ space ($0-2\pi$) gives

$$R(np) = \cos^2 \psi \frac{(\alpha + \beta)}{\frac{1}{2}(\alpha' + \beta' - \alpha - \beta)}$$

This can be written in terms of the expressions in 5-16a as

$$R(np) = \frac{\frac{2(A_0 + C_0)}{A_1 + C_1}}{.}$$

Zero-Field Absorption (ZFA)

The total intensity is just the zero-field intensity, which is given by $I_0 + 2I_{\pm}$ and using Eq. 5-15 we get

$$I_{ZF} = (m_x^2 + m_y^2)(\cos^2 \theta \sin^2 \psi + \sin^2 \theta) + 2m_z^2 \cos^2 \psi \cos^2 \theta \quad (5-19)$$

As expected this is independent of ϕ . Since the only quantity which can be varied in a given experiment is θ , it will be convenient to write Eq. 5-16 as

$$I_{ZF}(\theta) = a' + b' \sin^2 \theta$$

$$\text{with } b' = [(m_x^2 + m_y^2) - 2m_z^2] \cos^2 \psi \quad (5-20)$$

$$a' = (m_x^2 + m_y^2) \sin^2 \psi + 2m_z^2 \cos^2 \psi$$

Reference to Fig. 5-1 shows that for any orientation of \vec{H} , since \vec{E} is perpendicular to \vec{H} , a 90° rotation of \vec{E} about \vec{H} always leaves the \vec{E} vector in the aa' plane. Thus for $\theta=90^\circ$ we will get maximum ZF absorption, namely $I_{ZF}(90) = a' + b' = (m_x^2 + m_y^2)$; while for $\theta=0^\circ$ we get $I_{ZF}(0) = a'$.

This is in accord with the spin-orbit coupling results which showed that the molecular transition moment is largest in the y direction.

Thus, a plot of the ZF intensity vs. $\sin^2\theta$ should be linear. Further, if $I_{ZF}(\theta)/I_{ZF}(90)$ is plotted one finds that the slope and intercept can be written as

$$b = \{1 - I_c/I_a\} \cos^2\psi \quad (5-21)$$

and $a = \sin^2\psi + (I_c/I_a) \cos^2\psi$

where $\frac{I_c}{I_a} = 2m_z^2/(m_x^2 + m_y^2)$.

It can be seen that from such a plot it is possible to determine ψ if I_c/I_a is known. This polarization ratio would be measurable directly if the direction of propagation of the probe beam were exactly perpendicular to c . Since this is never certain, especially for the case of TMCBDT crystals, the measurement in which $I(0)/I(90)$ is a minimum would give the most accurate value of I_c/I_a .

To get the unpolarized ZFA we integrate Eq. 5-20 and obtain

$$I(np, ZFA) = a + \frac{1}{2} b \quad (5-22)$$

with a and b as defined in Eq. 5-21. As was previously defined the I here represents the measurement relative to $I(90)$.

Effect of Zero-Field Splitting Parameters

We now consider the effect of the ZFS parameters X , Y and Z on the Zeeman absorption spectrum of TMCBDT. To do this we find the eigenvalues and eigenvectors of Eq. 5-5, these will be denoted by ϵ_s^i and C_{sr}^i , respectively. Here i refers to molecule 1 or 2 while r is x, y or z and s refers to the triplet sublevel $-$, 0 or $+$. The method chosen for this diagonalization is outlined in Appendix I. The absorption intensity is then calculated using Eq. 5-11. It will be more convenient to describe the ZFS parameters in terms of the D and E parameters, defined in the usual way (113)

$$D = -(3/2)Z \quad \text{and} \quad E = (1/2)(Y-X) \quad (5-23)$$

The result for $D=E=0$ is that the eigenvalues are 0 and $\pm g\beta H$ and not a function of the field direction (ℓ, m, n). Thus the $\epsilon_+ - \epsilon_0 = \Delta_+$ and $\epsilon_- - \epsilon_0 = \Delta_-$ quantities are equal and this means that in the absorption spectrum the wings will be displaced equally from the center line. Also, the eigenvector of the $|-\rangle$ state is just the complex conjugate of that of the $|+\rangle$ state, (5-10) so the intensities of the two wing lines are equal. The intensity ratio is then given by Eqs. 5-17 and 5-18.

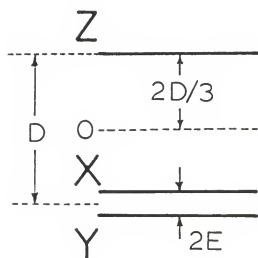
In the cases where D and/or E are not zero, the convention is to assign the z axis to that direction in which the spin-spin interaction is the greatest (112). Fig. 5-2(a) shows the zero-field splittings for D and E both negative. If the sign of D is changed, the value of the Z parameter and the center of gravity of the X and Y values reflect through zero. If the sign of E changes, the values of X and Y are interchanged. As was shown by Hochstrasser and Lin (112) it is possible to extract the values of D and E from low resolution optical Zeeman spectra of $T_1 \leftarrow S_0$ transitions in single crystals, provided that $g\beta H < 20|D|$. For values of $|D| \sim 0.2$ this requires fields in the vicinity of 40-45 kiloGauss.

In the particular case of the field directed along a molecular axis these authors give an approximate expression for the intensity imbalance in the wing lines. Defining $\gamma_g = \frac{X-Z}{4g\beta H} \sim \frac{D}{4g\beta H}$ this imbalance can be calculated as

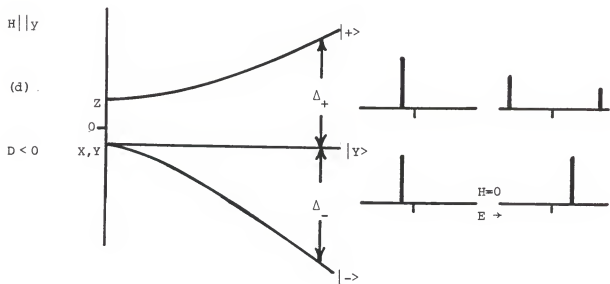
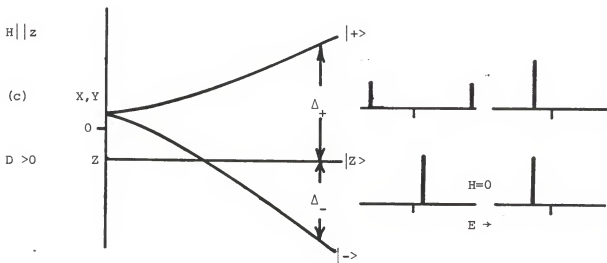
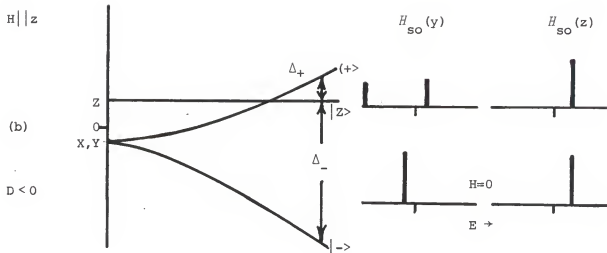
$$\frac{I_+}{I_-} = \left(\frac{1+\gamma_+}{1-\gamma_-} \right)^2 \quad (5-24)$$

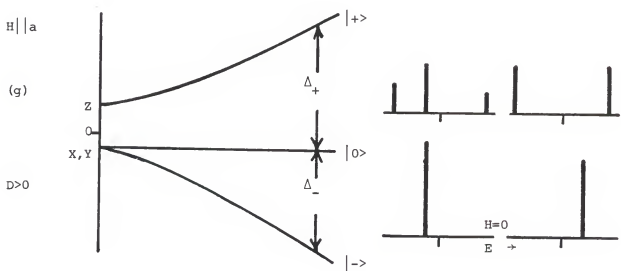
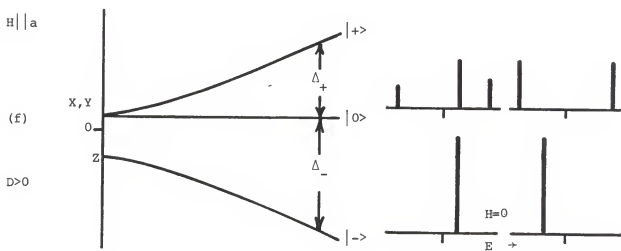
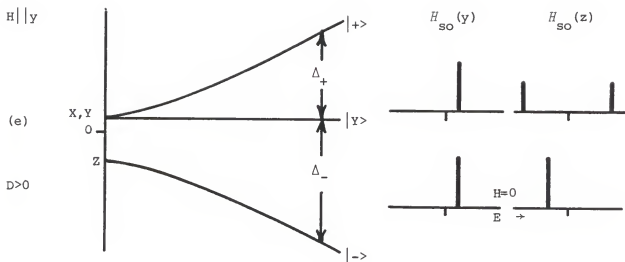
Figure 5-2. Effect of zero-field-splitting parameters on the Zeeman absorption spectra. For all cases E is assumed to be zero and only one spin-orbit route is active. The ordinate is energy and the abscissa magnetic field strength. For each case the histograms give the expected intensity pattern in zero-field and at some nonzero-field value. The relationships of the triplet state sublevels in zero-field are given in (a).

- (a) Relationship of zero-field-splitting parameters.
- (b) - (e) General cases.
- (c) - (g) Two examples applicable to TMCBDT.



(a)





It is seen that for $D > 0$ we will have $I_+ > I_-$ while for $D < 0$, $I_+ < I_-$ will be observed. This applies only for the field perpendicular to the z direction. If the field is parallel to the z direction, then $\gamma_z \approx \frac{E}{2g\beta H}$ and the imbalance in intensity will reflect the E parameter rather than the D parameter.

In addition to the intensity imbalance in the wing lines there will also be an imbalance in the line positions, that is $\Delta_+ \neq \Delta_-$. Under normal circumstances the E parameter is much smaller than the D parameter. Typically, for organic molecules where spin-orbit interaction is not large, D will be 5 to 10 times greater than E in magnitude. For these cases then, the imbalance in intensity is very small for the case of $H \parallel z$. The imbalance in Δ on the other hand is determined by D alone (115), for $H \parallel z$ the difference in Δ for the wing lines is $2D$ while for $H \perp z$ it is just D . These effects are diagrammed in Fig. 5-2(b-g), along with the expected intensity patterns for the cases in which only one spin orbit route is active ($H_{so}(u)$), calculated from Eqs. 5-17 and 5-18.

Figure 5-2(f) shows the situation when the field is aligned in the xy plane at an angle of 45° to the y axis. Eqs. 5-17 and 5-18 now give a ratio of $\frac{I_-}{I_+} = 2$ (for $D=E=0$). To obtain the results for non-zero D and E we diagonalize Eq. 5-5 and find, for $H_{so}(y)$ nonzero (one spin-orbit route active), that $I_+ > I_-$ for $D > 0$ and $I_+ < I_-$ for $D < 0$, as before. The intensities now are calculated from Eq. 5-11 using the eigenvectors.

Calculation of Zero-Field Splitting Parameters

Using the Optically Detected Magnetic Resonance technique (35) Maki, Svejda and Huber have measured the $|E|$ parameter for the molecule xanthione in an n-hexane Shpolskii matrix to be 0.0611 cm^{-1} . The D parameter was too large to measure using this technique. Burland, (36) however, reported that for xanthione in a xanthione single crystal host, the value of the D parameter is -11 and -20 cm^{-1} . These results were obtained from direct measurements of the phosphorescence from the lowest triplet state of the two xanthione guest sites in the host crystal. This unusually large value of D has been attributed by these authors to be due to large spin-orbit effects induced by the sulfur atom in the xanthione. It is estimated (35), using second order perturbation theory and estimates of state energies from experimental spectra, that $|D| > 0.77 \text{ cm}^{-1}$ in the xanthione $^3n\pi^*$ state (T_1), with D negative.

With these considerations in mind and the evidence of large spin-orbit coupling in TMCBDT we will apply the results of the calculations in Chapter 4 to estimate the value of the spin-orbit contribution to the zero-field parameters for TMCBDT.

The values of D for molecules in which the spin-orbit coupling effects are small are usually less than 1 cm^{-1} (102). For the specific case where the two unpaired electrons are localized on the same atom, a carbene radical in its ground triplet state (36), the value of $|D|$ is $\sim 0.7 \text{ cm}^{-1}$. With this in mind the spin-spin interaction is neglected and only the spin-orbit contribution to the zero field splitting parameters is calculated.

In these calculations it will be assumed that the zero-field tensor $\vec{S} \cdot \vec{\rho} \cdot \vec{S}$ is diagonal in the molecular axis system, which is taken to be, as before, with the y axis collinear with the C=S bonds, the x axis perpendicular to the molecular plane and the z axis through the ring carbon atoms and bisecting the C-CH₃ bonds, with the origin in the geometric center of the ring. It is also assumed that the g tensor is diagonal in this same coordinate system.

Following Hamerka (87) the matrix element for the interaction energy between two triplet sublevels is

$$H_{uv} = H_{uv}^{SS} + H_{uv}^{SO} = \langle {}^3\Psi_1^u | H_{SS} | {}^3\Psi_1^v \rangle - \sum_k \frac{\langle {}^3\Psi_1^u | H_{SO} | {}^1\Psi_k \rangle \langle {}^1\Psi_k | H_{SO} | {}^3\Psi_1^v \rangle}{(E_k - E_1)} \quad (5-25)$$

Here ${}^3\Psi_1^u$ and ${}^1\Psi_k$ are the zeroth-order wavefunctions for the T_1 state and k^{th} perturbing singlet state, while E_1 and E_k are their zeroth-order energies, respectively. To evaluate H_{uv}^{SO} we proceed in the same way as in Chapter 4. Because of the D_{2h} Point group symmetry, the nature of H_{SO} and the action of the spin operator S^- on the zero-field spin functions, we find that H_{uv}^{SO} is diagonal in this basis. Carrying out the spin operations as before we find

$$H_{uv}^{SO} = - \sum_k (E_k - E_1)^{-1} \langle \phi_1 | \frac{1}{2} R_u^- | \phi_k \rangle \langle \phi_k | \frac{1}{2} R_u^- | \phi_1 \rangle \delta_{uv} \quad (5-26)$$

The appropriate quantities from Table 4-2 are now substituted into the above:

$$\begin{aligned} X' &= H_{xx}^{SO} = -0.4525 \text{ cm}^{-1} \\ Y' &= H_{yy}^{SO} = -0.4233 \text{ cm}^{-1} \\ Z' &= H_{zz}^{SO} = -3.22 \times 10^{-4} \text{ cm}^{-1} \end{aligned} \quad (5-27)$$

Now imposing the requirement that the trace of the zero-field tensor be zero, we find $X = X' - \frac{1}{3} (X' + Y' + Z')$ and similar expressions for Y and Z.

This gives for the spin-orbit contribution to the calculated zero-field splitting parameters of TMBCDT

$$\begin{aligned} X &= -0.160 \text{ cm}^{-1} & D &= -0.439 \text{ cm}^{-1} \\ Y &= -0.131 \text{ cm}^{-1} & E &= +0.015 \text{ cm}^{-1} \\ Z &= +0.292 \text{ cm}^{-1} \end{aligned} \quad (5-28)$$

The largest contributions to each of these come from the ${}^1_{\sigma\pi}({}^1B_{3u})$ state at 3.62 eV for the X component, the two ${}^1_{\pi+}({}^1B_{2u})$ states at 4.55 and 5.32 eV, respectively, for the Y component and the ${}^1_{n+\sigma}({}^1B_{1u})$ state at 17.8 eV for the Z component.

The calculation predicts a positive E value and a negative D value. The sign of D is the same as that found for xanthione (36) but the magnitude is about 25 times smaller. If the excited state energies are too high as calculated by EHT, a reasonable assumption, we can expect that the values of X, Y and Z are underestimated by this calculation.

Influence of Triplet-State Perturbers

Hameka (116) considers the effect of triplet-triplet interactions arising as second order terms in the zero-field splitting parameters. However, he points out that the matrix elements arising from these are diagonal and as such shift all three triplet sublevels equally and therefore do not contribute to the zero field splitting since this is just the difference between the eigenvalues of the matrix. Using the triplet spin basis which transforms as the rotations in the point group of the molecule, it turns out that these matrix elements are indeed diagonal but do not contribute equally to the X, Y and Z parameters. This has since been recognized (35,117), however, but the expressions given by these authors are not very clear. Because of the importance

of spin-orbit effects in the TMCBDT this will be examined in some detail. Unfortunately due to lack of experimental data, as well as accurate calculations on excited states, for TMCBDT and xanthione, this may only be done qualitatively.

In Chapter 4 the perturbation of the ground electronic state by triplet states via the spin-orbit interaction was seen to be an important factor in the radiative properties of T_1 . The spin-orbit interaction can also couple T_1 with other triplet states (116) thus the T_1^x sublevel will have mostly $A_u \cdot {}^3\omega_x$ character with $B_{3u} \cdot {}^1\sigma_o$ character brought in by $H_{so}^-(x)$, $B_{2u} \cdot {}^3\omega_z$ brought in by $H_{so}^+(y)$ and $B_{1u} \cdot {}^3\omega_y$ via $H_{so}^+(z)$. Including these effects then gives the following result for the first-order perturbation-corrected wave function of the T_1^x sublevel, for example

$$\begin{aligned}
 {}^3\phi_x(A_u) = & {}^3\phi_x^o(A_u) + \sum_k \frac{(B_{3u}) \langle {}^1\phi_k^o | H_{so}^-(x) | {}^3\phi_x^o(A_u) \rangle}{E_1 - E_k} \cdot {}^1\phi_k^o \\
 & + \sum_{\ell} \frac{(B_{2u}) \langle {}^3\phi_{z,\ell} | H_{so}^+(y) | {}^3\phi_x^o(A_u) \rangle}{E_1 - E_{\ell}} \cdot {}^3\phi_{z,\ell} + \sum_{\ell} \frac{(B_{1u}) \langle {}^3\phi_{y,\ell} | H_{so}^+(z) | {}^3\phi_x^o(A_u) \rangle}{E_1 - E_{\ell}} \cdot {}^3\phi_{y,\ell}
 \end{aligned} \quad (5-29)$$

Similar expressions are obtained for the Y and Z sublevels of T_1 . As before we calculate the matrix elements of the operator

$$H = H_{so} + H_{ss}$$

using these corrected functions and find that only diagonal elements are nonzero. Again for the x sublevel we get

$$x' = \langle {}^3\phi_{x1}^o | H_{so} + H_{ss} | {}^3\phi_{x1}^o \rangle = \langle {}^3\phi_{x1}^o | H_{ss} | {}^3\phi_{x1}^o \rangle$$

1. See Equation 4-15, p. 99.

$$\begin{aligned}
& + \frac{(B_{3u})}{\sum_k} \frac{|\langle \phi_k^0 | H_{so}^- (x) | \phi_{x1}^0 \rangle|^2}{E_1 - E_k} + \frac{(B_{2u})}{\sum_\ell} \frac{|\langle \phi_{z,\ell}^0 | H_{so}^+ (y) | \phi_{x,1}^0 \rangle|^2}{E_1 - E_\ell} \\
& + \frac{(B_{1u})}{\sum_\ell} \frac{|\langle \phi_{y,\ell}^0 | H_{so}^+ (z) | \phi_{x,1}^0 \rangle|^2}{E_1 - E_\ell} . \quad (5-30)
\end{aligned}$$

The calculation then proceeds as in the previous section, and one finds that (neglecting $\langle H_{ss} \rangle$) $X' = Y' = Z'$, or that $D=E=0$. This is because in the EHT approximation the orbital part of the singlet and corresponding triplet wavefunctions are the same. This results in the same value for $\langle \phi_{z,1}^0 (B_{2u}) | H_{so}^+ (y) | \phi_{x,1}^0 \rangle$ appearing in X' and $\langle \phi_{2u}^0 (B_{2u}) | H_{so}^- (y) | \phi_{y1}^0 \rangle$ appearing in Y' . The corresponding energy denominators are also the same, for the same reason.

Now suppose we had reasonable SCF functions which adequately described the singlet and triplet states and reflected their energy splitting correctly. We could then calculate D-E from the difference of the X and Z elements, if E is small we can write

$$\begin{aligned}
D-E &= \langle \phi_{x1}^0 | H_{so} + H_{ss} | \phi_{x1}^0 \rangle - \langle \phi_{z1}^0 | H_{so} + H_{ss} | \phi_{z1}^0 \rangle \\
&= \langle \phi_{x1}^0 | H_{ss} | \phi_{x1}^0 \rangle - \langle \phi_{z1}^0 | H_{ss} | \phi_{z1}^0 \rangle \\
&+ \frac{(B_{3u})}{\sum_k} \left\{ \frac{|\langle \phi_k^0 | H_{so}^- (x) | \phi_{x1}^0 \rangle|^2}{E_1 - E_{k(s)}} - \frac{|\langle \phi_{yk}^0 | H_{so}^+ (x) | \phi_{z1}^0 \rangle|^2}{E_1 - E_{k(t)}} \right\} \quad (5-31) \\
&+ \frac{(B_{2u})}{\sum_\ell} \left\{ \frac{|\langle \phi_{z\ell}^0 | H_{so}^+ (y) | \phi_{x1}^0 \rangle|^2}{E_1 - E_{\ell(t)}} - \frac{|\langle \phi_{x\ell}^0 | H_{so}^+ (y) | \phi_{z1}^0 \rangle|^2}{E_1 - E_{\ell(t)}} \right\} \\
&+ \frac{(B_{1u})}{\sum_k} \left\{ \frac{|\langle \phi_{yk}^0 | H_{so}^+ (z) | \phi_{x1}^0 \rangle|^2}{E_1 - E_{k(t)}} - \frac{|\langle \phi_k^0 | H_{so}^- (z) | \phi_{z1}^0 \rangle|^2}{E_1 - E_{k(s)}} \right\}
\end{aligned}$$

It is assumed here that the sublevel splittings are negligible in comparison to the energy difference between the perturbed and unperturbed states. The subscripts (s) and (t) refer to the singlet and triplet

energy for the states whose orbital symmetry is the same. The second sum is clearly zero.

Now assuming there are perturbing states which lie close enough to T_1 so that the energy denominators are small, we see that D-E is then determined, at this level of approximation, by the sum of two factors: 1) the difference of the spin-spin matrix elements and 2) the difference of the square of spin-orbit matrix elements divided by the energy term for the singlet and that same quantity for the triplet. This second term appears for the two symmetry components involved. In the Y-X (=2E) calculation for example, the $H_{so}(z)$ component would contribute zero. Once again we examine only the factor due to spin-orbit coupling.

Using the method previously discussed in Chapter 4 and Table 4-2 we find for the B_{3u} sum that there are only 3 states, all σ_{-}^{*} , which dominate. These will reduce to

$$\frac{|\langle \sigma_{-}^{*} | R_x^{-} | n_{+} \pi_{-}^{*} \rangle|^2}{E_1 - E_s} \quad \text{and} \quad \frac{|\langle \sigma_{-}^{*} | R_x^{+} | n_{+} \pi_{-}^{*} \rangle|^2}{E_1 - E_t}$$

For the B_{1u} , the two largest contributors are both $n_{+} \sigma_{+}^{*}$ states.

Thus for the B_{3u} terms the integrals reduce to

$$\frac{\langle 1 | R_x^{-} | n_{+} \rangle}{E_1 - E_s} \quad \text{and} \quad \frac{\langle 3 | R_x^{+} | n_{+} \rangle}{E_1 - E_s + E_s - E_t}$$

While for the B_{1u} we have

$$\frac{|\langle 1 \sigma_{+}^{*} | R_z | \pi_{-}^{*} \rangle|^2}{E_1 - E_s} \quad \text{and} \quad \frac{|\langle 3 \sigma_{+}^{*} | R_z | \pi_{-}^{*} \rangle|^2}{E_1 - E_s + E_s - E_t}$$

The left superscripts 1 and 3 denote that the molecular orbital appearing in the integral is from the singlet $B_{3u}(B_{1u})$ state having energy E_s and from the triplet state of the same symmetry having energy E_t , respectively. The $E_1 - E_t$ may be expressed as the $E_1 - E_s$ separation plus $E_s - E_t$, the singlet-triplet energy separation. Using Y' and Z' we can get $D+E$ which will be of the same form as Eq. 5-31. Then, D and E can be obtained by adding and subtracting this and Eq. 5-31.

The above arguments demonstrate the origin of the spin-orbit contributions to the zero-field splitting parameters. Since the $R_z |\pi_-^* \rangle$ ($R_x |n_+ \rangle$) portion of the numerators is the same, the contribution to D will be due to the difference in the electron density distribution of the molecular orbital σ^* (σ) between the singlet and triplet state of B_{1u} (B_{3u}) symmetry. The singlet-triplet energy separation will also be important, but its magnitude will also be determined by the wavefunction differences between singlet and triplet states.

For approximate calculations the CNDO methods are often used (8), using the ground state wavefunction and virtual orbitals for the singly occupied excited molecular orbitals. In this case, the singlet and triplet wavefunctions are the same, however $E_s - E_t$ is then given by $2K$, where K is the exchange energy. For the $n_+ \pi_+^*$ state of cyclobutane-dione (8) (CBD, discussed in Chapter 2) for example, K is calculated to be $\sim 90 \text{ cm}^{-1}$ using the CNDO/S parameterization and $\sim 700 \text{ cm}^{-1}$ using the CNDO/2 parameters. At the single configuration *ab initio* level of approximation (see Chapter 2) a separate SCF calculation for the singlet and triplet states gives $E_s - E_t$ for the $n_+ \pi_+^*$ configuration of CBD as 3419 cm^{-1} . This shows the well known fact that there can be a very

large variation in $E_s - E_t$ depending on the method of calculation. Thus including effects due to triplet-triplet perturbations is justified only if one has very good quality wavefunctions. Because it is expected that configuration interaction in the singlet and triplet manifolds may shift states differently (again, because a given excited configuration, say $n_+ \sigma^*$, would have a different orbital wavefunction for the triplet and singlet states), it is not unreasonable to expect that CI would be important in this type of calculation.

Localized and Delocalized Excitations

As was discussed in Chapter 2, for the case of an $n\pi^*$ transition in a system containing two symmetry equivalent atoms which have a nonbonding orbital, Wadt and his coworkers (48) have shown that by relaxing the symmetry restriction on the wavefunction, the n orbital of the $n\pi^*$ state remains localized on the heteroatom and the π^* orbital adjusts to minimize the value of K for the singlet and maximize it for the triplet. This effect produces a large difference in the π^* orbital between the singlet and triplet states. If the same situation holds for $n\sigma^*$ transitions (or $\sigma\pi^*$ transitions), then it would follow that for these systems a large zero-field-splitting parameter, D , can be expected if the heteroatom(s) have relatively large spin-orbit coupling constants. Considering the case of CBD, it was shown in Chapter 2 that for the lowest $n\pi^*$ state the $E_s - E_t$ splitting in the orbital symmetry restricted wavefunction case (D_{2h}) is about 1700 cm^{-1} , while in the symmetry unrestricted calculation (C_s) this splitting is about 2700 cm^{-1} . This increase in S-T splitting due to a localized (Valence-Bond) description of the excited state would seem to give a larger calculated value of the zero-field splitting parameters.

So far the emphasis on the localized description calculations (see refs. in Chapter 2) has been on the determination of n orbital splittings, singlet and triplet energies and excited state geometry. It would be interesting to investigate the consequences of the localized description on the various matrix elements discussed above. In fact only compounds containing nitrogen and oxygen as the source of nonbonding electrons have thus far been investigated. One would tend to expect similar results to be found for thiocarbonyl containing compounds, except in those properties where spin-orbit coupling is important.

Comment on Xanthione

The spin-orbit coupling contribution to D for Xanthione calculated by Maki, Svedja and Huber (35) -0.77 cm^{-1} while the observed (36) D is -11 cm^{-1} for one of the Xanthione sites in the Xanthione host. For the other site Burland finds -20 cm^{-1} and claims the intersite difference of 11 cm^{-1} could easily be due to energy differences in the molecular (perturbing) states at the two sites. In view of the large shifts found for some aromatic hydrocarbons (72), ranging from 500 to 3000 cm^{-1} , and with an observed 425 cm^{-1} splitting between the Xanthione sites, this appears to be a reasonable assumption. No attempt was made, however, to explain the large discrepancy between the calculated and observed value for D .

In view of the preceding discussion we suggest two possible sources of error that give too low a calculated value for D . First, is the neglect of all perturbing states other than S_2 and T_2 . Capitanio, Pownall and Huber (31) have observed several ${}^1_{\pi\pi^*}$ states above T_1 :

two are A_1 and two are B_2 . Including the other A_1 state in the calculation would increase the value of X-Z. All other quantities being equal this would amount to an increase of ~50% (due to the energy denominator) in X-Z.

Second, relaxing the assumption that the orbital part of the wavefunction for the singlet and triplet states is the same means that if $|\langle {}^1\phi_{A_1}^o | H_{so}^- | {}^3\phi_1^o \rangle| < |\langle {}^3\phi_{A_1}^o | H_{so}^+ | {}^3\phi_1^o \rangle|$ this would tend to increase D by the square of that difference. We believe the arguments on localization with regard to the K integral support this idea. Capitanio, Pownall and Huber (31) also find that a CNDO/S-SECI calculation shows that the greatest change in electron density in the $\pi\pi^*$ transition (T_1) occurs on the C=S chromophore. This indicates that the π^* electron is rather localized on this chromophore rather than completely delocalized over the rings. In the same calculation these authors find that the second transition, $\pi\pi^*$, behaves in the same way. This corresponds to the lowest A_1 state. For such a system, where the unpaired electrons tend to have a high density in a localized region of the molecule it is reasonable to expect that the singlet-triplet differences in electron distribution would be large. Part of this difference is reflected by the molecular orbital coefficients on the sulfur atom. One center contributions to $\langle H_{so} \rangle$ from the sulfur contain the spin-orbit coupling constant (ζ) of $\sim 400 \text{ cm}^{-1}$. Using Eq. 4-25 we see that the contributions to X-Z may be written as

$$\frac{1}{4} \left\{ \frac{|\zeta c_{np_y} c_{\pi p_x}^s|^2}{-E_s} - \frac{|\zeta c_{np_y} c_{\pi p_x}^t|^2}{-(E_s - E_{st})} \right\}$$

The superscripts s and t refer to singlet and triplet molecular orbital coefficients and the energy denominators are as in Eq. 5-31. Because of the localization argument $|C_n C_\pi^t|$ is expected to be larger than $|C_n C_\pi^s|$.

If we now let $d = (C_\pi^t)^2 - (C_\pi^s)^2$ we can write for the contribution to X-Z from spin-orbit effects using Eq. 5-31 as

$$(X-Z)_{so} = \frac{1}{4} C_n^2 \zeta^2 \left\{ \frac{(C_\pi^s)^2}{E_s} - \frac{(C_\pi^s)^2}{E_s - E_{st}} - \frac{d}{E_s - E_{st}} \right\} \quad (5-32)$$

The first two terms are exactly as given by Maki, Svejda and Huber (35)

in their expression for D_{so} ; with the parameters these authors give

$(|\frac{1}{2} C_n C_\pi \zeta| = 97 \text{ cm}^{-1}$, $E_s = 8370 \text{ cm}^{-1}$ and $E_s - E_t = 4970 \text{ cm}^{-1}$) this amounts to -0.77 cm^{-1} . To estimate the importance of the third term, neglected by Maki, Svejda and Huber, we consider the localized $n\pi^*$ transition in CBD (Chapter 2).

To estimate the C_π^2 factors we use the net atomic populations of the π^* orbital on the excited oxygen atom. The difference in this quantity between the triplet state and singlet state should best reflect d. If we then assume that the same applies to TMCBDT we find that d \approx 0.07. Taking C_n^2 as 0.95 from the same calculation we then find for the neglected term

$$- \frac{(400)^2 (0.95) (0.07)}{4 (4970)} = -0.54 \text{ cm}^{-1}$$

This demonstrates that the amount neglected by assuming the same orbital wavefunction for the singlet and triplet states may be significant, particularly when the sulfur atom is involved (in the transition) because of its large spin-orbit coupling constant. The other $A_1(\pi\pi^*)$

state mentioned earlier, if included in a similar manner, could easily contribute another 50% of the above bringing the value for D_{SO} close to -2 cm^{-1} .

Experimental Details

Apparatus

The TMCBDT crystals were grown by sublimation in evacuated (10^{-3} torr), sealed glass tubes. TMCBDT used for this purpose was synthesized (118) by the procedure of Elam and Davis (119) from the corresponding dione (TMCBD) and phosphorus pentasulfide. The Zeeman measurements were taken using a pulsed magnet consisting of 110 windings around an 8 mm long, 2 mm (i.d.) steel tube. The crystal was attached to a 4 mm long fused quartz light pipe which was inserted in the coil bore.

The magnetic field was produced by charging a 76 μf capacitor to the appropriate voltage corresponding to the maximum field desired and discharging through the coil. The magnetic field strength was calibrated using the R lines of ruby with the optical arrangement described below. Fields up to 142 KGauss were used in the experiments. The entire assembly was either immersed in liquid helium for 4 K runs or in a flow tube through which the boil off allows temperature control from ~ 5 K to ~ 15 K.

The spectroscopic probe source was a Xe flashlamp which is triggered at the maximum magnetic field. The probe beam was sent through the sample to a 0.75 m Jarrell-Ash spectrometer. The dispersed light was focused at the target of a S.I.T. vidicon of an optical multichannel analyzer (Princeton Applied Research). The digitized spectra were then processed and plotted by computer. Nominally 5 exposures were coadded as a means of signal averaging.

Crystal Mounting

The TMCBDT crystals are extremely volatile and very soft so that great care had to be taken in handling and mounting them on the quartz lightpipe. The crystals grow in such a way that the ac face is usually parallel to the tangent plane to the glass tube at the location where the crystal develops. This means that the side attached to the glass is usually rounded and has to be polished flat and parallel to the other side. Most acceptable crystals are much larger than the diameter of the quartz lightpipe and have to be cut down to size. Because of these considerations it is almost impossible to obtain a mounted crystal which has the c axis exactly perpendicular to the coil axis, and therefore to the magnetic field direction. The Zeeman intensity pattern is very sensitive to magnetic field orientation with respect to the molecular axes (*vide supra*). This orientation must be properly considered when attempting to correlate calculated Zeeman intensity patterns with those observed in these experiments. Figure 5-3 shows the relationship among the various vectors of interest.

The important features are: first, the magnetic field is collinear with the direction of propagation of the analyzing light; second, the polarizer (for polarized runs) is oriented so that the analyzing beam is plane polarized and has the electric field vector always perpendicular to the magnetic field direction. Third, and most important, is the orientation of the crystal c axis with respect to the magnetic field (thus also defining its orientation with respect to \vec{E}) that is finally attained after polishing and mounting the crystal. Shown in Fig. 5-3 is the orientation in which the c axis is perpendicular to \vec{H}

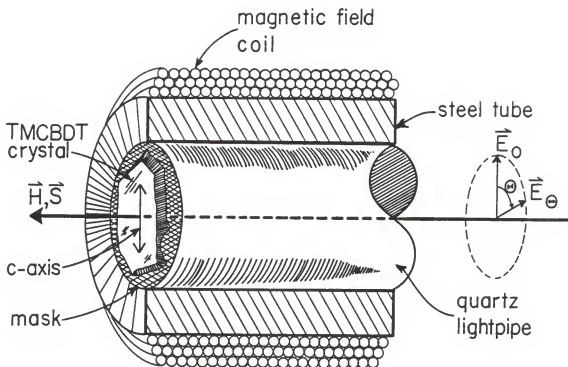


Figure 5-3. Light-pipe and coils assembly used in the Zeeman experiments. Details are explained in the text. \vec{S} is the Poynting vector; it defines the direction of propagation of the analyzing light which is collinear with the magnetic field, \vec{H} . The electric field vector of the analyzing light, \vec{E} , is shown for two polarizer orientations: $\theta = 0^\circ$ and $\theta = 90^\circ$.

Figure 5-4. Zeeman absorption spectrum at 1.6 K of the 594 nm band polarized perpendicular to c. Absorbance spectra of crystal A recorded on the Zeeman apparatus (see Fig. 5-3). The polarization is perpendicular to the c crystal axis. Both zero-field and high-field tracings are plotted on the same wavelength scale to show the shift in the peak position of the $|0\rangle$ transition with respect to the zero-field absorption. This shift indicates a finite zero-field splitting of the triplet state. The difference in the splittings Δ_+ and Δ_- of about 1 cm^{-1} and in the intensities I_+ and I_- further support this. See text and Table 5-6. The broad band to the red of 594 nm band is not due to TMCBDT, see text.

$$T = 1.6 \text{ K}$$

$$\Theta = 90^\circ$$

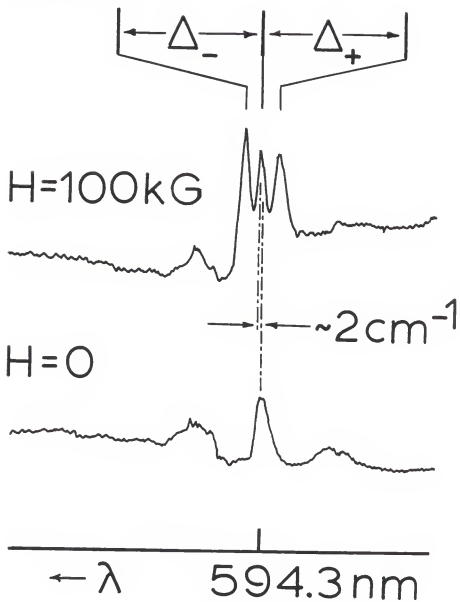
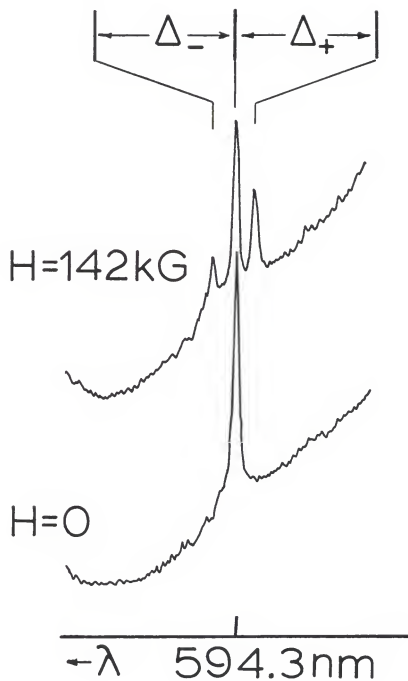


Figure 5-5. Unpolarized Zeeman absorption spectrum at 1.6 K of the 594 nm band. Absorbance spectra of crystal F recorded on the Zeeman apparatus (see Fig. 5-3) using unpolarized light. Both zero-field and high-field tracings are plotted on the same wavelength scale. The shift in peak position of the $|0\rangle$ transition is not as pronounced as in crystal A (see Fig. 5-4 and Table 5-6). The difference in the splittings Δ_+ and Δ_- and the I_+ and I_- intensity imbalance indicate a finite zero-field splitting and are discussed in the text. Values for these are also given in Table 5-6.

$T=1.6\text{K}$

Unpol.



($\psi=0$ in notation used in Fig. 5-1). The definition of the polarizer angle, θ , is such that $\theta=90$ gives the maximum observed zero-field signal. Spectra of the 5943 \AA region were taken for various settings of the polarizer.

Experimental Results

Low Temperature Results: 1.6 K

Zeeman absorption experiments on the 5943 \AA band of TMCBDT were performed at three different temperatures: 1.6 K, 5 K and 16 K. Due to experimental difficulties at 1.6 K only two crystals could be examined. In the first sample, crystal A, a zero-field absorption and a $\theta=90^\circ$ ($\parallel c$) polarization Zeeman absorption measurement was made. These results are shown in Fig. 5-4. In the second sample, crystal F, a zero field absorption spectrum and an unpolarized Zeeman absorption spectrum were recorded and are shown in Fig. 5-5.

With regard to crystal A zero-field absorption in Fig. 5-4, the broad band to the red of the 5943 \AA line is unexplained, but it is normally not seen and it is certainly not a spectral feature of TMCBDT. The broad band to the blue of the 5943 \AA band is a phonon sideband and low frequency mode as discussed in Chapter 3. The 10 cm^{-1} FWHM of the ZFA band in this sample is very large for such low temperature. The FWHM of the Zeeman absorption (taken at 100 KGauss, $\theta=90$) bands vary from 5 cm^{-1} for the $|0\rangle$ transition to $7-9 \text{ cm}^{-1}$ for the $|-\rangle$ and $|+\rangle$ transitions.

The imbalance in the Zeeman transitions should be noted. The $\Delta_-(\epsilon_- - \epsilon_0)$ and $\Delta_+(\epsilon_+ - \epsilon_0)$ are 8.8 and 10.5 cm^{-1} , respectively; their difference is 1.7 cm^{-1} . The intensity of the $|-\rangle$ transition is greater than that of the $|+\rangle$ transition; this seems to be so even if the peak of

the band which appears to be abnormally sharp is an artifact. The ratios are $I_{O-}/I_{+} = 0.78$, $I_{O-}/I_{+} = 1.19$ and $I_{+}/I_{-} = 0.65$.

Finally, we note that the Zeeman $|0\rangle$ transition maximum appears to be shifted to the red of the ZFA absorption at 5943 \AA by about 2 cm^{-1} .

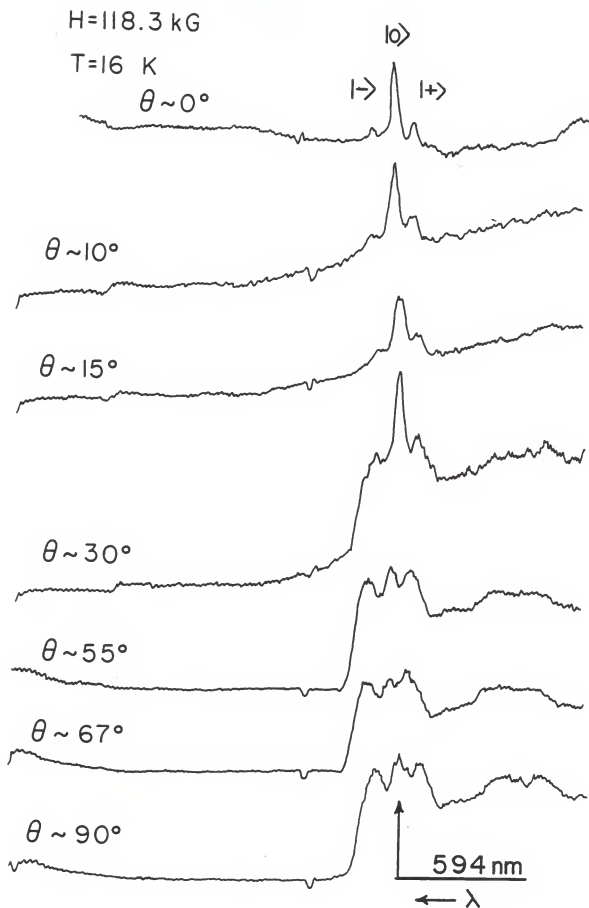
For crystal F (142 KGauss, unpolarized) we find a much smaller base line with essentially no phonon structure and sharper bands. In this case we find a FWHM of 3.5 cm^{-1} for both ZFA and Zeeman transitions. As in the previous sample there is an asymmetry in the Zeeman transitions. In this case, the intensity imbalance is unquestionable with the $|+\rangle$ transition being more intense than the $|-\rangle$ one. The ratios here are $I_{O-}/I_{+} = 2.78$, $I_{O-}/I_{+} = 1.85$ and $I_{+}/I_{-} = 1.50$, while the sublevel splittings are $\Delta_{-} = 12.3 \text{ cm}^{-1}$ and $\Delta_{+} = 11.4 \text{ cm}^{-1}$. The transition to the $|0\rangle$ Zeeman substate seems to be shifted to the red of the ZFA absorption by only $\sim 1.2 \text{ cm}^{-1}$ in this case.

The scarcity of data at this temperature is due to the crystals being jarred loose after only a few shots by turbulence which is generated in the liquid helium when the coils are energized. For this reason subsequent samples were run at higher temperatures, keeping the light-pipe assembly above the liquid helium. The temperature could then be varied by changing the height of the crystal above the liquid helium.

Temperatures above 4 K

The experiment at 16 K consisted of Zeeman absorption measurements on crystal B for various polarizer settings and are shown in Fig. 5-6; five shots were averaged for each polarizer angle in a field of 132 KGauss. For this case there are obviously phonon bands present for polarizer settings greater than 30° .

Figure 5-6. Polarized Zeeman absorption spectra of the 594 nm band at 16 K as a function of polarizer orientation. Absorbance spectra of crystal B taken as a function of polarizer orientation on the Zeeman apparatus (see Fig. 5-3). Wavelength increases from right to left. Each trace shown is the result of 5 averaged spectra. The variation of the Zeeman intensity ratio with the electric field vector orientation relative to the crystal axes is evident. See text and Table 5-4. The polarizer angles, θ , are in degrees relative to the orientation which gives minimum zero-field absorbance, ($\theta=0$).



As can be seen from Fig.5-6 the intensity ratios I_{O+}/I_{O-} and I_{O-}/I_{O+} change with θ ; starting at about 5 for $\theta=0$ ($\vec{E} \parallel$ projection of c onto crystal face) to about 1 for $\theta=90$ ($\vec{E} \perp c$). This behavior implies that more than one spin-orbit route is active (111), if it can be assumed that the magnetic field is along a crystal axis. In order to compare the ratios to the calculated values, peak heights were measured from a straight baseline, since the widths are nearly the same ($\sim 3.4 \text{ cm}^{-1}$). These ratios are collected in Table 5-2.

In the experiment in which crystal C was used (5 K) both absorption and emission spectra were taken. For the absorption spectra of the 5943 \AA band 5 shots were averaged for each polarizer angle at the highest magnetic field possible, 142 KGauss. These are shown in Fig. 5-7 and their intensity ratios are given in Table 5-3. Also taken were zero-field spectra as a function of polarizer angle (average of 5 shots), shown in Fig. 5-8. In addition, the same was done as a function of magnetic field strength but using unpolarized light; a neon (gas discharge) spectrum was taken in the region of the Ne 5974.628 and 5944.834 \AA lines using the same dispersion and OMA settings so that these could be plotted on the same scale as the spectra, shown in Fig. 5-9. These results also show a slight difference in the Δ_+ and Δ_- splittings. The emission spectra recorded for crystal C as a function of field strength are due to radiation from the trap at 6003 \AA . In this and all other Zeeman emission spectra recorded for this sample, only the $|-\rangle$ and $|0\rangle$ emission bands were detected. In an experiment in which the emission was recorded as a function of temperature between 5 K and 19 K, emission to the blue of 6003 \AA (due to the next higher

TABLE 5-2
OBSERVED RATIOS FOR THE ZEEMAN ABSORPTION (CRYSTAL B) OF THE
5943Å BAND AT 4.16 K AS A FUNCTION OF POLARIZER ANGLE. $\theta=90^\circ$
defines the maximum zero field absorption.
'Ave' = $\frac{1}{2}(I_o/I_+ + I_o/I_-)$.

θ^a	I_o/I_-^b	I_o/I_+	I_+/I_-	Ave.
0	5.80	4.14	1.40	4.97
10	4.14	3.22	1.29	3.68
15	3.38	2.59	1.31	2.99
30	1.90	2.22	0.86	2.06
55	0.898	1.33	0.68	1.11
67	0.808	1.05	0.77	0.93
90	0.964	1.35	0.71	1.16

a. θ is the polarizer angle in degrees, see Fig. 5-3.

b. The subscripts o, + and - refer to the triplet substates.
I denotes the intensity of the transition to that state.

Figure 5-7. Polarized Zeeman absorption spectra of the 594 nm band at 5 K as a function of polarizer orientation. Absorbance spectra of crystal C taken as a function of polarizer orientation on the Zeeman apparatus (see Fig. 5-3). Wavelength increases from right to left. Each trace shown is the result of 5 averaged spectra. The polarizer angles, θ , are in degrees relative to the orientation which gives minimum zero-field absorbance ($\theta=0$). The intensity variation with polarizer orientation relative to the crystal axes is not as evident here. See text and Table 5-3.

$H=142$ kG
 $T=5.2$ K

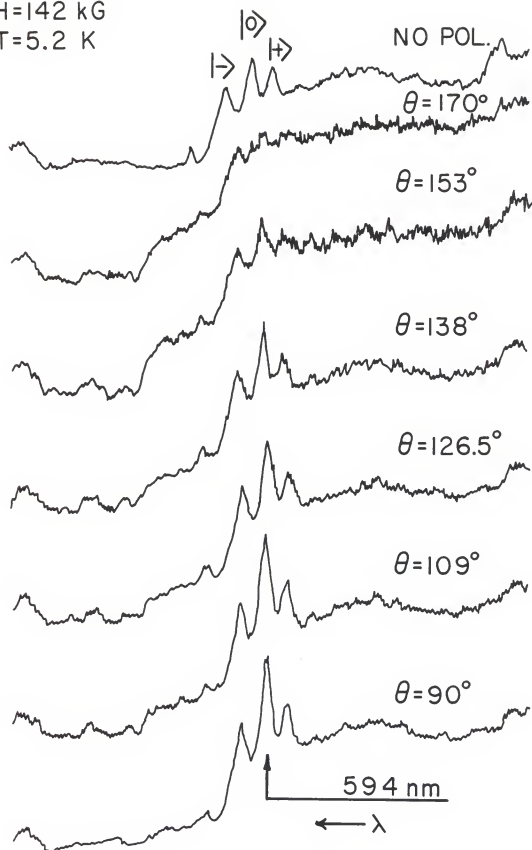


TABLE 5-3
OBSERVED RATIOS FOR THE ZEEMAN ABSORPTION (CRYSTAL C) OF THE
5943A BAND AT $\sim 5^\circ\text{K}$ AS A FUNCTION OF POLARIZER ANGLE. $\theta=90^\circ$
defines the maximum zero field absorption. 'NP' means
unpolarized measurement. 'Ave' = $\frac{1}{2}(I_o/I_+ + I_o/I_-)$.

θ^a	I_o/I_-^b	I_o/I_+	I_+/I_-	Ave.
170	0.93	1.92	0.49	1.42
153	1.31	2.37	0.55	1.84
138	1.51	2.00	0.75	1.75
126.5	1.39	2.38	0.58	1.89
109	1.68	2.09	0.80	1.89
90	1.59	2.29	0.69	1.94

NP	1.28	1.87	0.68	1.57

a. θ is the polarizer angle in degrees, see Fig. 5-3.

b. The subscripts o, + and - refer to the triplet substates.

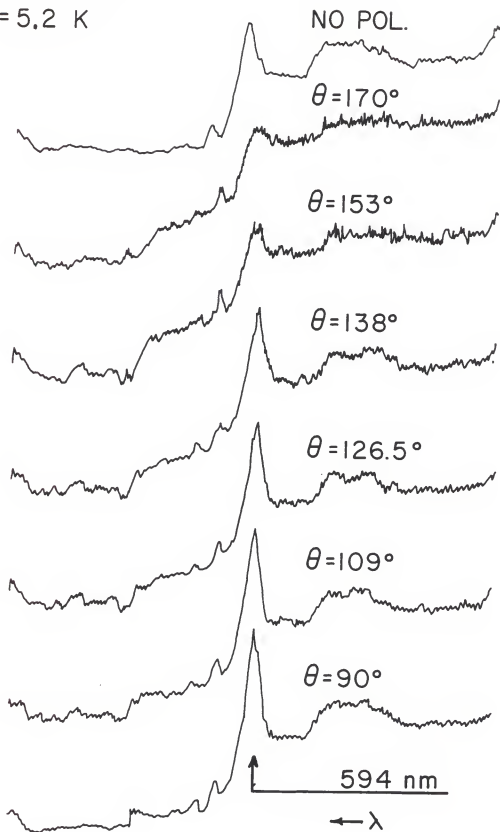
I denotes the intensity of the transition to that state.

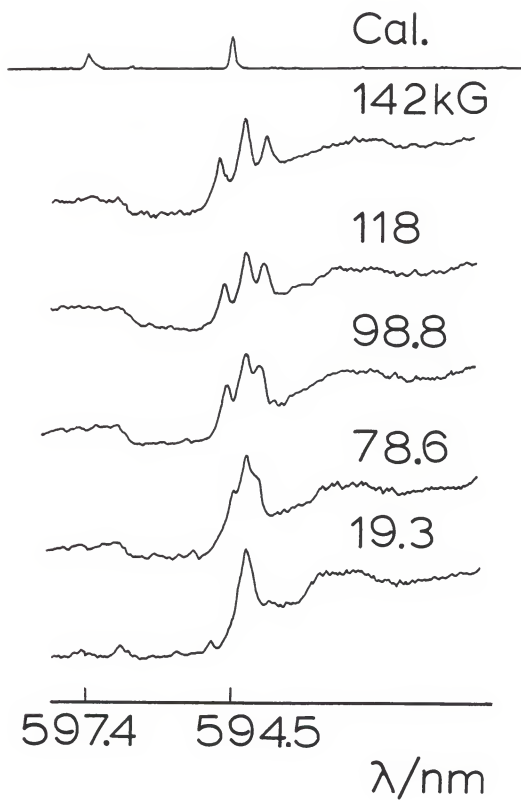
Figure 5-8. Polarized zero-field absorption spectra of the 594 nm band at 5 K as a function of polarizer orientation. Absorption spectra taken in zero-field (ZFA) using the Zeeman apparatus (see Fig. 5-3) as a function of polarizer orientation. Each trace is the average of 5 spectra taken for crystal C at the same polarizer settings for those spectra recorded in high field (Fig. 5-7); recording the ZFA and high-field spectra in the same experiment insures identical alignment in both measurements. The intensity at each polarizer setting relative to that at $\theta=90^\circ$ is given in Table 5-4. This information is used to determine the orientation of the c crystal axis relative to the direction of the incident light, \hat{s} in Fig. 5-3. See text, p. 137 ff.

Figure 5-9. Unpolarized Zeeman absorption spectra of the 594 nm band at 5 K as a function of magnetic field strength. The spectrum labeled 'cal.' records the Ne calibration lines (discharge tube) whose wavelengths are given on the horizontal axis. The other traces are the average of 5 absorption spectra taken at the indicated field strengths, measured in kiloGauss. The imbalance in the Δ_+ and Δ_- splittings (see text, p. 138-144) are given in Table 5-5.

ZERO FIELD

T = 5.2 K



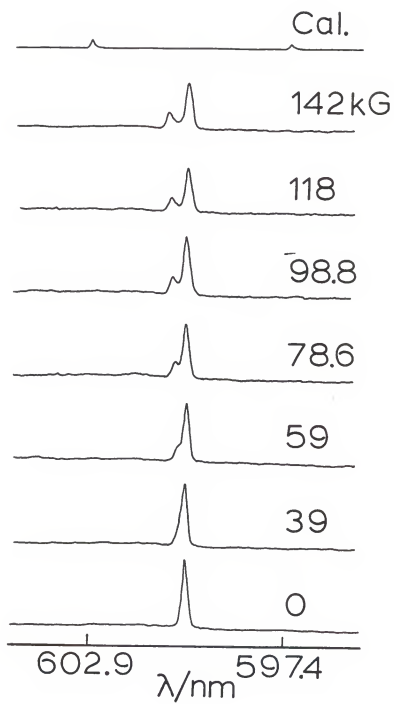


lying trap) grows in as the temperature drops below 8 K. This emission, although much weaker than that of the 6003 Å trap, also seems to have intensity in the $|-\rangle$ and $|0\rangle$ transitions. The field dependent emission results are introduced here for comparison with the field dependent absorption results and are given in Fig. 5-10. The sublevel splittings Δ_+ and Δ_- are given in Table 5-5 with the estimated errors.

Measurement Errors

The dispersion calculated from the separation of the neon calibration lines in the absorption run (Fig. 5-9) is 0.3071 Å/unit (120). The ϵ_0 line is 5 units to lower wavelength than the 5944.834 Å Ne line giving a value of $\epsilon_0 = 5943.30 \text{ Å}$ which compares very well with $5943.10 \pm 0.18 \text{ Å}$ found for the J_c component of the 0-0 band of crystal D in the zero-field 1.6K absorption run with a Wollaston prism as described in Chapter 3. Since there are 500 OMA channels covering a spectral range of about 109.3 Å this gives approximately 0.22 Å/channel , which, for the ϵ_0 line, is $\sim 0.62 \text{ cm}^{-1}/\text{channel}$. If we estimate the error for the line position in these determinations as due mainly to the line position measurement we may take the error as ± 0.5 unit or about $\pm 0.15 \text{ Å}$. This amounts to about 1 OMA channel, or roughly $\pm 0.6 \text{ cm}^{-1}$. Considering the difference between the ϵ_0 lines measured by the two very different methods to be 0.20 Å (~ 1 channel) we estimate the error as $\pm 0.25 \text{ Å}$ or $\pm 0.71 \text{ cm}^{-1}$. Since this is the error in each ϵ , the error in Δ_+ is $\sqrt{2} (0.7) = \pm 1.0 \text{ cm}^{-1}$ and since the zero field splitting parameter D is related to the difference between Δ_+ and Δ_- the error in its estimate would be about $\pm 1.5 \text{ cm}^{-1}$.

Figure 5-10. Unpolarized Zeeman emission spectra of the 600 nm trap at 5 K as a function of magnetic field strength. The spectrum labeled 'cal.' records the Ne calibration lines (discharge tube) whose wavelengths are given on the horizontal axis. The other traces are emission spectra of the 600 nm trap at the indicated field strengths. The splittings are given in Table 5-5. Note the absence of the $|+\rangle$ transition band.



Two spectra were taken for $H=98.8$ KGauss and the difference in the ϵ_+ and ϵ_- line position relative to that of ϵ_0 was at most one unit, or $\sim 0.3 \text{ \AA}$ (0.85 cm^{-1}). They should be a good estimate of the error in Δ from magnetic field fluctuations and other instrumental instabilities. Also from these two measurements we can estimate the error to be expected in the intensity. This is found to be 1 unit for I_0 , 3 units for I_- and 4 units for I_+ . For these two runs the intensity ratios are

$$I_0/I_+ = 1.48 \quad \text{and} \quad 1.67 \quad \% \text{ diff} \quad 13\%$$

$$I_0/I_- = 1.48 \quad \text{and} \quad 1.61 \quad \% \text{ diff} \quad 9\%$$

$$I_+/I_- = 1.00 \quad \text{and} \quad 0.96 \quad \% \text{ diff} \quad 4\%$$

From these we estimate the error in the intensity ratios to be about $\pm 10\%$.

To insure that the total intensity reaching the photomultiplier tube was independent of polarizer angle, a $\lambda/4$ plate was inserted between the monochromator and photomultiplier tube. We therefore estimate that any error caused by additional polarization due to the grating is much less than 10%.

Another source of error in determining the band positions and intensities of the Zeeman transitions arises because of the broad sloping background due to the phonon modes. This is not believed to be a problem in cases like that in Fig. 5-5 because the background variation is linear in the region of the entire multiplet. In a case similar to that in Fig. 5-7, where the Zeeman multiplet appears to be on the shoulder of a broad gaussian feature, it may be expected that the baseline will not contribute equally to all three components.

To estimate this error a computer simulation was performed in which a Zeeman multiplet made up of gaussian bandshapes having symmetrical energy distribution ($\Delta_+ = \Delta_-$) and a known ratio (I_0/I_{\pm}) was added to a broad gaussian feature. The relative positions, intensities and bandwidths are taken from a typical experimental result, and the plot scaled so as to resemble the latter as much as possible. Only a few examples were done this way for an estimate; a systematic study of error as a function of the various parameters was not carried out. A straight baseline was drawn under the Zeeman multiplet and intensities (peak heights) measured from it. From the ratios I_0/I_{\pm} of 1.3 and 2 used for a HWHM of 1.6 cm^{-1} an error in the 'observed' ratios of 4% and 6%, respectively, was found. In the case of a ratio of 2 and a HWHM of 2 cm^{-1} the error was higher, being 5 and 16% for the low and high energy components. Thus it appears that the broader the band, the greater the error. The error in the position of the Zeeman components is about 8%, at most.

On the average, the errors in the intensity caused by this type of baseline subtraction are ~10-12%, about the same as that estimated above. The error in a Δ_+ or Δ_- would be estimated as 8%; at higher fields this is about 1 cm^{-1} , within the error limits estimated previously.

Discussion

Temperatures above 4K

It is worth mentioning here that initially the Zeeman experiments were carried out on TMCBDT crystals only to determine which bands in the system originating at 5943 Å were due to the $T_1(^3A_u) \leftarrow S_0(^1A_g)$ transition.

No particular attention was given to the crystal orientation and mounting. The splitting pattern observed in that experiment showed that the transitions to the $|-\rangle$ and $|+\rangle$ substates were more intense than that to the $|0\rangle$ substate. This is inconsistent with the results of the ZFA experiment at 1.6 K (crystal E) which showed that the intensity of the 5943 \AA band system was polarized $\perp c$. This latter observation leads to the assignment of ^3Au to the T_1 state, with the intensity and polarization being due to spin-orbit coupling with singlet states whose electric dipole allowed transitions are polarized along the C=S bonds in TMCBDT. In turn this implies a single spin-orbit route, which means that for the TMCBDT case a ratio I_0/I_{\perp} of 2 should be seen with the magnetic field \perp to the ac crystal face, and should be independent of polarization. An experiment to verify this was carried out using crystal A mounted as shown in Fig. 5-3, with the field believed to be \perp to the ac face. The crystals chosen for the experiments were similar in crystal habit to that of crystal D, for which the orientation of the c axis was determined by x-ray diffraction (76). A polarizing microscope was then used to determine the orientation of the c axis; the orientation with respect to the exposed face may change with polishing or mounting.

The only spectrum recorded for this crystal was for a \perp polarization with an observed ratio of $I_0/I_{\perp} \approx 1$. This was not in agreement with the expected pattern. Next, crystal B was mounted for a 16 K experiment in which spectra were recorded as a function of polarization. The results here showed a substantial difference between the intensity ratio observed with the electric field vector, \vec{E} , parallel to the c axis: $I_0/I_{\perp} \approx 4$, and that with \vec{E} perpendicular to the c axis: $I_0/I_{\perp} \approx 1$.

To interpret these results assuming that \vec{H} was \perp to the ac face we set $\psi=\phi=0$ in Eq. 5-16. The expected ratio is

$$\left(\frac{I_o}{I_+} \right)_{\psi=\phi=0} = \frac{2[\frac{1}{2}(R_x^2 + 1) - R_x] \tan^2 \theta}{2R_z^2 + [\frac{1}{2}(R_x^2 + 1) + R_x] \tan^2 \theta}$$

For $\theta=0$ this gives $I_o/I_+ = 0$ while for $\theta=90$ we get a ratio which approaches 2 as R_x approaches zero. Thus, while a value of $R_x \cong +0.17$ is required to give a ratio of ~ 1 at $\theta=90$, it is impossible to get a ratio of 5 for $\theta \cong 0$ and this field orientation unless $R_z = 0$. In this case $R_x \cong -0.17$ results in a ratio of ~ 4 . This situation is not possible because the transition moment ratio R_x is a molecular property and will not change during an experiment or, from crystal to crystal. Allowing for an error in the measurement of θ near 0° is only meaningful if $R_z \neq 0$. In this case, however, the maximum ratio will still be 2.

Thus it is apparent that while the Zeeman intensity ratio varies with polarization in the crystal B data, implying the presence of an additional spin-orbit route, no satisfactory values for transition moment ratios could be found to explain the data with the assumption that \vec{H} was \perp to the ac face.

The restriction that \vec{H} be along a crystal axis was removed and the formulas for the Zeeman ratio for an arbitrary field direction were applied. The data for the crystal C showed much less variation of intensity ratio with polarization.

Comparing the 90° measurement with the 10° and unpolarized ones, we find a difference of about 28% and 19%, respectively. Thus there is little difference between the two extreme polarizer settings. From this data, one would conclude that only one spin-orbit route is active,

and by comparison with the theoretical result in Fig. 5-2(f) confirm it to the $H_{SO}(y)$ (or $H_{SO}(x)$). Further, we can see from the above discussion that the field must be nearly perpendicular to the ac plane of the unit cell.

The intensity of the ZFA bands in Fig. 5-8 is given in Table 5-4 along with those from two other runs on crystals D and E. This shows that the band intensity varies with θ according to Eq. 5-20 for the three bands at 5943 \AA , 5926 \AA and 5836 \AA . A least squares fit of $I(\theta)/I(90)$ vs $\sin^2 \theta$ of the data for crystal C gives a reasonably good straight line with a slope of ~ 0.75 and intercept of about 0.25. Since crystal D was run at 1.6 K with a Wollaston prism both $\perp c$ and $\parallel c$ polarizations were photographed simultaneously. From the densitometer tracings the ratio I_c/I_a was found to be ~ 0.0047 . This is the lowest observed value for I_c/I_a in all the runs made on TMCBDT; as pointed out previously, this means that the angle ψ was zero and that I_c/I_a is ~ 0.005 . This further leads to a ratio of z-polarized to y-polarized transition moments of about 0.05, assuming $m_x = 0$. The spin-orbit coupling results in Table 4-4 agree fairly well with this result. Now substituting this value of I_c/I_a into Eq. 5-21 with the slope of 0.75 we find $\psi \approx \pm 29.8^\circ$. Using $I_c/I_a = 0$ we find $\psi \approx 30^\circ$.

This shows that in the Zeeman experiment using crystal C the angle which the analyzing beam and magnetic field made with the aa' plane was $\sim 30^\circ$. Now, setting $R_x = 0$, $R_z = 0.05$, $\psi = 30^\circ$ and calculating the Zeeman intensity ratio for various values of the angle ϕ (cf. Fig. 5-1) and the zero field parameters, $D=E=0$, using Eq. 5-16, gives a resulting fit of the calculated I_o/I_{\pm} not in good agreement with the average ratios in Table 5-2.

TABLE 5-4
ZERO-FIELD ABSORPTION VS. POLARIZATION

θ^a (deg)	$I(\theta)/I(90)^b$				
	Crystal C ^c	Crystal E ^d			Crystal D ^e
		I	II	III	
0	-	0.519	0.441	0.434	0.00471
5	-	0.519	0.441	0.434	-
10	0.264	0.556	0.451	0.472	-
25	-	0.602	0.490	0.528	-
27	0.352	-	-	-	-
40	-	0.673	0.578	0.623	-
42	0.637	-	-	-	-
53.5	0.758	-	-	-	-
57	-	0.772	0.735	0.792	-
71	0.835	-	-	-	-
86	-	1.00	1.00	1.00	-
90	1.00	-	-	-	1.00
96	-	1.00	1.00	1.00	-
α^f	0.2483 ± 0.091	0.5164	0.5435	0.4309	
b	0.7476 ± 0.058	0.4578	0.4210	0.5557	
r^2	0.9766	0.9753	0.9688	0.9924	
Standard Error	0.049	0.043	0.089	0.010	

continued

TABLE 5-4 continued

- a. θ , defined in Fig. 5-1 and 5-3, is the angle between the \vec{E} vector and the projection of the c axis onto a plane \perp to \vec{H} and \vec{S} (Poynting vector).
- b. $I(\theta)/I(90) = a + b \sin^2 \theta$, see p. 137 in text.
- c. Data from experiments performed on Zeeman apparatus, $T = 5.2 \pm 1$ K, for the 594 nm band.
- d. Data from experiments performed on Cary 14 at 10K. (I) 594 nm band, (II) 593 nm band, (III) 584 nm band.
- e. Data from densitometer tracings of measurements using Wollaston prism apparatus at 1.6 K (see Chapter 3).
- f. Results of least squares fit using equation in (b.) above.

TABLE 5-5
OBSERVED Δ VALUES FROM FIELD DEPENDENT ABSORPTION OF 5943Å BAND AND
EMISSION OF 6003Å TRAP. (In the emission only the ϵ_0 and ϵ_- lines
are seen).

H(K \circ)	ϵ_-^a	ϵ_+	Δ_-^b	Δ_+^b	$ \Delta_- - \Delta_+ $	ϵ_-	Δ_-^c
142	16905.83+0.71	16833.19+0.71	-15.18+1.0	12.18+1.0	3.0+1.5	16638.77+0.71	-15.18+1.0
118.3	16808.84 "	16831.50 "	-12.17 "	10.49 "	1.7 "	16641.20 "	-12.65 "
98.8	16811.03 "	16828.45 "	-9.98 "	7.44 "	2.5 "	16642.98 "	-10.96 "
78.6	16813.21 "	16824.10 "	-7.80 "	3.08 "	4.7 "	16645.51 "	- 8.43 "
59	-	-	-	-	-	16648.04 "	- 5.91 "
39	-	-	-	-	-	16649.73 "	- 4.22 "

a. All entries in Table are in cm^{-1} except H which is in kiloGauss.

b. ϵ_- taken as 16821.01 cm^{-1} for all traces. $\Delta_+ = \epsilon_+ - \epsilon_0$; see text, p. 138 ff.

c. ϵ_0 taken as 16653.94 cm^{-1} (6002.92Å), the 6003Å trap emission.

Since there are four parameters which can be varied (two angles ψ and ϕ , R_x and R_z) it is convenient to plot the calculated ratio (Eq. 5-16) as a function of the angle θ for various sets of parameter combinations to determine the functional behavior.

Zeeman Ratio as Function of R_x , R_z , ψ and ϕ

Again, consider the case of one spin-orbit route: $R_x = R_z = 0$; taking the molecular transition moment along y (\parallel C-S bonds). For $\psi = \phi = 0$ I_o/I_{+} is independent of polarization and is 2. While this is close to the values observed for crystal C it is not at all in agreement with the data from crystal B, as discussed above. That different crystals give varying results in the Zeeman pattern implies that the field orientation must be different, assuming both crystals have the identical faces developed. On the other hand, since the crystals are very soft, they can be polished so as to distort the face containing the c axis so that after polishing the c axis is at an angle to the flat side on which the probe beam and magnetic field impinge. Both of these situations are equivalent and can be visualized with the aid of Fig. 5-1 and 5-3. Furthermore, the transition moment ratios R_x and R_z , if different from zero, are not expected to change from crystal to crystal because they represent a molecular property. Thus it is reasonable to assume that what gives rise to the different Zeeman results from crystal to crystal are the different values of ψ and ϕ in each case.

The plots in Fig. 5-11 ($\psi=5^\circ$) and 5-12 ($\psi=20^\circ$) show the ratio I_o/I_{+} as a function of θ for various values of ϕ , while Figs. 5-13 ($R_x=0$) and 5-14 ($R_z=0$) show the effects of transition moment ratios. These are self explanatory. It should be emphasized that a small change

Figure 5-11.

Effect of ϕ on the calculated Zeeman intensity ratio for $\psi=5^\circ$ and one spin-orbit route in the absence of zero-field splitting. The plots in Fig. 5-11 to Fig. 5-16 were made with the program RAMPIT described in the Appendix. Equations 5-16 and 5-16a are used with the variables as defined in the text. The curve without tic marks is the zero-field absorption calculated using Eq. 5-20. 'RATIO' means $I_{O/I}$ and 'THETA' is varied from 0° to 180° . The angles ψ and ϕ are defined in Fig. 5-1. ψ is the angle which the magnetic field, H , and incident light propagation direction, S , make with the aa' plane in the unit cell (see also Fig. 3-1). ϕ is the angle which H and S make with the $-a'$ axis of the unit cell. F_x and R_z are the ratio of the free molecule transition moments: (m_x/m_y) and (m_z/m_y) , respectively. Here m_y is taken as the largest transition moment and is directed along the C-S bonds. In the calculation, as in the derivation of Eq. 5-16, it is assumed that both molecules in the unit cell absorb. Note the sensitivity for θ near 0° and 180° , even though only m_y is non-zero.

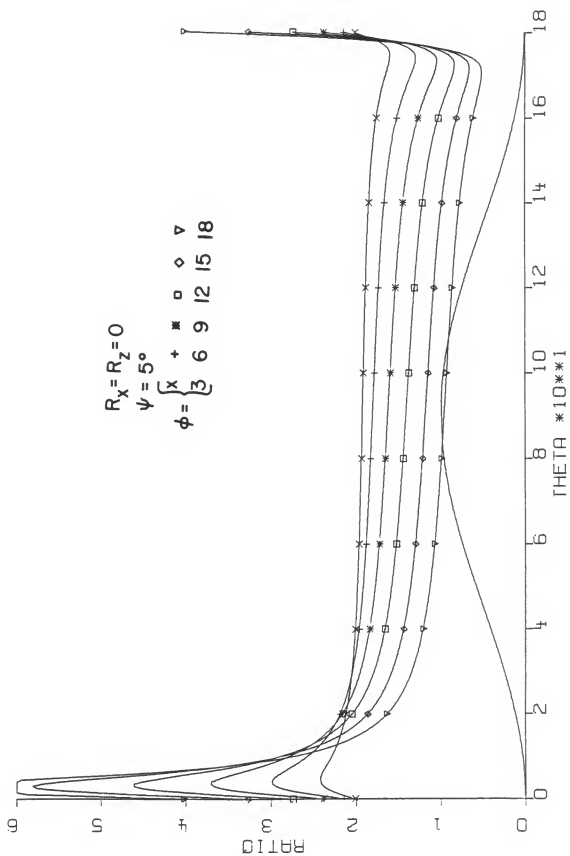


Figure 5-12. Effect of ϕ on the calculated Zeeman intensity ratio for $\psi=20^\circ$ and one spin-orbit route in the absence of zero-field splitting. (See caption in Fig. 5-11.)

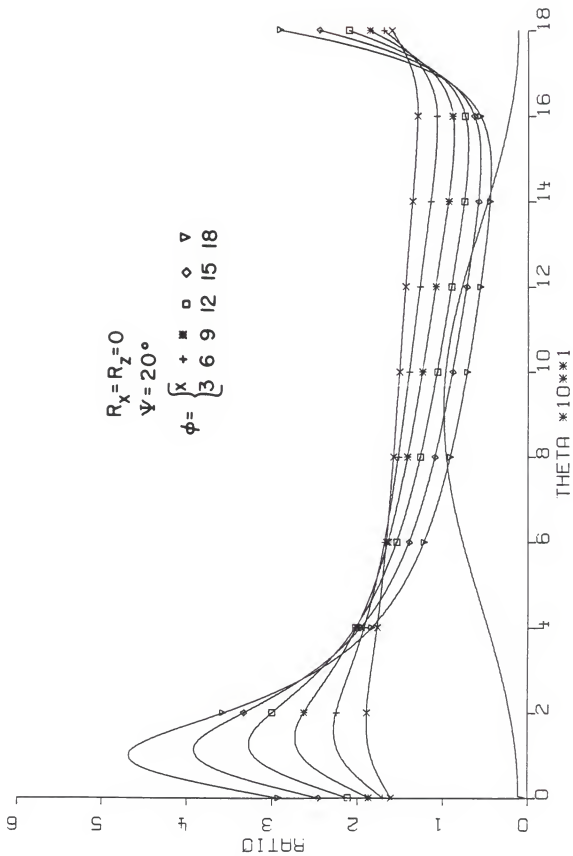


Figure 5-13.

Effect of z spin-orbit route on the Zeeman intensity ratio in the absence of zero-field splitting. See caption in Fig. 5-11 for definitions. This is the case for two spin-orbit routes calculated for the case where the magnetic field is not aligned with a crystal symmetry axis. R_z defines the ratio of their transition moments. Note that varying R_z has the same effect on the ratio for θ near 0° and 180° as varying ϕ has in the case of one spin-orbit route (cf. Fig. 5-11, 5-12). Also, at $\theta=90^\circ$ the Zeeman ratio is independent of m_z , see page 135.

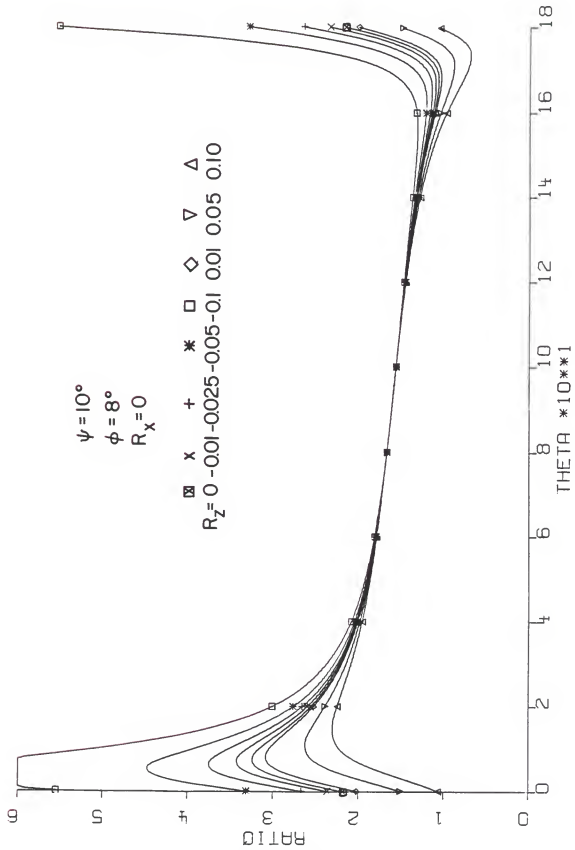
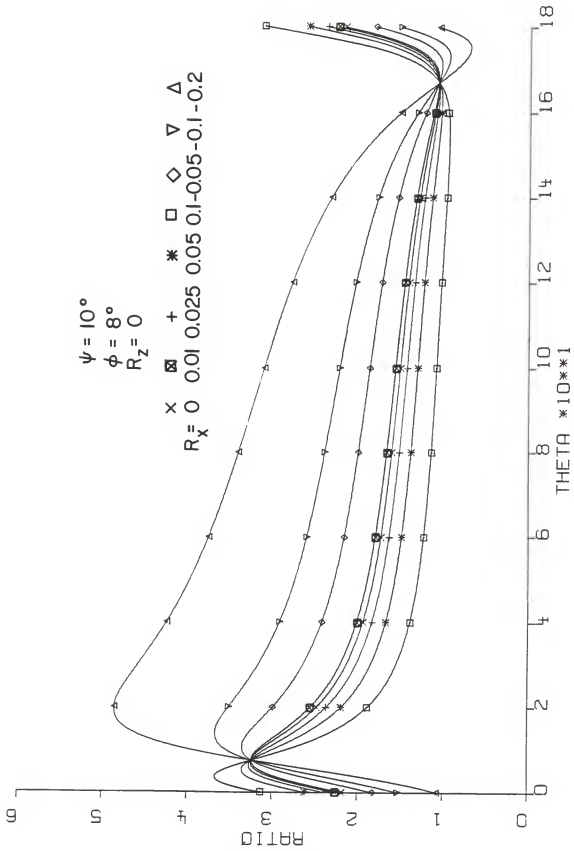


Figure 5-14. Effect of x spin-orbit route on the Zeeman intensity ratio in the absence of zero-field splitting. See caption in Fig. 5-11 for definitions. For values of $R_x > 0$ the ratio exhibits a θ dependence similar to that for various ϕ values, see Fig. 5-11. From Eq. 5-16 it is seen that factors containing R_x and ϕ are not linearly independent.



in field orientation away from a crystal symmetry axis can cause a very large change in the Zeeman pattern. Also a small activity in a second spin-orbit route ($R_z = \pm 0.05$ or 5%) can manifest itself as a large difference (~50%) in the Zeeman intensity ratio at the proper polarization (in this case $\theta \approx 0$).

We can superimpose the experimental points of Tables 5-2 and 5-3 on the various theoretical curves and find that for $R_x = R_z = 0$ and $\psi \approx 10^\circ$ each set of data points fits well for a particular value of ϕ .

As shown in Fig. 5-15, the data for crystal B fit the curve corresponding to $\phi \approx 17^\circ$ while $\phi = 2^\circ$ is found to fit the data for crystal C best. The calculation was repeated with $R_z = -0.01$ and $R_x = +0.003$ from the spin-orbit coupling calculation (Fig. 5-16) but no noticeable change in the fit was observed.

The difference between this value of ψ and the value of 30° determined in the ZFA intensity vs. θ plot can easily be accounted for by noting that the error in the ZFA intensity due to the underlying phonon structure being measured as part of the band increases with decreasing θ . Thus subtracting out this contribution, if it could be determined, would decrease the intercept.

It is important to note that as a consequence of the magnetic field not being aligned exactly in a crystal plane of symmetry (ψ or ϕ not zero) there is a difference between a measurement taken at a polarizer angle θ and one taken at $-\theta$. Equation 5-16 shows that this is due to the coefficient B_0 which is proportional to $\sin \psi \cdot \sin 4\phi$. Thus the measurements are very sensitive to the angle ϕ .

Figure 5-15. Comparison of the calculated Zeeman ratio for the y spin-orbit route with average experimental ratios as a function of polarizer orientation. See caption in Fig. 5-11 for definitions. The data points are circled:

- ⊗ - data for crystal C at 5K.
- ⊕ - data for crystal B at 16K.

The values of the average experimental ratios $\{ \frac{1}{2}(I_o/I_+ + I_o/I_-) \}$ for both sets of data are given in Tables 5-2 and 5-3. The values of $\psi=10^\circ$ and $\phi=2^\circ$ best reproduced the data for crystal C, while $\psi=10^\circ$ and $\phi=17^\circ$ fit best for crystal B.

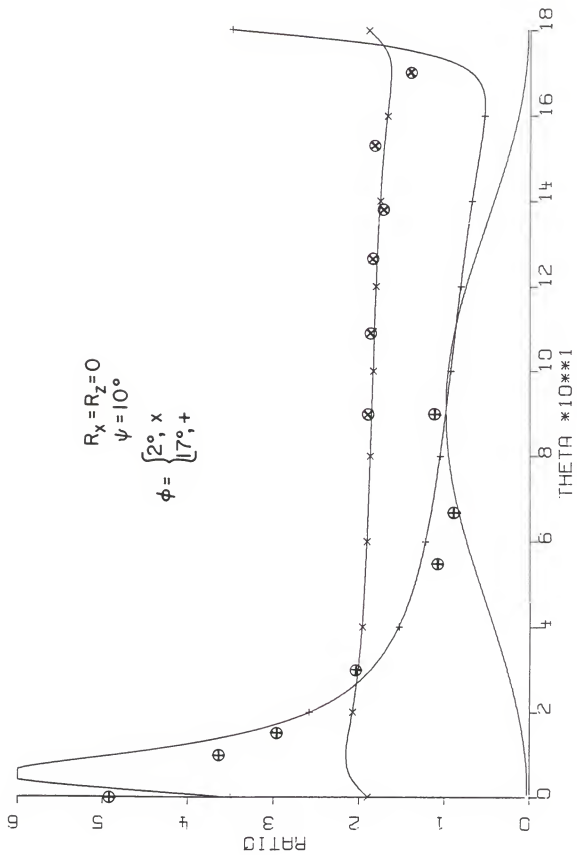
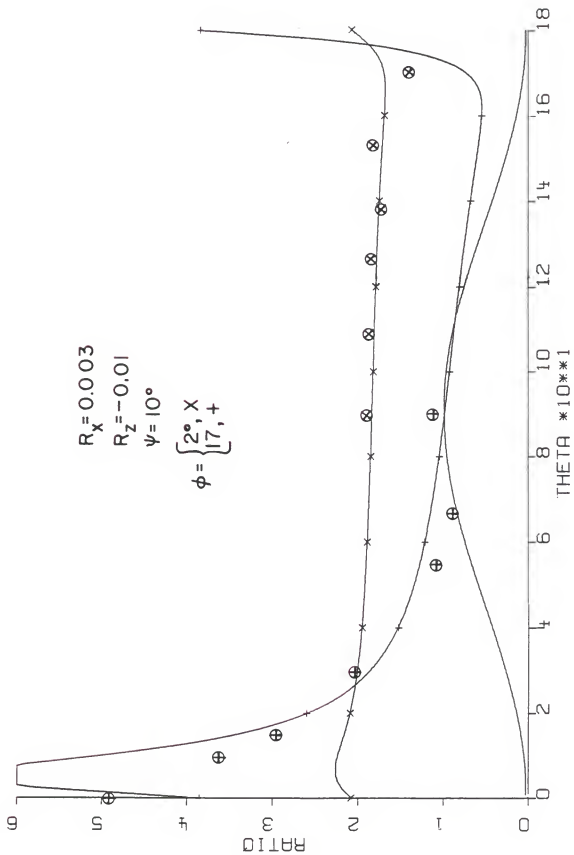


Figure 5-16. Comparison of the theoretical Zeeman ratio using the transition moments determined from the EHT-spin-orbit-coupling calculation. See Captions in Fig. 5-11 and Fig. 5-15 for definitions. The calculated values of R_z and R_x are too small to significantly alter the fit.



The B_0 term arises from the dependence of the magnetic substate eigenvectors on the field direction. This effect has been elucidated by Castro and Hochstrasser (111a) and we will paraphrase their explanation. In the magnetic field the spin functions of the triplet sublevels are expressed as linear combinations of the zero-field spin functions (spin quantized along the field) so that the field induces interference terms among the zero-field transition moments. Thus for a given magnetic substate the electric field of the radiation that induces the transition does not necessarily coincide with a molecular symmetry axis. The relative phases of the zero-field transition moments will then become important in the intensity expression. Also important is the fact that for zero field the intensity still depends on θ and ψ , but the ϕ dependence vanishes because of the uniaxial nature of the crystal.

Several different methods were used to fit the Zeeman data. A fit to the data from crystal B could be obtained with a particular set of R_x , R_z , ψ and ϕ but when these same R_x and R_z values were used in fitting the data for crystal C no satisfactory fit could be found for any value of ψ and ϕ . One reason for this is that ϕ values ranging from 0 to 90° were used for both sets of data. The plotted functions were helpful in determining the best set of parameters quickly, rather than printing out tables of calculated and observed values as functions of the angles and moment ratio parameters.

Summary

The data examined thus far demonstrate that in TMCBDT one spin-orbit route is active and that its axis is along the C=S bonds. This is consistent with the results of the spin-orbit calculation. The dependence

of the Zeeman ratio on the polarization of the analyzing light is explained by an improper alignment of the magnetic field. The reason for this is due to the nature of the crystal and has been discussed previously. Although the data can be explained by including a small amount of ($R_z=0.01$) of a second spin-orbit route in a direction $\parallel c$, with $R_z = 0.05$ the fit improves from the crystal B data but becomes worse for the crystal C data. With the low resolution used and the underlying broad phonon bands present at these temperatures the data do not warrant a more precise fitting procedure. Therefore we conclude that the variation of Zeeman intensity with polarization is due mainly to lack of field alignment with a crystal axis and not to additional spin-orbit routes.

Low Temperature and Field Dependent Results

As mentioned previously, the intensity imbalance observed in the 1.6 K Zeeman spectra and the field dependent Zeeman splittings observed in both the absorption and emission data of crystal C suggest that a sizeable zero-field splitting exists in TMCBDT. Based on the results of the spin-orbit calculation this effect is estimated to be larger in TMCBDT than in its carbonyl analogue.

To assess the magnitude of D the eigenvalues of Eq. 5-5 were plotted as a function of magnetic field strength for various values of D and for various field orientations (ψ, ϕ sets). The Δ_+ and Δ_- from Table 5-5 were then plotted on the same scale and an approximate fit determined. Acceptable fits could be found for various values of D in the range of ~ 1.5 to 3.5 cm^{-1} . The choice of axis systems were: a) the molecular z axis parallel to the crystal c axis and the molecular y along the C=S bonds, (largest transition moment along y); b) the

molecular y and z axes interchanged with respect to the choice above, (transition moment now along z). In all cases the g tensor was assumed isotropic and the D tensor diagonal. The principal axis system for both of these was assumed the same and coincident with the molecular symmetry axes.

Whenever a reasonable fit was found using these plots, the predicted intensity ratio as calculated using the eigenvectors of Eq. 5-5 in Eq. 5-11 was always reversed with respect to the experimental results (cf. Table 5-3). That is, the observed $I_+/I_- < 1$ while that calculated using the D value from the fit gave $I_+/I_- > 1$.

To seek a possible explanation for this discrepancy, the Zeeman transitions were plotted for each of the two molecules in the unit cell. Because of the zero-field parameters the eigenvalues of the two molecules are no longer the same for a nonsymmetric field orientation. (A symmetric field orientation, $\phi=0$ for example, renders the molecules magnetically equivalent and restores the equality of the eigenvalues). The differences depend mainly on D since it is normally much larger than E . If the linewidths of the Zeeman transitions are sufficiently narrow ($< 1 \text{ cm}^{-1}$) it is found that the sum of the two intensity patterns is different than if the eigenvalue differences are ignored.

Furthermore, it is noticed that in the data of crystal C only the unpolarized absorption exhibits the $\Delta_+ \neq \Delta_-$ asymmetry. The high field data would also be expected to do so, but does not.

For the case tried in the procedure just described, namely $\psi=10^\circ$, $\phi=2^\circ$, $D=+2 \text{ cm}^{-1}$, $E=-0.05 \text{ cm}^{-1}$, $R_x = R_z = 0$ and the axis system choice (b) above, the FWHM for each band was taken as the approximate

width measured in the experimental data ($\sim 5 \text{ cm}^{-1}$). The unpolarized absorption, and polarized absorption for various values of θ were plotted. The Δ_+ and Δ_- values were then determined from the plot in the same way as was done for the experimental data. The difference in Δ values, i.e., $\Delta_+ - \Delta_-$, was found to be greater in the unpolarized simulation than in the polarized one; the difference being due to different intensities for each molecule between the polarized and unpolarized case.

Specifically, with the above parameters we get 1 cm^{-1} and 0.4 cm^{-1} for the unpolarized and 90° polarization, respectively. This result taken together with the large widths due to elevated (with respect to the sharper 1.6 K lines) temperatures can possibly account for the discrepancy. This follows since what is observed is a sum of intensities and energy distributions, while the Δ_+ and Δ_- are plotted as a function of field strength using the eigenvalues of molecule one only. (Those of molecule two are superimposable on those of one in the scale used in the plot.)

We will now use this simulation method to explain the results for crystals A and F at 1.6 K.

If we examine the Zeeman patterns in Figs. 5-4 and 5-5 we find that the overall ratio $I_o/I_{\pm}(\text{ave})$ of crystal F is similar to that of crystal C, while for sample A (90° Pol.) a ratio of ~ 1 resembles that in the data of crystal B. Using the same parameters, respectively, we first calculate the eigenvalues and eigenvectors (cf. Eq. 5-5). Then, assuming one spin-orbit route, the intensities were calculated according to Eq. 5-11. The unpolarized result is obtained as explained previously.

Table 5-6 compares the results for both 1.6 K cases with the previously mentioned results. The agreement is quite good. Some of the simulation results are shown in Figs. 5-17 and 5-18.

Table 5-7 contains the result of the calculation using these same parameters for comparison with the data from crystals B and C (cf. Tables 5-2 and 5-3, respectively). As was seen for the case of $D=E=0$ the angles $\psi=10^\circ$ and $\phi=2^\circ$ reproduce the average I_0/I_+ well. And now by including the zero-field splitting the intensity imbalance in the crystal C case is predicted very well but is only determined qualitatively in the case of crystal B.

It can be seen (cf. Table 5-7) that the intensity ratios of the Zeeman transitions are very well reproduced at $\theta=90$. This is the most intense spectrum observed and expected to be more accurate. As θ decreases to zero the total intensity decreases also and the difference between calculated and observed intensity ratios becomes larger. Nevertheless, the trend in the average ratio and the intensity imbalance is fairly well reproduced by the parameters chosen. The unpolarized result was not reproduced well in this case, however. It was found that the parameter $|E|$ if kept small (<0.1) influences neither the intensity pattern nor the eigenvalues very much. The parameter D , on the other hand, influences the I_+/I_- ratio a great deal, and the average ratio I_0/I_+ to a smaller extent.

The data for crystal B are expected to be less accurate at higher θ values because the phonon modes are polarized perpendicular to c . It can be seen from Fig. 5-6 that at $\theta=0$ the baseline is flat. The calculated ratio I_+/I_- follows the observed trend, starting out at a value larger than 1 and decreasing as θ increases. For this case,

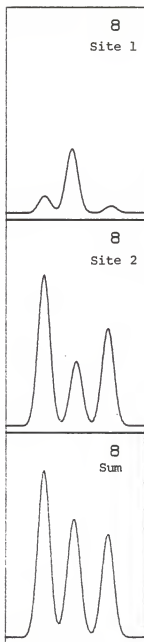
TABLE 5-6
COMPARISON OF CALCULATED TO EXPERIMENTAL ZEEMAN MEASUREMENTS AT 1.6 K

Parameters	Crystal A		Crystal F	
ψ (deg)	~ 10		~ 10	
ϕ (deg)	~ 17		~ 2	
D (cm^{-1})	+2.5		-2.5	
E (cm^{-1})	+0.05		+0.05	
θ (deg)	90		Unpolarized	
H (KG)	~ 100		~ 142	
Results	Calculated ^b	Observed	Calculated ^b	Observed
Δ_+ ^a	9.68	~ 10.5	12.8	~ 11.4
Δ_-	8.59	~ 8.8	13.8	~ 12.3
$ \Delta_+ - \Delta_- $	~ 1.1	~ 1.7	1.0	~ 0.9
I_0/I_-	0.71	0.78	2.29	2.78
I_0/I_+	1.15	1.19	1.45	1.85
I_+/I_-	0.62	0.65	1.58	1.50
ZFA- 0>	-1.35	+2	~ 1.2	$\sim 0.9-1.8$
FWHM ^c	4.1(2.0)	7	3.44(3.4)	~ 3.5

a. All 'calculated' Δ values and ratios are obtained from simulated spectra.

b. Z molecular axis is parallel to C=S bonds; y is || to c.

c. Values used for individual bands in parantheses.



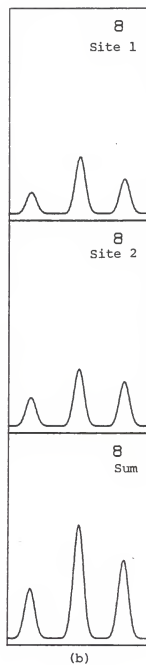
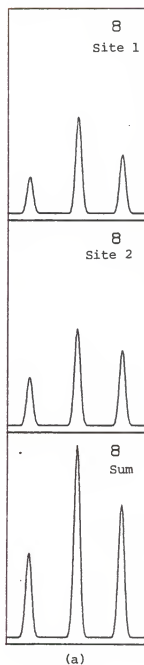
Crystal A

Figure 5-17. Simulated Zeeman spectra of crystal A for the two molecules in the unit cell and their sum. The parameters used to calculate the spectra are:

Molecular z axis \parallel C=S bonds.
 $H = 100 \text{ kGauss}$, $g_{\text{iso}} = 2.0023$,
 $D = +2.5 \text{ cm}^{-1}$,
 $E = +0.05 \text{ cm}^{-1}$, $R_x = R_y = 0$,
 $\psi = 10^\circ$, $\phi = 17^\circ$ and $\theta = 90^\circ$.

Figure 5-18. Simulated Zeeman spectra of crystal F for the two molecules in the unit cell and their sum. Parameters used to calculate the spectra are:

Molecular z axis along C=S bonds
H = 142KGauss
g_{iso} = 2.0023
 $\psi=10^\circ$, $\phi=2^\circ$
D = -2.5 cm⁻¹
E = 0.05 cm⁻¹
R_x = R_y = 0
Unpolarized



Crystal F

TABLE 5-7 continued

Ratio	2.08	1.33	1.56		5.87	3.30	1.78
Expt.	1.31	2.37	0.55		4.14	3.22	1.29
138	0.024	0.067	0.040	15	0.007	0.053	0.013
	0.074	0.146	0.114		0.007	0.005	0.010
	0.098	0.212	0.154		0.014	0.058	0.023
Ratio	2.17	1.38	1.57		4.09	2.47	1.65
Expt.	1.51	2.00	0.75		3.38	2.59	1.31
126.5	0.042	0.114	0.068	30	0.012	0.099	0.024
	0.096	0.190	0.148		0.045	0.029	0.063
	0.137	0.303	0.216		0.057	0.128	0.087
Ratio	2.21	1.40	1.57		2.23	1.47	1.52
Expt.	1.39	2.38	0.58		1.90	2.22	0.86

continued

TABLE 5-7 continued

109	0.069	0.185	0.111	55	0.020	0.164	0.039
	0.117	0.234	0.182		0.151	0.097	0.211
	0.186	0.418	0.293		0.171	0.261	0.250
Ratio	2.25	1.43	1.58		1.53	1.04	1.46
Expt.	1.68	2.09	0.80		0.898	1.33	0.68
90	0.088	0.235	0.142	67	0.022	0.178	0.042
	0.117	0.235	0.182		0.201	0.128	0.281
	0.205	0.470	0.325		0.222	0.306	0.323
Ratio	2.29	1.45	1.58		1.38	0.949	1.45
Expt.	1.59	2.29	0.69		0.808	1.05	0.77
Unpolarized	0.073	0.122	0.046	90	0.019	0.163	0.038
	0.094	0.121	0.060		0.257	0.163	0.359
	0.167	0.242	0.106		0.276	0.326	0.397
Ratio	1.45	2.28	0.634		1.18	0.821	1.44
Expt.	1.28	1.87	0.68		0.964	1.35	0.71

however, the I_O/I_+ and I_O/I_- is very sensitive to θ in the range where $\theta < 20^\circ$, therefore a small error in polarizer setting would change the ratio significantly.

Discrepancies

The data is well reproduced in most cases discussed so far, but there are some inconsistencies. First, the sign of D is different for crystal F and crystal A, in Table 5-6. Second, the intensity ratio I_+/I_- for crystal C is explained by $D > 0$, but a plot of the eigenvalues as a function of H shown in Fig. 5-19 does not fit the observed unpolarized data, plotted on same scale. These discrepancies may arise if the principal axes of Δ are not coincident with the molecular axes, or are coincident but rotated by 90° or 180° . In the present calculation this possibility is not taken into account. While all the other quantities are calculated in a field-fixed frame, the zero-field tensor is not. Transformation of this tensor by the appropriate similarity transformation using a matrix whose components are the direction cosines between the various pairs of axes in the zero-field (molecular) axis system and the field-fixed system (121).

\bar{D} and \bar{g} Tensor Consideration

Thus far the principal axes (X,Y,Z) of the \bar{D} tensor have been assumed to be along the molecular symmetry axes, ie. X||x, Y||y and Z||z. Now consider a transformation which gives Z||x, Y||y and X||z. For $D = -3$ and $E=0$ this amounts to

$$\bar{D} = \begin{bmatrix} -1 & 0 & 0 \\ 0 & -1 & 0 \\ 0 & 0 & +2 \end{bmatrix} \rightarrow \begin{bmatrix} +2 & 0 & 0 \\ 0 & -1 & 0 \\ 0 & 0 & -1 \end{bmatrix} = \bar{D}'$$

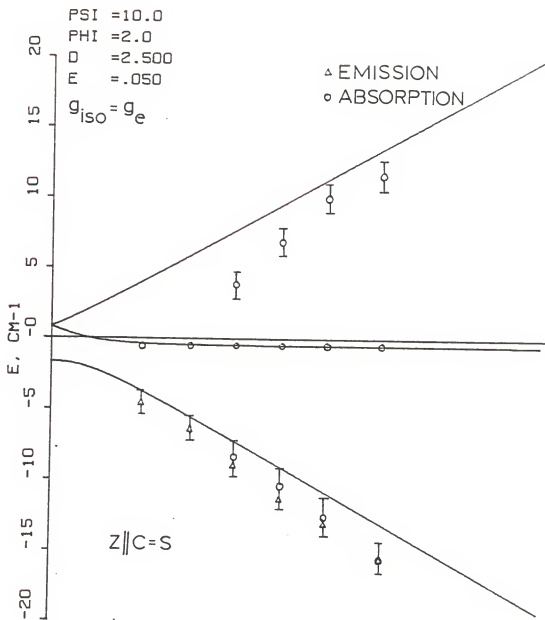


Figure 5-19. Plot of calculated and experimental band positions as a function of magnetic field strength for $D > 0$ and spin axes coincident with molecular symmetry axes. All experimental values given in Table 5-5.

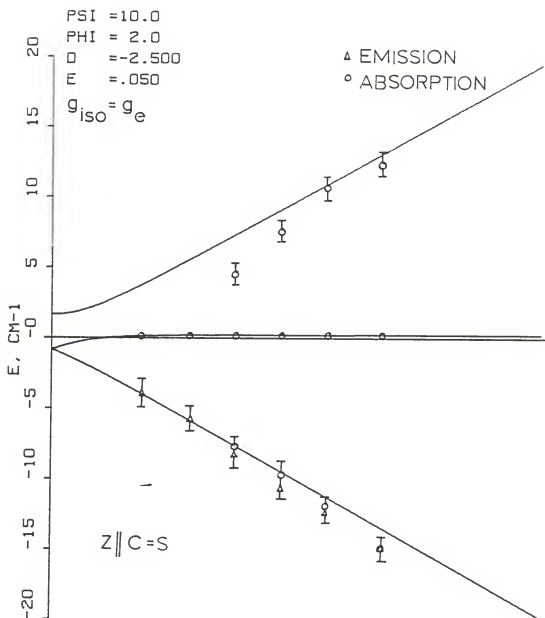


Figure 5-20. Plot of calculated and experimental band positions as a function of magnetic field strength for $D < 0$ and spin axes coincident with molecular symmetry axes. All experimental values given in Table 5-5.

Using D' in Eq. 5-5 now gives the pattern in Fig. 5-21 and the polarized intensities in Table 5-8 for the crystal C orientation of $\psi \sim 12^\circ$ and $\phi \sim 2^\circ$. We now get good agreement of both intensity imbalance and Δ imbalance for this set of data. This result simply means that the magnetic axis of symmetry is not the same as the molecular axis along which the electronic transition is polarized.

Further, the magnetic axes may not lie along the molecular axes because of molecular distortion in the $^3\pi\pi^*$ state observed (T_1). This would mean that the D tensor would have to be expressed in the field fixed-axis system and in turn give results dependent on the field orientation.

Since the data for crystals F and A are taken at different field orientations we cannot expect the signs of D to be the same because the orientations are not the same.

From the above considerations it follows that the g tensor should also be transformed to the field-fixed system. However if it is isotropic as we have assumed, this will amount to transforming a unit matrix and will not change anything. On the other hand we do have evidence for a large spin-orbit contribution to the zero-field splitting parameter D . Therefore there should also be a strong influence on g from this effect.

According to Stone (122) the g tensor for a molecule in an orbitally nondegenerate triplet state may be approximated by

$$g^{zz} = 2 + \frac{1}{3} \sum_p \sum_n \sum_k \frac{\langle \psi_p | \ell_k^3 | \psi_n \rangle \langle \psi_n | \zeta_k \ell_k^z | \psi_p \rangle}{\epsilon_p - \epsilon_n},$$

Where ψ_p are occupied and ψ_n are virtual orbitals and ϵ_i their energies. k labels the atomic centers while ζ_k is the spin-orbit coupling constant

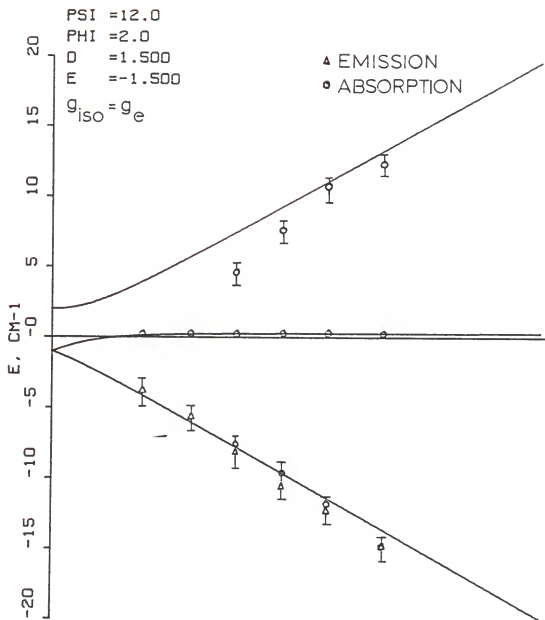


Figure 5-21. Plot of calculated and experimental band positions as a function of magnetic field strength for the case of non-coincident molecular symmetry and spin axes. All experimental values given in Table 5-5.

TABLE 5-8

INTENSITIES FOR CRYSTAL C CALCULATED USING $X=+2$, $Y=Z=1$. (Coordinate system is with Z molecular axis parallel to the crystal C axis and Y along C=S bonds. $T_1 \leftarrow S_0$ transition moment along Y. The other parameters are: $\psi=12^\circ$, $\phi=2^\circ$, $g=g_e$, $E=0.05$ cm⁻¹ and $H=142$ KGauss. Table entries are as in Table 5-7.)

θ	I_-	I_o	I_+	θ	I_-	I_o	I_+
170	0	0	0	126.5	0.059	0.108	0.042
	0.022	0.032	0.017		0.142	0.204	0.105
	0.022	0.032	0.017		0.201	0.313	0.147
Ratio	1.44	1.95	0.74	Ratio	1.55	2.12	0.73
Expt.	0.93	1.92	0.49	Expt.	1.39	2.38	0.58
153	0.009	0.016	0.006	109	0.100	0.183	0.071
	0.066	0.095	0.049		0.171	0.246	0.127
	0.075	0.111	0.055		0.271	0.429	0.198
Ratio	1.48	2.01	0.74	Ratio	1.58	2.17	0.73
Expt.	1.31	2.37	0.55	Expt.	1.68	2.09	0.80

continued

TABLE 5-8 continued

138	0.033	0.061	0.024	90	0.131	0.240	0.094
	0.111	0.160	0.082		0.168	0.242	0.125
	0.145	0.221	0.106		0.300	0.482	0.218
Ratio	1.53	2.08	0.73	Ratio	1.61	2.21	0.73
Expt.	1.51	2.00	0.75	Expt.	1.59	2.29	0.69

and ℓ_k^z is the orbital angular momentum operator on atom k . Here the frozen orbital approximation is used and state energies are calculated as molecular orbital energy differences using singly excited configurations. This is the same procedure used in the spin-orbit calculations in Chapter 4.

Note that the g_ν tensor depends on the first power of the spin-orbit coupling constant while D_ν is proportional to its square. Both tensors depend on the first power of the energy difference between the state in question (T_1) and the perturbing state.

Batley and Bramly (117) investigated the effect of spin-orbit coupling on the g_ν and D_ν tensors in carbonyl $^3\Pi^*$ and $^3\Pi^*$ states and give the following simple relation for the change in g_ν from the free electron value g_e as a function of the change in D_ν due to spin-orbit coupling

$$\Delta g_{zz} = g_e - g_{zz} = \frac{6\Delta Z}{\zeta}$$

where ΔZ is the spin-orbit contribution to the principal value Z of the zero-field tensor. This change in g_ν is derived by considering only one center terms. In the present case, ζ , the spin-orbit coupling constant is therefore for sulfur. If we estimate ΔZ as $+3 \text{ cm}^{-1}$ and use $\zeta_S = 390 \text{ cm}^{-1}$, *vide supra*, we find $\Delta g_{zz} = -0.046$. This gives a g_{zz} of 1.956. The change is negative because the $^3\Pi^*$ state is lowest and the energy denominator will be negative because perturbing states will lie above it.

Applying this result to TMCBDT we find, using the same transformation as for D_ν ,

$$\underset{\sim}{g} = \begin{bmatrix} 2.0023 & 0 & 0 \\ 0 & 2.0023 & 0 \\ 0 & 0 & 1.956 \end{bmatrix} \rightarrow \begin{bmatrix} 1.956 & 0 & 0 \\ 0 & 2.0023 & 0 \\ 0 & 0 & 2.0023 \end{bmatrix}$$

In Eq. 5-4, the Zeeman term should now be written as

$$\beta H_o (\ell \ m \ n) \begin{bmatrix} 1.946 & 0 & 0 \\ 0 & 2.0023 & 0 \\ 0 & 0 & 2.0023 \end{bmatrix} \begin{bmatrix} S_x \\ S_y \\ S_z \end{bmatrix}$$

where the spin operators are referenced in the molecule-fixed axes, and the other quantities have their usual meaning. Since $\underset{\sim}{D}$ is still diagonal in the field-fixed system the zero-field term is the same.

When Eq. 5-5 is now diagonalized and the intensity calculations done we find little change in the intensity ratios and very little change in the plotted eigenvalues as a function of field strength. Only a slight increase in $|+\rangle$ slope is noticeable above ~ 130 KGauss. The intensity of the $|0\rangle$ transition increases at the expense of the $|+\rangle$ and $|-\rangle$ transitions, hence the ratios for all the polarizations increase. For the value of g used here this increase amounts to $\sim 5\%$.

Thus we conclude that the zero-field parameters are far more important than the $\underset{\sim}{g}$ tensor in the Zeeman absorption spectra of TMCBDT. It is shown that all the data are consistent with a value of $|\underset{\sim}{D}| \sim 2$ to 3 cm^{-1} and $|\underset{\sim}{E}| \sim 0$. The choice of axes system for consistency of sign seems to be dependent on the crystal orientation in the field, which implies a $\underset{\sim}{D}$ tensor whose principal axes are rotated with respect to the molecular axes. From the spin-orbit coupling analysis of Chapter 4 (cf. Table 4-2) it may be seen that large $\langle H_{so} \rangle$ matrix elements are found in the molecular x (out of plane) and y (along C=S bonds) directions. However electric dipole allowed transition moments

only contribute intensity polarized along the y direction. Thus, the spin-orbit coupling interaction has the effect of rotating the zero-field tensor \hat{D} relative to the molecular framework; that is, it causes the magnetic axis of symmetry to be out of plane rather than along the C=S bonds.

Summary of Zeeman Absorption Experiments

In this Chapter we have demonstrated that only the spin-orbit route along the molecular axis collinear with the C=S bonds is active and, by taking proper account of the magnetic field direction, the observed Zeeman absorption spectra can be successfully explained. Additional spin-orbit routes (components of H_{so} along other molecular directions) are not necessary to improve the fit based on our experimental error. It is estimated that if present, these must be < 0.05 when described as transition moment ratios. This is $< 2.5 \times 10^{-3}$ as an intensity contribution. This compares well with a value of $\sim 1.6 \times 10^{-3}$ as found in the ZFA measurement on crystal D.

An expression has been derived which gives the Zeeman ratio for the case of negligible zero-field splitting as a function of field orientation. It is demonstrated that for certain field directions highly variable intensity ratios are found even for the case of one spin-orbit route.

The effect of zero-field parameters on the absorption spectra has been investigated in a qualitative manner using first and second order perturbation theory and the results applied to the TMCBDT spectrum. A value of $\sim 3 \text{ cm}^{-1}$ can be deduced from the available spectra and that this value agrees well with that found for xanthione by Burland (36).

A more reasonable estimate and explanation for the origin of $D = -11 \text{ cm}^{-1}$ for xanthione is given than that available in the literature (35,36). In this regard it is found that for thio-carbonyl chromophores the spin-orbit contribution to the zero-field splitting parameters arising from differences in electron density at the sulfur atom, between the singlet and corresponding triplet perturbing states should not be neglected. In the literature (35,36,117) the assumption has been made that these terms are negligible and reasoning about the zero-field parameters centers around energy denominators.

As another consequence of field orientation, it is found that a consistent reproduction of the data necessitates that the zero-field tensor be expressed in the field fixed system. The g tensor, while expected to drop below the free electron value along the molecular axis collinear with the C=S bonds, does not change the result appreciably.

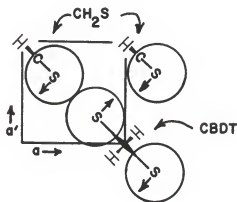
CHAPTER 6 CONCLUSIONS AND SUGGESTIONS

Through these experiments it has been demonstrated that the first band in the $n\pi^*$ absorption region reported by Ballard and Park (12) is due to the ${}^3n\pi^*$ state. The unusual occurrence of a $T \leftarrow S$ transition possessing intensity comparable to a spin allowed $S \leftarrow S$ transition is understood on the basis of the large spin-orbit contributions of the sulfur atoms. It was shown that the transition ${}^3A_u \leftarrow {}^1A_g$ is polarized exclusively along the C=S bonds. In this light, the other weak transitions at the blue edge of the band, near 24300 cm^{-1} , should be examined by Zeeman spectroscopy as they are comparable in intensity to the lowest 3A_u . The ${}^3B_{2g}$ states can only be seen if vibronic-spin-orbit coupling is very large. This is not known with certainty at this time, but it is expected to be small if at all present.

The explicit nature of the DMP model proposed in Chapter 3 should be further investigated both theoretically and experimentally. It was stated in Chapter 3 (see Fig. 3-7) that consideration of the unit cell geometry, the molecular geometry, and the atomic van der Waals radii shows that there are two regions in the unit cell where a large amount of steric hindrance should occur. An INDO calculation on both the ground state and triplet excited state could be carried out along the B_{2g} lattice vibrational coordinate. An energy lowering

is expected as the sulfur atoms, which initially have their van der Waals clouds in contact (see Fig. 3-7), move away from one another. As the molecules move further along this coordinate, however, the sulfur atoms approach those of another set of translationally equivalent molecules; this will again raise the energy.

To carry out this calculation two thioformaldehyde molecules and one CBDT molecule are sufficient. The diagram below (view is along c crystal axis) shows the arrangement of these molecules. Their motions in the aa' plane are indicated. The thioformaldehyde molecules are simply pivoted about the carbon atom to simulate the motion of the other CBDT molecules.



Since the ${}^3n\pi^*$ excited state is expected to have elongated C=S bonds, the above could be repeated using the C=S bond lengths in CBDT found by a separate calculation on the ${}^3n\pi^*$ state of an isolated CBDT molecule. The effect of the increased bond lengths in CBDT should be to raise the barrier in the DMP and cause the energy minimum to occur at a somewhat greater B_{2g} lattice displacement.

Thus far only region A in Fig. 3-7 has been considered. A similar approach to that just described could be applied to region B in Fig. 3-7. In this way the magnitude of both effects or their combination can be determined.

Experimental investigation of matrix isolated TMCBDT (in a rare gas or nitrogen matrix) in the infrared as well as in the visible region of the spectrum can now be done in our laboratory using Fourier Transform or conventional spectroscopy.

The IR spectrum as a function of temperature, down to 10K, should indicate whether or not the ground state DMP is due to the intramolecular torsion mode. If this is true the appearance of g type vibrations at low temperature is expected because 90% of the molecules are in the 0^+ level at 10K. Because this level is below the barrier, these molecules should now be bent in the C_{2v} symmetry point group. The b_{3g} and b_{2g} vibrations (in D_{2h} symmetry) now become allowed since they correlate with the b_1 and b_2 symmetry species (see Table 3-4 for the correlation). Conversely, investigation of the Raman spectrum of the matrix isolated TMCBDT at low temperatures would demonstrate whether or not the u vibrations normally not seen in planar TMCBDT become allowed in the bent molecule.

The $T_1 \leftarrow S_0$ transition can be investigated in a matrix environment; in this case the phonon sideband should not be the same as that in the single crystal spectrum. Indeed, the absence of this band (cf. Fig. 3-2, +47 and +59 cm^{-1}) in the matrix isolated spectrum would indicate that lattice vibrations alone are responsible for its appearance in the single crystal spectrum.

The observed zero-field splitting in TMCBDT is about -1 to -3 cm^{-1} , whereas in XS it is about -11 cm^{-1} (36). Based on the location of perturbing states relative to T_1 in the two molecules it is reasonable that TMCBDT should have a much lower D than XS. For example if Ballard and Park's assignment of the intense band at 45000 cm^{-1} to a $\pi\pi^*$ state is correct, then this is most likely the perturbing state for T_1 (cf. Table 4-2). This would mean that the spin-orbit-coupling contribution this state makes to D in TMCBDT is now almost 7 times less than for XS, if only the $\pi\pi^*$ contribution is taken into account, since the corresponding state in XS is only $\sim 5000 \text{ cm}^{-1}$ above T_1 . Thus it may be that because of the larger separation between the $\pi\pi^*$ and $n\pi^*$ states of TMCBDT the D value will be small in spite of having 2 sulfurs in the molecule. This is the most reasonable conclusion that can be drawn on the basis of the present data.

Also, the contribution by this $\pi\pi^*$ state to the transition moment is smaller than that calculated from the EHT energies (cf. Fig.2-4) and the weight of the ${}^3B_{2g}$ perturbing states is even greater in intensity enhancement.

As an extension of the theory in Chapter 5 one may integrate the expressions for the unpolarized ratio over the angles ϕ and ψ and obtain a formula for the Zeeman intensity ratio for a random distribution of molecules in the magnetic field, such as would be expected from a matrix isolated sample. A look at the transition moments for the operators involved in the MCD theory using these equations should not be difficult. Thus far no C type terms have been reported in the MCD of molecules;

this is because they arise from a degenerate ground state (which is split by the magnetic field) and most organic molecules normally do not belong to this category.

In Chapter 4 it was pointed out that over 70% of the transition moment magnitude comes from triplet perturbations of the ground state. Suppose that the ground state wavefunction is adequately described by Eq. 4-5, then the ground state singlet wavefunction has triplet character mixed in by H_{so} . If this perturbation is strong enough, it may be possible to observe C-type terms in the MCD spectrum of matrix isolated TMCBDT (or XS).

The absence of the $|+\rangle$ band in the Zeeman emission spectra at temperatures below 20K (see Fig. 5-10) may be explained by assuming that the radiationless processes out of this level completely mask the radiative pathway. While this may be true in zero field, it seems unlikely in high field because the states are completely mixed, the various rate constants therefore become linear combinations of the ones belonging to the zero field states (123).

Alternately, consider the possibility that the 600 nm trap is due to an excited electronic state which is localized on a disoriented molecule within the bulk of the crystal. These occurrences are called X-traps and have recently been examined in 4,4'-p-dichlorobenzophenone by Peretti et al. (124). In such a situation it is possible that the excited electronic states could be significantly perturbed in such a way as to reduce the energy gap between the $^3_n\pi^*(A_u, T_1)$ state and the lowest $^1_{\pi\pi^*}$ perturbing state. This could then increase the zero-field splitting (D) significantly. Then, if D is on the order of

20 cm^{-1} or greater (cf. in XS traps D is -11 cm^{-1} and -20 cm^{-1} (86)), the emission from the $|+\rangle$ state would not be seen below 20K due to the small fraction of molecules in this state. Thus the Zeeman emission experiments on single crystal TMCBDT should be performed at higher temperatures, 77K for example, to see if emission grows in to the blue of the two bands observed in Fig. 5-10.

The *ab initio* calculations completed thus far should certainly be extended to include CI. It is expected that an accurate prediction of the $n\pi^*$ states will be obtained. The calculation of the lowest $\pi\pi^*$ states would also be useful.

Using the changes in electron density at various positions within the molecule it should be possible to predict the nature of the vibrations that are active in the transition. This has been briefly reported (60) for the vertical transitions to the $^{1,3}n\pi^*$ states calculated in the SCSCF approximation.

It is hoped that the arguments presented here spark renewed interest in the theoretical consideration of this molecule in this research group, and by others.

APPENDIX I

To facilitate calculation and plotting of the various Zeeman related equations in Chapter 5, the laboratory computer was chosen rather than the University computer. This is a NICOLET 1180 mini-computer which accepts NICOLET Assembler and an enhanced version of Basic. Although a diagonalization routine can now be written in FORTRAN 77 and called from a library by a Basic program, FORTRAN was not available at the time these calculations were initiated. Thus another method for the diagonalization of the spin Hamiltonian matrix, Eq. 5-5, was chosen. That method is briefly described here.

The secular equation is written as a set of coupled homogeneous equations from which the eigenvalues are found by setting the determinant of the secular equation equal to zero. Evaluating the determinant gives a cubic equation whose roots are the eigenvalues.

The secular equation is

$$C_x (X-\lambda) + C_y (-ibn) + C_z (ibm) = 0$$

$$C_x (ibn) + C_y (Y-\lambda) + C_z (-ib\ell) = 0$$

A1

$$C_x (-ibm) + C_y (ib\ell) + C_z (Z-\lambda) = 0$$

Because the matrix is Hermitian the eigenvalues are real. Using the tracelessness of the ρ tensor condition, namely, that

$$X + Y + Z = 0$$

and the relationship of the direction cosines

$$\ell^2 + m^2 + n^2 = 1$$

the characteristic equation reduces to

$$\lambda^3 + q\lambda + r = 0 \quad A2$$

$$\text{with} \quad q = XY + XZ + YZ - b^2 \quad A3$$

$$r = b^2 (X\ell^2 + Ym^2 + Zn^2) - XYZ \quad A4$$

$$\text{and} \quad b = g\beta H_O.$$

The eigenvalues are the roots of Eq. A2 and may easily be found by a trigonometric substitution:¹

$$\text{let} \quad \cos\phi = -4r/a^3 \quad \text{and} \quad a = 2(-q/3)^{1/2}$$

then the eigenvalues are

$$\lambda_1 = a \cos (\phi/3) \quad (a)$$

$$\lambda_2 = a \cos (\phi/3 + 2\pi/3) \quad (b) \quad A5$$

$$\lambda_3 = a \cos (\phi/3 + 4\pi/3) . \quad (c)$$

To get the eigenvectors, the coefficient ratios are found from A1. The quantity $C_x C_z^{-1}$ may be obtained from A1 by eliminating C_y using (a) and (c) and $C_y C_z^{-1}$ is found by eliminating C_x using (b) and (c). C_z is arbitrarily taken as real and the normalization condition

$$C_x C_x^* + C_y C_y^* + C_z C_z^* = 1$$

is used to solve for C_x , C_y and C_z expressed as functions of

1. This is taken from "C.R.C. Standard Mathematical Tables" 13th Edition, R. C. Weast, S. M. Selby and C. D. Hodgman, Editors; The Chemical Rubber Co., Cleveland, OH. p366.

ℓ, m, n, X, Y, Z, b and λ . Substituting each of the eigenvalues from A5 into these expressions will then give a set of coefficients, the eigenvector, for that eigenvalue.

After some algebra the final results are

$$C_x = \frac{-Z_3 Z_1^* |Z_2|}{|Z_1| \cdot \Sigma} \quad (a)$$

$$C_y = \frac{-Z_3 Z_2^* |Z_1|}{|Z_2| \cdot \Sigma} \quad (b) \quad A6$$

$$C_z = \frac{|Z_1| \cdot |Z_2|}{\Sigma} \quad (c)$$

The Z_i are complex quantities and $|Z_i| = (Z_i Z_i^*)^{1/2}$,
with $(i = 1, 2, 3)$:

$$Z_1 = (X-\lambda)\ell - ibmn \quad (a)$$

$$Z_2 = (Y-\lambda)m + ib\ell n \quad (b)$$

$$Z_3 = (Z-\lambda)n + ib\ell m \quad (c)$$

$$\begin{aligned} \text{and } \Sigma = & (X-\lambda)^2 \ell^2 [(Z-\lambda)^2 n^2 + b^2 \ell^2 (1-\ell^2)] \\ & + (Y-\lambda)^2 m^2 [(X-\lambda)^2 \ell^2 + b^2 m^2 (1-m^2)] \\ & + (Z-\lambda)^2 n^2 [(Y-\lambda)^2 m^2 + b^2 n^2 (1-n^2)] \\ & + b^4 (\ell mn)^2. \end{aligned} \quad (d) \quad A7$$

The program ZFS8N, listed below, utilizes the above method with the Zeeman equations of Chapter 5 to calculate the intensity ratios for the general case of arbitrary field direction, multiple spin-orbit routes and nonzero D and E. The input prompting is self-explanatory.

The diagonalization routine EIGCH (see ref. 114) has been used to check the results using ZFS8N and in all cases tested the eigenvalues and eigenvectors were identical (except for the arbitrary phase in the eigenvectors).

The program to simulate the calculated Zeeman spectra in Figs. 5-17 and 5-18 is called ZFSPKS. It uses the intensity and position of the bands for each molecule in the unit cell obtained from ZFS8N to calculate the spectrum. A Gaussian lineshape is assumed for each transition. Based on the HWHM input by the user it calculates the spectrum by adding the contribution from each transition at each wavelength. The START buttons on the NIC-1180 computer are used as an amplification factor; this number appears on the plot in the upper right-hand corner. This multiplier is the combined value of the START buttons divided by 1024 and may be changed in between plots by the user.

This program can be used to plot combinations of one or more Gaussians; up to six total. The variables J1 and J2 define the first and last bands in the sum. The variable F1 defines the branch to take: plot another combination, change parameters or exit. The variables W1 and W3 define the initial and final values of the horizontal axis, respectively.

The program RATPLT was used to plot the functional dependence of I_{\perp}/I_{\parallel} on the polarizer angle, θ . The program uses Equations 5-16 and 5-16a and the Nicolet plotting routines to produce the plots shown in Figure 5-11 through 5-16. The present prompting statements are terse, but understandable. The present version also does not loop over transition moment ratios (R_x and R_z), so the plots of Fig. 5-13 and 5-14 were made by successive runs with the axes-drawing statements omitted.

```

10 REM          ZFSB...   NOV. 3, 1981 .....
11 REM          NOV 16--- CHANGES FOR MOL Z // C=S BONDS.
20 REM
30 REM          ZEEHAN INTENSITY RATIOS FOR TRIPLET CASE.
35 REM
40 REM          ZERO FIELD PARAMETERS ARE INCLUDED.
50 REM          EIGENVALUES AND EIGENVECTORS ARE CORRECT
60 REM          FOR THE GENERAL DIRECTION AND D,E NOT ZERO.
70 REM          -----
80 REM
950 DIM I(2,2),I9(2,2),E9(2,2),G2(2,2)
955 DIM L1(2,2), M1(2,2), N1(2,2)
960 DIM G3(2,2),G4(2,2),G5(2,2),G6(2,2),G7(2,2)
970 DIM I7(2,2)
975 DIM G(2)
980 DIM I2(2),I3(2),I4(2)
1000 DIM C0(2,2),C1(2,2),W(2),M(2)
1010 DIM R(2),R1(2)
1020 DIM A0$(5),A1$(2),A2$(2)
1022 DIM A3$(4),A9$(3)
1030 DIM X0(2),Y0(2),Z0(2),Z1(2),Z2(2),Z3(2),Z4(2),Z5(2)
1060 REM STRING INITIALIZATION.
1065 LET A1$(0)=" X "
1070 LET A1$(1)=" Y "
1080 LET A1$(2)=" Z "
1090 LET A2$(0)=" R "
1100 LET A2$(1)=" I "
1102 LET A3$(0)=" AXIS"
1104 LET A3$(1)=" "
1106 LET A3$(2)="S B0"
1108 LET A3$(3)="NDS "
1110 LET A3$(4)=" Z//C"
1121 REM
1130 LET B=4.6699E-5
1140 LET P0=3.141592654
1160 LET S7=1/SQR(2)
1170 LET B0=9.9999E-1
1599 REM INPUT SECTION... DATA SELECT...
1600 REM
1602 PRINT"ENTER DATE & COMMENT (<21 CHR):";
1603 INPUT A9$(0),A9$(1),A9$(2),A9$(3)
1605 PRINT"USE EXPTL. VALUES FROM SET # ";
1610 INPUT S0
1612 PRINT "ENTER '0' FOR";A3$(4);A3$(0);" OR '2' FOR";A3$(4);A3$(2);A3$(3)
1614 INPUT F4
1620 GO SUB 9000 [ REST OF INPUT: ZFS. PRAAMS.]
1625 GO SUB 9060 [ FIELD DIRECTION.]
1630 GO SUB 9500 [ T.M. RATIOS]

```

```

1640 GO SUB 12000
1650 GO SUB 14000
1652 PRINT
1654 PRINT "UNPOLARIZED INFO:"
1656 FOR K1=1 TO 2
1657 PRINT"KRAD:";I7(0,K1);TAB(20);I7(1,K1);TAB(35);I7(2,K1)
1658 PRINT TAB(5);I9(0,K1);TAB(20);I9(1,K1);TAB(35);I9(2,K1);" SITE";K1
1660 NEXT K1
1662 PRINT TAB(5);I2(0); TAB(20); I2(1); TAB(35); I2(2); " SUM";W2;" ZFA"
1664 PRINT TAB(5);R9(0); TAB(20); R9(1); TAB(35); R9(2); "RATIO"
1666 PRINT
1668 PRINT"EMISSION: KRAD(SUMS) (-)=";I4(0);" (0)=";I4(1);" (+)=";I4(2)
1670 LET I5=I4(1)/I4(0)
1672 LET I6=I4(2)/I4(1)
1675 PRINT " RATIO: (0/-)=";I5; " (+/0)="; I6
1700 GO SUB 13000
2000 REM READ EXPTL DATA
2001 REM
2005 RESET
2010 LET J2=6
2020 IF S0=1 THEN 2080
2025 LET J2=5
2029 REM SKIP FIRST SET
2030 FOR J=0 TO 6
2040 READ T, W1,W2,W3
2050 NEXT J
2060 FOR J3=0 TO J2
2065 READ T
2080 FOR J4=0 TO 2
2090 READ R1(J4)
2092 NEXT J4
2100 GO SUB 15000 [ CALC. INTENSITY RATIOS.]
2110 GO SUB 16000 [ AS F(POL.)- PRINT'EM]
2120 NEXT J3
3000 REM
3001 REM BRANCH SECTION
3002 REM
3005 PRINT
3010 PRINT "ENTER BRANCH(ES): ";
3020 CALL BSTRGL(A0$,1)
3025 LET F9=1
3030 FOR J=0 TO 10
3040 IF A0$(J)="M" THEN 3200
3050 IF A0$(J)="B" THEN 1605
3052 IF A0$(J)<>"A" THEN 3060
3055 GO SUB 9060
3060 IF A0$(J)<>"R" THEN 3080
3070 GO SUB 9500
3080 IF A0$(J)<>"Z" THEN 3100
3090 GO SUB 9000
3100 IF A0$(J)<>"P" THEN 3120

```

```

3110 GO TO 1650
3120 IF ASC(A0$(J))=141 THEN 1640
3130 IF A0$(J)="S" THEN 3250
3140 NEXT J
3150 PRINT"BRANCH????";
3160 GO TO 3020
3200 CALL EXIT
3250 STOP
3251 REM
3500 REM
5000 REM
5001 REM DATA
5002 REM
5010 DATA 0,4.6,3.29,1.4
5020 DATA 10,4.14,3.22,1.29
5030 DATA 15,3.38,2.59,1.31
5040 DATA 30,1.89,2.35,0.80
5050 DATA 55,0.898,1.33,0.68
5060 DATA 67,0.808,1.05,0.77
5070 DATA 90,0.964,1.35,0.71
5080 DATA 170,1.00,1.71,0.585
5090 DATA 153,1.00,1.78,.562
5100 DATA 138,1.43,2.00,.715
5110 DATA 126.5,1.32,2.32,0.569
5120 DATA 109,1.56,2.00,0.780
5130 DATA 90, 1.50,2.26,0.664
5140 DATA 00,1.11,1.67,0.665
9000 REM INPUT SR. ZFS PARAMETERS.
9001 REM
9010 PRINT "ENTER G: (XX, YY, ZZ), D, E, H ";
9012 LET F9=0
9020 INPUT G(0),G(1),G(2),D,E,H1
9021 LET D3=D/3
9022 LET X=D3-E
9023 LET Y=D3+E
9024 LET Z=-2*D3
9025 RETURN
9060 PRINT"ENTER PSI, PHI: ";
9070 INPUT P1,P2
9075 LET F9=0
9080 LET P9=57.29577951
9090 LET S1=SIN(P1/P9)
9100 LET C4=COS(P1/P9)
9102 LET C5=C4*C4
9104 LET C7=S1*C4
9110 LET S2=SIN(P2/P9)
9120 LET C2=COS(P2/P9)
9121 LET S0=S2*C2
9122 LET S4=S2+C2
9124 LET S5=S2-C2
9125 LET S6=S7*C4

```

```

9126 LET U0=-S4*S5
9127 LET U2=U0*C5
9128 LET U3=S8*C5
9129 LET U4=S5*C7
9130 LET U5=S4*C7
9131 LET N=-S1
9132 LET L=S6*S5
9135 LET H0=S6*S4
9136 LET S6=S1*S1
9138 LET L1(1,0)=L
9140 LET L1(2,0)=H0
9142 LET H1(1,0)=-H0
9144 LET H1(2,0)=L
9146 LET H1(1,0)=H
9148 LET H1(2,0)=N
9150 LET L1(1,2)=L
9152 LET L1(2,2)=H0
9154 LET H1(1,2)=N
9156 LET H1(2,2)=N
9158 LET H1(1,2)=H0
9160 LET H1(2,2)=-L
9162 FOR J1=1 TO 2
9164 FOR J=0 TO 2 STEP 2
9166 LET L1(J1,J)=L1(J1,J)*G(0)
9168 LET H1(J1,J)=H1(J1,J)*G(1)
9170 LET H1(J1,J)=H1(J1,J)*G(2)
9172 NEXT J
9174 NEXT J1
9190 RETURN
9500 REM INPUT SR FOR T.H.'S
9504 PRINT"ENTER MX,";
9505 IF F4=0 THEN 9510
9506 PRINT " MZ, MY";
9508 GO TO 9520
9510 PRINT " MY, MZ";
9520 INPUT H(0),H(1),H(2)
9535 LET H9=H(0)+2+H(1)+2
9540 RETURN
11000 REM SUBROUTINE FOR EIGENVALUES AND VECTORS
11002 LET H=B*H1
11005 IF (ABS(D)+ABS(E))>0 THEN 11040
11010 LET W(0)=-H
11015 LET W(1)=0
11020 LET W(2)=H
11025 GO TO 11190
11040 LET R0=(L*L*X+M0*M0*Y+N*N*Z)*H+H-X*Y*Z
11050 LET Q=X*Z+X*Y+Y*Z-H*H*(L*L+M0*M0+N*N)
11060 LET Q1=Q/3
11070 LET V=-R0/(2*SQR(-Q1*Q1*Q1))
11080 LET V1=V
11090 IF V1>=0 THEN 11110

```

```

11100 LET V1=ABS(V1)
11110 LET P=ATN(SQR(1-V1*V1)/V1)
11120 IF V>=0 THEN 11140
11130 LET P=P0-P
11140 LET W0=2*SQR(-01)
11150 LET W(0)=W0*COS(P/3)
11160 LET W(1)=W0*COS((P+P0*2)/3)
11170 LET W(2)=W0*COS((P+P0*4)/3)
11180 GO SUB 11500 [SORT EIGENVALUES ' ' '0' '+' ]
11190 GO SUB 11950 [ZERO VECTORS]
11200 LET F5=0
11210 IF ABS(L/G(0))<B0 THEN 11260
11220 LET F8=0
11230 LET F6=1
11240 LET F7=2
11250 GO TO 11350
11260 IF ABS(H0/G(1))<B0 THEN 11310
11270 LET F8=1
11280 LET F6=0
11290 LET F7=2
11300 GO TO 11350
11310 IF ABS(N/G(2))<B0 THEN 11360
11320 LET F8=2
11330 LET F6=0
11340 LET F7=1
11350 LET F5=1
11360 IF (ABS(D)+ABS(E))=0 THEN 11450
11370 IF F5=0 THEN 11430
11380 LET T2=0.5*ATN(2*H/D)
11390 IF F8<2 THEN 11410
11400 LET T2=P0/4
11410 GO SUB 11600
11420 GO TO 11480
11430 GO SUB 11700
11440 GO TO 11480
11450 IF F5=1 THEN 11400
11452 LET B3=SQR(2*(1-N*N))
11454 LET C0(0,1)=L
11456 LET C0(1,1)=H0
11458 LET C0(2,1)=N
11460 LET C0(0,2)=-L*N/B3
11462 LET C0(1,2)=-H0*N/B3
11464 LET C0(0,0)=C0(0,2)
11466 LET C0(1,0)=C0(1,2)
11468 LET C0(2,2)=B3/2
11470 LET C0(2,0)=C0(2,2)
11472 LET C1(0,2)=H0/B3
11474 LET C1(0,0)=C1(0,2)
11476 LET C1(1,0)=L/B3
11478 LET C1(1,2)=-C1(1,0)
11480 RETURN

```

```

11497 REM
11498 REM   SORT EIGENVALUES   '- ' '0' '+'
11499 REM
11500 FOR J=0 TO 1
11510 LET J1=J+1
11520 FOR J2=J1 TO 2
11530 IF W(J)<W(J2) THEN 11570
11540 LET W1=W(J)
11550 LET W(J)=W(J2)
11560 LET W(J2)=W1
11570 NEXT J2
11575 NEXT J
11578 FOR J=0 TO 2
11579 LET E9(J,K1)=W(J)
11580 NEXT J
11590 RETURN
11599 REM   SR FOR VECTORS .... CASE C.... H// AXIS....
11600 LET C9=COS(T2)
11610 LET S9=SIN(T2)
11620 LET C0(F0,1)=1
11630 LET C0(F6,2)=C9
11640 LET C0(F7,0)=C9
11650 LET C1(F6,0)=-S9
11660 LET C1(F7,2)=-S9
11670 RETURN
11699 REM   SR FOR VECTORS.....CASE D.....
11700 FOR J=0 TO 2
11710 LET X0(J)=X-W(J)
11720 LET Y0(J)=Y-W(J)
11730 LET Z0(J)=Z-W(J)
11740 LET Z1(J)=(X0(J)*L)↑2+(H*M0*H)↑2
11750 LET Z2(J)=(Y0(J)*M0)↑2+(H*L*N)↑2
11760 LET Z3(J)=(Z0(J)*N)↑2+(H*M0*L)↑2
11770 LET Z4(J)=SQR(Z1(J)*(Z2(J)+Z3(J))+Z2(J)*Z3(J))
11780 LET Z5(J)=SQR(Z1(J)/Z2(J))
11790 LET C0(0,J)=-X0(J)*Z0(J)-(H*M0)↑2)*L*N/(Z5(J)*Z4(J))
11800 LET C1(0,J)=-(Z0(J)*N*N+X0(J)*L*L)*H*M0/(Z5(J)*Z4(J))
11810 LET C0(1,J)=-(Y0(J)*Z0(J)-(H*L)↑2)*M0*N*Z5(J)/Z4(J)
11820 LET C1(1,J)=+(Z0(J)*N*N+Y0(J)*M0*M0)*H*L*Z5(J)/Z4(J)
11830 LET C0(2,J)=SQR(Z1(J)*Z2(J))/Z4(J)
11835 LET C1(2,J)=0
11870 NEXT J
11880 RETURN
11881 REM
11949 REM   SR TO ZERO VECTORS .....
11950 FOR I1=0 TO 2
11955 FOR J=0 TO 2
11960 LET C0(J,I1)=0
11965 LET C1(J,I1)=0
11970 NEXT J
11975 NEXT I1

```



```

11988 KLEUKN
11999 REM
12000 REM PRINT SR. FOR ZFS PARMS, TM'S & H DIRECTION.
12001 REM
12002 PRINT
12003 PRINT
12004 PRINT
12007 PRINT A9$(0);A9$(1);A9$(2);A9$(3)
12008 PRINT
12009 PRINT "MOLECULAR";A3$(4);A3$(F4);A3$(F4+1)
12010 PRINT "FIELD=";H1;" G."
12020 PRINT"G: XX=";G(0);" YY=";G(1);" Z=";G(2);" D =" ;D;" E =" ;E
12030 PRINT"PSI=";P1;" PHI=";P2
12032 PRINT "M(X)="; M(0);
12034 IF F4=0 THEN 12040
12036 PRINT " M(Y)="; M(2); " M(Z)="; M(1)
12038 GO TO 12045
12040 PRINT " M(Y)="; M(1); " M(Z)="; M(2)
12045 PRINT
12046 RETURN
12049 IF F9=1 THEN 12180
12050 PRINT "EIGENVALUES AND VECTORS:"
12060 PRINT TAB(6);"-";TAB(16);"0";TAB(26);"+"
12070 PRINTTAB(2);W(0);TAB(12);W(1);TAB(22);W(2)
12080 FOR J=0 TO 2
12090 PRINT
12100 PRINT A1$(J);
12110 FOR K=0 TO 1
12120 PRINT A2$(K);
12130 FOR J1=0 TO 2
12135 ON K+1 GO TO 12140,12145
12140 PRINT C0(J,J1);
12142 GO TO 12150
12145 PRINT C1(J,J1);
12150 NEXT J1
12155 PRINT
12158 PRINT " ";
12160 NEXT K
12170 NEXT J
12180 RETURN
13000 REM HEADER SR. FOR INTENSITIES.
13010 PRINT
13020 PRINT"THETA";TAB(8);"I0/I-";TAB(23);"I0/I+";TAB(38);"I+/I-";" ZFA"
13025 PRINT " OR I- ";TAB(23);" I0 ";TAB(38);" I+"
13030 RETURN
14000 REM SUBR. TO CALCULATE G(S,U) TERMS FROM EIGENVECTORS.
14001 REM K1 IS MOLECULE INDEX
14002 REM I1 IS SUBLEVEL INDEX
14003 REM J IS ZF BASIS INDEX
14004 REM ALL TERMS DEFINED ON P 281-289
14005 REM G'S ZEROED IN SR. TO ZERO VECTORS.

```

```

14006 REM
14010 FOR J=0 TO 2
14012 LET I2(J)=0
14016 LET I4(J)=0
14018 NEXT J
14019 LET W2=0
14020 FOR K1=1 TO 2
14021 LET K2=K1+F4
14022 IF F9=1 THEN 14090
14025 LET L=L1(K1,F4)
14030 LET H0=M1(K1,F4)
14040 LET N=M1(K1,F4)
14050 PRINT
14060 PRINT " MOLECULE #";K1
14065 GO SUB 11000 [EIGENVALUES AND VECTORS..
14070 PRINT "L=";L/G(0);" M=";H0/G(1);" N=";N/G(2)
14080 GO SUB 12050 [ PRINT EIGENVALS & VECTS.
14081 REM SWITCH VECTORS AFTER PRINTING.
14082 IF F4=0 THEN 14090
14084 GO SUB 16200 [SWITCH IF Z//C=S]
14090 FOR I1=0 TO 2
14095 LET W0=0
14100 FOR J=0 TO 2
14110 REM EIGENVALUES STORED IN E9(J,K1) IN SR 11500
14120 LET W(J)=H(J)+2*(C0(J,I1)+2+C1(J,I1)+2)
14125 LET W0=W0+W(J)
14130 NEXT J
14132 LET I7(I1,K1)=W0
14135 LET I4(I1)=I4(I1)+W0
14140 LET H2=(W(0)+W(1))/2
14150 LET H3=W(0)-W(1)
14160 LET H4=W(2)
14170 LET H5=M(1)*M(2)/S7*(C0(1,I1)*C0(2,I1)+C1(1,I1)*C1(2,I1))
14180 LET H6=M(0)*M(2)/S7*(C0(0,I1)*C0(2,I1)+C1(0,I1)*C1(2,I1))
14190 LET H7=M(0)*M(1) *(C0(0,I1)*C0(1,I1)+C1(0,I1)*C1(1,I1))
14200 LET H9=H3+U3+H7*U2
14210 LET H0=H2*(S6+1)+H4*C5
14220 ON K2 GO TO 14222,14230,14240,14250
14222 LET H0=H0+H9+H6*U4-H5*U5
14225 GO TO 14260
14230 LET H0=H0-H9+H5*U4+H6*U5
14232 GO TO 14260
14240 LET H0=H0+H9+H6*U4+H5*U5
14242 GO TO 14260
14250 LET H0=H0-H9+H6*U5-H5*U4
14260 LET G2(I1,K1)=H2
14270 LET G3(I1,K1)=H3
14280 LET G4(I1,K1)=H4
14290 LET G5(I1,K1)=H5
14291 LET G6(I1,K1)=H6
14292 LET G7(I1,K1)=H7

```

```

14293 LET H8=H8/2
14294 REM I2,I9 & W2 ARE UNPOLARIZED QUANTITIES, SO H8/2 AS ON P 286.
14295 LET I9(I1,K1)=H8
14300 LET I2(I1)=I2(I1)+H8
14305 LET W2=W2+H8
14310 NEXT I1
14320 NEXT K1
14325 LET W2=W2/M9
14330 REM UNPOLARIZED RATIOS.
14340 LET R9(0)=I2(1)/I2(0)
14350 LET R9(1)=I2(1)/I2(2)
14360 LET R9(2)=I2(2)/I2(0)
14380 RETURN
15000 REM SR TO CALC. INTENSITY RATIOS AS F(THETA).
15001 REM
15010 LET C3=COS(T/P9)
15020 LET S3=SIN(T/P9)
15022 LET C6=S3*C3
15024 LET S3=S3*S3
15026 LET C3=C3*C3
15028 LET C8=S3-S6*C3
15030 LET E0=C4*C6
15035 LET E1=S6*C3+S3
15040 LET E2=U0*C8+4*S1*C6*S0
15050 LET E3=S8*C8-S1*C6*U0
15060 LET E4=C3*U4+E0*S4
15070 LET E5=C3*U5-E0*S5
15072 REM
15075 LET W1=0
15076 LET I3(0)=0
15077 LET I3(1)=0
15078 LET I3(2)=0
15080 FOR K1=1 TO 2
15081 LET K2=K1+F4
15090 FOR I1=0 TO 2
15100 LET H8=G2(I1,K1)*E1+G4(I1,K1)*C5*C3
15110 LET H9=G3(I1,K1)*E3+G7(I1,K1)*E2
15120 ON K2 GO TO 15125,15130,15135,15140
15125 LET H8=H8+H9+G6(I1,K1)*E4-G5(I1,K1)*E5
15126 GO TO 15160
15130 LET H8=H8-H9+G6(I1,K1)*E5+G5(I1,K1)*E4
15131 GO TO 15160
15135 LET H8=H8+H9+G6(I1,K1)*E4+G5(I1,K1)*E5
15136 GO TO 15160
15140 LET H8=H8-H9+G6(I1,K1)*E5-G5(I1,K1)*E4
15160 LET I(I1,K1)=H8
15170 LET I3(I1)=I3(I1)+H8
15175 LET W1=W1+H8
15180 NEXT I1
15185 NEXT K1
15186 LET W1=W1/M9
15187 REM

```

```

15190 LET R(0)=I3(1)/I3(0)
15200 LET R(1)=I3(1)/I3(2)
15210 LET R(2)=I3(2)/I3(0)
15290 RETURN
16000 REM PRINT INTENSITY RATIOS FOR EACH POL.
16010 PRINT
16015 PRINT T;
16016 FOR K1=1 TO 2
16017 PRINT TAB(5);I(0,K1);TAB(20);I(1,K1);TAB(35);I(2,K1);" SITE";K1
16018 NEXT K1
16019 PRINT TAB(5);I3(0);TAB(20);I3(1);TAB(35);I3(2);" SUM"
16020 PRINT TAB(5);R(0);TAB(20);R(1);TAB(35);R(2);" RATIO ";W1;" ZFA"
16030 PRINT TAB(5);R1(0);TAB(20);R1(1);TAB(35);R1(2);" EXPT"
16050 RETURN
16200 REM INTERCHANGE VECTORS C(Y,I1) AND C(Z,I1)
16210 FOR I1=0 TO 2
16215 LET T9=C0(1,I1)
16220 LET T8=C1(1,I1)
16225 LET C0(1,I1)=C0(2,I1)
16230 LET C1(1,I1)=C1(2,I1)
16235 LET C0(2,I1)=T9
16240 LET C1(2,I1)=T8
16245 NEXT I1
16250 RETURN
69000 END

```

```

70 REM ..... I F S P K S ,.....
80 REM
90 REM
100 DIM A(20),U(20)
110 DIM X(325),Y(325)
120 CALL PLOTS
130 LET L2=0.69315
140 LET N=320
150 PRINT "ENTER W1,W3 ";
160 INPUT W1,W3
170 PRINT"ENTER SIZE OF BOX (HORIZ,VERT) : ";
180 INPUT H1,V1
190 LET W2=(W3-W1)
200 LET X0=W2/N
210 LET W2=W2/H1
220 LET P1=INT(10/V1)
230 LET P=0
240 IF F1>0 THEN 330
250 PRINT "ENTER ENERGIES : "
260 FOR I=1 TO 6
270 INPUT W(I)
280 NEXT I
290 PRINT "ENTER INTENSITIES : "
300 FOR I=1 TO 6
310 INPUT A1(I)
320 NEXT I
330 PRINT"ENTER HUHM, J1, J2, F1: ";
340 INPUT B,J1,J2,F1
350 LET B1=0.469719*V1/B
360 ON F1 GO TO 370, 370, 290, 250, 150, 850
370 FOR I=1 TO 6
380 LET A(I)=A1(I)*B1
390 NEXT I
400 FOR I=0 TO N
410 LET X(I)=W1+I*X0
420 LET Y(I)=0.1
430 CALL FSWITCH(S1,S2)
440 LET S1=S1/1024
450 IF S1>0 THEN 470
460 LET S1=1
470 FOR J=J1 TO J2
480 IF A(J)=0 THEN 570
490 LET E1=(X(I)-W(J))/B
500 LET E1=E1*L2
510 IF E1>9 THEN 570
520 ON F1 GO TO 530, 560
530 LET Y2=A(J)*EXP(-E1)
540 LET Y(I)=Y(I)+S1*Y2
550
560
570
580
590
600
610
620
630
640
650
660
670
680
690
700
710
720
730
740
750
760
770
780
790
800
810
820
830
840
850
860
870
880
890
900
910
920
930
940
950
960
970
980
990

```

```

550 GO TO 570
560 LET Y(I)=Y(I)+A(J)*X(I)/W(J)*EXP(-E1)
570 NEXT J
580 NEXT I
590 LET X(N+1)=W1
600 LET X(N+2)=W2
610 LET Y(N+1)=0
620 LET Y(N+2)=1
630 IF F3=1 THEN 730
640 LET F3=1
650 LET X1=0.5
660 LET Y1=10.5-V1
670 CALL FDPLOT(X1,Y1,-3)
680 PRINT "CHANGE ORIGIN? (0 OR 1) ";
690 INPUT F2
700 IF F2=0 THEN 730
710 INPUT X1,Y1
720 CALL FDPLOT(X1,Y1,-3)
730 CALL FLINE(X,Y,N+1,1,0,1)
740 CALL FDPLOT(0,0,3)
750 GO SUB 860
760 GO SUB 920
770 LET P=P+1
780 IF P<P1 THEN 830
790 LET V2=(P-1)*V1
800 LET P=0
810 CALL FDPLOT(H1,V2,-3)
820 GO TO 330
830 CALL FDPLOT(0,-V1,-3)
840 GO TO 330
850 CALL EXIT
860 REM BOX SUBR.
870 CALL FDPLOT(H1,0,2)
880 CALL FDPLOT(H1,V1,2)
890 CALL FDPLOT(0,V1,2)
900 CALL FDPLOT(0,0,2)
910 RETURN
920 REM PRT FACTOR SR.
930 LET S3=.1+V1/25
940 LET X2=H1-S3*2-.05
950 LET Y2=V1-S3-.1
960 CALL FNUMBER(X2,Y2,S3,S1,0,2,2)
970 CALL FDPLOT(0,0,3)
980 RETURN
990 END

```

```

50 REM ..... PROGRAM R A T P L T ..... DEC. 1981
100 DIM X(200),Y(200)
105 DIM G$(3)
110 LET Q9=57.29578
120 LET Q8=2/Q9
150 PRINT"ENTER PSI (IN,FIN,DEL): ";
155 INPUT P1,P2,P3
160 PRINT "          PHI          : ";
165 INPUT P4,P5,P6
166 LET P7=0
167 LET P8=90
168 LET D3=0.5
169 GO TO 180
170 PRINT "          THETA          : ";
175 INPUT P7,P8,D3
180 PRINT"ONE ROUTE,PLOT,PRINT? (E.G.:YN): ";
185 CALL BSTRGL(G$,1)
190 IF G$(1)="Y" THEN 250
195 PRINT "ENTER RX,RZ : ";
200 INPUT R8,R9
210 LET R4=R8*R8+1
220 LET R7 =R4+2*R8
230 LET R6=R4-2*R8
240 LET R5=2*R9*(R9-R8-1)
250 IF G$(2)="N" THEN 300
255 CALL PLOTS
260 CALL FDPLOT(1.5,1.5,-3)
300 FOR Q0=P1 TO P2 STEP P3
310 LET Q1=Q0/Q9
320 LET S1=SIN(Q1)
330 LET C1=COS(Q1)
340 LET T1=S1/C1
350 IF G$(2)="N" THEN 810
380 LET G1$="THETA"
385 LET G2$="RATIO"
400 CALL FAXIS(0,0,G1$,5,9,0,0,10,2,2)
410 CALL FAXIS(0,0,G2$,5,6,90,0,1,2,2)
800 LET J=-1
810 FOR Q2=P4 TO P5 STEP P6
815 LET Q3=Q2*Q8
820 LET S2=SIN(Q3)+2
830 LET C2=COS(Q3)+2
840 LET S4=SIN(2*Q3)
845 IF G$(2)="N" THEN 860
850 CALL FDPLOT(0,0,3)
860 IF G$(1)="Y" THEN 10000
900 REM FOR 2 OR MORE ROUTES.
910 LET A0=S1*S1*((R7+S2*R6)/2+R5)
920 LET B0=S1*S4*R6/2

```

```

930 LET C0=R6*C2/2
940 LET A1=R4*T1+T1-A0
950 LET D1=R4/(C1+C1)-C0
960 GO TO 10100
10000 REM FOR 1 ROUTE ONLY (SAME FOR EITHER X OR Y)
10010 LET A0=S1*S1*(1+S2)/2
10020 LET B0=S1*S4/2
10025 LET C0=C2/2
10030 LET A1=T1+T1-A0
10040 LET D1=1/(C1*C1)-C0
10100 LET N=-1
10105 FOR T=P7 TO P8 STEP D3
10110 LET N=N+1
10120 LET X(N)=T
10125 LET Y(N)=0
10130 IF T=0 THEN 10190
10140 IF T=90 THEN 10250
10145 LET T2=T/Q9
10150 LET T3=SIN(T2)/COS(T2)
10160 LET I0=2*(A0+T3*(B0+C0*T3))
10170 LET I1=A1+T3*(D1*T3-B0)
10180 GO TO 10300
10190 LET I0=2*A0
10200 LET I1=A1
10210 GO TO 10300
10250 LET I0=2*C0
10260 LET I1=D1
10300 IF I1>0 THEN 10350
10310 PRINT"I1=0 : ";Q0;Q2;T;A0;B0;C2;A1;D1;T3
10320 LET Y(N)=6
10350 LET Y(N)=I0/I1
10360 IF Y(N)<=6 THEN 10380
10370 LET Y(N)=6
10380 NEXT T
10385 IF G*(3)="N" THEN 10500
10390 FOR I=0 TO 180 STEP 10
10400 PRINT I;X(I);Y(I)
10410 NEXT I
10500 IF G*(2)="N" THEN 11100
10900 LET Y(N+2)=1
10910 LET X(N+2)=10
10920 LET J=J+1
11000 CALL FLINE(X,Y,N+1,1,10,J)
11100 NEXT Q2
11200 IF G*(2)="N" THEN 12200
12000 CALL FDPLOT(0,0,3)
12010 CALL FDPLOT(11,0,-3)
12200 NEXT Q0
12300 PRINT "WANT MORE? (Y,N): ";
12310 INPUT H4$
12320 IF H4$="Y" THEN 150
12330 CALL EXIT
13000 END

```


APPENDIX II

The programs listed here were used to carry out the calculations in Chapter 4. The main program is called SPINORBT and is listed first. Three subroutines are required to run the program, MOMENT, LOPER, and MOVE. Presently these are stored in the NERDC TCP system in files of the same name under the access number 22031001,10.

The subroutines can be called from other programs as well, for example, MOMENT calculates transition moments as outlined in Chapter 4; this method follows the approximations made by Ellis and his coworkers (92,105).

The comments in each listing define the input and output variables and a sample input is provided at the end. For a given EHT run, any number of NAMELIST (&INPUT...&END) data sets may be concatenated.

The output is labelled and requires no additional explanation. The notation for the states in the integrals appearing on the output is: the orbital numbers are used to label the MO's, with #1 being the highest unoccupied (virtual) orbital and #N being the lowest occupied orbital. For TMCBDT some of these orbitals are given in Fig. 2-4, MO number 25 is the HOMO and 24 is the LUMO.

The eigenvalues are printed but not the eigenvectors. It would be useful to optionally print the eigenvectors as well, but this was not included in the present version.

S P I N O R B T 12-79

PAGE 2

NO DEFAULTS ARE PRESENTLY INCLUDED IN THE PROGRAM, SO ALL THE
 NAMELIST VARIABLES MUST BE SPECIFIED. THESE ARE DEFINED BELOW.
 SEE THE STATEMENT: NAMELIST /INPUT/ LIST..... FOR THE LIST
 OF THESE INPUT VARIABLES.

A SAMPLE INPUT LISTING IS GIVEN AFTER THE SUBROUTINES.
 THIS IS ONE FOR THE CASE OF THE TRIPLET N(+)PI*(-)
 STATE OF TETRAMETHYLCYCLOBUTANEDIITHIONE. (LOWEST TRIPLET).
 SINGLET AND TRIPLET PERTURBING STATES WHICH ARE LESS
 THAN 20 E.V. OR SO ARE INCLUDED.

AN ENTRY LIKE: 13*4.5 0. 3. 3*0.0 IN A NAMELIST DATA
 INPUT STREAM MEANS: 13 CONSECUTIVE FLOATING POINT VALUES OF
 4.5 ARE READ, FOLLOWED BY 1 INTEGER OF VALUE 0, FOLLOWED BY
 4.5 ARE READ, FOLLOWED BY 2 INTEGER VALUES OF 0 AND 3.
 FOLLOWED BY 3 FLOATING POINT ZEROS. MIXED MODE IS ALLOWED,
 BUT ALL THE ABOVE WOULD BE READ INTO A SINGLE VECTOR OF LENGTH
 13+2*3=18. IF THE VECTOR IS DIMENSIONED > 18, ZEROS ARE
 PADDED IN.
 REFER TO THE 'NAMELIST' FEATURE IN THE 'FORTRAN IV LANGUAGE
 MANUAL'. (IBM).

THE ORDER OF INPUT ON UNIT 5 (CARD READER, OR EQUIVALENT) IS:
 NB, NOCC, NA, NH, COMMENT (413 ON FIRST LINE)
 80 CHR. COMMENT NEXT LINE)
 R. THE COORDINATES X,Y AND Z FOR EACH ATOM, HYDROGENS FIRST,
 NA, NH LINES (CARDS) (EACH: 3 F 15.6)
 C INPUT NAMELIST
 VARIABLES AND THEIR VALUES.....
 &END

 VARIABLE DEFINITIONS:

EPS EIGENVALUES, IN E.V.
 C EIGENVECTORS.
 S OVERLAP MATRIX. SEE ABOVE FOR DIMENSIONALITY.
 CT EIGENVECTOR OF MO IN TRIPLET STATE. ALWAYS IN THE
 R.H.S. OF <SINGLET | H(SO) | TRIPLET>.
 CS EIGENVECTOR OF MO IN SINGLET STATE. ALWAYS IN THE
 L.H.S. OF ABOVE INTEGRALS.
 SO SPIN-ORBIT-COUPLING CONSTANTS. STORED IN VECTOR OF
 LENGTH NA. ONLY FOR NON-HATOMS.
 ETA SLATER EXPONENTS STORED IN ARRAY OF LENGTH NA.
 R THE ATOMIC COORDINATES. ORIGIN OF MOLECULE FIXED

```

COORDINATE SYSTEM MUST BE AT THE CENTER OF MASS OF THE MOLECULE OTHERWISE THE *.A* TERMS IN THE TRANSITION MOMENT MUST BE CORRECTED.
MATRIX OF DIMENSION R(3,NH+NA).
NUMBER OF HYDROGEN ATOMS.
NUMBER OF NON-H
VECTOR OF LENGTH NA TO STORE THE NAMES OF ATOMS.
VECTOR OF LENGTH 40 TO STORE THE OPERATOR INDEX*. THIS CORRESPONDS TO .LR* IN SUBROUTINE *LOPER*. USE 1,2 OR 3 FOR THE X,Y OR Z COMPONENTS OF H(SO). SAME AS KIJ. FOR INDIVIDUAL VALUE OF ILR. INDEX FOR SINGLET ORBITALS. VECTOR OF LENGTH 40. SAME AS IIS FOR INDIVIDUAL VALUE OF ILR. SAME AS IIS, BUT FOR TRIPLET. SAME AS IS, BUT FOR TRIPLET. INDEX FOR COMMON ORBITAL WHICH DOES NOT APPEAR IN H(SO). USED TO COMPLETE OUTPUT LABELS FOR STATES. SAME AS IK. NUMBER OF ORBITALS. DIMENSION OF EIGENVALUES, ETC. NUMBER OF OCCUPIED ORBITALS. LABEL FOR MULTIPLICITY. SEE MULT IN MOMENT S-R. (*,NA) MATRIX CONTAINING THE ATOM INDICES DESCRIBING THE BONDING TO AN ATOM. FOR EXAMPLE, NN(1,5),NN(2,5),NN(3,5),NN(4,5) = 4,6,10,11 MEANS THAT ATOM # 5 (IN THE SEQ. 1,NA) IS BONDED TO ATOM #5 4,6,10 AND 11. THIS IS USED TO DIFFERENTIATE ONE CENTER, NEAREST A NEIGHBOR (DUE TO OVERLAP, THE OPERATOR IS STILL A ONE CENTER TYPE) AND OTHER CONTRIBUTIONS TO H(SO). SEE $P IN MOMENT S-R. LOGICAL VARIABLE. IF TRUE (=TRUE, OR .T) PRINT BREAKDOWN OF CONTRIBUTIONS TO <H(SO)>. IF FALSE (=FALSE, OR .F) PRINT ONLY TOTALS. SET TO TRUE FOR ONE CENTER ONLY CALCULATION. SET TO FALSE TO INCLUDE OVERLAP TERMS, THESE ARE DIVIDED INTO NEAREST NEIGHBOR, ETC. SEE .NN*. IF TRUE, WRITES ON LOG UNIT 2 THE TOTALS. THE TWO ORBITAL INDICES OF THE TRIPLET STATE IN THE TRANSITION. THRESHOLD FOR TERMS IN SUM. NOT IMPORTANT FOR ENT. THRESHOLD FOR VECTORS. IGNORE IF <V(OR T)FRESH. MAXIMUM NUMBER OF PERTURBING STATES IN THE SUM. THIS IS THE *40* IN .ILR*, IIS*, ETC. IT REPRESENTS THE MAXIMUM NUMBER OF TERMS IN THE SUM OF EQ. 4-12, BUT INCLUDING ALL 3 COMPONENTS OF H(SO).

```



```

14  TR(J,I)=0.0
    ETOT=0.0
    DO 15 I=1,N OCC
      J=NB-I+1
      ETOT=ETOT+EPS(J)
      ETOT=ETOT*2.00
      WRITE(6,503) ETOT,N OCC
      READ(5,INPUT,END=1000)
      WRITE(6,610) VTRESH,VTRESH
      ENU=(EPS(TRI(2))-EPS(TRI(1)))*8065.0
      DO 200 M=1,MAX
        MULT=MMULT(M)
        IS=IIS(M)
        JT=IJT(M)
        K=IK(M)
        LR=ILR(M)
        KIJ=LR
        IF(IS.EQ.0 .OR. K.EQ.0 .OR. JT.EQ.0 .OR. LR.EQ.0) GO TO 210
        EJK=EPS(K)-EPS(IS)
        EJK=EPS(K)-EPS(JT)
        EIK=EIK+THE SINGLET ENERGY (ABOVE G.S.)
        EIK=EIK+THE TRIPLET ENERGY (ABOVE G.S.)
        IF (K.LE.(NB-N OCC)) GO TO 16
        EIK=-EIK
        EJK=-EJK
        DEC=EJK-EIK
        DE=DEC*8065.
        EIK=EIK*8065.
        EJK=EJK*8065.
        WRITE(6,604) COMMT,IS,K,TYPE(LR),JT,K
        NO=NA+NH
        CALL MOVE(C,CS,CT,IS,JT,NB)
        CALL LOPER (CT(N0+1),LR,NA,SO,20 )
      SOC=0.0
      SOT=0.0
      SNN=0.0
      IF ($PRT) WRITE(6,600)
      DO 100 KR=1,3
        KR0=N0+(KR-1)*NA
        DO 90 IR=1,NA
          IR0=KR0+IR
          IF(ABS(CT(IR0)).LT.VTRESH) GO TO 90
          DO 80 KL=1,3
            KL0=N0+(KL-1)*NA

```

S P I N O R B T 12-79

PAGE 6

```

DO 70 IL=1,NA
  IL0=KL0+IL
  IF (ABS(CS(IL0)).LT.VTRESH) GO TO 70
  $NN=.FALSE.
  $OT=.FALSE.
  $OC=.FALSE.
  OTYPE=BLANK
  IF (IL.NE.IR) GO TO 50
  $OC=.TRUE.
  OTYPE=OCTR
  GO TO 65
50 DO 60 J=1,4
  IF (NN(J,IL).NE.IR) GO TO 60
  $NN=.TRUE.
  OTYPE=NNBR
  GO TO 65
60 CONTINUE
  $OT=.TRUE.
  OTYPE=OTHR
  IOV=IL0+KF(IR0)
  IF ($ONE.AND.NOT.$OC) GO TO 70
  T=CS(IL0)*CT(IR0)*S(IOV)
  IF (ABS(T).LT.VTRESH) GO TO 70
  IF ($OT) $OT=$OT+T
  IF ($OC) $OC=$OC+T
  IF ($NN) $NN=$NN+T
  IF ($PRT) WRITE(6,601) OTYPE,TYPE(KL),ATOM(IL),
    * CS(IL0),TYPE(KR),ATOM(IR),CT(IR0),S(IOV),T
  CONTINUE
70 CONTINUE
80 CONTINUE
90 CONTINUE
100 CONTINUE
110 TOT=$OC+$NN+$OT
  TOTDE=TOT/DE
  IM=I*AG
  HSOME=TOTDE
  IF (IR-2) 111,112,113
  FOR (I,SO) X Y Z
  IS FOR ALL 3 OF THESE HSUB(I), I= 1, 2, 3
  IS FOR THE TRIPLET SUBSTATES ONE CENTER CONTRIBUTIONS.
  $OC CONTAINS THE SUM OF " NEAREST NEIGHBOR "
  $NN " " " ALL " OTHER "
  $OT " " " " " "
  TOTDE IS THE TOTAL/DELTA E
  HSOME IS THE FINAL TERM. EQ. 4-20.
  TERM IS A TERM IN THE SUM OF EQ. 4-12.

```

```

S P I N O R B T      12-79

111  IF (K.NE.IS) H SOME=TOTDE/SQR2
      HSUB(1)=-HSOME
      HSUB(2)=+HSOME
      HSUB(3)=0.0
      GO TO 115
112  IM=BLANK
      IF (K.NE.IS) H SOME=+TOTDE/SQR2
      HSUB(1)=HSOME
      HSUB(2)=HSOME
      HSUB(3)=0.0
      GO TO 115
113  H SOME=-HSOME
      IF (K.EQ.IS) H SOME=HSOME*SQR2
      HSUB(1)=0.0
      HSUB(2)=0.0
      HSUB(3)=HSOME
115  WRITE(6,602) SOC,SNN,SOT,TOT,TOTDE,HSOME,IM
C
      IF (MULT.EQ.TRIP) GO TO 130
      IL=IS
      IR=K
      GO TO 140
130  IF (TRI(1).NE.K) GO TO 132
      IL=TRI(2)
      IR=JT
      GO TO 140
132  IF (TRI(2).EQ.JT) GO TO 133
      WRITE(6,606) TRI,K,JT
      GO TO 200
133  IL=TRI(1)
      IR=K
140  CALL MOVE(C,CS,CT,IL,IR,NB)
      CALL MOMENT(CS,CT,IL,IR,ATOM,ETA,R,KIJ,TM,SPRTM,.FALSE.,
*
      TERM,TM*HSOME TERM
      WRITE(6,603)
      DO 150 I=1,3
      HSUB(I)=HSUB(I)*TM
150  TR(KIJ,I)=TR(KIJ,I)+HSUB(I)
      WRITE(6,607) HSUB
C
200  CONTINUE
SUM=0
DO 170 I=1,3
170  TRMT(I)=0

```


M O M E N T 12-79

```

SUBROUTINE MOMENT CALCULATES THE TRANSITION MOMENT
<I|P|U> . SEE CHAPTER 4 AND REFERENCES THEREIN.

THE T.M. INTEGRAL IS DIVIDED INTO 'A' AND 'B'
TYPE CONTRIBUTIONS. SEE PAGE 109. THESE ARE PRINTED
(IF $P=.TRUE.) FOR EACH ATOM. THE TOTAL FOR EACH
ATOM IS PRINTED. 'S' ORBITAL, AND 'P' ORBITAL.
CONTRIBUTIONS ARE ALSO SPECIFIED.
IF $P=.FALSE. ONLY THE TOTAL 'A' AND 'B' CONTRIBUTIONS
ARE GIVEN.

UNITS:
DISTANCES ARE IN ANGSTROMS
FINAL RESULT IS IN DEBYES

ARGUMENT DEFINITIONS:
CL EIGENVECTOR OF ORBITAL IN INITIAL STATE
CR EIGENVECTOR OF ORBITAL IN FINAL STATE
IS ORBITAL INDEX OF INITIAL STATE
IK ORBITAL INDEX OF FINAL STATE
ATOM ARRAY CONTAINS STRINGS FOR ATOMIC SYMBOLS
ETA ARRAY CONTAINS THE SLATER EXPONENTS OF THE ATOMS
R ARRAY CONTAINS THE COORDINATES IN ANGSTROMS
K HAS VALUE OF 1,2 OR 3 FOR X,Y OR Z RESPECTIVELY.
TM THIS IS THE OPERATOR R(U), U=1,2 OR 3.
$P LOGICAL VARIABLE (TRUE=.TRUE.=T, OR FALSE=.FALSE.=F)
USED TO PRINT THE CONTRIBUTION BREAKDOWN FOR TM:
T = PRINT ALL TOTALS.
F = PRINT ONLY TOTALS.
$AVE LOGICAL VARIABLE USED TO FLAG STORAGE OF TOTALS ON DISK.
NH NORMALLY NOT NEEDED.
NA NUMBER OF HYDROGEN ATOMS IN THE MOLECULE.
THE NUMBER OF ALL OTHER TYPES OF ATOMS IN MOLECULE.
THE COORDINATES ARE GIVEN IN THE SAME ORDER AS THE
EHT INPUT: HYDROGENS FIRST, THEN ALL OTHERS.
ANY QUANTITY WHICH IS ATOM DEPENDENT IS ENTERED
IN THE ARRAY (E.G. ETA, R, ATOM) IN THE SAME ORDER
AS THE COORDINATES.
MULT CONTAINS THE STRING 'SING' OR 'TRIP' TO PRINT
SINGLET OR TRIPLET FOR A SINGLET-SINGLET
TRANSITION OR A TRIPLET-TRIPLET TRANSITION, RESPECTIVELY.
IU THE LOGICAL UNIT NUMBER FOR STORAGE OF FINAL
RESULTS ON DISK. IF $AVE=.TRUE.

```

COMMENT 12-79

```
C
C
C VARIABLE DEFINITIONS:
C CON1 SORT(2)*ELECTRON CHARGE)
C CON2 $*0./.(25SORT(3)).A.=AO=BOHR RADIUS.
C A1 CONTRIBUTIONS TO TOTAL *B.* TYPE TERMS FROM HYDROGEN ATOMS.
C T1 TOTAL *A.* CONTRIBUTIONS.
C B1 TOTAL *B.* CONTRIBUTIONS.
C AC VALUE OF NON-H ATOM *A.* CONTRIBUTION.
C BC BOVALUE OF NON-H ATOM *B.* CONTRIBUTION.
C B2 " "
C
C NOTES AND BUGS:
C PRESENTLY ONLY WORKS FOR PRINCIPAL QUANTUM NUMBER=2 ATOMS
C (OUTER SHELL). FOR PQN=3.. SULFUR, FOR EXAMPLE, MUST
C MULTIPLY ALL *B.* TYPE TERMS BY 7/5=1.400. FOR REASON
C SEE TEXT P. 110-111 AND THE TWO EQUATIONS ON PAGE 111.
C PRESENTLY REQUIRES COORDINATES AND EIGENVECTORS TO BE
C SPECIFIED IN THE FORMAT OF THE EHT PROGRAM, QCPE #64.
C
C SUBROUTINE MOMENT (CL,CR,IS,K,K,ATOM,ETA,R,K,TM,$P,$SAVE,
C NH,NA,MULT,I,U)
C IMPLICIT LOGICAL*(I,$)
C DIMENSION CL(I),CR(I),ATOM(I),ETA(I),R(3,22)
C DIMENSION $TYPE(3),$2P(2),$ORB(2)
C DATA $B/1H /,$$TYPE/'X'',$Y'$',Z'/,$$2P/'S'`,`P'/$
C
C EPS=0.0005
C CON1=-6.7924395
C CON2=0.763892
C A1=0.0
C DO 100 I=1,NH
C IF ($P) WRITE(6,602)
C IF ((ABS(CL(I))*.LT.EPS).OR.(ABS(CR(I))*.LT.EPS)
C *.OR.(R(K,I).EQ.0.0)) GO TO 100
C A1=A1+CL(I)*CR(I)*R(K,I)*CON1
C CONTINUE
C IF ($P) WRITE(6,609) A1
C T2=0.0
C TAB=0.0
C TB1=0.0
C DO 150 I=1,NA
C IF ($P) WRITE(6,600) I, ATOM(I)
C A2=0.0
C L$=NH+I
C DO 130 J=1,4
C J1=J-1
C L$=L$+J1+LS
C IF ((ABS(CL(L$))*.LT.EPS).OR.(ABS(CR(L$))*.LT.EPS))

```

M O M E N T 12-79

```

*      .OR.(RK,LS).EQ.0.0)) GO TO 130
AC=CL(L)*CR(L)*RK,LS)*CONI
A2=A2+AC
IF (.NOT. SP) GO TO 130
$ORB(1)=$2P(2)
$ORB(2)=$TYPE(J1)
GO TO 126
$ORB(1)=$2P(1)
$ORB(2)=$B
WRITE(6,610) ATOM(I),SORB,AC
CONTINUE
IF (SP .AND. A2.NE.0.0) WRITE(6,611) A2
C=CONI*CON2/ETA(I)
LPK=K*NA+LS
B2=0.0
B0=0.0
IF ((ABS(CL(LS)),LT,EPS).OR.(ABS(CR(LPK)),LT,EPS)) GO TO 140
B0=CL(LS)*CR(LPK)*C
IF (SP) WRITE(6,612) IS,$TYPE(K),IK,B0
IF ((ABS(CL(LPK)),LT,EPS).OR.(ABS(CR(LS)),LT,EPS)) GO TO 145
B2=CL(LPK)*CR(LS)*C
IF (SP) WRITE(6,612) IK,$TYPE(K),IS,B2
B1=B0*B2
IF (SP.AND. B0.NE.0.0 .AND. B2.NE.0.0) WRITE(6,613) B1
AB=B1+A2
IF (SP .AND. AB.NE.0.0) WRITE(6,614) ATOM(I), AB
TA2=TA2+A2
TB1=TB1+B1
TAB=TAB+AB
CONTINUE
TA=TA2+A1
TM=TM+AB+A1
WRITE(6,601) MULT,IS,$TYPE(K),IK,TA,TB1,TM
IF (.SAVE) WRITE(IU) MULT,K,IS,IK,TM
RETURN

C      FORMAT(1H0,13.2X,A4,
600      FORMAT(///,10X,22HTRANSITION MOMENT FOR ,A4,SHLET <,12.1X,A2,
601      *      13.1H> (DEBYES):,///,1H,15X,SUM OF A TERMS =,F13.3,
*      *      //,1H,15X,SUM OF B TERMS =,F13.3,///,1H,15X,
*      *      TOTAL T.M. =,F17.3/)
C      FORMAT(1H1)
602      FORMAT(1H0,*,* CONTRIBUTIONS TO TRANS. MOMENT (DEBYES) **,
609      *      //,5X,HYDROGENS,F15.5,
*      *      //,5X,24HATOM ORB. CONTRIBUTION,/)

```

M O M E N T 12-79

PAGE 4

```
610 FORMAT(1H,5X,A4,2X,2A1,2X,F14.3)
611 FORMAT(1H,11X,*,SUM(A),*,F8.3)
612 FORMAT(1H,5X,B,*,S(12,*)P,A1,*,(12,*)*,F10.3)
613 FORMAT(1H,11X,*,SUM(B),*,F10.3)
614 FORMAT(1H,5X,A4,*,TOTAL,*,F13.3)
C
END
```

PAGE 1

L O P E R 12-79

```

C SUBROUTINE LOPER
C ORBITAL ANGULAR MOMENTUM OPERATOR, L, ON THE MOLECULAR
C ORBITAL IN THE KEY. THIS IS ACCOMPLISHED BY INTERCHANGING
C THE ATOMIC ORBITAL COEFFICIENTS FOR THE ATOM ON WHICH THE
C OPERATION TAKES PLACE. THE INTERCHANGE HAS THE SAME EFFECT
C AS THE ROTATION OF A P ORBITAL BROUGHT ABOUT BY L.
C THE ORBITAL COEFFICIENT IS MULTIPLIED BY THE SPIN-ORBIT
C CALCULATION TO AN OVERLAP INTEGRAL.
C
C ARGUMENT DEFINITIONS:
C LRHAS VALUE OF 1,2 OR 3 FOR X,Y OR Z COMPONENT OF
C THE SPIN-ORBIT OPERATOR.
C NANUMBER OF NON-H ATOMS IN THE MOLECULE.
C SOVECTOR CONTAINING THE SPIN-ORBIT-COUPLING CONSTANTS
C FOR THE NA ATOMS.
C
C NOTES AND BUGS:
C WORKS ONLY FOR EHT-FORMAT EIGENVECTORS. EASY TO CHANGE TO
C CND0/IND0 OR OTHERS.
C
C SUBROUTINE LOPER (C,LR,NA,SO,*)
C DIMENSION T(20),C(1),SO(1)
C INTEGER*4 LOP(3,3)/0,1,2, 1,2,0, 2,0,1/
C
C IF(LR.LT.1.OR. LR.GT.3) GO TO 20
C I0=LOP(1,LR)*NA
C I1=LOP(2,LR)*NA
C I2=LOP(3,LR)*NA
C
C DO 10 I=1,NA
C C(I+I0)=0.0
C T(I) =C(I+I1)*SO(I)
C C(I+I1)=-C(I+I2)*SO(I)
C C(I+I2)= T(I)
C
C RETURN
C WRITE(6,100) LR
C FORMAT('///', ***** L OPERATOR UNDEFINED.....',
C * , READ NEXT NAMELIST *****//)
C RETURN 1
C END

```

M O V E 12-79

PAGE 1

C THIS SUBROUTINE MOVES THE TWO EIGENVECTORS NEEDED FOR
 C A SPIN-ORBIT INTEGRAL INTO <CL AND CR>.
 C THE FULL EIGENVECTOR MATRIX FROM THE EHT OUTPUT IS
 C STORED AS THE SINGLY SUBSCRIPTED VARIABLE 'C'.

```

SUBROUTINE MOVE (C,/CR/,/CL/,IR,IL,NB)
DIMENSION      C(I),CL(I),CR(I)
FL(L)=NB*(L-1)
KL0=FL(IL)
KR0=FL(IR)
DO 10 I=1,NB
  KL=KL0+I
  KR=KR0+I
  CL(I)=C(KL)
  CR(I)=C(KR)
RETURN
END

```

10

PAGE 1

SAMPLE INPUT FOR SPINORBT

```

THE FIRST LINE (CARD) OF THE DATA INPUT FOR S P I N O R B T
PROGRAM IS 52 28 10 12
THE FOLLOWING IS TO AID1 IN DECIPHERING COLUMNS ONLY. LEAVE OUT.7
4
5
6
12345678901234567890123456789012345678901234567890
52 28 10 12
** JAN 5, 1979 DITHIONE S.O. COUPLING & OSCILL. STRENGTH CALC ENTWF
2.075068 1.147565 0.0
-2.075068 1.147565 0.0
-2.075068 -1.147565 0.0
1.315648 2.460271 0.875579
-1.315648 2.460271 -0.875579
-1.315648 2.460271 0.875579
1.315648 -2.460271 -0.875579
-1.315648 -2.460271 0.875579
-1.315648 -2.460271 -0.875579
0.0 0.0 1.049015
0.0 0.0 -1.049015
0.0 1.115135 0.0
0.0 -1.115135 0.0
-1.323484 1.880792 0.0
-1.323484 1.880792 0.0
-1.323484 -1.880792 0.0
0.0 0.0 2.657015
0.0 0.0 -2.657015
EI INPUT
COMMT=, DITHIONE JAN 5 1979 USING EXTENDED HUCKEL WF.
ATOM= C1., C3., C2., C4., CM 1., CM 2., CM 3., CM 4.,
. S1., S2
SD=8*28.0*2*382.0, ETA=8*1.625*2*1.817.
NM=3.4*9.0, 3.4*10.0, 1.2*5.6, 1.2*7.8, 3.3*0.3*0.4*3*0.4*3*0.4*3*0.
1.3*0.2*3*0.
ILR=6*3.3*2.5*1.6*3.7*2.4*1.
IIS=29.3*4.41.49.21.14.18.16.36.19.40.27.44.50.3*25.
26.32.42.33.39.43.46.47.52.25.28.35.25.25.
IJT=4*25.4*25.2*4.25.15.23.20.9*4.12.2*24.17.13.
IK=4*24.4*25.24.25.4*24.3*25.
26.32.42.33.39.43.46.47.52.25.28.35.25.25.
SPRT MEI=SAVE=F,SPRT=I.
SONE=I.
TRI=25.24.
MMULI=14*SING*.17*TRIP.

```


SAMPLE INPUT FOR SPINORBT

VTRESH=0.001,
YTRESH=0.1,
&END

PAGE 2

REFERENCES

1. H. L. McMurry, J. Chem. Phys. 9, 231 (1941).
2. H. L. McMurry, *ibid.*, p. 241.
3. J. Sidman and D. S. McClure, J. Am. Chem. Soc. 77, 6461 (1955).
4. F. O. Nicolaisen, O. F. Nielsen and M. Vala, J. Mol. Struct. 13, 349 (1972).
5. M. Vala, I. Trabjerg and E. N. Svendsen, Acta Chem. Scand. A28, 37 (1974).
6. R. Spafford, J. Wrobel and M. Vala, Mol. Phys. 27, 1241 (1974).
7. R. Spafford, J. Baiardo, J. Wrobel and M. Vala, J. Am. Chem. Soc. 98, 5217 (1976).
8. J. Baiardo, R. Spafford and M. Vala, J. Am. Chem. Soc. 98, 5225 (1976).
9. R. Spafford and M. Vala, J. Photochem. 8, 61 (1978).
10. E. A. LaLancette and R. E. Benson, J. Am. Chem. Soc. 83, 4867 (1961).
11. E. M. Kosower, J. Chem. Phys. 38, 2813 (1963).
12. R. E. Ballard and C. H. Park, Spectrochimica Acta 26A, 43 (1970).
13. R. Hoffman, A. Imamura and W. J. Hehre, J. Am. Chem. Soc. 90, 1499 (1968).
14. J. R. Swenson and R. Hoffman, Helv. Chim. Acta 53, 2331 (1970).
15. R. Hoffman, Accts. Chem. Res. 4, 1 (1971).
16. R. Hoffman, J. Chem. Phys., 39, 1397 (1963).
17. J. A. Pople and D. L. Beveridge, *Approximate Molecular Orbital Theory*, McGraw-Hill, New York, N.Y., 1970.
18. D. Cowan, R. Gleiter, J. A. Hashmall, E. Heilbronner and V. Hornung, Angew. Chemie Intl. Ed. 10, 401 (1971).

19. D. W. Turner, C. Baker, A. D. Baker and C. R. Brundle, *Molecular Photoelectron Spectroscopy*, Wiley-Interscience, London, 1970.
20. R. D. Gordon, M. Caris and D. G. Newman, *J. Mol. Spectrosc.*, 60, 130 (1976).
21. R. Gleiter, E. Heilbronner and V. Hornung, *Helv. Chim. Acta* 55, 255 (1972).
22. F. Brogli, E. Heilbronner and T. Kobayashi, *Helv. Chim. Acta* 55, 274 (1972).
23. E. Heilbronner, V. Hornung, F. H. Pinkerton and S. F. Thames, *Helv. Chim. Acta* 55, 289 (1972).
24. D. Dougherty and S. P. McGlynn, *J. Am. Chem. Soc.* 99, 3234 (1977).
25. D. Dougherty, P. Brint and S. P. McGlynn, *J. Am. Chem. Soc.* 100, 5597 (1978).
26. J. C. D. Brand, H. Callomon, D. C. Moule, J. Tyrrell and T. H. Goodwin, *Trans. Far. Soc.* 61, 2365 (1965).
27. T. Oka, A. R. Knight and R. P. Steer, *J. Chem. Phys.* 63, 2414 (1975); *ibid.* 66, 699 (1977).
28. H. Okabe, *J. Chem. Phys.* 66, 2058 (1977).
29. S. D. Gupta and M. Chowdhury, *J. Chem. Phys.* 53, 1293 (1970).
30. D. S. L. Blackwell, C. C. Liao, R. O. Loufty, P. de Mayo and S. Paszyc, *Mol. Photochem.* 4, 171 (1972).
31. D. A. Capitanio, H. J. Pownall and J. R. Huber, *J. Photochem.* 3, 225 (1974).
32. M. Mahaney and J. R. Huber, *Chem. Phys. Lett.* 30, 410 (1976); *J. Photochem.* 5, 333 (1976).
33. U. Bruhlman and J. R. Huber, *J. Photochem.* 10, 205 (1979).
34. R. Rajee and V. Ramamurthy, *J. Photochem.* 11, 135 (1979).
35. A. H. Maki, P. Svejda and J. R. Huber, *Chem. Phys.* 32, 369 (1978).
36. D. M. Burland, *Chem. Phys. Lett.* 70, 508 (1980).
37. P. deMayo, *Accts. Chem. Res.* 9, 52 (1976).
38. C. D. Shirrell and D. E. Williams, *Acta Cryst.* B29, 1648 (1973).
39. J. Hurst and M. Vala, unpublished work, 1976.

40. J. J. Worman, E. Schmidt, E. S. Olson, W. P. Jensen and R. Schultz, *Spectrochimica Acta* A32, 1415 (1976).
41. J. Behan, R. A. W. Johnstone, J. J. Worman and T. P. Fehlner, *J. Mol. Struct.* 40, 151 (1977).
42. P. K. Basu, U. Chandra Singh, K. N. Tantry, V. Ramamurthy and C. N. R. Rao, *J. Mol. Struct. (Theochem)* 76, 237 (1981).
43. I. Trabjerg, J. Baiardo and M. Vala, "The 5943 Å Triplet Band System of 2,2,4,4-tetramethyl-1,3-cyclobutanedithione", Thirty-Fourth Symposium on Molecular Spectroscopy, Columbus, Ohio, 1979. Paper MG13.
44. Details are given in Chapter 5.
45. R. D. Gordon, S. E. Gransden and R. Marion, *J. Mol. Spectrosc.*, 81, 340 (1980).
46. J. K. Crawley and R. D. Gordon, *J. Phys. Chem.*, 85, 3776 (1981).
47. W. R. Wadt and W. A. Goddard III, *J. Am. Chem. Soc.*, 97, 2034 (1975).
48. W. R. Wadt, W. A. Goddard III and T. H. Dunning, *J. Chem. Phys.* 65, 438 (1976).
49. D. A. Kleier, R. L. Martin, W. R. Wadt and W. R. Moomaw, "Localized Excitations and the Geometry of the Excited States of Pyrazine" in press. We are grateful to Prof. Moomaw for a preprint of this work.
50. L. E. Nitsche and E. R. Davidson, *Chem. Phys. Lett.* 58, 171 (1978).
51. M. Hehenberger, *Chem. Phys. Lett.*, 46, 117 (1977).
52. C. P. Keijzers, P. S. Bagus and J. P. Worth, *J. Chem. Phys.* 69, 4032 (1978).
53. H. T. Jonkman, *Broken Orbital Symmetry in Excited and Ionized States of Molecules*, Ph.D. Thesis, University of Groningen, The Netherlands, 1975. The author is grateful to Dr. Jonkman for a copy of his thesis.
54. W. Von Niessen, W. P. Kraemer and G. H. F. Diercksen, *Chem. Phys.* 41, 113 (1979). This work contains many references to many-body Green's function methods and other PES interpretative theories.
55. I. Trabjerg and H. U. Güdel, *Acta Chem. Scand.* A28, 8 (1974).
56. See references in Chapter 4.
57. The usefulness of this technique in discriminating spin-orbit contributions is discussed in Chapter 5.

58. See, for example W. A. Goddard III, T. H. Dunning, Jr., W. J. Hunt and P. J. Hay, *Accts. Chem. Res.* 6, 368 (1973).
59. J. J. Wendoloski, Thirty-Fifth Symposium on Molecular Spectroscopy, Columbus, Ohio, 1980. Paper WF12.
60. J. Baiardo and M. Vala Thirty-Sixth Symposium on Molecular Spectroscopy, Columbus, Ohio, 1981. Paper MHL.
61. The orbital plots were made with the HIDEPLOT program package, written by Dr. N. H. F. Beebe. We are grateful to QTP for making it available to us.
62. S. Canuto, O. Goscinski and M. Zerner, *Chem. Phys. Lett.* 68, 232 (1979).
63. J. Almlöf, Proceedings of the Second Seminar on Computational Problems in Quantum Chemistry, Strassburg, 1972 (Max-Planck-Institute, München, 1973), (unpublished).
64. P. S. Bagus, B. Liu, D. McLean and M. Yoshimine, IBM Res. Rep. RJ 1077 (1972), (unpublished).
65. T. H. Dunning, Jr., *J. Chem. Phys.* 53, 2823 (1970).
66. C. E. Dykstra and H. F. Schaefer III, *J. Am. Chem. Soc.* 97, 7210 (1975); *ibid.* 98, 401 (1976).
67. M. Hehenberger, private communication of U. Wahlgren's notes on the description of a revision of ALCHEMY.
68. M. C. Riche and M. M. Janot, *C. R. Acad. Sci. Paris, Ser. C*, 275, 543 (1972).
69. J. C. Decius and R. M. Hexter, *Molecular Vibrations in Crystals*, McGraw-Hill Inc., New York, N.Y., 1977.
70. R. M. Hochstrasser, *Molecular Aspects of Symmetry*, W. A. Benjamin, Inc., New York, N. Y., Chapter 10.
71. G. F. Koster, J. O. Dimmock, R. G. Wheeler and H. Statz, *Properties of the Thirty-two Point Groups*, M. I. T. Press, Cambridge, Mass., 1963.
72. A. S. Davydov, *Theory of Molecular Excitons*, McGraw-Hill, Inc., New York, N. Y., 1962. Translated by M. Kasha and M. Oppenheimer, Jr., Chapter 1.
73. B. Di Bartolo and R. C. Powell, *Phonons and Resonances in Solids*, John Wiley and Sons, New York, N. Y., 1976. Chapter 10.

74. R. M. Hochstrasser and P. N. Prasad, J. Chem. Phys. 56, 2814 (1972); and "Optical Spectra and Relaxation in Molecular Solids", in *Excited States*, Vol. 1, E. C. Lim Ed.; Academic Press, New York, N.Y. 1973.
75. A spectrum which could have been described by an ℓ of 2 to 3 was observed only once at ~ 20 K by J. Hurst (unpublished work) during experiments prior to the x-ray determination of the c axis location (76).
76. Dr. Fleming Hansen determined this for us; we are grateful for his assistance.
77. The author is indebted to Prof. Martin Vala, and Dr. Ib Trabjerg (of the Department of Physical Chemistry, H.C. Ørsted Institute, University of Copenhagen) for photographing the TMCBDT spectra described in this chapter and the Zeeman spectra in Chapter 5. Dr. Trabjerg's assistance with the experiments performed during his brief visit to the U. of F. (April 1978) is also appreciated.
78. Y. Toyozawa, Supplement of the Progress of Theoretical Physics, Number 12, 1959. Page 111.
79. J. B. Coon, N. W. Naugle and R. D. McKenzie, J. Mol. Spectrosc. 20, 107 (1966).
80. J. P. Baiardo, in preparation (unpublished).
81. E. B. Wilson, J. C. Decius and P. C. Cross, *Molecular Vibrations*, McGraw-Hill Inc., New York, N.Y., 1955. Chapter 3.
82. Ref. 81, Appendix III.
83. Ib Trabjerg, private communication.
84. J. R. Henderson, Douglas Report SM-45807, Douglas Aircraft Co., 1964.
85. R. M. Hochstrasser, J. Chem. Phys. 47, 1015 (1967).
86. D. S. McClure, J. Chem. Phys. 20, 682 (1951); *ibid.*, 17, 905 (1949).
87. H. F. Hamerka, *Advanced Quantum Chemistry*, Addison-Wesley Publishing Company, Reading, Mass. 1965. P. 197.
88. C. A. Hutchison and B. W. Mangum, J. Chem. Phys. 29, 952 (1958); *ibid.* 34, 908 (1961).
89. R. H. Clarke and R. M. Hochstrasser, J. Chem. Phys. 48, 745 (1968).
90. H. Sternlicht and H. M. McConnell, J. Chem. Phys. 35, 1793 (1961).
91. R. M. Hochstrasser and T. S. Lin, J. Chem. Phys. 49, 4929 (1968).

92. R. L. Ellis and H. H. Jaffe, "Electronic Excited States of Organic Molecules", in *Electronic Structure Calculation. Part B: Applications*, G. A. Segal, Editor; Plenum Press, New York, 1977.
93. L. Goodman and V. G. Krishna, *Rev. Mod. Phys.* 35, 541 (1963).
94. M. Blume and R. E. Watson, *Proc. Roy. Soc.* A270, 127 (1968); *ibid.*, A271, 565 (1963).
95. J. L. Ginsburg and L. Goodman, *Mol. Phys.* 15, 441 (1968).
96. J. A. Pople and G. A. Segal, *J. Chem. Phys.* 43, S136 (1965).
97. Ib Trabjerg and M. Vala, in preparation.
98. C. A. Masmanidis, H. H. Jaffe and R. L. Ellis, *J. Chem. Phys.* 79, 2052 (1975).
99. J. C. Slater, *Quantum Theory of Matter*, McGraw-Hill, Inc. New York, N. Y., 1968. Page 225.
100. G. Lancelot, *Mol. Phys.*, 29, 1099 (1975).
101. E. B. Moore, W. C. Cook and A. R. M. Ram, authors. QCPE Program N-64. Quantum Chemistry Program Exchange, Indiana University, Bloomington, Indiana.
102. T. Azumi, S. P. McGlynn and M. Kinoshita, *Molecular Spectroscopy of the Triplet State*, Prentice-Hall Inc., Englewood Cliffs, New Jersey; 1969. ca. page 189.
103. In Eqs. 4-10 and 4-11 the complex conjugates of $\langle H_{so} \rangle$ arise. H_{so} is Hermitian and pure imaginary so we have

$$\langle {}^3B_{1g} | H_{so} | {}^1\psi_o \rangle^* = - \langle {}^3B_{1g} | H_{so} | {}^1\psi_o \rangle = \langle {}^1\psi_o | H_{so} | {}^3B_{1g} \rangle$$
 and since the latter two integrals reduce to $-(\langle p' | R | n \rangle)$ and $-\langle n | R | p' \rangle$ we write the denominator as $-(E_l - E_o)$ and have:

$$\frac{+\langle p' | R | n \rangle}{E_o - E_l} = \frac{-\langle n | R | p' \rangle}{E_o - E_l} = \frac{\langle n | R | p' \rangle}{E_l - E_o}$$
104. Ref. 102, ca. page 247.
105. R. L. Ellis, G. Kuehnlenz and H. H. Jaffe, *Theor. Chim. Acta* 26, 131 (1972).
106. See ref. 17, Appendix B.
107. For energy optimized exponents of the neutral atom, see E. Clementi and D. L. Raimondi, *J. Chem. Phys.* 38, 2686 (1963).
108. J. C. Slater, *Phys. Rev.* 36, 57 (1930).

- 109a.) J. H. Van der Waals and M. S. DeGroot, in *The Triplet State*, Beirut Symposium, 1967; A. Zahlan, Editor. Cambridge University Press, Cambridge, England 1967. Page 101.
- b.) T. Azumi, C. M. O'Donnell and S. P. McGlynn, *J. Chem. Phys.* 45, 2735 (1966).
- 110.D. P. Craig and S. H. Walmsley, "Visible and Ultraviolet Absorption by Molecular Crystals" in *Physics and Chemistry of the Organic Solid State*, D. Fox, M. M. Labes and A. Weissberger, Editors; Volume I, Chapter 10; Interscience Publishers, New York, 1963.
- 111a.) G. Castro and R. M. Hochstrasser, *Solid State Communication* 3, 425 (1965); *ibid.*, *J. Chem. Phys.* 48, 637 (1968).
- b.) S. Dym, R. M. Hochstrasser and M. Schafer, *J. Chem. Phys.* 48, 646 (1968).
- c.) R. M. Hochstrasser, *J. Chem. Phys.* 47, 1015 (1947).
- 112.R. M. Hochstrasser and T. S. Lin, *J. Chem. Phys.* 49, 4929 (1968).
- 113a.) N. M. Atherton, *Electron Spin Resonance, Theory and Applications*, (Ellis Horwood Series in Physical Chemistry), Halsted Press, New York, N.Y., 1973. Chapter 5.
- b.) A. Carrington and A. D. McLachlan, *Introduction to Magnetic Resonance with Application to Chemistry and Chemical Physics*, Harper and Row, New York, N.Y. 1967.
- 114.The EIGCH subroutine in the IMSL mathematical package handles complex Hermitian matrices. The 3x3 in this case can also be solved analytically, see Appendix I.
- 115.As E becomes larger it will also influence Δ . Because of the convention that z be the axis of greatest spin-spin interaction, and the definitions of D and E, however, it turns out that $|D| > |E|$ is usually true. It is not inconceivable, however for X,Y and Z to be such that $|D|$ and $|E|$ are comparable.
- 116.H. F. Hameka in ref. 109a, p. 24-25. Also see page 199 of ref.102. Contributions by quintet states are neglected on the basis of large excitation energies. The triplet perturbers of T_1 do not contribute to radiative properties and were heretofore neglected. Because of the like spins T-T coupling occurs via H_{so}^+ , cf. Eq. 4-15
- 117.M. Batley and R. Bramley, *Chem. Phys. Lett.* 15, 337 (1972).
- 118.We are grateful to the members of the Organic Division of the H.C. Ørsted Institute for the synthetic work.
- 119.E. U. Elam and H. L. Davies, *J. Org. Chem.* 32, 1562 (1967).

120. A ruler with $1/64$ " graduations was used to measure peak heights and line positions etc.. In the text a "unit" refers to $1/64$ ".

121. In lieu of a tensor analysis text, see ref. 113a, section 4.2 and ref. 113b, Appendix D.

122. A. J. Stone, Proc. Roy. Soc. A271, 424 (1963).

123. A. Hammer, M. Schworer and H. Sixl, Chem. Phys. Lett. 5, 434 (1970).

124. P. Peretti, P. Ranson and Y. Rousset, Chem. Phys. 56, 135 (1981).

BIOGRAPHICAL SKETCH

Joseph P. Baiardo was born on June 1, 1946, in Ozzano, Monferrato, Italy. In 1957 his family immigrated to the U.S. He graduated from St. Michael Central High School in Chicago in 1964 and received a Bachelor of Science in chemistry from Loyola University of Chicago in 1968. From then until 1971 he served on the faculty of Notre Dame High School for Boys in Niles, Illinois, where he taught chemistry and physics. In 1971 he began graduate studies in chemistry at the University of Florida leading to the degree of Doctor of Philosophy.

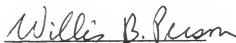
On June 30, 1973, he married Nancy Elaine Tyszkowski of Brookline, Massachusetts. They now have three sons, Joseph A. (7) Jonathan (5) and Justin (2).

I certify that I have read this study and that in my opinion it conforms to acceptable standards of scholarly presentation and is fully adequate, in scope and quality, as a dissertation for the degree of Doctor of Philosophy.



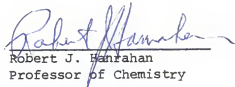
Martin T. Vala, Chairman
Professor of Chemistry

I certify that I have read this study and that in my opinion it conforms to acceptable standards of scholarly presentation and is fully adequate, in scope and quality, as a dissertation for the degree of Doctor of Philosophy.



Willis B. Person
Professor of Chemistry

I certify that I have read this study and that in my opinion it conforms to acceptable standards of scholarly presentation and is fully adequate, in scope and quality, as a dissertation for the degree of Doctor of Philosophy.



Robert J. Henrhan
Professor of Chemistry

I certify that I have read this study and that in my opinion it conforms to acceptable standards of scholarly presentation and is fully adequate, in scope and quality, as a dissertation for the degree of Doctor of Philosophy.



John R. Sabin
Professor of Physics

I certify that I have read this study and that in my opinion it conforms to acceptable standards of scholarly presentation and is fully adequate, in scope and quality, as a dissertation for the degree of Doctor of Philosophy.



Zoran Pop Stojanovic
Professor of Mathematics

This dissertation was submitted to the Graduate Faculty of the Department of Chemistry in the College of Liberal Arts and Sciences and to the Graduate Council, and was accepted as partial fulfillment of the requirements for the degree of Doctor of Philosophy.

May 1982

Dean, for Graduate Studies
and Research